NASA Contractor Report 177626

Aerodynamic Control of NASP-Type Vehicles Through Vortex Manipulation

Volume II

Static Wind Tunnel Tests

Carlos J. Suárez, Brian R. Kramer, Brooke C. Smith, and Gerald N. Malcolm

CONTRACT NAS2-13196
September 1993

National Aeronautics and Space Administration

NASA Contractor Report 177626

Aerodynamic Control of NASP-Type Vehicles Through Vortex Manipulation

Volume II

Static Wind Tunnel Tests

Carlos J. Suárez, Brian R. Kramer, Brooke C. Smith, and Gerald N. Malcolm

Eidetics International, Inc.
3415 Lomita Blvd.
Torrance, CA 90505

Prepared for
Ames Research Center
CONTRACT NAS2-13196
September 1993

National Aeronautics and
Space Administration

Ames Research Center
Moffett Field, California 94035-1000

PAGE _____ INTENTIONALLY BLANK

TABLE OF CONTENTS

NOMENCLATURE

A_{ref}	reference wing area
b	wing span
c	wing chord
L	reference length = total length of the model
$C\mu$	momentum coefficient of blowing = $\dot{m}j\ Vj / q\ A_{ref}$
$\dot{m}j$	mass flow rate of the blowing jet
q	free-stream dynamic pressure
V_∞	free-stream velocity
Vj	average exit velocity of the blowing jet
α, AOA	angle of attack
β	sideslip angle
ϕ	roll angle
Φ	azimuth angle (from the windward meridian)
de	elevon deflection (+ down)
dr	rudder deflection (+ right)
CN	normal force coefficient
Cm(b)	body axes pitching moment coefficient
Cn(b)	body axes yawing moment coefficient
Cl(b)	body axes rolling moment coefficient
Cy(b)	body axes side force coefficient
CL	stability axes lift coefficient
ΔCn(b)	body axes yawing moment increment
ΔCl(b)	body axes rolling moment increment
ΔCy(b)	body axes side force increment
Cp	pressure coefficient
$Cn\beta$	directional derivative
$Cl\beta$	lateral derivative
R/L30	blowing on the right/left side with a reservoir pressure of 30 psi, which corresponds to a $C\mu$ = 0.00075*
B30	blowing on both sides simultaneously with a reservoir pressure of 30 psi, which corresponds to a $C\mu$ = 0.00075*
*	L/R/B 40, 50 and 60 correspond to $C\mu$ = 0.001, 0.00125 and 0.0015, respectively

LIST OF FIGURES

SUMMARY

Forebody Vortex Control (FVC) is an emerging technology that has received widespread and concentrated attention by many researchers for application on fighter aircraft to enhance aerodynamic controllability at high angles of attack. This technology has also been explored in this research program for potential application to a NASP-type configuration. Wind tunnel tests, using 6-component force and moment and surface pressure measurements, have been conducted to evaluate a number of forebody jet blowing schemes. The configuration tested has a slender, circular cross-section forebody and a 78° swept delta wing. Blowing jets were implemented on the leeward side of the forebody with small circular tubes tangential to the surface at various longitudinal locations that could be directed aft, forward, or at angles in between. Jet blowing on each side of the forebody individually and on both sides simultaneously were evaluated. The effects of blowing are observed primarily in the yawing and rolling moments and are highly dependent on the jet configuration and the angle of attack. Effectiveness is also evaluated at sideslip conditions. Results show that the baseline flow field, without blowing activated, is quite sensitive to the geometry differences of the various protruding jets, as well as being sensitive to the blowing, particularly in the angle of attack range where the forebody vortices are naturally asymmetric. In addition to the static forces, moments and pressures, an assessment was made at the time lag of the flow field response to the initiation of blowing. The time response was very short, on the order of the time required for the flow disturbance to travel the distance from the nozzle to the specific airframe location of interest at the free stream velocity. Overall, results indicate that sizable yawing and rolling moments can be induced with modest blowing levels. However, direct application of this technique on a very slender forebody would require thorough wind tunnel testing to optimize the jet location and configuration.

AERODYNAMIC CONTROL OF NASP-TYPE VEHICLES THROUGH VORTEX MANIPULATION

VOLUME II: STATIC WIND TUNNEL TESTS

1.0 INTRODUCTION

One of the most significant and ambitious programs in the aerospace industry in the near future will be the development and eventual flight test of the National Aero-Space Plane (NASP). A high proportion of the technological research now being conducted to support the development of a NASP is concentrated in the hypersonic regime. In addition to excellent hypersonic performance, however, high-quality low-speed flight must also be achieved. Conceivably, configurations optimized for hypersonic flight may experience adverse low-speed aerodynamic phenomena dominated by separated and vortex flows, such as wing rock or non-zero yawing moments at zero sideslip, which could complicate the effort for achieving good handling qualities during the takeoff and the approach and landing phases. Using conventional control effectors such as rudder or aileron to overcome the effects of these adverse phenomena and satisfy low-speed flight quality criteria may result in a weight increment over and above that which exists if hypersonic flight quality were the only concern. Using non-conventional vortex control effectors, on the other hand, may potentially satisfy low-speed flight quality criteria with a substantially lower weight penalty. The principal mechanism to accomplish a saving in weight is with fluid amplification, where a small fluidic input, such as surface blowing in the forebody region, results in large output control forces and moments to the airframe by influencing the vortex flow field.

The powerful forebody vortices are one of the main causes of aircraft instabilities at high angles of attack. An effective means of suppressing the instabilities in this flight regime is, therefore, to directly control these vortices. Recent research efforts on fighter-type aircraft indicated that some of the most promising methods for Forebody Vortex Control (FVC) are movable forebody strakes, rotatable nose-tip and nose-boom devices, and blowing on the forebody surface. The use of symmetrically deployed forebody strakes has been shown to be effective in forcing naturally-occurring asymmetric vortices at high angles of attack to be symmetric. The large forebody side forces and resulting yawing moments at zero sideslip are therefore reduced or eliminated. The use of asymmetrically deployed forebody strakes has been investigated for possible application to controlling the yawing moment[1,2]. Rotatable nose-tip devices are also found to be effective in controlling the forebody flow. These devices are in the forms of a small cylinder attached to the tip[3], machined flats[3], elliptic tips[4], and small vortex generators[5]. Miniature, rotatable strakes attached to the nose-boom of an F-16 also influence the forebody vortex flow field, creating forces and moments that can be used for additional control[6]. Due in part to the concern about strakes and mechanical surfaces interfering with forebody radar operation, various forebody blowing techniques to control the forebody vortex orientations have also been investigated as alternatives to mechanical devices. Two main forms of blowing have been studied: (1) blowing from a localized jet [2,7,8], and

(2) blowing from a tangential slot[2,8-12]. In either form, blowing was found to be highly effective in controlling the vortex orientation.

The Phase I technical results (Ref. 13) show that it is potentially feasible to utilize vortex manipulation with blowing to provide the necessary control forces for a NASP-type configuration, as well as fighter configurations, at low speeds. The mass flow requirements for blowing scaled to a full-size NASP based on sub-scale experiments appear to be low, well within practical limits of acquiring the required mass flow through engine bleed or similar sources. The resulting control moments, based on wind tunnel studies of fighter configurations, can be greater than those generated by a typical rudder. The vertical tail area and structural weight may be reduced, and thus, can potentially lead to an improvement in the hypersonic drag performance. Preliminary tests in the water tunnel, as part of this Phase II investigation, also showed that blowing can produce sizable forces and moments at angles of attack between 20° and 30°.

It is important to note that at the time the research contract with NASA was awarded, there was no specific design for the NASP yet selected. The models used in the Phase I study and in this investigation are based on drawings of a generic, preliminary NASP configuration provided by the duPont Aerospace Co., Inc. The configuration that now appears from the consolidated NASP design team, however, is significantly different. Even thought it still has highly-swept wings, the fuselage has a blunt forebody, so the lateral/directional stability problems will be different. This by no means diminishes the value of this research program; the general results obtained in this study can be applied to similar configurations, such as the High Speed Civil Transport (HSCT) or any other supersonic/hypersonic advanced configuration. Also, the basic fluid mechanics associated with blowing will be better understood. Despite the dissimilarity between the current NASP and the configurations used in this investigation, the models will still be referred to as NASP-type configurations.

The Phase II research effort includes static and dynamic ("free-to-roll") water tunnel tests, static and dynamic wind tunnel tests, and a simulation exercise. It is the intention of this report (Volume II of a Final Report) to summarize the results of the static wind tunnel tests performed on this configuration.

2.0 TECHNICAL OBJECTIVES

The principal objectives of the Phase I study were to identify, early-on in the technology development phase of NASP, the potential adverse low-speed aerodynamic phenomena associated with typical NASP configurations (which are optimized for high-speed flight), and to investigate potential solutions to these problems. The idea was to utilize vortex control methods similar to those investigated for fighter aircraft at high angles of attack as an alternative method or an augmentation to conventional methods of aerodynamic control of the National Aero-Space Plane. The Phase I study showed that blowing could be utilized to manipulate the forebody vortices and to create forces that could be used for control. That study, however, was qualitative, based on flow visualization. The Phase II study was structured to quantify and optimize those force and moment inputs. The overall goal was to develop the

technology of forebody vortex control by blowing to a level where it could be seriously considered as a viable candidate for incorporation into the flight control system of this type of aircraft. Results from the Phase II research were expected to provide high-confidence in the aerodynamic performance benefits to the generic NASP configuration with forebody blowing. A six degree-of-freedom simulation was performed to evaluate the advantages of the blowing system for take-off and approach and landing tasks, where the angle of attack is sufficiently high to require enhanced controllability.

Water tunnel tests were conducted prior to the wind tunnel test to evaluate different blowing techniques and to perform a preliminary "screening", so only the best blowing configurations were investigated in the wind tunnel. Both slot blowing and jet blowing were studied in the water tunnel. Slot blowing did not show significant improvements over jet blowing in terms of behavior and magnitude of the forces and moments produced, therefore, it was decided to investigate only the jet blowing technique in the wind tunnel test. The results of that water tunnel test are extensively discussed in Volume I of this Final Report.

The specific objectives of the static wind tunnel tests are listed below:

1. Evaluate and quantify the effectiveness of jet blowing for controlling the forebody vortices of a NASP-type configuration.

2. Investigate the effects of different parameters on the blowing process, such as nozzle location, blowing direction and mass flow rate. Force, moment and pressure measurements will be performed for each of the blowing schemes.

3. Study and quantify the time response (time lag) of the vortex system to the blowing inputs, by using surface-mounted dynamic pressure transducers (Endevco) to acquire surface pressure changes in response to blowing activation.

3.0 EXPERIMENTAL SETUP

The experiments were conducted in the NASA Ames Research Center 7 x 10 Foot Wind Tunnel. It is a closed-throat, single return atmospheric tunnel with about 10% air exchange accomplished by means of a ventilating tower. The tunnel is powered by a single 8-blade, 8.5 m (28 ft) diameter fan driven by a 1600 HP synchronous motor located in the nacelle in the return passage.

The model used in this test (which was twice the scale of the water tunnel model), can be seen in Figs. 1 and 2. The forebody has a length-to-base diameter ratio of 6, and is circular in cross-section. The wing is a sharp-edge delta with a 78° sweep. This NASP-type configuration possesses characteristics that may be considered as similar to certain forebody/leading edge extension (LEX) and missile forebody/canard combinations.

The forebody of the model is provided with three rings of static pressure ports at F.S. 7.6 cm, 20.3 cm and 47 cm (3", 8" and 18.5"). The first two stations have 20 static

pressure ports each, while the last station has 8 ports on the leeward side. A PSI system with a 48-channel module, which is shown in Fig. 2a, was used to measure the forebody pressure distributions at the selected stations. Endevco dynamic pressure transducers were located on the forebody at F. S. 10.2 cm, 30.5 cm and 50.8 cm (4", 12" and 20") and Φ = 150° radially, and on each wing at 93 cm and 118.4 cm (36.6" and 46.6") from the tip. These transducers monitored the dynamic pressure changes produced by blowing and provided useful time lag data. A 6-component sting balance internal to the model was utilized to acquire force and moment data.

The blowing ports are located at F.S. 3.2 cm and 12.5 cm (1.25" and 4.9") and Φ = 150° radially, as seen in Fig. 2b. The blowing was controlled by two fast-acting solenoid valves (Fig. 2c). The total pressure and temperature in a chamber very close to each of the nozzle exits were measured to determine the mass flow rate and the blowing coefficient $C\mu$. In order to obtain the different blowing rates, the reservoir pressure was varied from 30 psi to 60 psi, and for this total pressure range, the flow was choked at the nozzle exit.

Most of the tests on this configuration were performed at a dynamic pressure q = 1915 Pa (40 psf), which corresponds to a free stream velocity of 55 m/sec (180 ft/sec), and a Reynolds number of 570,000 based on the body diameter. The test was performed for an angle of attack range from 0° to 30° and for a sideslip angle range from -10° to 10°. The model is sting mounted in the center of the test section with the wings in the vertical plane (Fig. 2d). The different blowing techniques investigated, which are illustrated in Fig. 3, include: aft blowing from the forward location, aft blowing at an angle, forward blowing from the aft and forward locations, and combined blowing.

4.0 RESULTS AND DISCUSSION

4.1 Force and Moment Measurements

Force and moment data were acquired using a 1.5" MK-II sting balance. The data are presented in body axes, with the addition of lift coefficient in stability axes for selected configurations.

4.1.1 Baseline Configuration

The flow field for slender forebody configurations is very sensitive to any disturbance in the nose region. A small change in the geometry of the body of revolution will affect the flow field characteristics significantly. Even if the geometry is not changed, an increase in angle of attack at zero sideslip is sufficient to create large asymmetries in the vortices with the associated asymmetric forces and moments. The configuration tested in this study, being a slender, circular cross-section forebody, was found to be extremely sensitive to any disturbance or change in geometry. In order to evaluate blowing, small nozzles were located near the tip of the model; these blowing ports, protruding from the body surface, definitely influence the baseline flow characteristics. It is important to make clear at this point that each blowing method

investigated is compared to the appropriate baseline, since even the minimal change in nozzle orientation or location can, by itself, modify the forebody vortex pattern significantly. After the nozzle geometry was changed, the non-blowing characteristics of the new baseline configuration were determined, and the particular blowing method was then evaluated as an increment with respect to said baseline.

Six coefficients (CN, Cm(b), Cn(b), Cl(b), Cy(b) and CL) are presented in Fig. 4 for the "clean" configuration (no blowing ports) and for a configuration with nozzles (baseline A), which corresponds to tangential blowing straight aft. The effect of the ports on the longitudinal characteristics is almost negligible, although the configuration with the blowing nozzles presents a slightly higher normal force and a lower nose-down pitching moment coefficient for angles of attack greater than 20°, due mainly to additional forebody "lift". Large differences are observed in the lateral/directional characteristics. The yawing moment curve (Fig. 4c) indicates that the blowing ports cause the forebody vortices to become asymmetric at a lower angle of attack when compared to the clean configuration. The baseline configuration shows an asymmetric vortex pattern starting at $\alpha = 15°$. Very strong asymmetries are evident for this configuration between $\alpha = 25°$ and 30°, while the asymmetries shown by the clean configuration are significantly reduced in this angle of attack range. The rolling moment coefficient reveals a similar behavior, with the clean configuration maintaining a much smaller asymmetric moment for most of the angle of attack range investigated. The baseline rolling moment curve is zero up to $\alpha = 10°$, negative from $\alpha = 10°$ to 23°, and positive at higher angles of attack.

The effects of sideslip on the longitudinal characteristics are minimal (Fig. 5a and 5b). The only difference is the expected reduction in the normal force for all the sideslip conditions (especially for $\beta = 5°$) at angles of attack higher than 20°. The yawing moment curves depicted in Fig. 5c indicate that the directional stability is slightly positive (i. e., β and Cn are the same sign) to angles of attack of approximately 10°. This stability is provided by the vertical tail. As the angle of attack is increased, the effect of the vertical tail is diminished, the forebody vortices become stronger and the destabilizing effect of the forebody is predominant. The forebody vortex asymmetry observed at $\beta = 0°$ is reversed for the positive sideslip at angles of attack greater than 20°, as denoted by the negative yawing moment. In general, the initial asymmetry appears to be very strong, since it is not enhanced with negative sideslip at angles of attack higher than 25°. The effect of sideslip on rolling moment (Fig. 5d) is favorable through most of the angle of attack range, in the sense that a positive sideslip produces a negative rolling moment compared to the $\beta = 0°$ data and vice versa. The side force is relatively symmetric (about $\beta = 0°$) for the $\beta = 5°$ and -5° cases up to $\alpha = 20°$ and at $\alpha = 30°$. Between 20° and 30° angles of attack, the asymmetry is stronger with positive sideslip than with negative β. The $\beta = -10°$ case produces a more positive side force than the $\beta = -5°$ case only to $\alpha = 20°$; beyond that angle of attack, the asymmetry in the forebody vortices is apparently reduced, and from 25° to 30° angle of attack, the values of the side force for the $\beta = 0°$ and $\beta = -10°$ are almost equal. Figure 6 depicts the directional derivative Cn_β and the lateral derivative Cl_β.

The first plot indicates positive directional stability for angles of attack lower than 10° ($Cn_\beta > 0$), neutral stability at $\alpha = 10°$, and negative stability for angles of attack greater than 10° ($Cn_\beta < 0$). The lateral stability is positive (Cl_β is negative) for the entire angle of attack range.

The same coefficients are presented in Fig. 7 for the tail off configuration, still with the same blowing nozzles (A). Again, no major changes are observed in the longitudinal characteristics. Without the vertical tail, the main contributor to the yawing moment change with sideslip is the forebody, and it is a destabilizing contribution. A positive yawing moment is produced for negative sideslip angles, mainly resulting from the positive side force created in the forebody. The effect of sideslip on rolling moment on this configuration is still favorable, i. e., a positive rolling moment is produced for negative sideslips. It is important to note that the asymmetries in the baseline flow for the tail off case are significantly reduced compared to the tail on configuration, indicating strong interactions between the vortices and the vertical tail.

4.1.2 Effect of Control Surface Deflections

A limited control surface deflection study was performed in order to obtain benchmark values of the conventional control power for later comparison with the control power that can be obtained with blowing. The model is provided with a rudder and with elevons on each wing (see Fig. 1) that were deflected differentially as ailerons and together as an elevator. The results for two elevator deflections (30° and -30°) are presented in Fig. 8, and the trends are as expected. Most of the effect is observed in the longitudinal coefficients (CN, Cm(b) and CL), with the downward deflection producing an increase in normal force and a more negative pitching moment than the shown by the baseline case. A small effect is observed in the lateral/directional coefficients, especially in the yawing moment and side force.

Figure 9 reveals the results for the differential elevon deflections. The primary effect, as expected, is in the rolling moment coefficient (Fig. 9d). For a +/- 30° deflection, the value of the rolling moment coefficient change produced is approximately 0.035. This incremental value with respect to the baseline is almost constant for most of the angle of attack range. A very interesting result is the coupling of the ailerons with the directional characteristics. The differential elevon deflection induces also a significant change in yawing moment and in side force, as shown in Figs. 9c and 9e. It appears that the differential elevon deflection is affecting the flow near the vertical tail, creating a pressure gradient over this surface with the associated side force and yawing moment.

The deflection of the rudder, shown in Fig. 10, does not affect the longitudinal coefficients, and minimal changes are seen in the rolling moment curves. The majority of the changes are evident in the yawing moment and side force coefficients (Figs. 10c and 10e). A rudder deflection of 30° produces a change in yawing moment compared to the baseline case of about 0.03-0.04. At angles of attack between 20° and 25°, it is evident that a progressive deflection of the rudder from 15° to 30° does not necessarily produce a larger yawing moment. This is most likely due to the interaction of the asymmetric forebody vortices with the tail in that region. The side force shows a continuous negative increment with respect to the baseline with rudder deflection. The

magnitude of the yawing moment increment is important to keep in mind for later comparison with the changes in yawing moment obtained by blowing. The effect of the rudder under sideslip conditions ($\beta = -10°$) is presented in Fig. 11. Trends are similar to the $\beta = 0°$ case in terms of yawing moment increments. The side force curves show positive increments for positive or negative deflections at angles of attack greater than 20°, denoting changes in the position of the center of pressure. At angles of attack above 15°, the positive deflection of the rudder results in a positive yawing moment increment (as desired), but in near-zero or positive side force increment, implying that the center of pressure shifts forward and the contribution of the forebody is increased in a direction opposite to the tail contribution. From the yawing moment data, the rudder is still effective, but the overall flow field changes sufficiently to also produce a positive side force. The reason for this is not clear. The flow visualization experiments in the water tunnel showed that, at angles of attack higher than 25°, the forebody vortices burst close to the vertical tail, so it is possible that interactions between the rudder and the vortex's burst point might influence the flow field in the forebody region. The effect of the rudder deflection on the rolling moment is larger than for the zero sideslip case, and produces a negative rolling moment increment for rudder deflections in either direction. Perhaps the rudder deflection is influencing the flow on the wing near the trailing edge sufficiently to produce negative roll inputs in both cases.

4.1.3 Effect of Blowing (Aft Blowing, Nozzle A)

The first blowing technique evaluated was blowing straight aft, tangentially to the forebody surface, from the forward location (see Fig. 1). Blowing from the left and right sides, and from both sides simultaneously, were investigated extensively. The results for left blowing appear in Fig. 12, and as expected, blowing does not affect the longitudinal characteristics significantly. The only change observed is a small reduction in normal force for the high blowing coefficient cases at angles of attack greater than 22°. Figs. 12c-e reveal the effect of left side blowing on the lateral/directional coefficients. Blowing is not effective at angles of attack below 15°; at $\alpha = 15°$, blowing starts producing a nose-left or negative yawing moment. Confirming the water tunnel test results, the blowing jet appears to be delaying separation on that side of the forebody, inducing a left-vortex-low pattern and the associated negative side force and yawing moment coefficients (with respect to the baseline). Between 15° and 23° angles of attack, the magnitude change in yawing moment increases as the blowing coefficient is increased and the trends appear to be well-behaved. Blowing at the highest $C\mu = 0.0015$ induces a negative change in the yawing moment coefficient of about 0.06 at $\alpha = 20°$, larger than the increment produced by a 30° rudder deflection. The effect of blowing on the rolling moment coefficient appears to be also favorable, in the sense that it reduces the asymmetric rolling moment, especially at the highest blowing coefficient. At this $C\mu$, a positive rolling moment increment is observed between $\alpha = 15°$ and 23°, while a negative increment is observed between 23° and 30° angles of attack. There is obviously some interactions of vortices with either the tail or wing surfaces at angles of attack between 20° and 25°, since the direction of the rolling and yawing moments reverse. The side force and the increments in side force,

yawing moment and rolling moment coefficients with respect to the baseline are plotted in Figs. 12e-h.

Figure 13 shows the effect of blowing on the right side of the forebody, and again, no changes are observed in the longitudinal characteristics. The effects on the lateral/directional characteristics are quite different than for the left side blowing case. Even though a small positive side force is generated at angles of attack higher than 25°, the yawing moment increment generated with respect to the baseline is negative, as in the left side blowing case. This could be due to several reasons, such as, for example, the initial vortex asymmetries and the location of the blowing ports. The initial forebody asymmetry, as denoted by the baseline yawing moment curve, is very strong, and apparently, blowing on this side (which means blowing into the vortex that is already closest to the forebody) and in this angle of attack range cannot enhance that asymmetry much more. The blowing ports are probably located too far forward, and therefore, very close to each other, so the jets are actually influencing the flow characteristics on both sides of the forebody and the net effect of blowing is diminished. The impact of right side blowing on the rolling moment coefficient is minimal.

The changes in the lateral/directional characteristics produced by blowing on both sides simultaneously are shown in Fig. 14. This technique appears to be very efficient for eliminating the initial natural asymmetries. The advantage of this scheme is the fact that significant yawing moment and rolling moment coefficient increments (0.03 and 0.02, respectively) can be obtained when blowing at the minimum blowing coefficient ($C\mu$ = 0.00075). Actually, the yawing and rolling moment coefficients obtained when blowing at the two lowest rates present almost zero values throughout the entire angle of attack range. The mass flow rates corresponding to these blowing coefficients appear to be well within the practical limits of full size blowing requirements, based on studies related to fighter configurations with available engine bleed for the required pressurized air source.

When the vertical tail is removed, blowing strongly influences the vortex flow field and it appears that the trends are better behaved than for the tail on configuration, probably because the interaction between the vortices and the vertical tail is not present. Fig. 15 shows left-hand-side blowing for the no tail configuration. At the minimum blowing coefficient, the initial asymmetries in yawing and rolling moment are totally eliminated. As $C\mu$ is increased, a negative yawing moment is obtained, which increases with both angle of attack and blowing rate. At 30° angle of attack and the maximum blowing rate ($C\mu$ = 0.0015), left side blowing induces a negative change of 0.09 in yawing moment coefficient with respect to the baseline. Unfortunately, similar yawing moment increments are not obtained when blowing on the right side (Fig. 16). In general, left, right and simultaneous blowing produce a negative, positive and almost zero yawing moments, respectively, as seen in Fig. 16b. However, the initial asymmetry presented by this configuration showed a positive yawing moment, therefore, as in the tail on case, the increment produced by right side blowing is minimal. Apparently, blowing on the right side from this port location and at these blowing coefficients is not sufficient to enhance the vortex asymmetry at zero sideslip.

The effect of blowing under sideslip conditions was also investigated. Figure 17 reveals the results for blowing at $\beta = 5°$. Left blowing is destabilizing in yawing moment, as denoted in Fig. 17a, in which a negative yawing moment increment is observed for most of the angle of attack range for a nose-left attitude. Blowing on the right side at the highest blowing coefficient ($C\mu = 0.0015$) induces a positive or stabilizing yawing moment increment between $\alpha = 20°$ and 25°, that tends to bring the nose back to a zero sideslip condition. At $\beta = -5°$ (Fig. 18), blowing on the left side at $C\mu = 0.0015$ also produces a nose-left yawing moment which has an stabilizing effect, and blowing on the right side is not effective (Fig. 18d-f). Not much change in the rolling moment coefficient is observed. Depicted in Fig. 19 are results for $\beta = -10°$. Blowing on the left side at the maximum $C\mu$ tends to reduce the initial asymmetry up to 25° angles of attack, as shown in Fig. 19a. The trends are not well behaved, probably because there are strong interactions between the forebody vortices and the vertical tail. Blowing on the right side (Fig. 19e) enhances the asymmetry and produces a constant positive increment in yawing moment (destabilizing) of about 0.02 from $\alpha = 20°$ to 30°.

4.1.4 Effect of Blowing (Aft Blowing, Nozzles B30IN and B30OUT)

It was reported in Ref. 7 that by rotating the nozzles inboard 60°, the magnitude of the yawing moment increment obtained by blowing was increased significantly. In an effort to investigate the sensitivity of blowing to a change in the nozzle angle, the ports were turned inboard 30°. This experiment illustrated how sensitive this configuration is to changes in geometry. Just by changing the orientation of the nozzles, the baseline flow is modified substantially, as denoted by the yawing and rolling moment curves in Figs. 20a and 20b. Not only the magnitude of the initial asymmetries is modified, but their sign (i.e., the vortex orientation) is totally changed with respect to the previous baseline (A) as well. Later in the test, when the nozzle angle was changed to 45° inboard, the non-blowing flow characteristics were influenced in such a way that the dynamics of the model/sting system were totally modified. The model vibrated so violently with this nozzle configuration that data could not be recorded at this condition.

Since the initial asymmetry for this configuration presents a left-vortex-low pattern, as indicated by the negative values of the yawing moment curve, blowing on the left side is not very effective. A negative yawing moment increment of about 0.02 is obtained for angles of attack between 20° and 30°. Blowing on the right side produces a very large positive change in side force up to $\alpha = 27°$. That positive change in side force induces a positive change in yawing moment, however, the trends are very unpredictable, as seen in Fig. 20e. At $\alpha = 20°$, the largest change in yawing moment is produced when blowing at the lowest rate ($C\mu = 0.00075$). At $\alpha = 25°$, the increments are minimum, and at 30° angle of attack, a change in yawing moment of approximately 0.08 is obtained when blowing with the highest $C\mu = 0.0015$. This increment is much larger than any change induced by the previous blowing configuration, denoting the influence of blowing direction. A positive rolling moment increment is observed for the

right blowing case between $\alpha = 22°$ and 30°. It is evident that the orientation of the nozzles is an extremely important parameter in the blowing process.

The blowing nozzles were turned outboard 30° and the results are presented in Fig. 21. The non-blowing flow field characteristics are again different than for previous configurations. The blowing ports are apparently acting as small strakes, reducing the initial asymmetries, especially in the yawing moment coefficient shown in Fig. 21a. The coefficient has an almost zero value for most of the angle of attack range. This blowing scheme did not prove very efficient. Ref. 7 reported that outboard blowing creates a force away from the blowing side. Some evidence of that trend is observed in these data for some blowing coefficients and angles of attack, but in general, this form of blowing does not appear to provide an advantage over the previous blowing schemes investigated.

4.1.5 Effect of Blowing (Forward Blowing, Nozzles C and D)

Forward blowing was also evaluated as a possible means of lateral/directional control. The results of forward blowing from the aft location are presented in Fig. 22. Left blowing induces a negative yawing moment, and it seems to be more efficient than right blowing. Both of them produce similar negative yawing moment changes at $C\mu = 0.0015$, but left blowing is more efficient at the lowest blowing coefficients. Neither left nor right blowing from this location is sufficient to enhance the vortex asymmetry and produce a positive change in yawing moment. It is difficult to speculate on the mechanism of this blowing technique, but it appears that both jets are influencing more the right side of the forebody, promoting an earlier separation on that side and forcing the initial right-vortex-low pattern to be symmetric. The results from blowing on both sides simultaneously seem to be independent of mass flow rate, and the net effect is to produce an almost zero yawing and rolling moments (Fig. 22g and 22h). Trends at $\beta = -10°$ are shown in Fig. 23, and as expected from results at $\beta = 0°$, left blowing is more effective than right blowing. In general, blowing from one side of the forebody loses effectiveness when the aircraft is yawed too much towards the side of the blowing port. Blowing on the left side can reverse the right-vortex-low asymmetry, and blowing on the right side enhances the asymmetry but only for angles of attack between 25° and 30° and at the lower blowing rates (Figs. 23d and 23e).

The results for forward blowing from the forward location agree with the water tunnel test (Volume I of this Final Report), and with the results presented in Ref. 2 for a generic fighter configuration. At high angles of attack, and at low blowing coefficients, forward blowing produces the opposite effect when compared to aft blowing, i.e., blowing on the left side at $C\mu = 0.00075$ produces a positive (nose-right) change in yawing moments for angles of attack greater than 25° (Fig. 24a). As the blowing coefficient is increased, this trend is reversed and a negative increment is produced. Between 15° and 25° angles of attack, however, the effect of left and right blowing on the yawing moment is the same, and in both cases, the asymmetry is completely eliminated at the highest blowing coefficient. For angles of attack greater than 25°, blowing at $C\mu = 0.0015$ on the left side (Fig. 24a) and on the right side (Fig. 24d), induces negative and positive increments in yawing moment, respectively. The effect of forward blowing at the highest $C\mu$ on side force and rolling moment coefficients is

similar for left or right blowing, probably because with the blowing nozzles so far forward and therefore, very close to each other, the forward jet acts like a vortex spoiler and affects both left and right vortices almost equally. The jets are apparently too far forward to be useful.

4.1.6 Effect of Blowing (Combined Blowing, Nozzles E1 and E2)

This technique combines aft blowing on one side (left) and forward blowing on the other side (right) applied simultaneously. The concept behind this blowing method is to delay separation on the left side (by means of aft blowing), and to promote early separation on the opposite side (by means of forward blowing). Results are revealed in Fig. 25, and a negative increment in the lateral/directional coefficients is produced. These changes appear to be better behaved than in all the other techniques tested before. An increase in blowing coefficient causes an almost proportional increase in the increments produced, and at $C\mu = 0.0015$, the initial asymmetries are completely eliminated. Limitations in the testing time did not allow for evaluation of the other combination, i.e., aft blowing on the right side and forward blowing on the left side.

A quick test on blowing aft and forward on the same side simultaneously (see Fig. 3) was also performed but only for the two lower blowing coefficients (Fig. 26). Negative increments are obtained when blowing at these two rates, except near $\alpha = 25°$. It can be speculated that for blowing to be effective over the entire angle of attack range, a combination technique that uses two jets to reinforce the effects of blowing might be the best solution for obtaining maximum yawing moment inputs.

4.2 Pressure Measurements

Static pressures were measured on the forebody at three different stations using a PSI electronic scanner. The pressure distributions are presented at selected angles of attack, both for the non-blowing baselines and for all the blowing techniques investigated, and they are plotted against azimuth angles. Ports with azimuth angles Φ between 1° and 179° are on the right side of the forebody; the left side contains ports with Φ between 181° and 359° ($\Phi = 0° = 360°$ is the windward meridian).

4.2.1 Baseline Configuration

The pressure distributions at the three forebody stations for the non-blowing case of the configuration with nozzle A (blowing straight aft) are presented in Fig. 27. The pressures show a symmetric vortex flow field for the $\alpha = 15°$ case, and a asymmetric pattern is evident starting at 20° angle of attack, as denoted by the lower pressures on the right side of the forebody. This indicates a higher suction on the right side, and a right-vortex-low pattern, confirming the force and moment measurements, where the yawing moment curve presented a large positive value for angles of attack greater than 15° (see Fig. 4c).

The pressure distributions for the same baseline at different sideslip conditions are shown in Figs. 28, 29 and 30 for the $\beta = 5°$, -5° and -10° cases, respectively. The

β = 5° and -5° cases present mirror images only for the ports located on the windward side. The pressures at the ports located between Φ = 72° and 288° reveal different aspects of the flow, such as vortex position, separation, etc., and because of the natural asymmetries in the flow at zero sideslip, very different pressure distributions can be expected in that forebody region for the β = 5° and -5° cases. The pressures show an almost symmetric vortex pattern for the β = 5° case up to 25° angles of attack. At α = 30°, the asymmetric vortex pattern switches sign (left-vortex-low). At -5° sideslip, the asymmetry indicated by the pressures is similar to the baseline case, with a right-vortex-low pattern. This asymmetric pattern, however, is not enhanced for the β = -10° case, as seen in Fig. 30. The asymmetry is apparently reduced, and the vortices appear to be interacting with the opposite forebody sides, as denoted by the pressure distribution at station 3, where a much lower pressure is observed on the left side of the forebody, contradicting the distributions observed in stations 1 and 2 for the same condition.

The forebody pressure distribution for the tail off case, shown in Fig. 31, reveals similar characteristics as the tail on case up to 25° angles of attack. At α = 30°, the distribution at station 2 is slightly different, and the asymmetric pattern observed is not as dramatic as for the tail on configuration. The interactions between the forebody vortices and the vertical tail apparently do not influence the forebody vortex flow field at angles of attack lower than 30°.

4.2.2 Effect of Blowing (Aft Blowing, Nozzle A)

The effect of blowing at α = 15° and 20° are shown in Figs. 32 and 33, respectively, and no major changes are observed. The three blowing schemes (left, right, both) produce a slight increase in pressure at α = 15°. At α = 20°, an indication of the effect of blowing is noticed, as the initial asymmetry observed in stations 2 and 3 is eliminated completely. At α = 25° and 30° (Figs. 34 and 35), the pressure distributions confirm the force and moment measurements. Starting with the initial right-vortex-low asymmetry, left blowing makes the pressure distribution symmetric when blowing at the highest $C\mu$ = 0.0015, as evident in stations 2 and 3 in Figs. 34a and 35a. Not much effect is observed for right blowing, as indicted in Figs. 34b and 35b for α = 25° and 30°, respectively. Simultaneous blowing (Fig. 35c) reduces the large initial asymmetry at 30° angle of attack at the lowest blowing coefficient ($C\mu$ = 0.00075). A combination of the effects of left and right blowing appears to be beneficial in this case.

The hysteresis in the blowing process was also investigated, and it is illustrated in Fig. 36 at α = 30°. Blowing was applied on the left side and the mass flow was increased to the maximum rate. The results in Fig. 36a (increasing rate portion) agree with the pressure distributions depicted in Fig. 35a, showing good repeatability between similar type runs (in both runs, the mass flow of the blowing jet was increased from zero to the maximum rate). The mass flow rates were then decreased until zero blowing, and the pressures show some hysteresis (Fig. 36b). Changes in pressure on the leeward side of the forebody are not as evident as in the previous figure (36a), and

the non-blowing case (baseline A) presents a slightly different vortex pattern. The asymmetry still has the same orientation, but the magnitude is decreased.

Figures 37 and 38 show the effects of blowing at 25° and 30° angles of attack, respectively, for the tail off configuration. As shown by the force measurements, left blowing produces a large change in side force and yawing moment at $\alpha = 30°$. Figure 38 appears to confirm those results; left blowing at $C\mu = 0.00125$ produces a large change in the pressure distribution, reversing completely the initial asymmetry, as observed in stations 2 and 3.

4.2.3 Effect of Blowing (Aft Blowing, Nozzles B30IN and B30OUT)

The effect of changing the orientation of the nozzles in the vortex flow field is clearly shown also by the forebody pressure distribution. By turning the nozzles inboard 30°, the baseline characteristics are changed completely with respect to the previous case (nozzle configuration A), and a left-vortex-low asymmetry is observed at 30° angle of attack. Left-hand-side blowing produces small changes at $\alpha = 25°$, as shown in Fig. 39a. The large positive changes in side force produced by right blowing are reflected in the pressure changes in stations 2 and 3 shown in Fig. 39b. At 30° angle of attack, the asymmetry is slightly enhanced when blowing on the left side, and totally reversed when blowing on the right side (Fig. 40b). Large changes in pressures are observed in all the stations, but especially in stations 2 and 3. The pressures decrease on the right side and increase significantly on the left side; higher suction is created on the right side and a large positive yawing moment is induced.

When the nozzles are turned outboard 30°, it was speculated that these blowing ports physically act as small strakes, eliminating the large forebody vortex asymmetries. Figs. 41 and 42 show pressure distributions for this configuration at $\alpha = 25°$ and 30°, respectively, and an almost symmetric pattern is observed for the baseline at both angles of attack. However, the effects of blowing are not as dramatic as the changes in the baseline flow, as the force and moment measurements had shown in section 4.1.4. At $\alpha = 25°$, the effect of blowing is minimum. At $\alpha = 30°$, right and left blowing create opposite asymmetries. Left blowing produces a left-vortex-low asymmetry, as shown in Fig. 42a, while right blowing induces a right-vortex-low asymmetry (Fig. 42b).

4.2.4 Effect of Blowing (Forward Blowing, Nozzles C and D)

The local effect of the blowing jet in some forebody areas is evident in Fig. 43, which shows pressure distributions for forward blowing with nozzle C at $\alpha = 25°$. The majority of the changes are seen in station 1, which is in front of the blowing ports. Left blowing (Fig. 43a) clearly affects the left leeward side of the forebody, while right blowing does the opposite (Fig. 43b). Apparently, the blowing jet is promoting an early separation on the blowing side; however, this behavior is not being reflected on side force or yawing moment changes, probably because this is only a local effect produced by the jets in a small forebody region. Behind the ports (stations 2 and 3), small changes are produced by left blowing that tend to decrease the initial

asymmetry, while right blowing does not show any major effect on the pressures. At $\alpha = 30°$ (Fig. 44), similar trends are observed.

Figures 45 and 46 show forward blowing from the forward location at $\alpha = 25°$ and 30°. No major effects on the pressure are noticed at $\alpha = 25°$. The results at $\alpha = 30°$ reveal again the disadvantage of this method, i.e., changes are not well-behaved and control reversals with blowing rate are observed. This is clearly illustrated in Fig. 46b, especially in station 2. Starting with the non-blowing case, that presents a slight right-vortex-low asymmetry, forward blowing (right side) at the lowest $C\mu = 0.00075$, completely reverses the asymmetry, inducing a negative yawing moment, as seen previously in the force measurements. On the other hand, by blowing at the highest $C\mu = 0.0015$ on the same forebody side, the asymmetry is reinforced, and a positive yawing moment increment is obtained.

4.2.5 Effect of Blowing (Combined Blowing, Nozzles E1 and E2)

Combined blowing with nozzle E1 at 25° and 30° angle of attack is shown in Figs. 47 and 48. As in the case of the C nozzle, the local effect of the blowing jet is evident on the right side of station 1. This effect is more noticeable at $\alpha = 30°$, where the blowing jet appears to be lifting the right vortex off the surface, therefore increasing the pressure on that side of the forebody. Changes in pressure are also observed in stations 2 and 3 (Fig. 48), with the aft blowing jet apparently influencing the left vortex, pulling it closer to the surface and inducing a negative yawing moment increment. The changes produced by this blowing scheme seem to be gradual and well-behaved.

Figs. 49 and 50 present results for combined blowing with nozzle E2 (simultaneous aft and forward blowing on the left side) at $\alpha = 25°$ and 30°. Only two blowing rates are presented, but at $\alpha = 30°$, the effects are noticeable in station 2, where changes in pressure on both sides of the forebody occur for the $C\mu = 0.001$ case, again inducing a negative side force increment.

4.3 Time Lag Measurements

In an effort to quantify the dynamic response of the control forces to a blowing input, the model was provided with fast time response pressure transducers (Endevco). These transducers are located on both sides of the forebody and on the wings at selected stations (see Figs. 1 and 2).

Fig. 51 shows the effect of aft blowing at $\alpha = 25°$ on the pressures measured (in raw counts) at two forebody positions (Endevcos 1 and 2), and on two wing positions (Endevcos 9 and 10). The response is almost instantaneous; a lag of about 0.005 seconds (between the start of the blowing pressure rise to the first noticeable change in forebody pressure) is observed in the forebody, so it can be speculated that the yawing moment changes will be almost instantaneous. The Endevcos on the wing show a longer time lag, but that is likely due to the fact that these transducers are farther downstream. At this free stream speed, it takes about 0.018 seconds for the flow

to reach that Endevco location on the wing. Figure 51b shows that the changes in pressure are observed about 0.020 seconds after the blowing pressure starts building up, and the maximum pressure changes occur about 0.020 seconds after the set blowing pressure is reached. The response of the rolling moment gage (in raw counts) is also plotted in this figure, and it shows a very fast response (about 0.010 seconds after the left and right pressures start changing).

Fig. 52 shows similar data at $\alpha = 30°$, and the pressures on the forebody start changing almost immediately after blowing is turned on. Depicted in Fig 52b is the response of the side force gage (in raw counts), and again, a very fast response is observed. It appears that the mean value of the side force change is obtained approximately 0.015 to 0.020 seconds after the blowing pressure reaches its maximum value. This time response is consistent with data presented in Ref. 7. The transducers located on the wing, in this case presented at two different stations, show similar behaviors. The Endevcos located at the aft wing station appear to respond 0.005 seconds later than the ones at the forward station (Figs. 52c and 52d), but again, that is likely due to the time it takes the free stream flow to reach the second station. When blowing on the right side (Fig. 53), it is seen that the changes in the forebody pressures near the blowing ports are very rapid, as denoted by the instantaneous pressure change measured by Endevco 2. Force and moment measurements showed that this blowing scheme did not produce any changes in yawing or rolling moments, and that is confirmed by the outputs of Endevco 9 and 10, where no changes in pressure are noticeable in Fig 53b. The simultaneous blowing technique (Fig. 54) shows a very fast response also. Similar behavior is observed at $\beta = -10°$ in the forebody transducers for left blowing (Fig. 55a) and right blowing (Fig. 55b).

Finally, Fig. 56 shows results for forward blowing (Nozzle C). The first two graphs illustrate the response of a transducer that is located in front of the blowing nozzle, clearly showing the unsteadiness of the signal when blowing is on. The transducers located on the forebody behind the blowing ports (Figs. 56c and 56d) and on the wings (Figs. 56e and 56f) present similar time responses as the observed for the other blowing scheme, i.e., aft blowing.

According to the results obtained in this part of the experiment, it can be speculated that the response of the control forces created by blowing is almost instantaneous. The time for the configuration flow field to react to a blowing input at the front of the forebody is approximately the time required for the disturbance to travel the length of the model. No major time lags or overshoots were observed for any of the blowing techniques investigated.

5.0 CONCLUSIONS

A detailed investigation of the effect of various jet blowing schemes on a NASP-type configuration was performed in a wind tunnel. The main conclusions of this study can be summarized as follows:

1. The configuration investigated, having a slender forebody, is extremely sensitive to small changes in forebody geometry and to disturbances in the flow field.

The sole presence of the small blowing ports near the tip of the forebody can cause strong asymmetries at angles of attack higher than 15°.

2. Blowing straight aft is capable of producing significant changes in the lateral/directional characteristics for angles of attack greater than 15°. These changes are strongly dependent on the initial flow field asymmetries. Left side blowing at $C\mu = 0.0015$ produces a negative change in yawing moment, with a magnitude comparable to a rudder deflection of 30°. The blowing jet is delaying separation on the left side of the forebody, creating a higher suction on that side and a negative side force. Right side blowing, however, does not produce a similar increment in yawing moment and side force, probably because the large initial vortex asymmetry (right-vortex-low) cannot be enhanced much more at these blowing coefficient and angle of attack ranges. Simultaneous blowing eliminates the vortex asymmetry at the lowest $C\mu = 0.00075$.

3. In addition to angle of attack and blowing rate, aft blowing appears to be very sensitive to changes in nozzle direction. By turning the nozzles inboard 30°, the yawing moment increments produced by blowing are magnified at some angles of attack. The behavior of this blowing technique is still very dependent on blowing side.

4. Forward blowing can also affect the lateral/directional characteristics of this configuration but, in general, the results present unpredictable and non-linear trends, with large control reversals in the angle of attack range investigated. This confirms the results obtained in the water tunnel investigation.

5. Combined blowing, i.e., blowing aft on one side and forward on the other, reveal interesting results, with significant changes in side force, yawing moment and rolling moment coefficients. These increments are gradual and well-behaved for this combination (aft blowing on the left side and forward blowing on the right side), but time limitations did not allow for testing the other combination.

6. The forebody pressure distributions present excellent agreement with the force and moment measurements. These pressures also show interesting aspects of the flow, such as forebody vortex position, local effects of the blowing jets, etc.

7. The dynamic response of the forces and pressures to the blowing inputs was also evaluated. Neither of the blowing techniques investigated presents major time lags or overshoots. The response of the pressures on the forebody is almost instantaneous, while the wing transducers show a lag that correspond to the convective time, i.e., the time it takes the free stream flow to reach those wing stations.

In general, it was shown that blowing can be used to generate additional control forces and moments that would improve the handling qualities of a NASP-type configuration. The results, however, also show that an extensive and thorough optimization of some of the blowing parameters (especially port location and direction) is still necessary to take this control technique to a flight test program. This investigation definitely showed that, first of all, the blowing rates necessary to obtain additional forces and moments to enhance controllability are well within the practical limits of full size mass flow requirements. Secondly, the increments in forces and

moments are comparable, and sometimes larger, than a full rudder deflection. Even though the rudder of this configuration is still effective at 30° angle of attack, blowing offers the possibility of decreasing the size of the vertical tail, therefore reducing weight and drag and improving high speed performance.

6.0 ACKNOWLEDGMENTS

Support for this work is provided by NASA Ames Research Center under contract NAS2-13196. The technical monitor is Mr. Larry Meyn of the Fixed-Wing Aerodynamics Branch. We would also like to acknowledge the efforts of Mr. Bert Ayers for his high quality work in constructing the wind tunnel model.

7.0 REFERENCES

1. Murri, D.G. and Rao, D.M., "Exploratory Studies of Actuated Forebody Strakes for Yaw Control at High Angles of Attack," AIAA-87-2557-CP, August 1987.

2. Malcolm, G.N., Ng, T.T., Lewis, L.C., and Murri, D.G., "Development of Non-Conventional Control Methods for High Angle of Attack Flight Using Vortex Manipulation," AIAA-89-2192, July 31-August 1-2, 1989.

3. Zilliac, G., Degani, D., and M. Tobak, "Asymmetric Vortices on a Slender Body of Revolution," AIAA-90-0388, January 1990.

4. Moskovitz, C., Hall, R., and DeJarnette, F., "Experimental Investigation of a New Device to Control the Asymmetric Flowfield on Forebodies at Large Angles of Attack," AIAA-90-0068, January 1990.

5. Ng, T. T. and Malcolm, G. N., "Aerodynamic Control Using Forebody Strakes," AIAA-91-0618, Jananuary 1991.

6. Suárez, C. J., Malcolm, G. N., Ng, T. T., "Forebody Vortex Control with Miniature, Rotatable Nose-boom Strakes", AIAA-92-0022, January 1992.

7. Guyton, R. W., Maerki, G., "X-29 Forebody Jet Blowing", AIAA-92-0017, January 1992.

8. LeMay, S. P., Sewall, W. G., Henderson, J. F., "Forebody Vortex Flow Control on the F-16C Using Tangential Slot and Jet Nozzle Blowing", AIAA-92-0019, January 1992.

9. Tavella, D.A., Schiff, L.B., and Cummings, R.M., "Pneumatic Vortical Flow Control at High Angles of Attack," AIM-90-0098, January 1990.

10. Rosen, B. and Davis, W., "Numerical Study of Asymmetric Air Injection to Control High Angle-of-Attack Forebody Vortices on the X-29 Aircraft," AIAA-90-3004, August 1990.

11. Ng, T. T. and Malcolm, G. N., "Aerodynamic Control Using Forebody Blowing and Suction," AIAA-91-0619, January 1991.

12. Ng, T. T., Suárez, C. J., Malcolm, G.N., "Forebody Vortex Control Using Slot Blowing," AIAA-91-3254, September 1991.

13. Ng, T. T., "Aerodynamic Control of NASP-type Vehicles Through Vortex Manipulation", Eidetics International TR89-009, 1989.

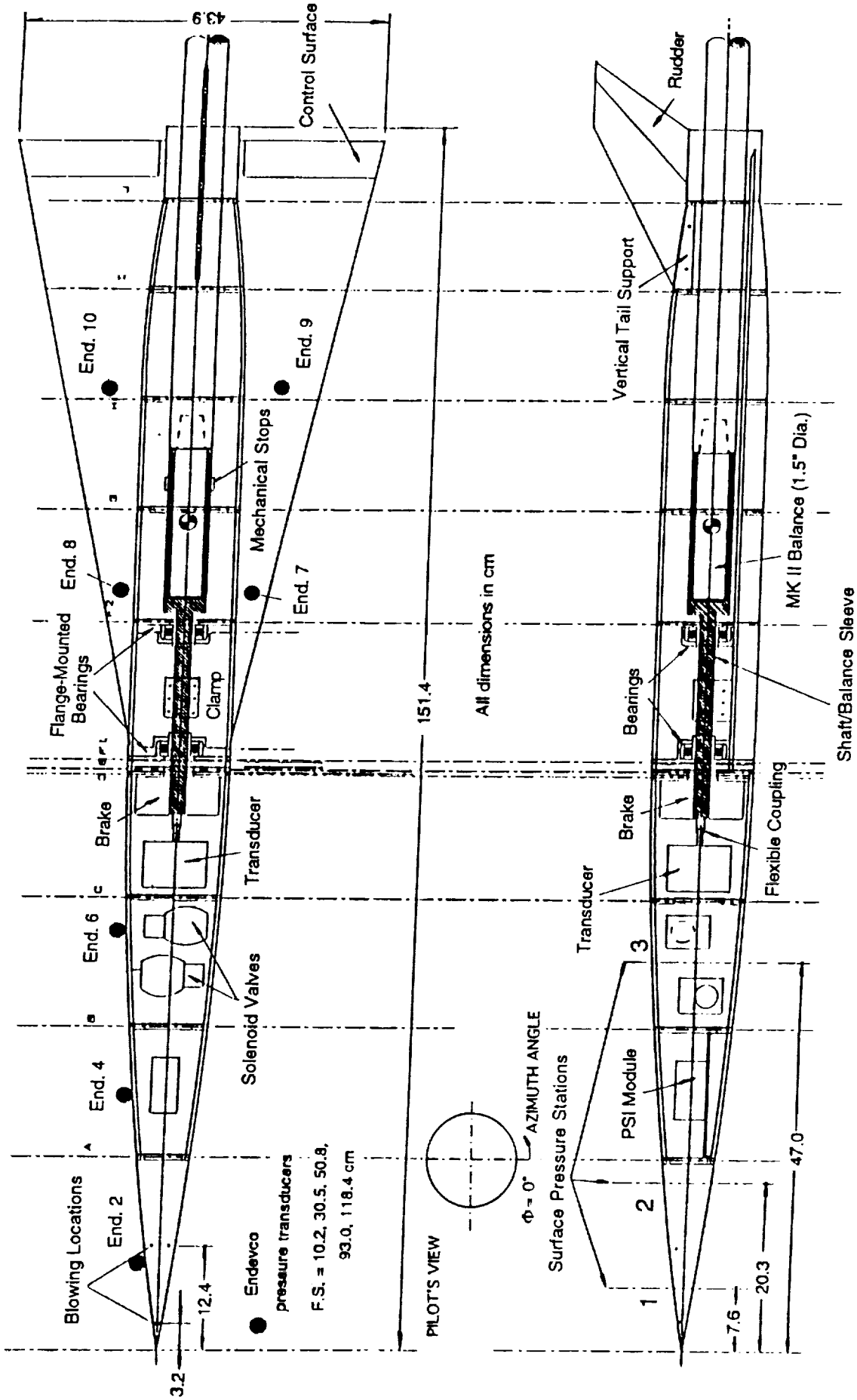

Figure 1 - Schematics of Wind Tunnel Model

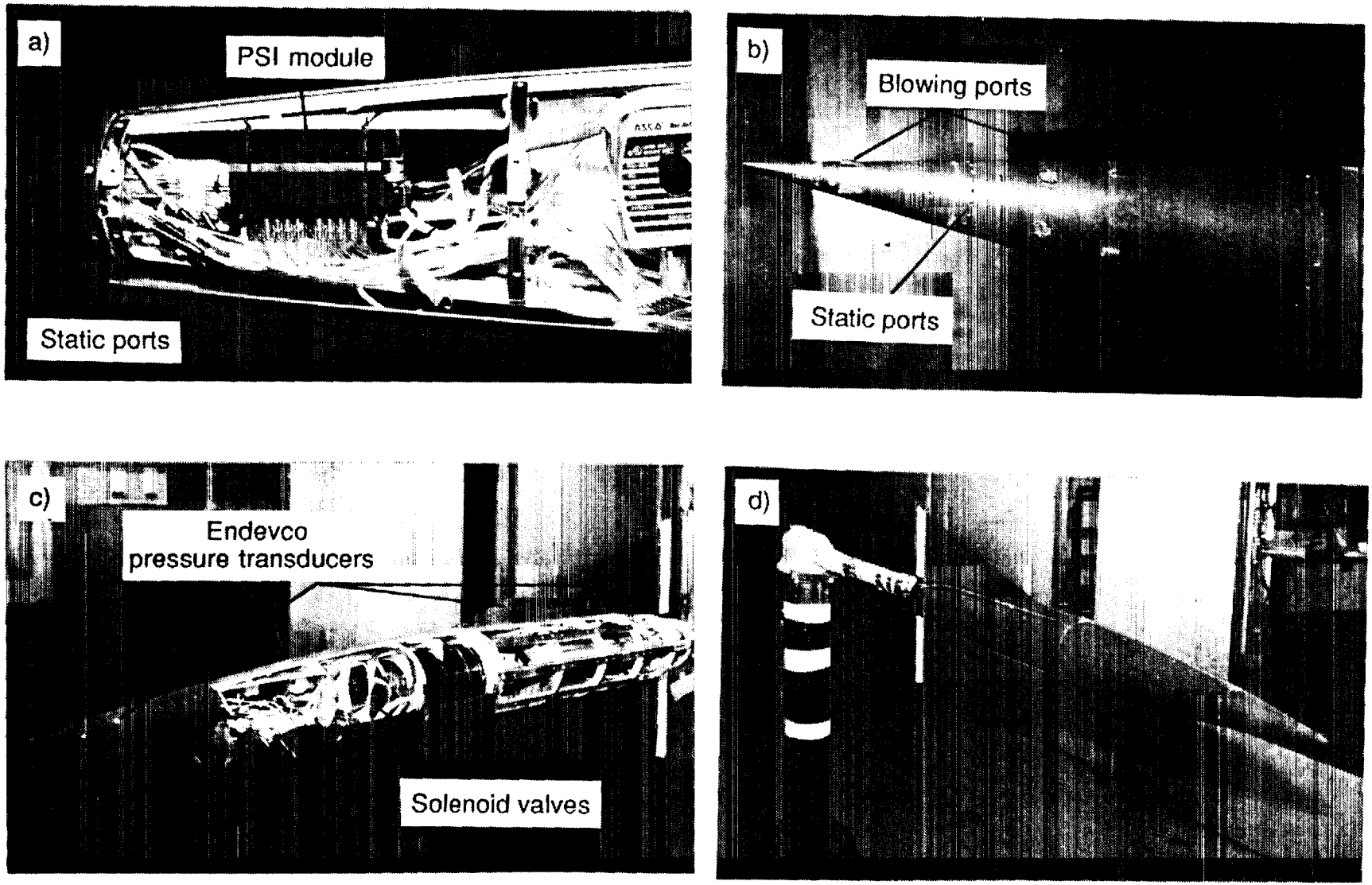

Figure 2 - Photos of Wind Tunnel Model

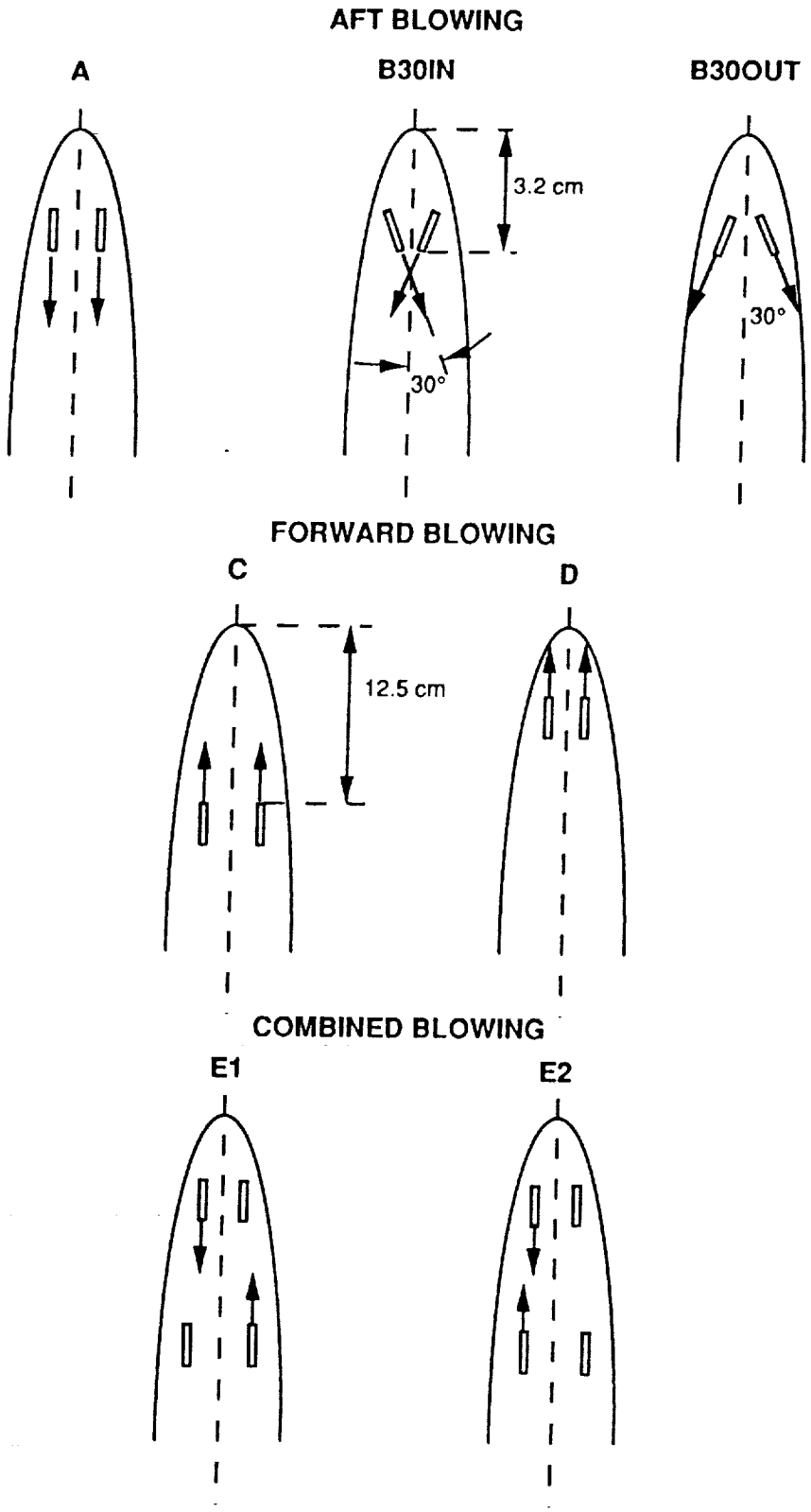

Figure 3 - Schematics of Different Blowing Schemes

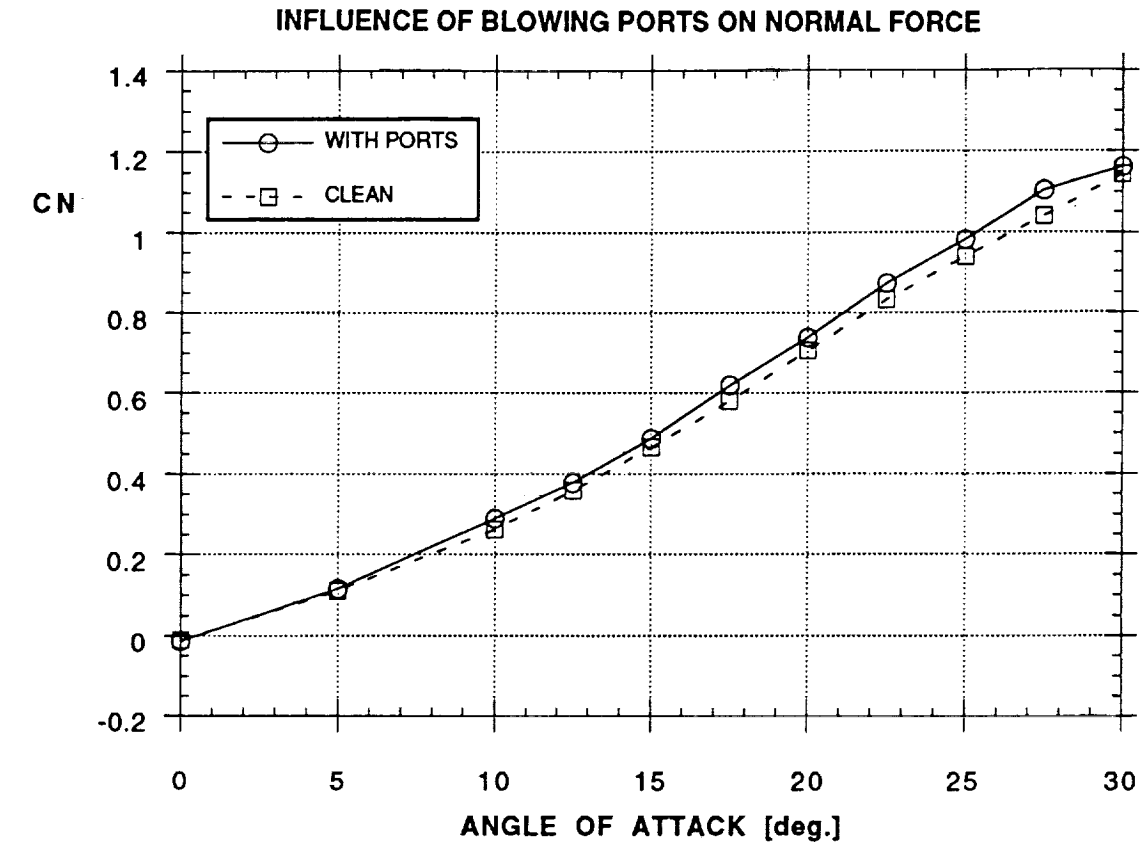

a)

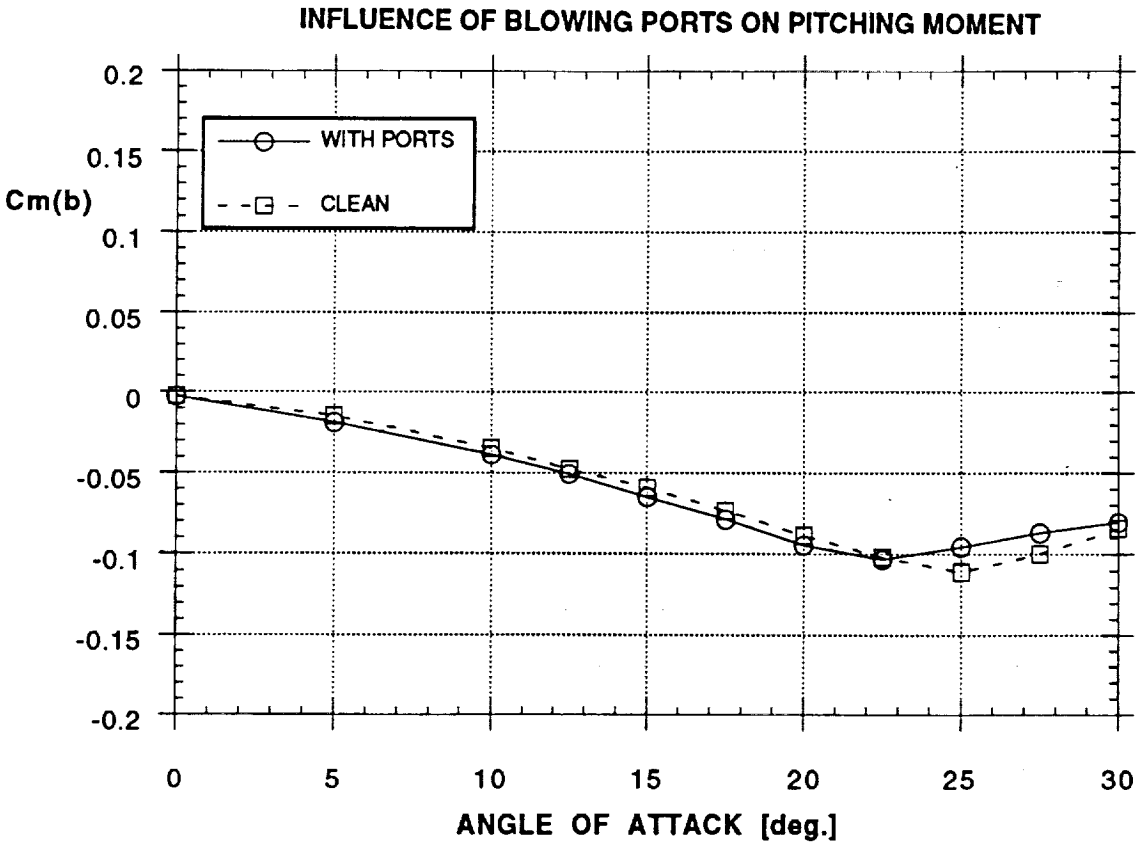

b)

Figure 4 - Influence of Blowing Ports on Forces and Moments (No Ports vs. Baseline A)

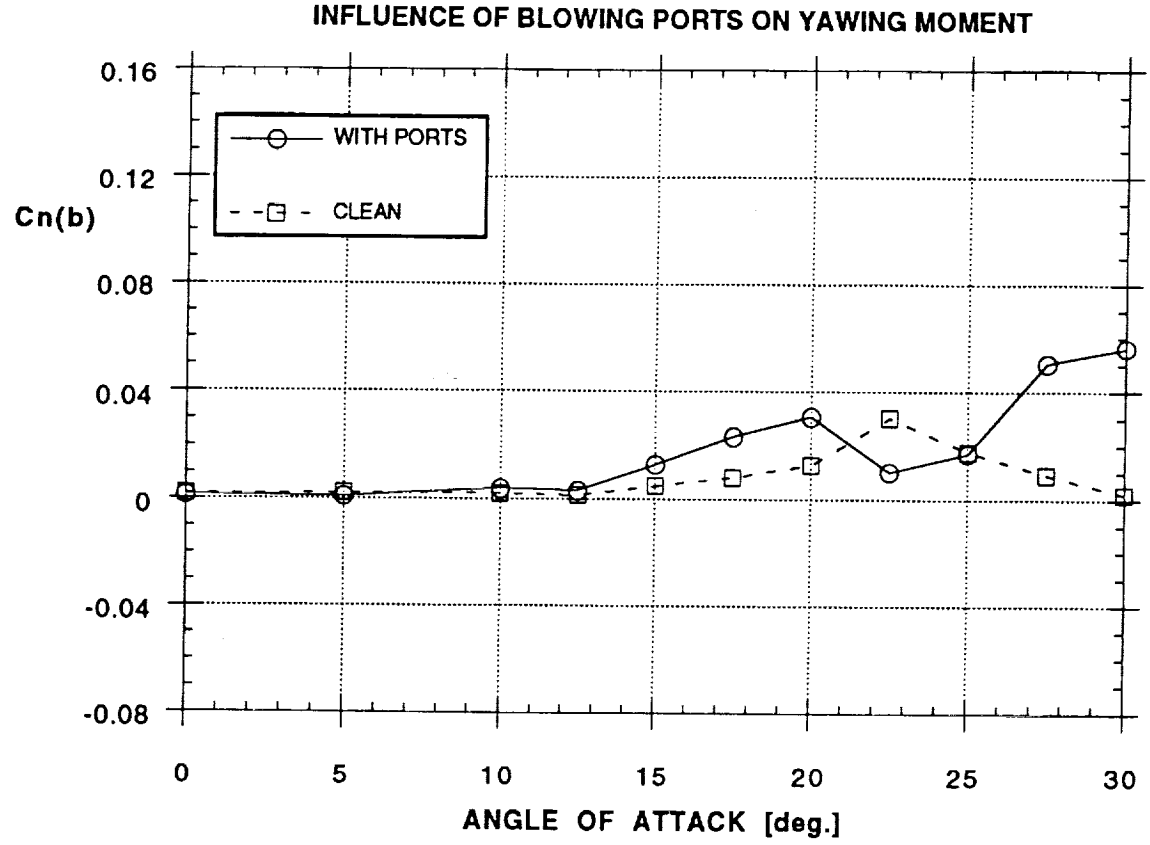

c)

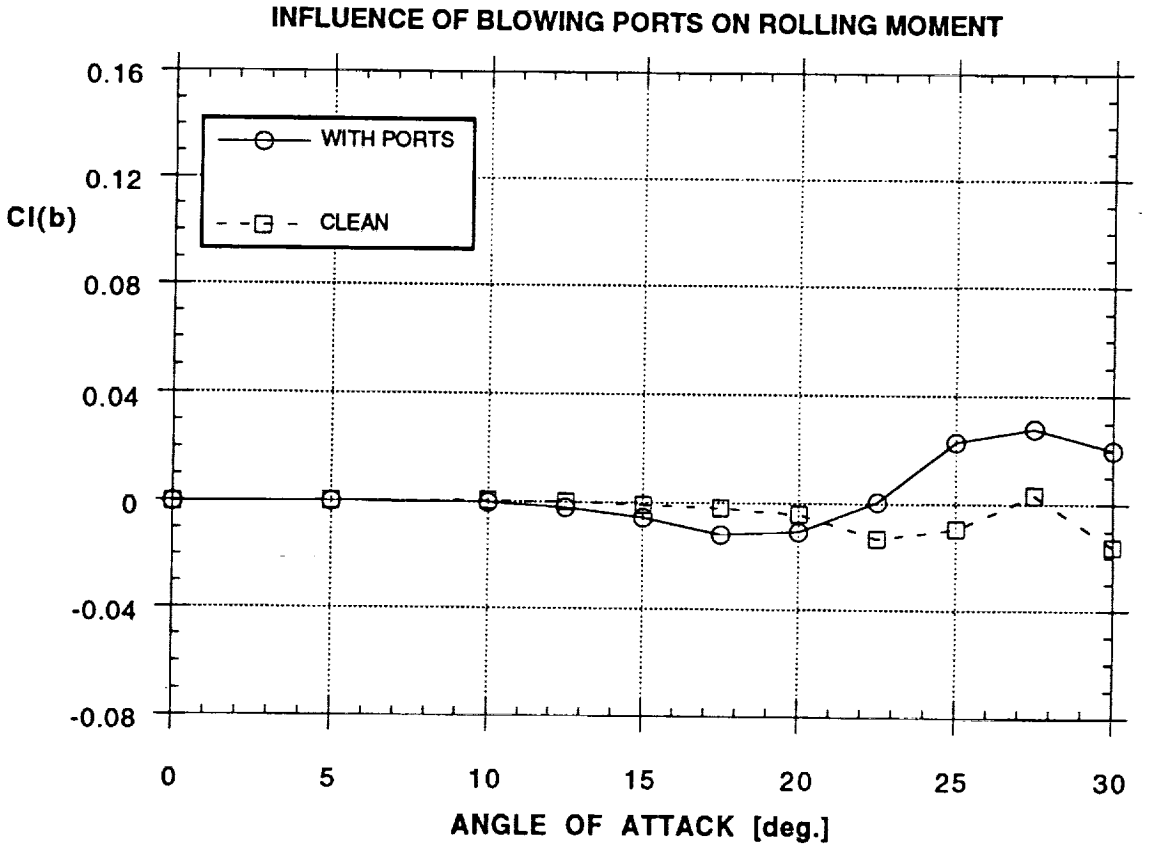

d)

Figure 4 - Continued

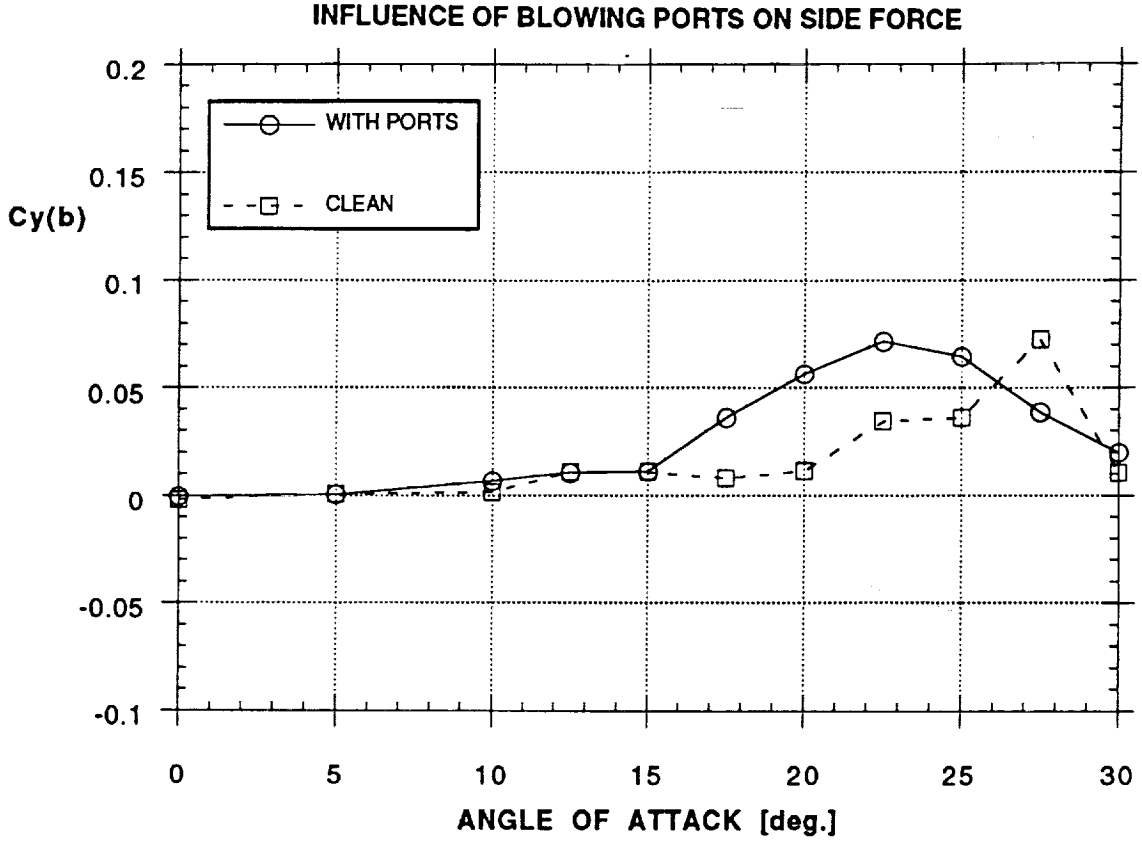

e)

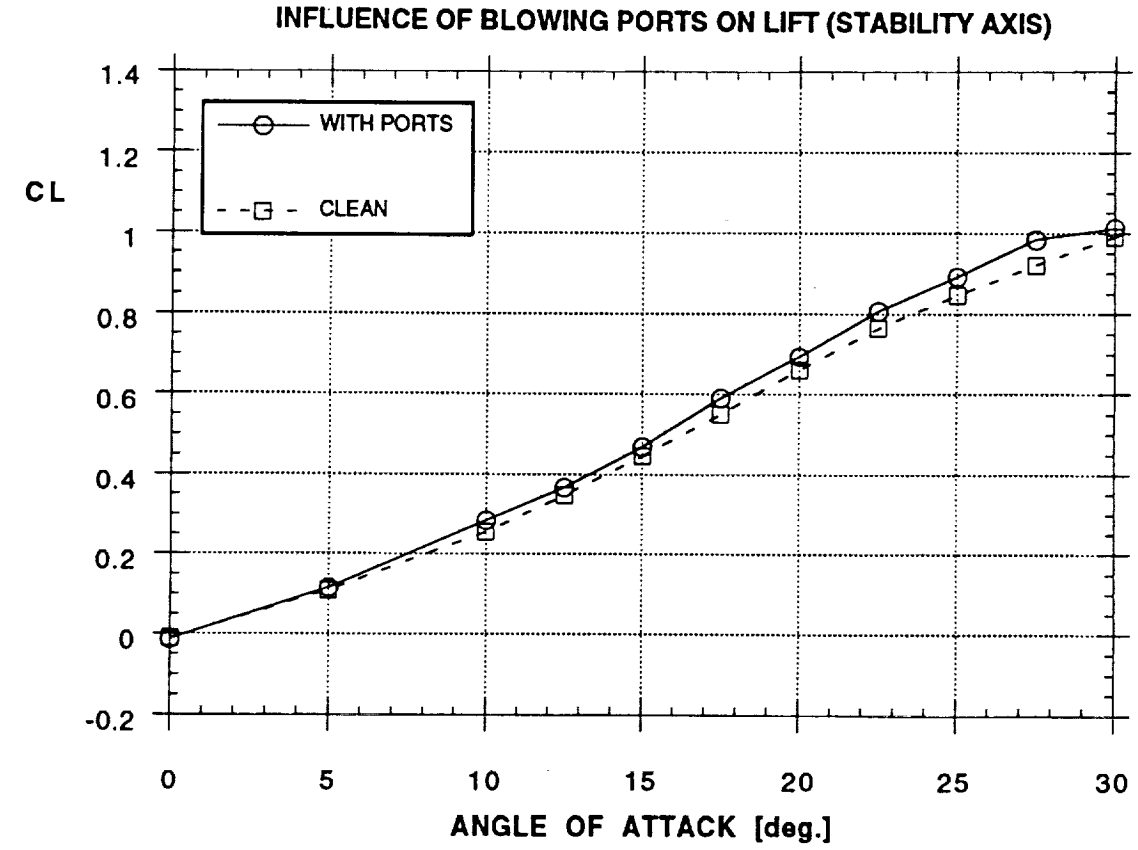

f)

Figure 4 - Concluded

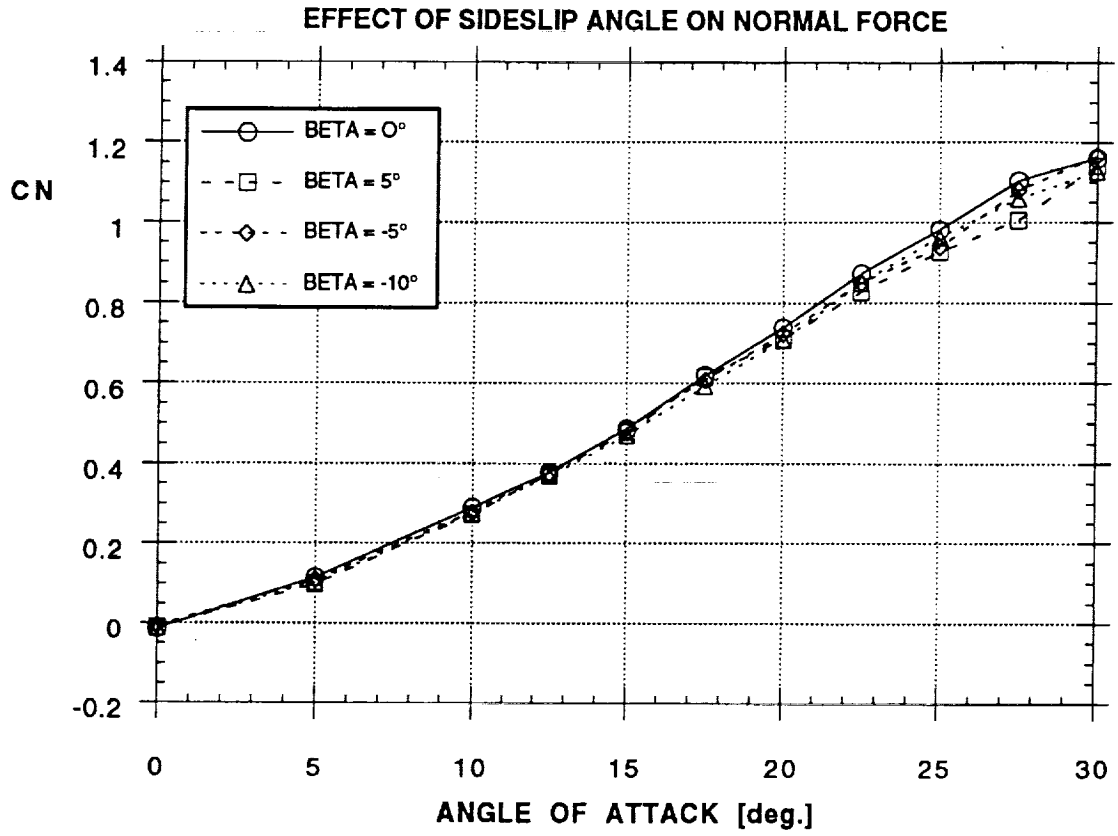

a)

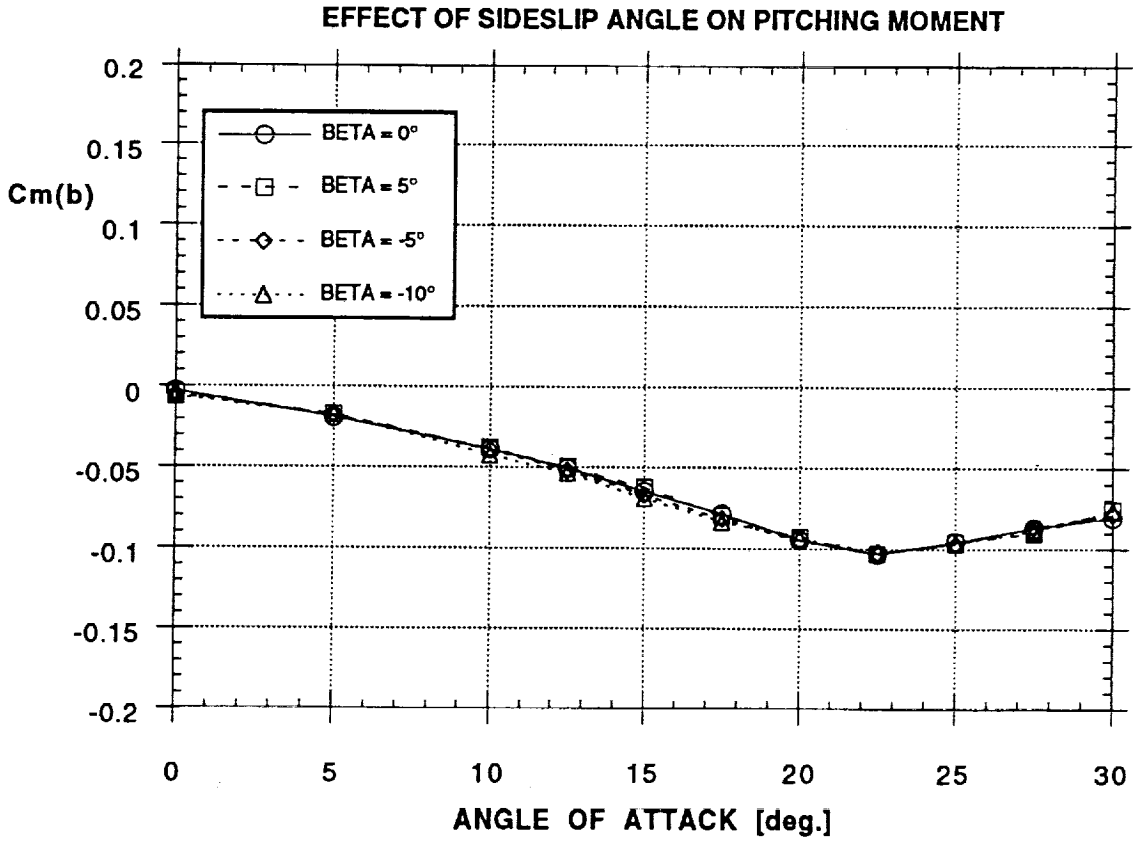

b)

Figure 5 - Effect of Sideslip Angle on Forces and Moments (Baseline A)

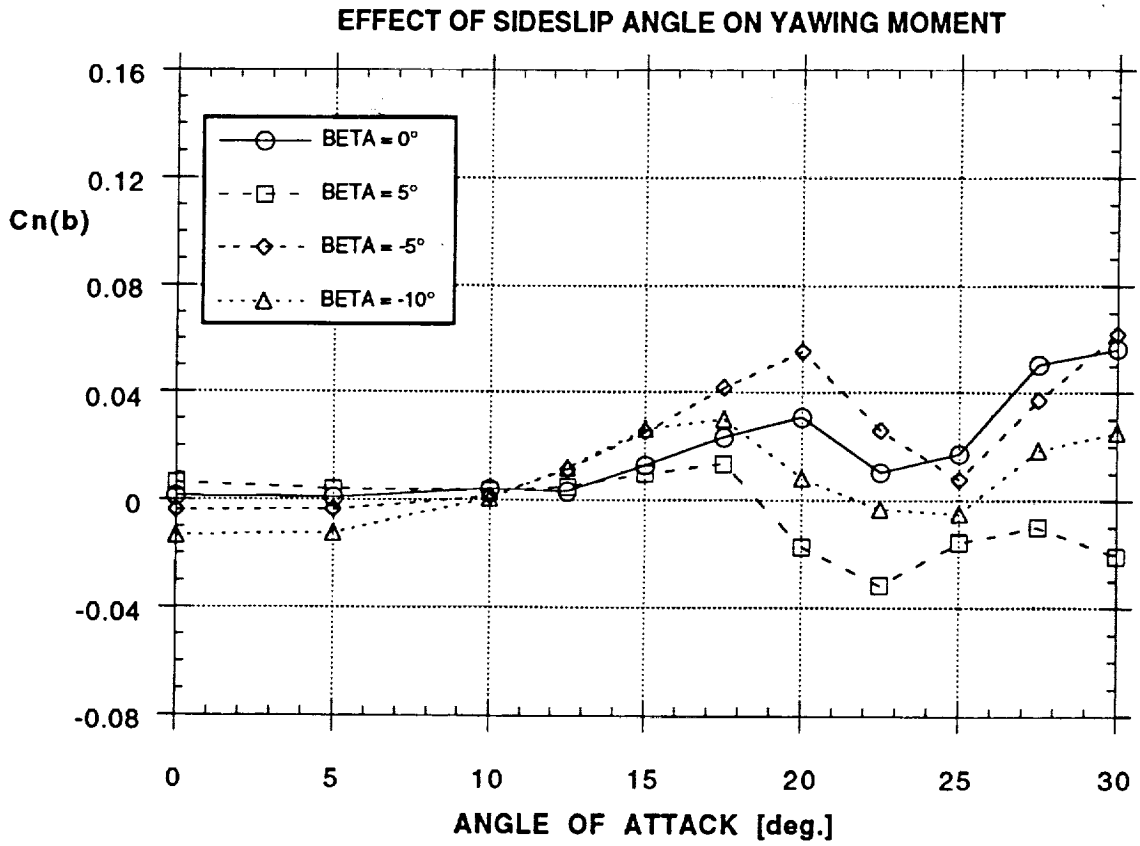

c)

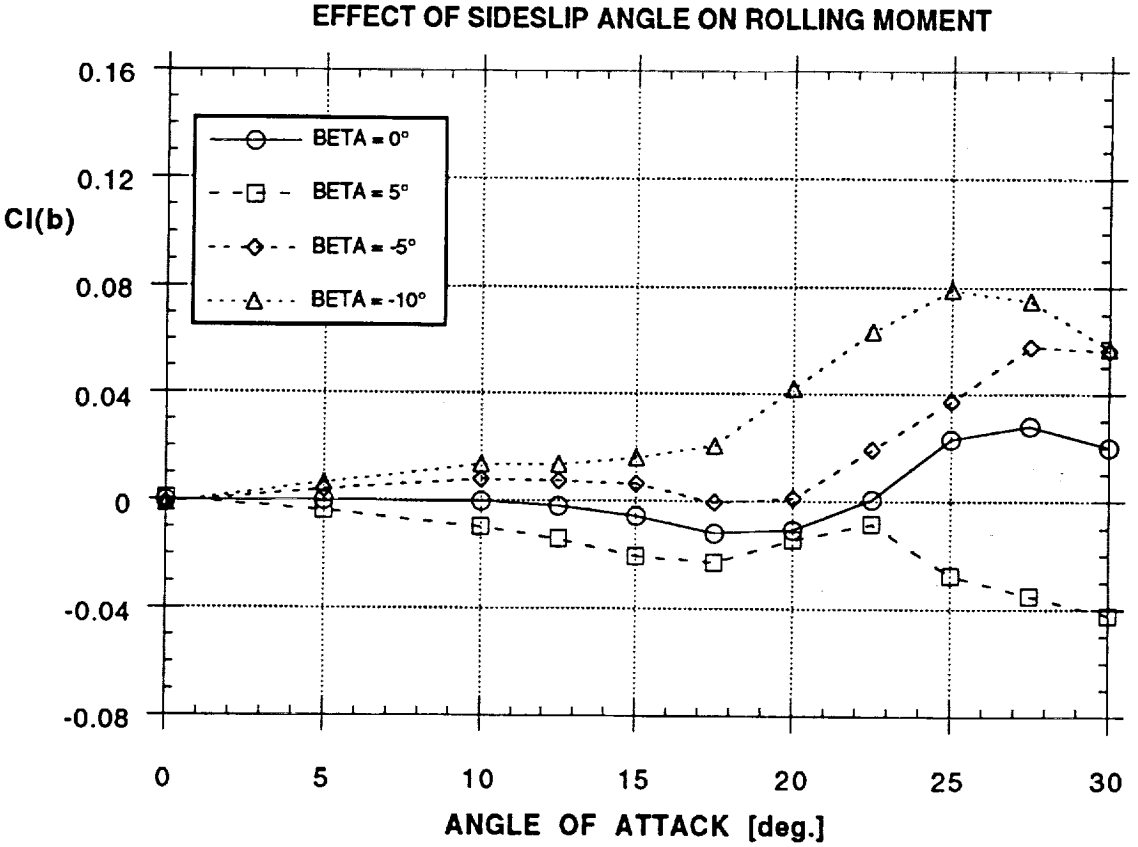

d)

Figure 5 - Continued

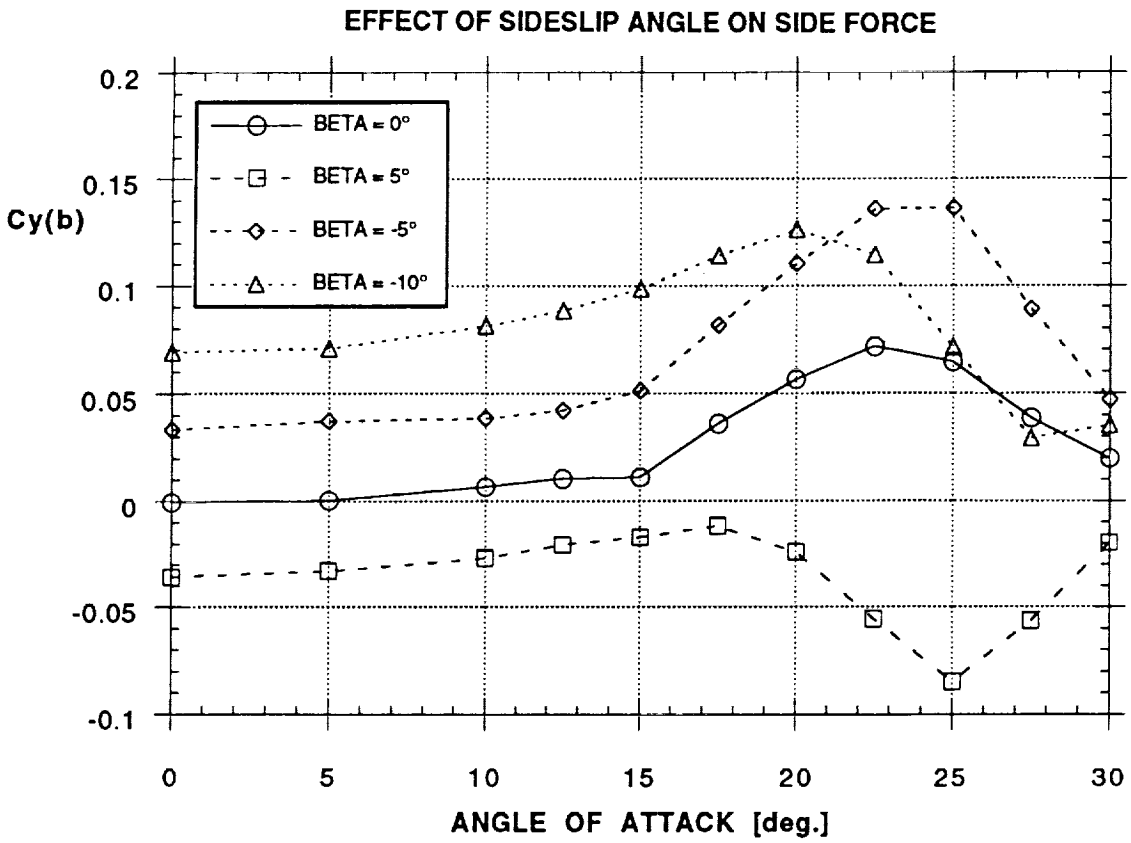

e)

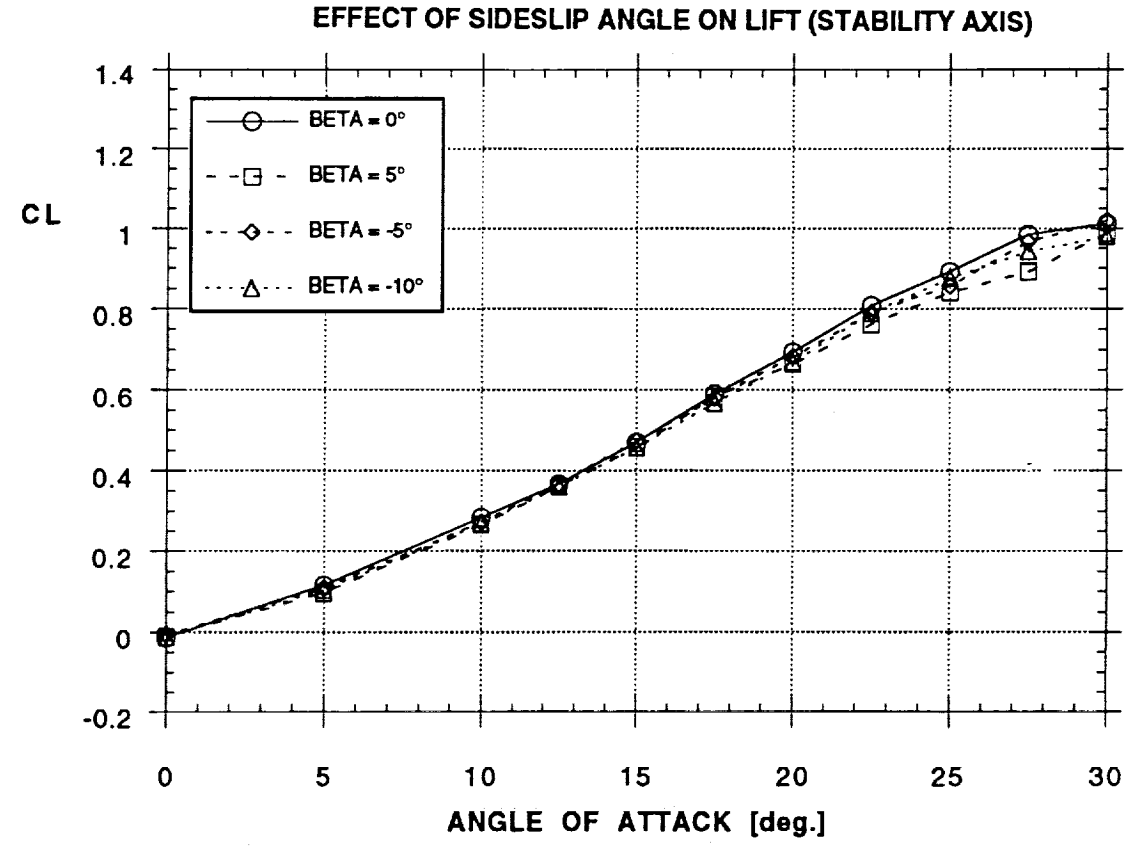

f)

Figure 5 - Concluded

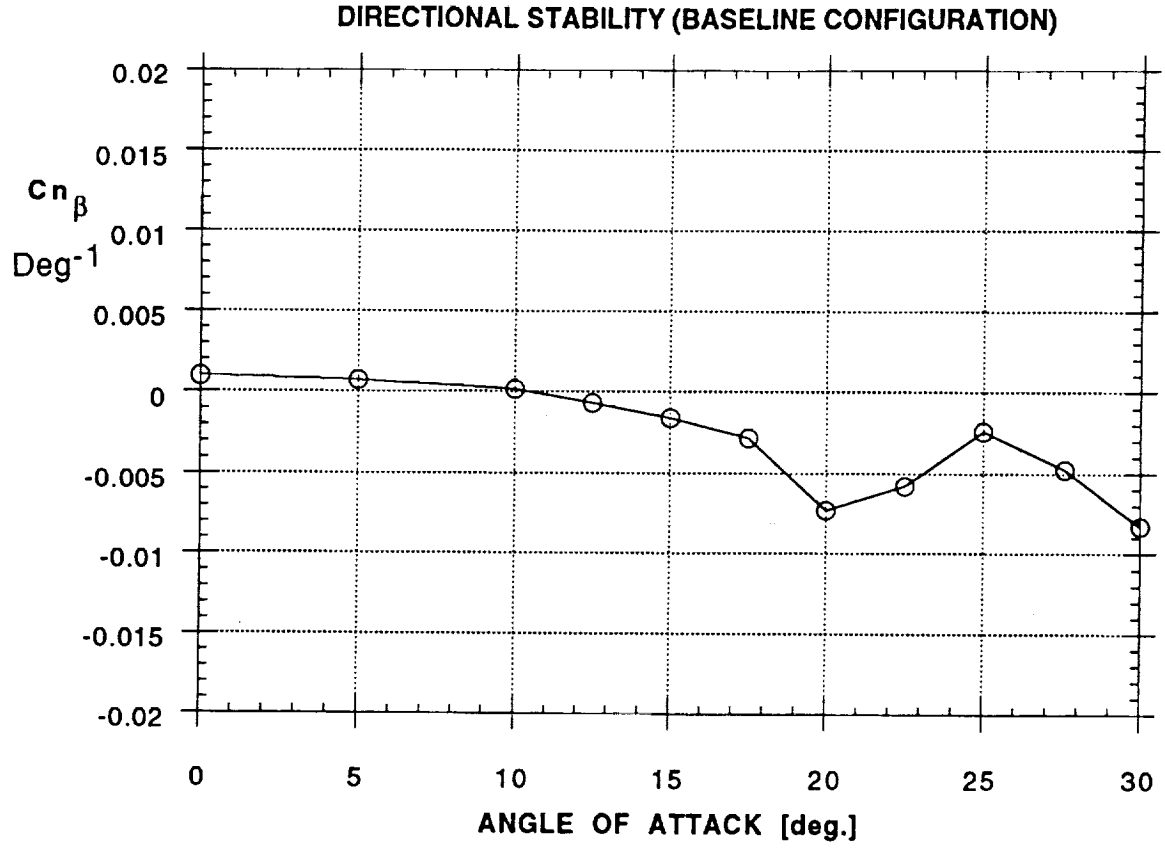

a)

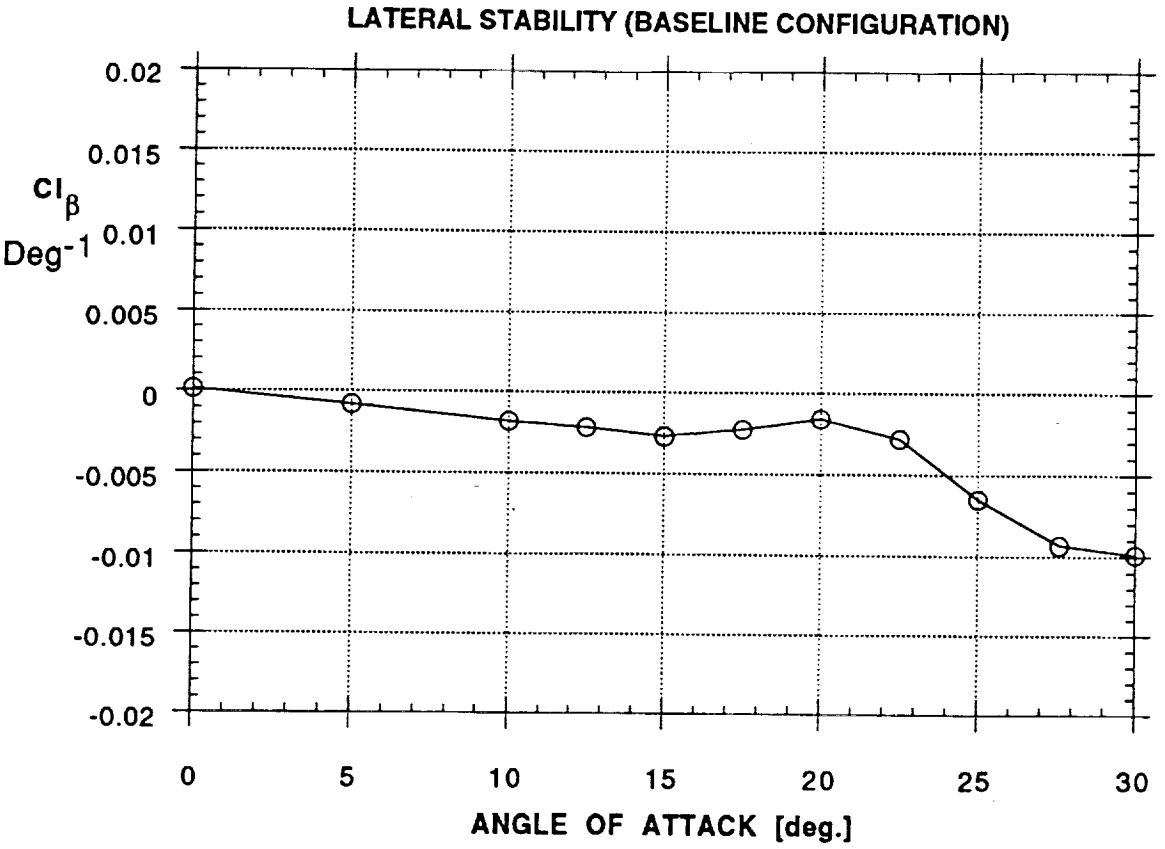

b)

Figure 6 - Directional and Lateral Derivatives (Baseline A)

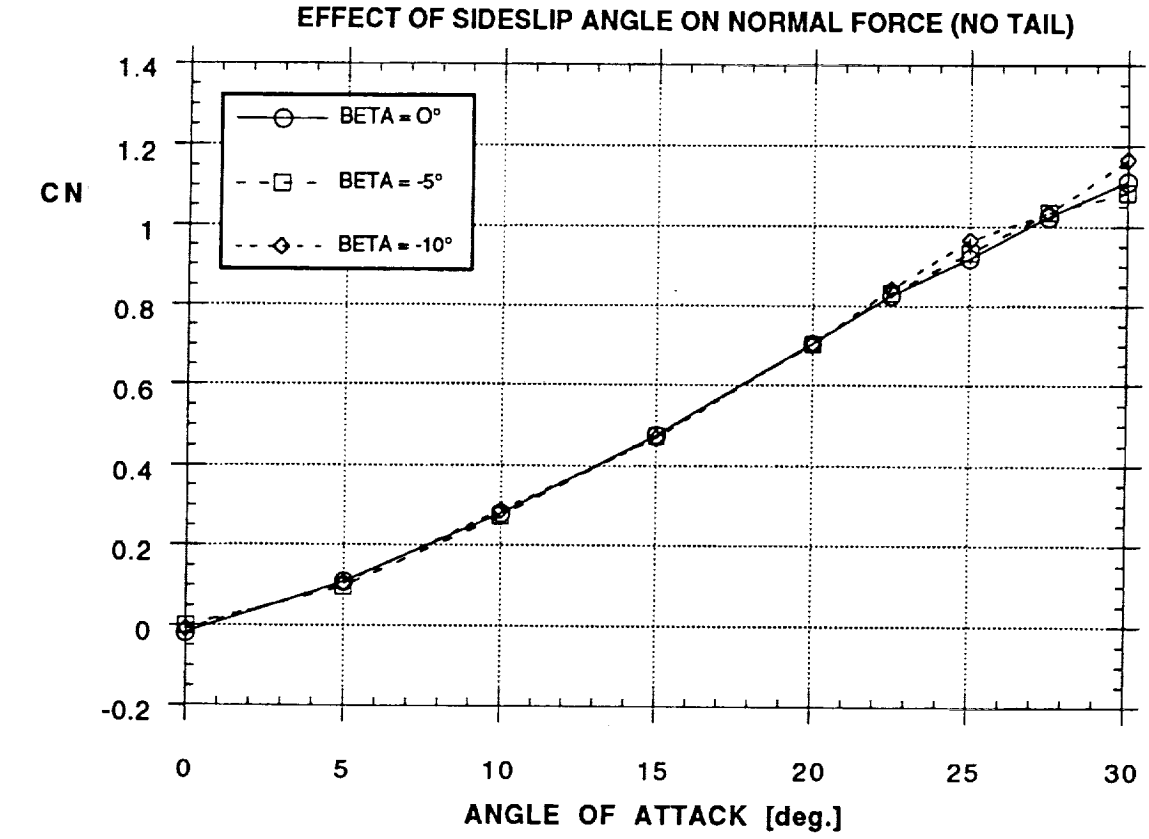

a)

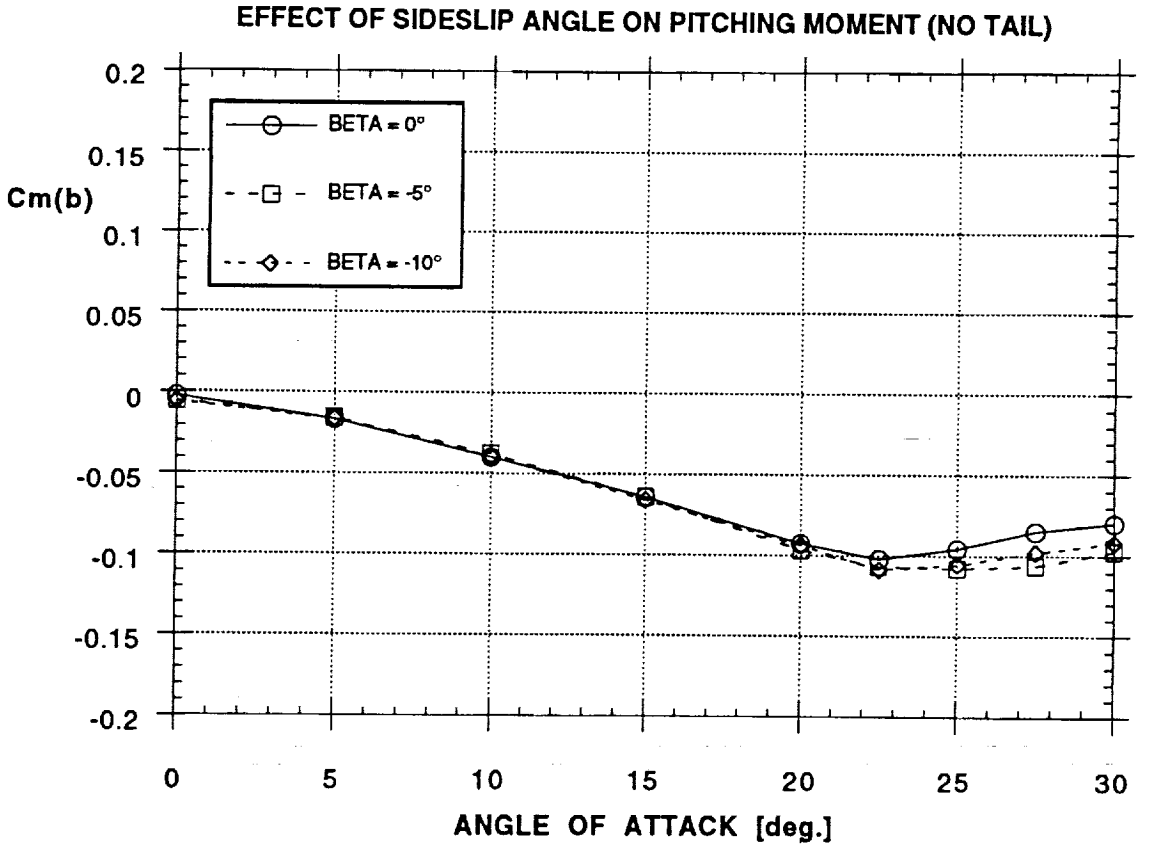

b)

Figure 7 - Effect of Sideslip Angle on Forces and Moments (No Tail)

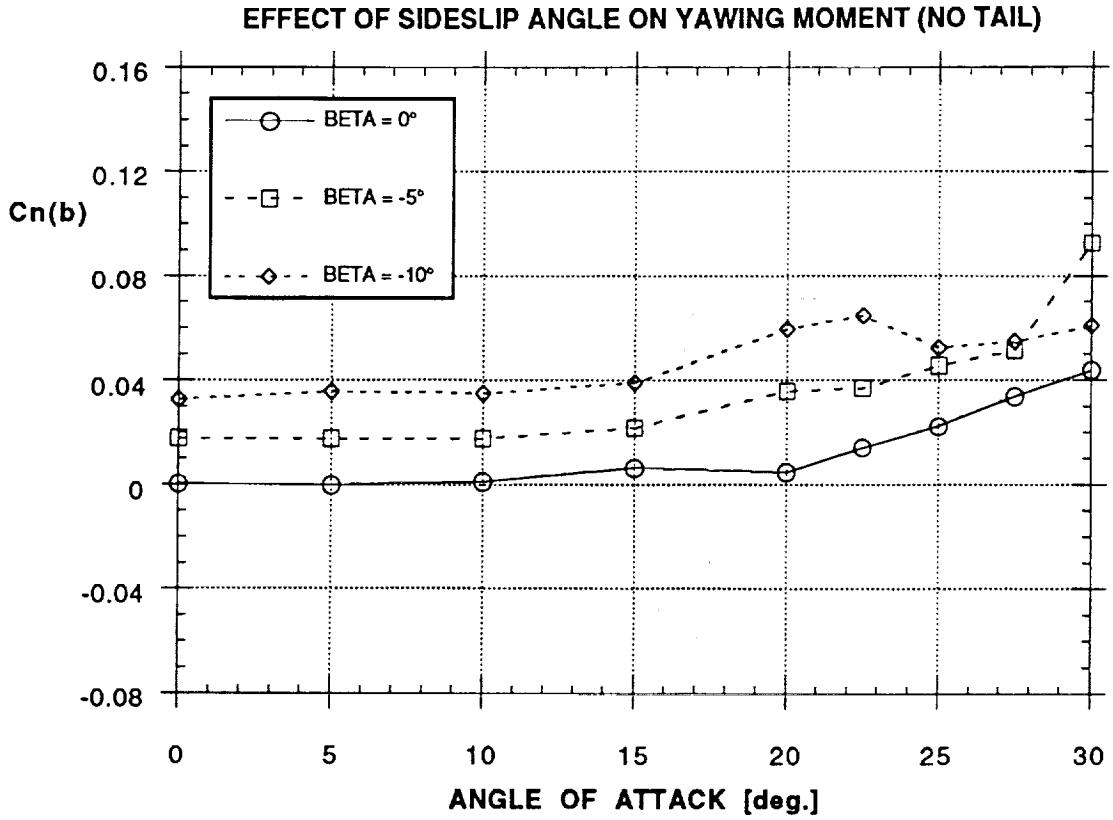

c)

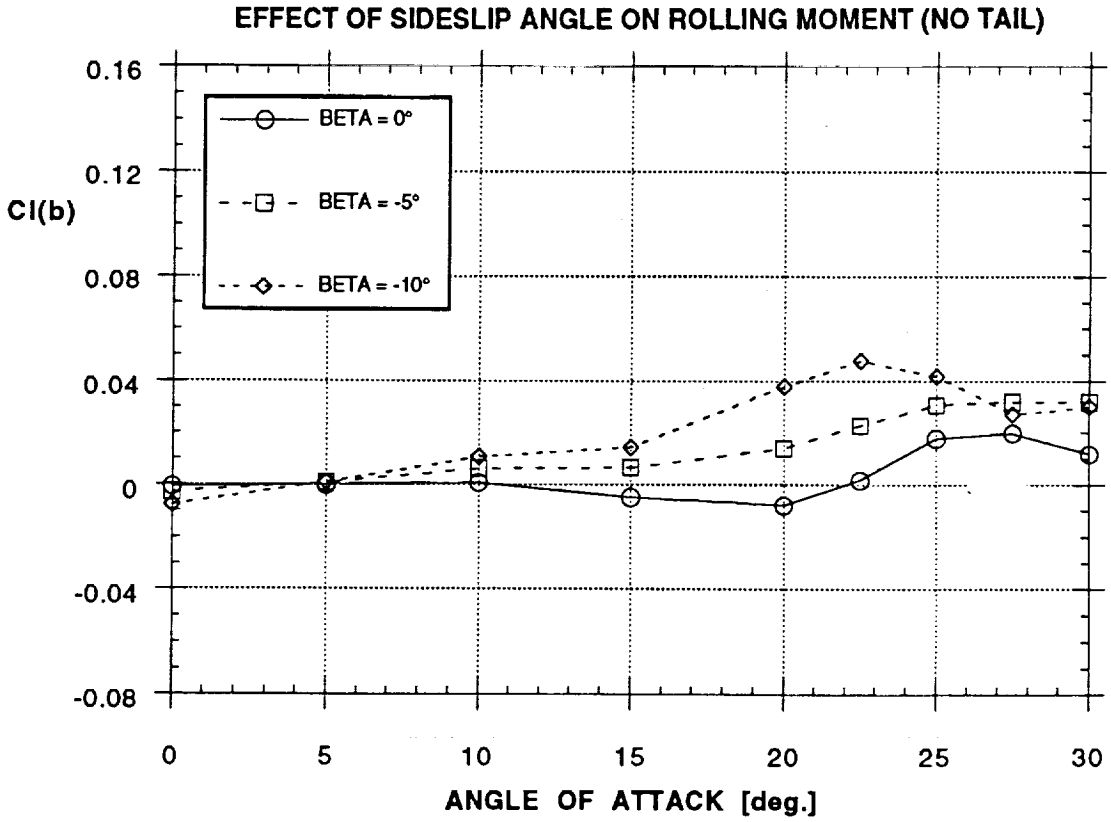

d)

Figure 7 - Continued

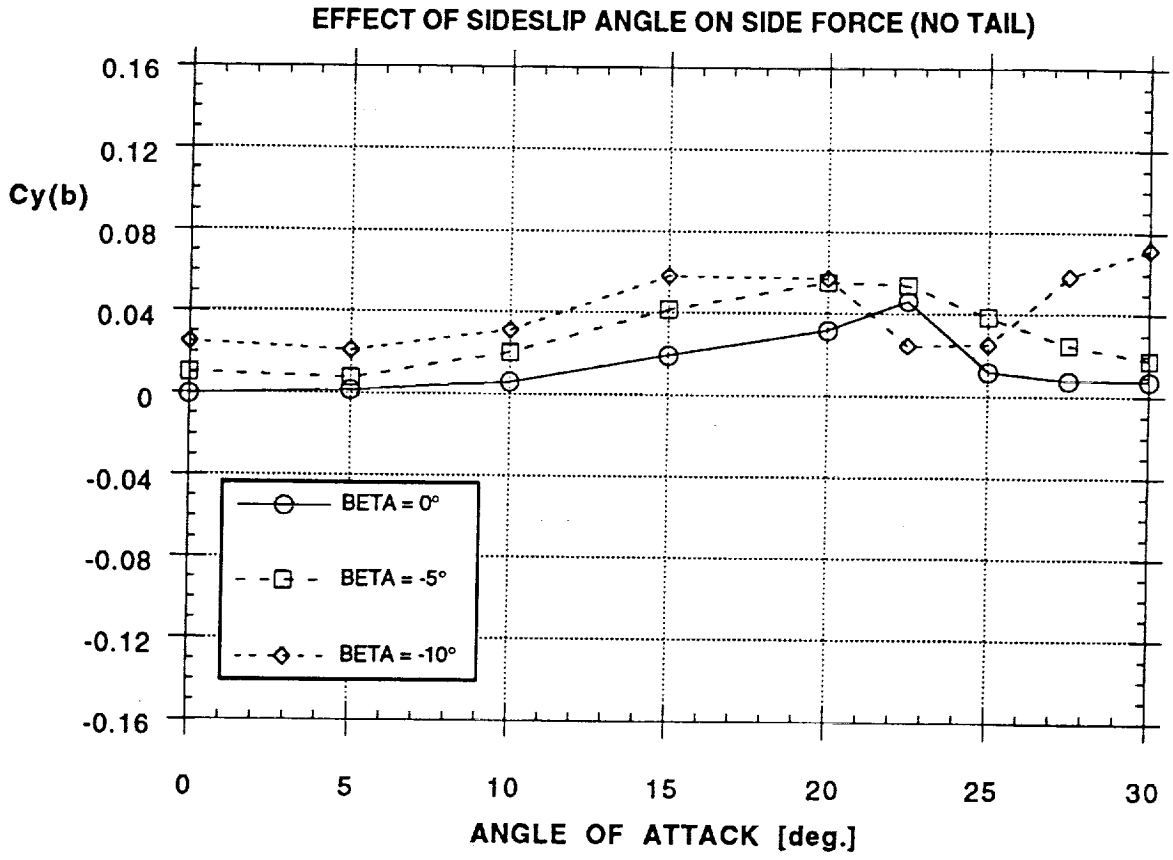

e)

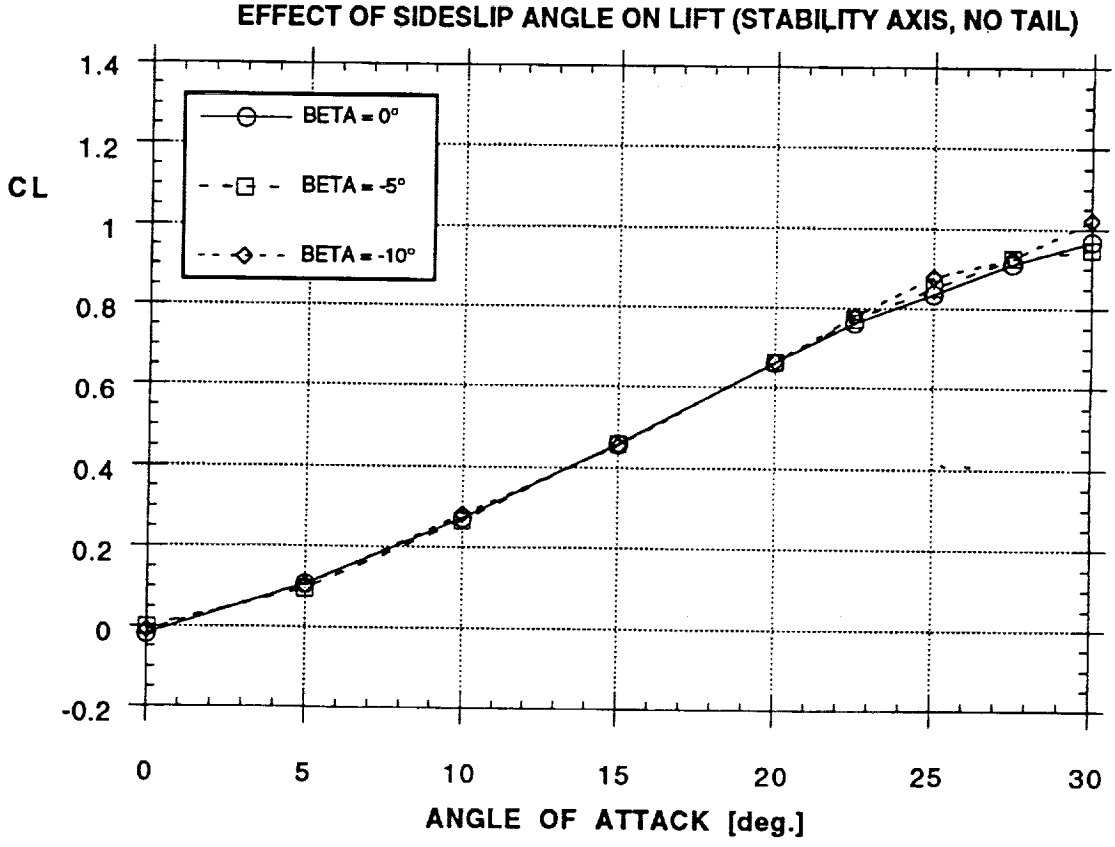

f)

Figure 7 - Concluded

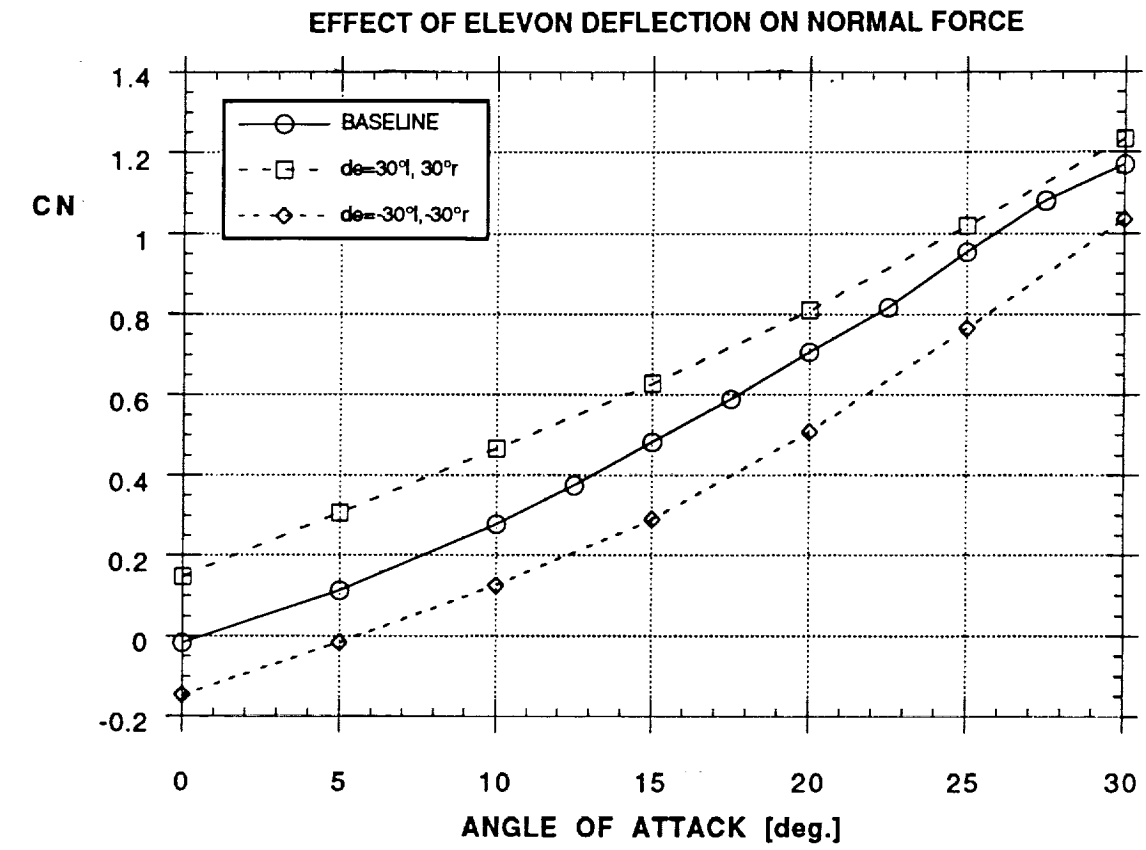

a)

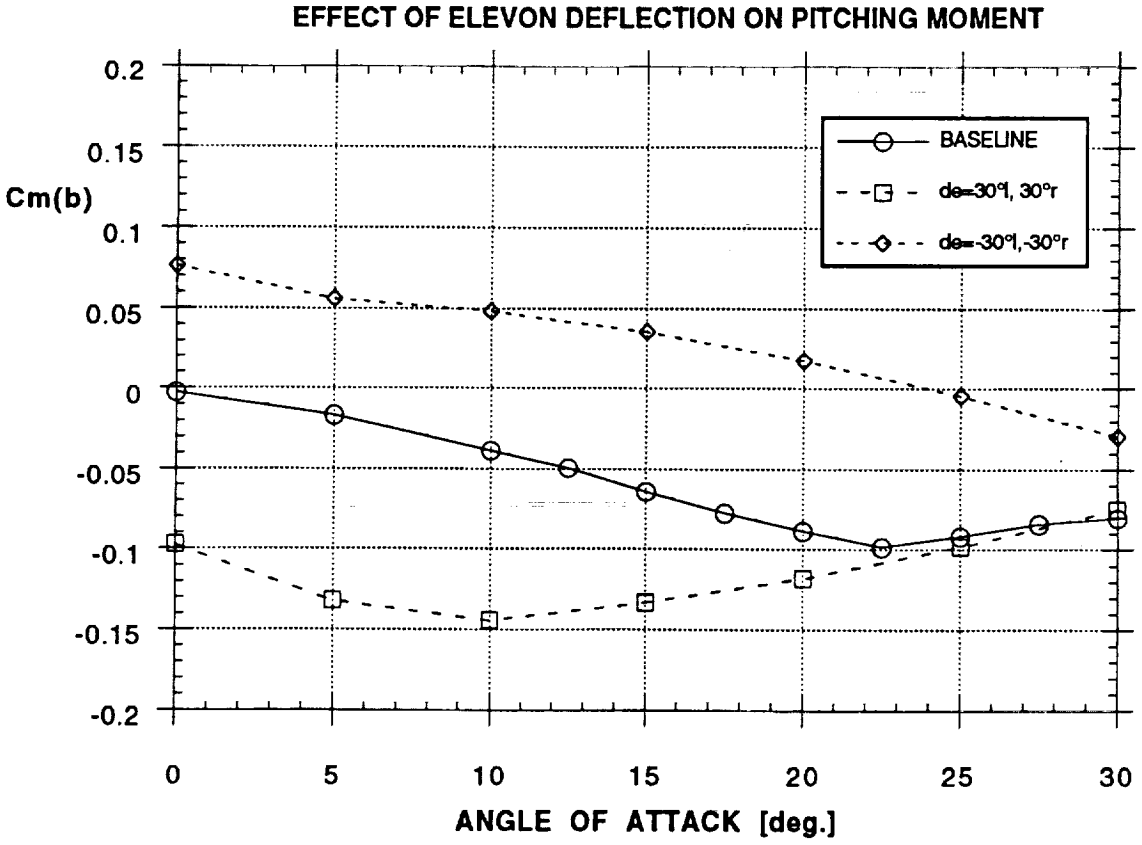

b)

Figure 8 - Effect of Elevon Deflection on Forces and Moments

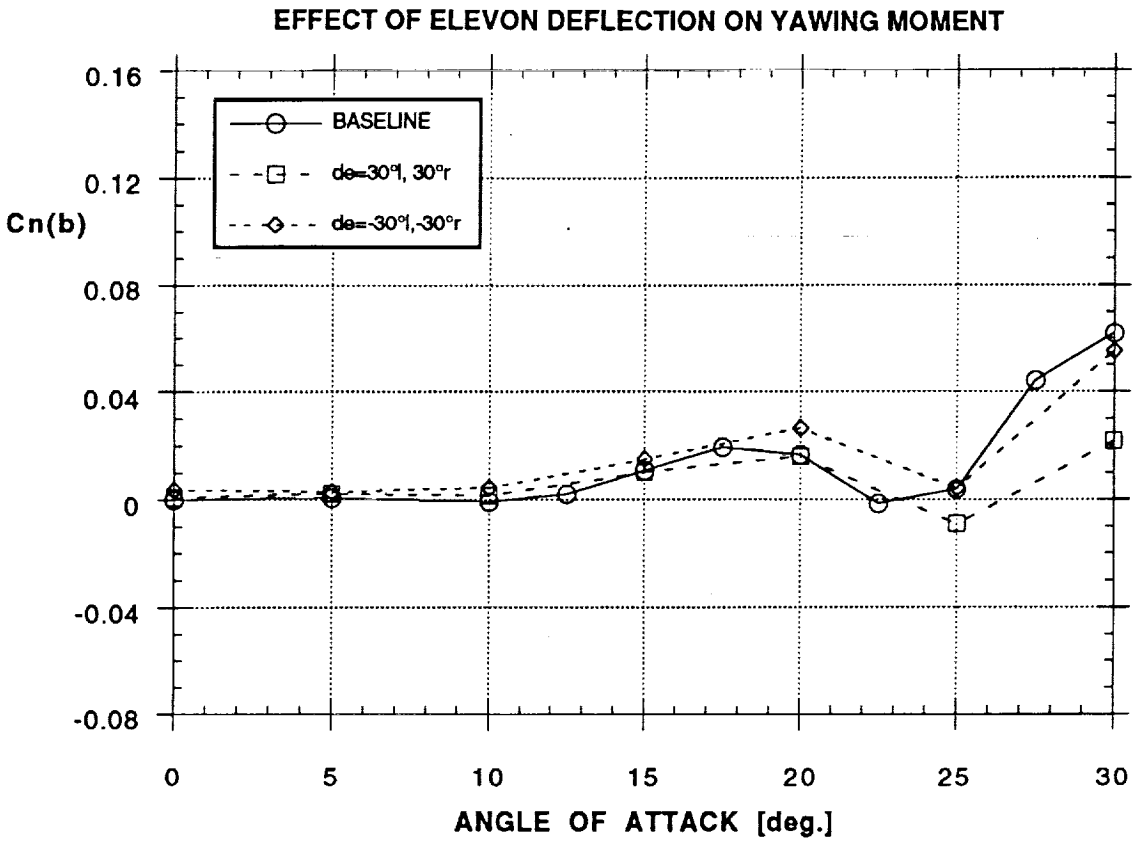

c)

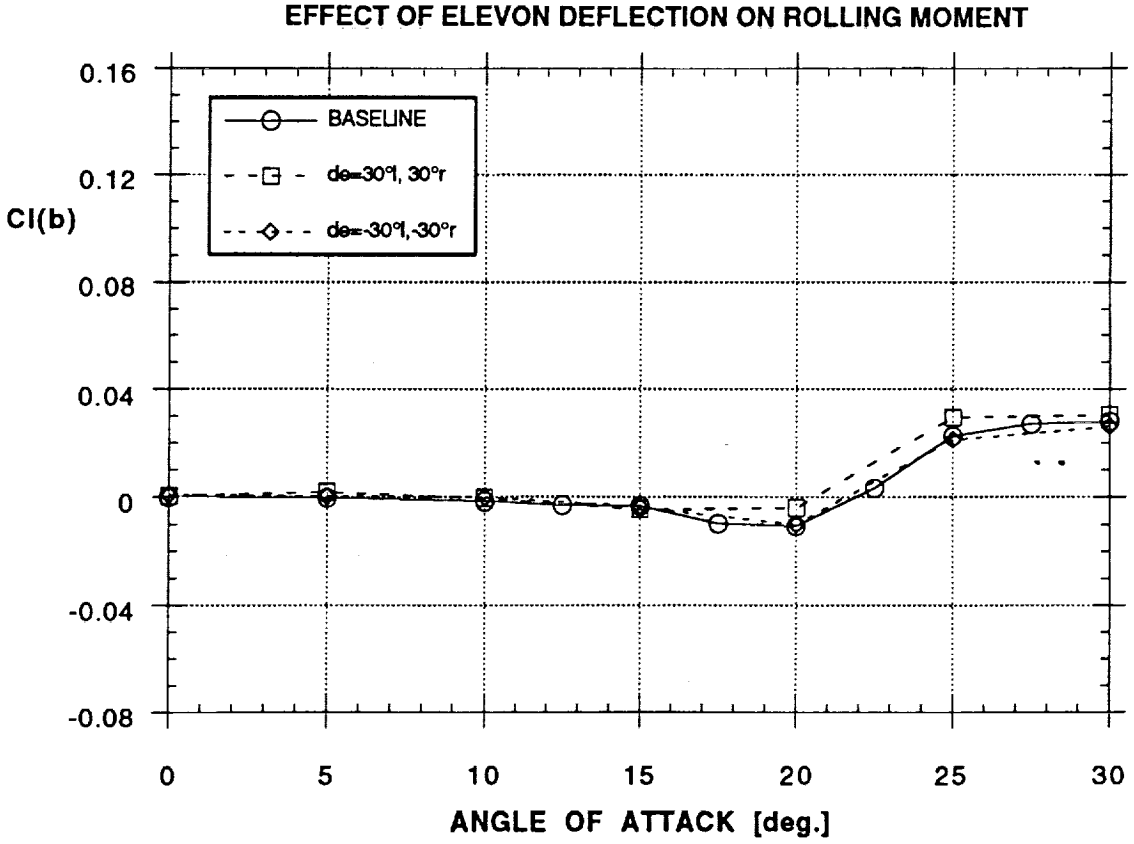

d)

Figure 8 - Continued

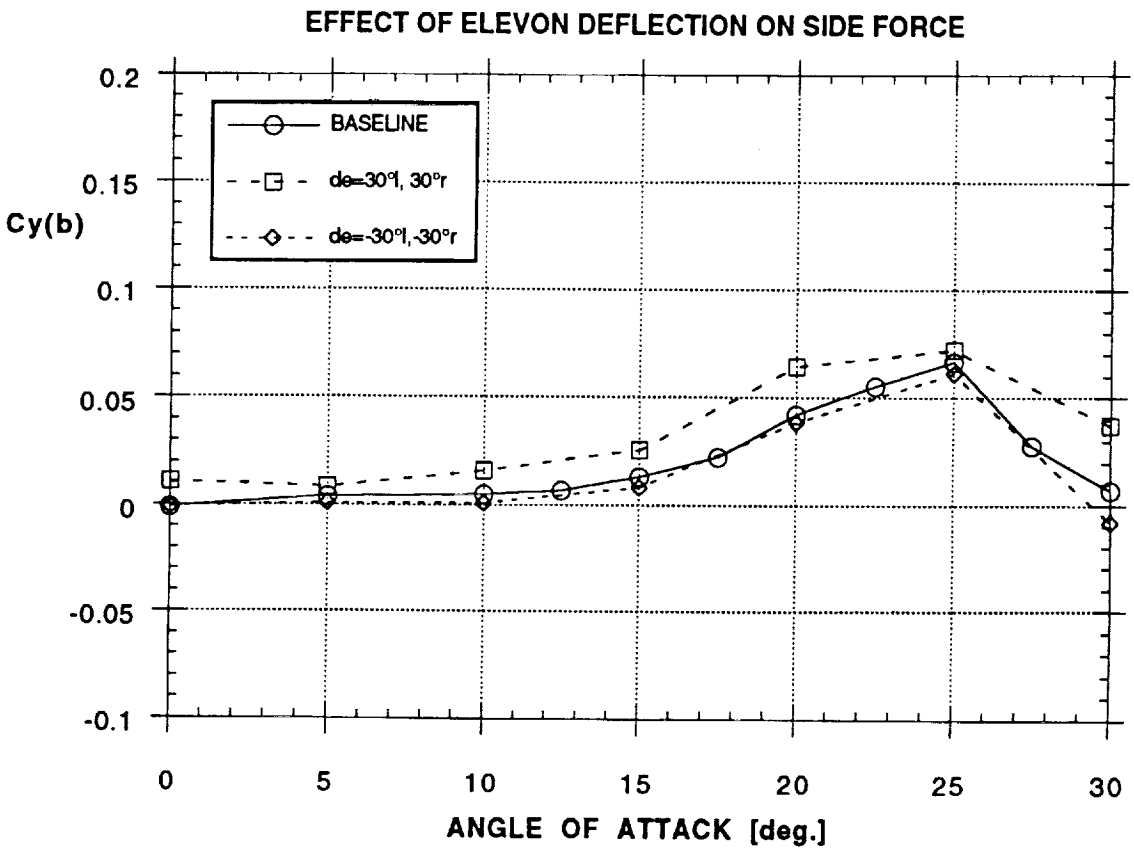

e)

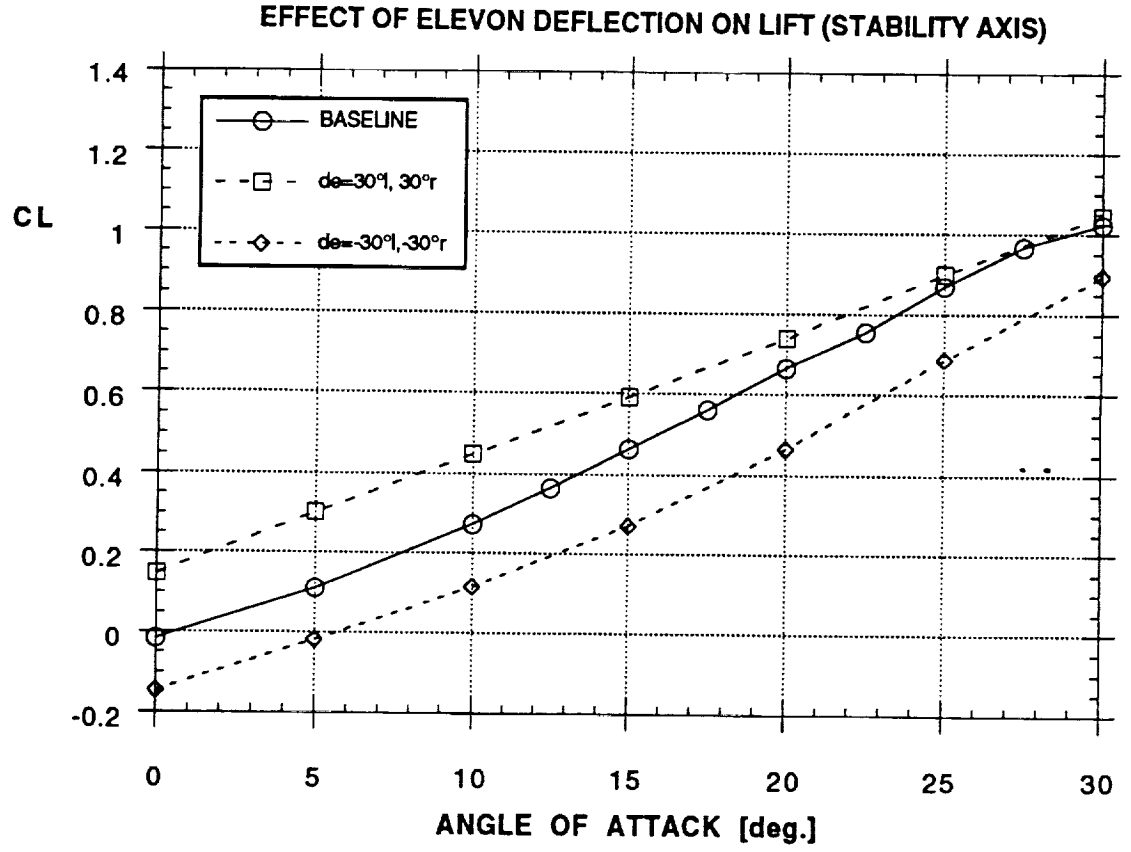

f)

Figure 8 - Concluded

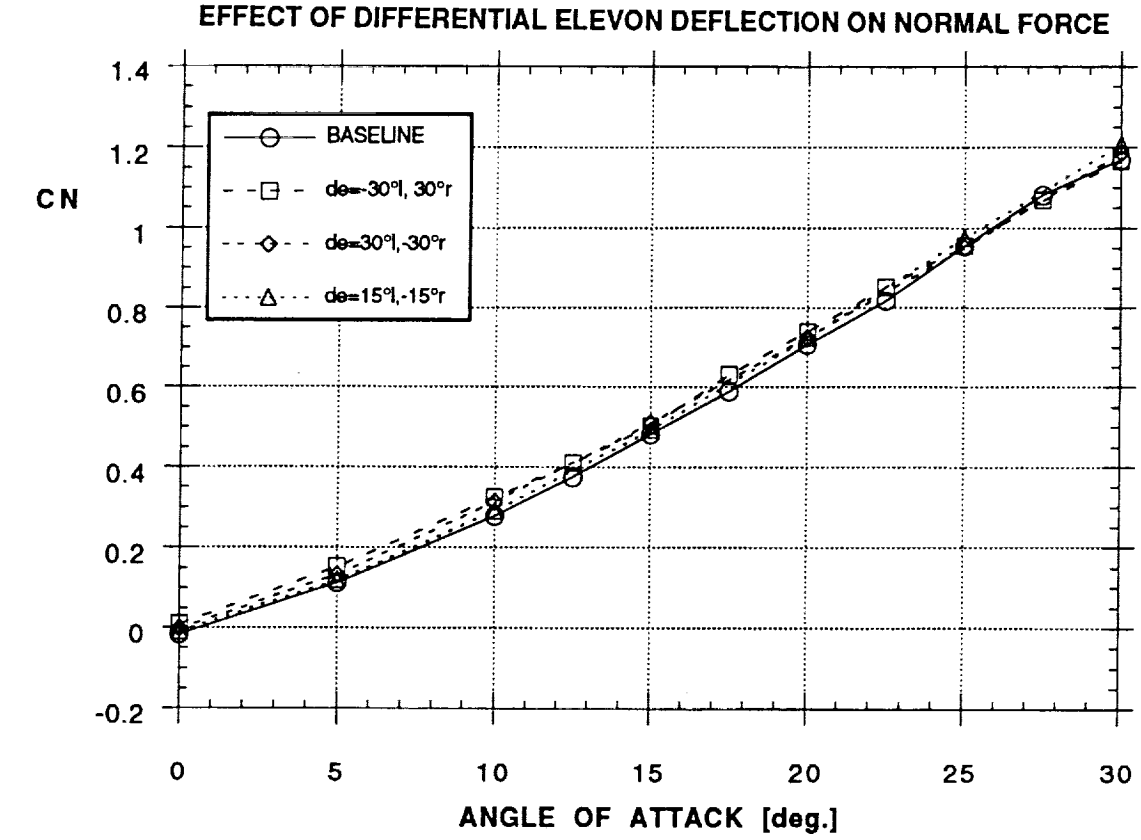

a)

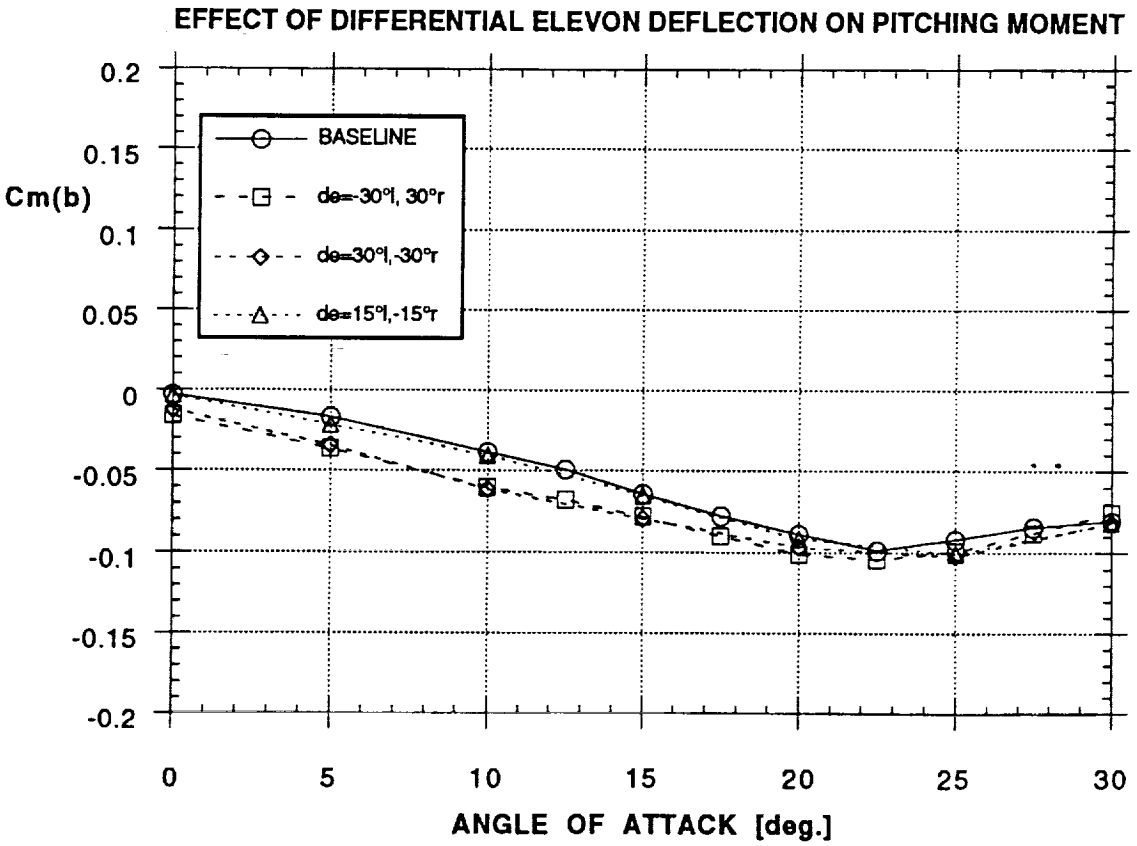

b)

Figure 9 - Effect of Differential Elevon Deflection (ailerons) on Forces and Moments

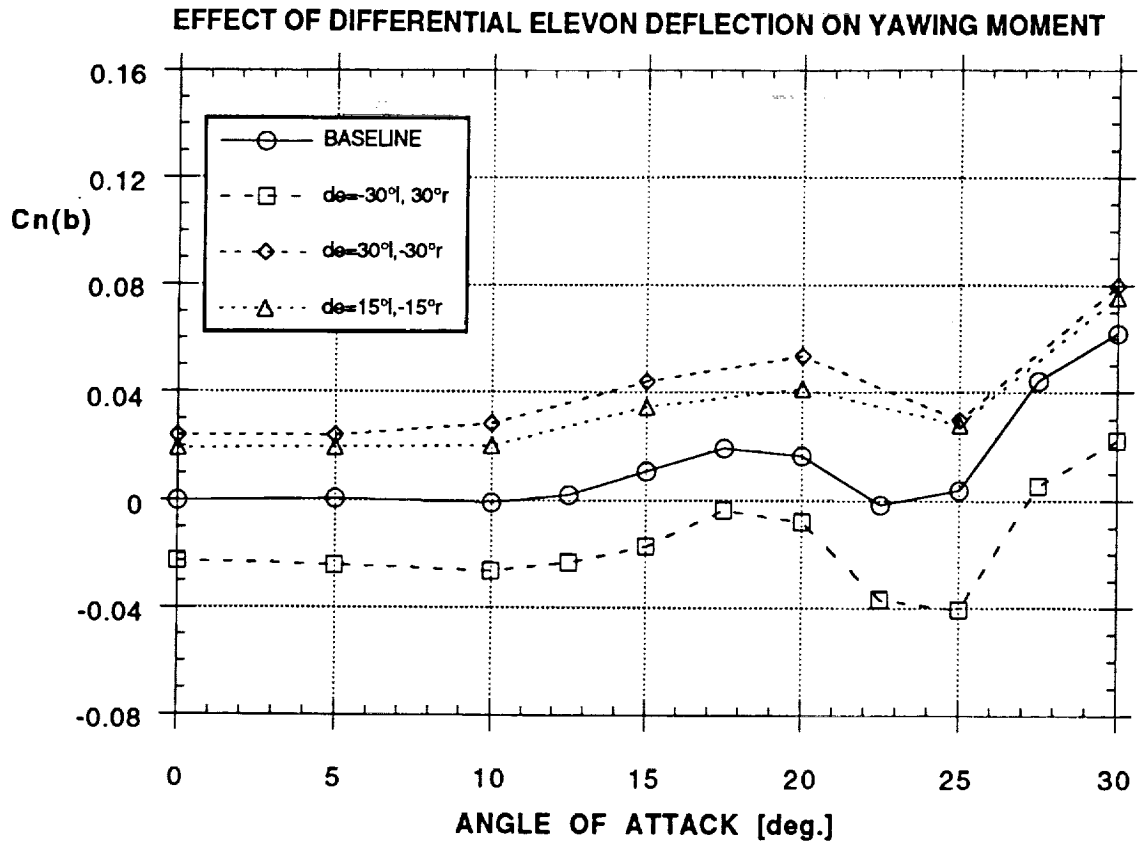

c)

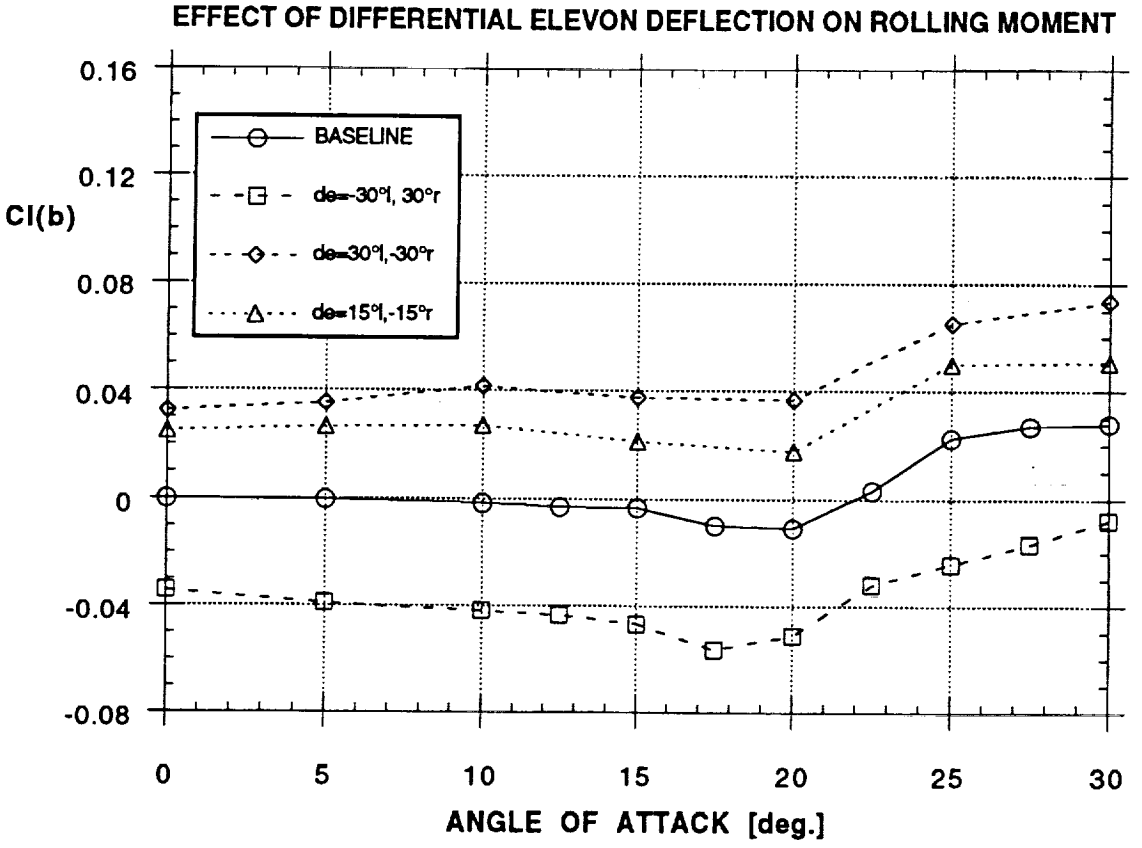

d)

Figure 9 - Continued

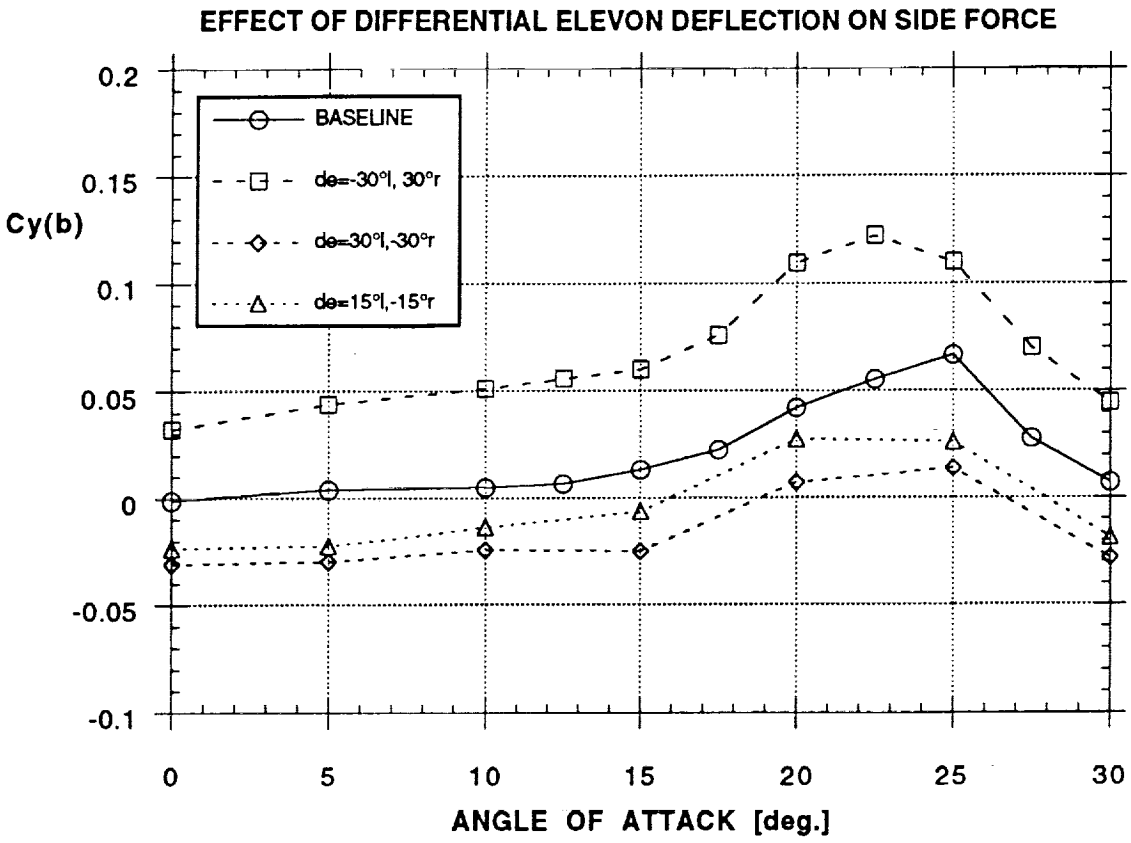

e)

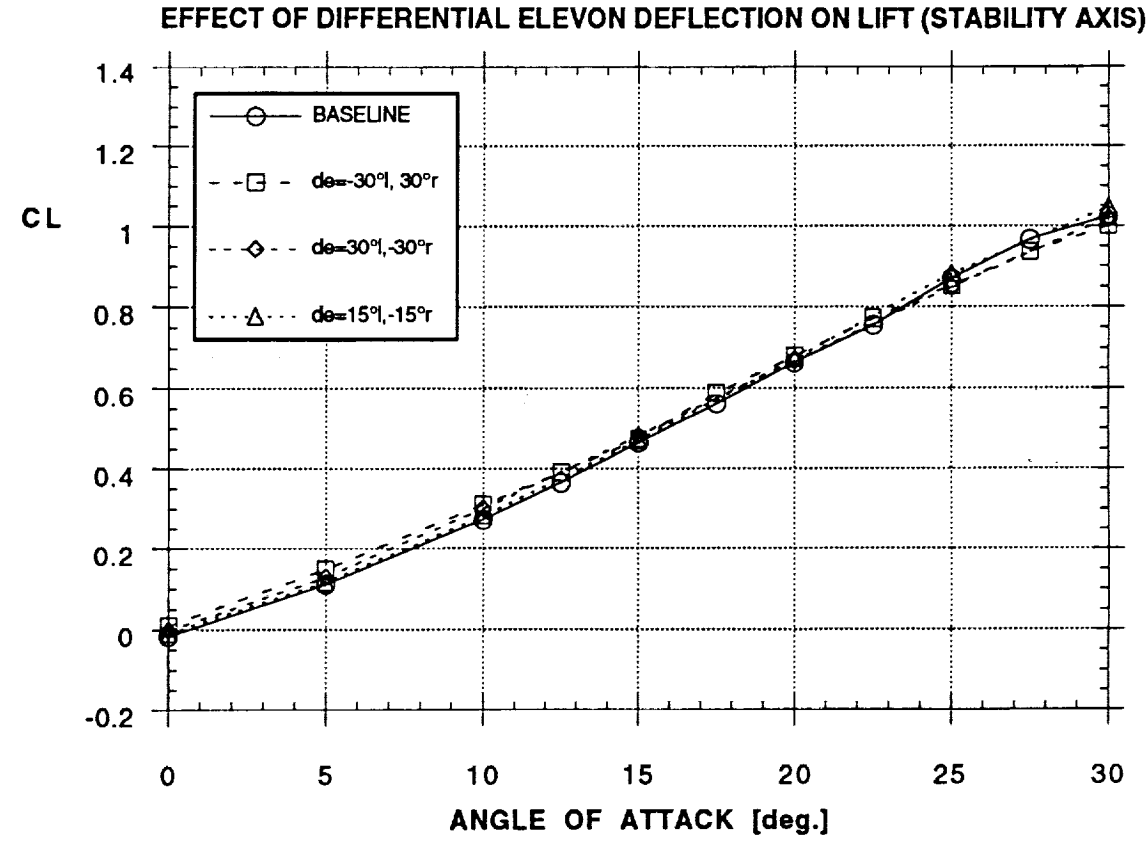

f)

Figure 9 - Concluded

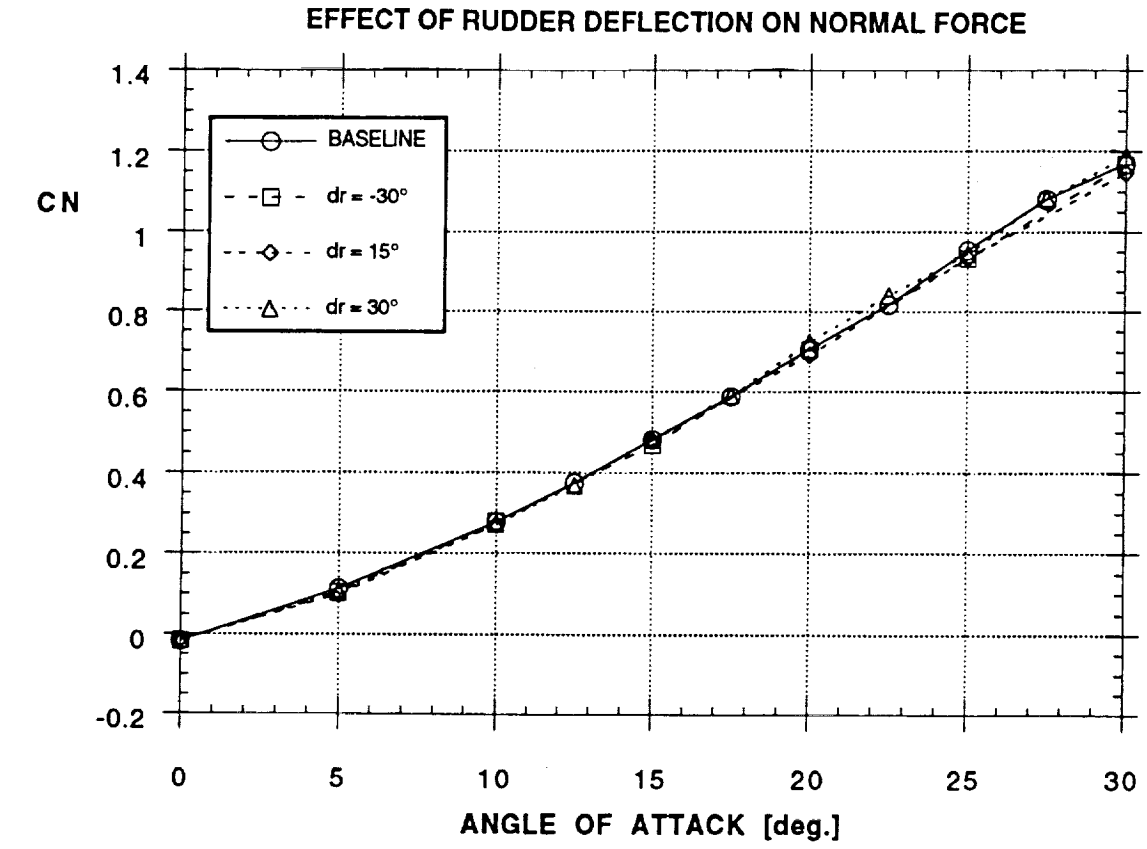

a)

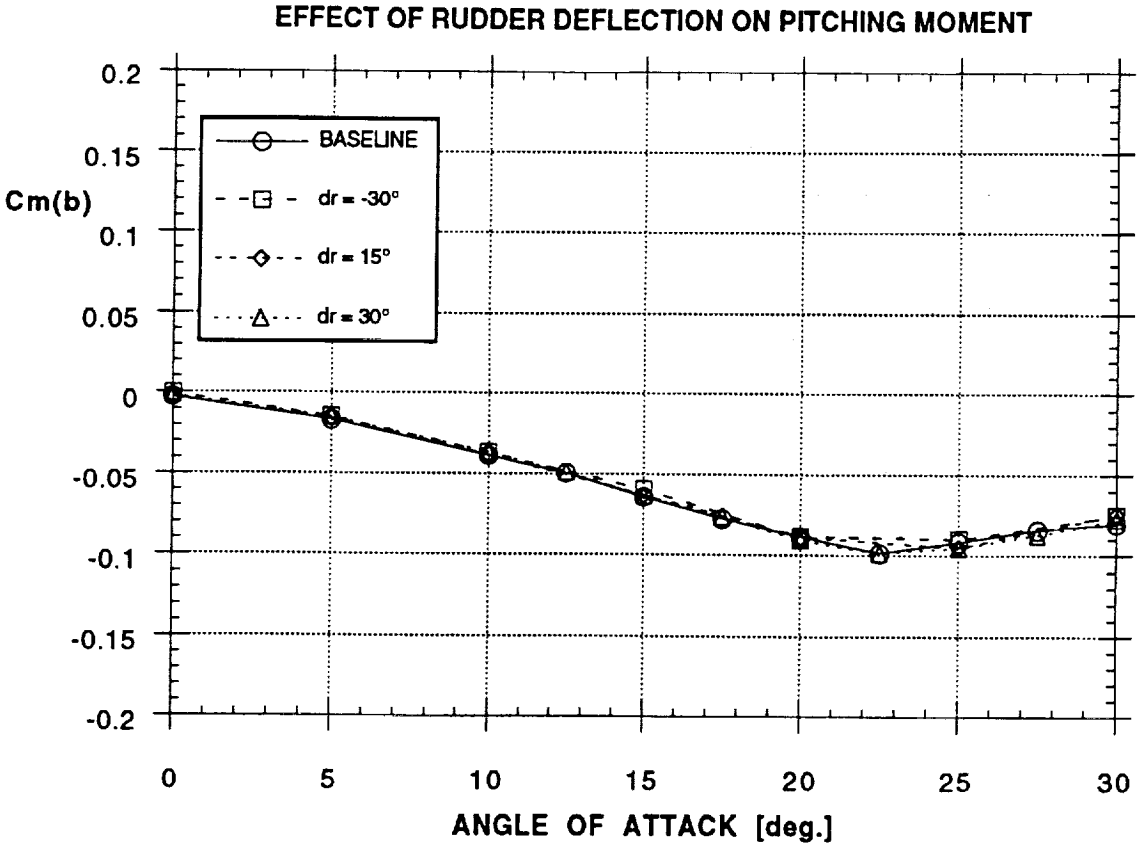

b)

Figure 10 - Effect of Rudder Deflection on Forces and Moments

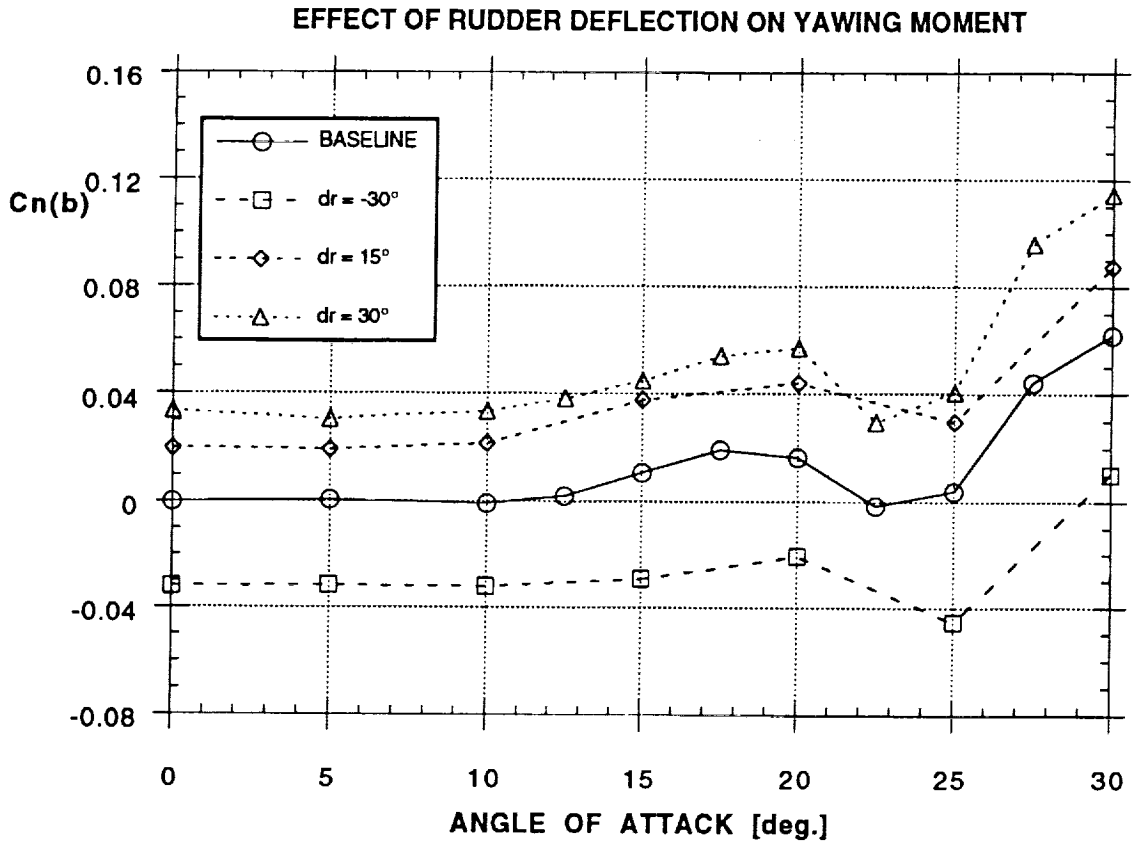

c)

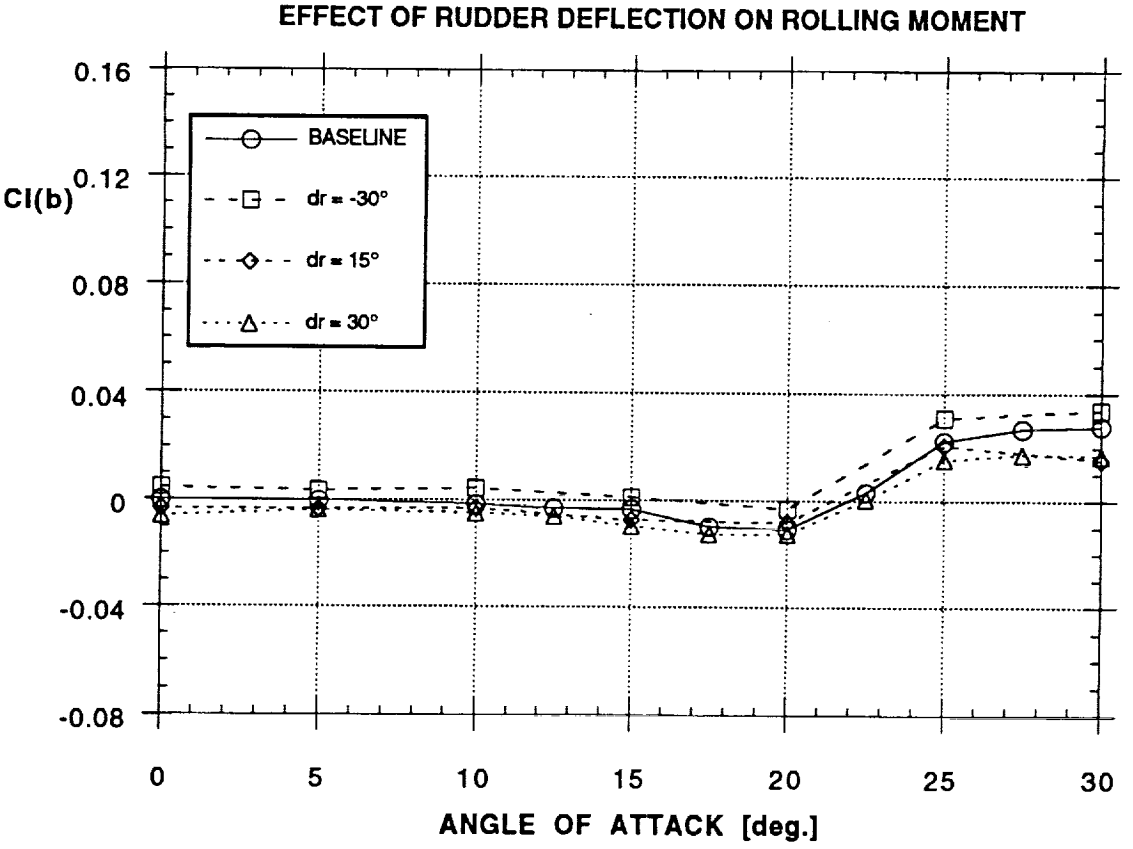

d)

Figure 10 - Continued

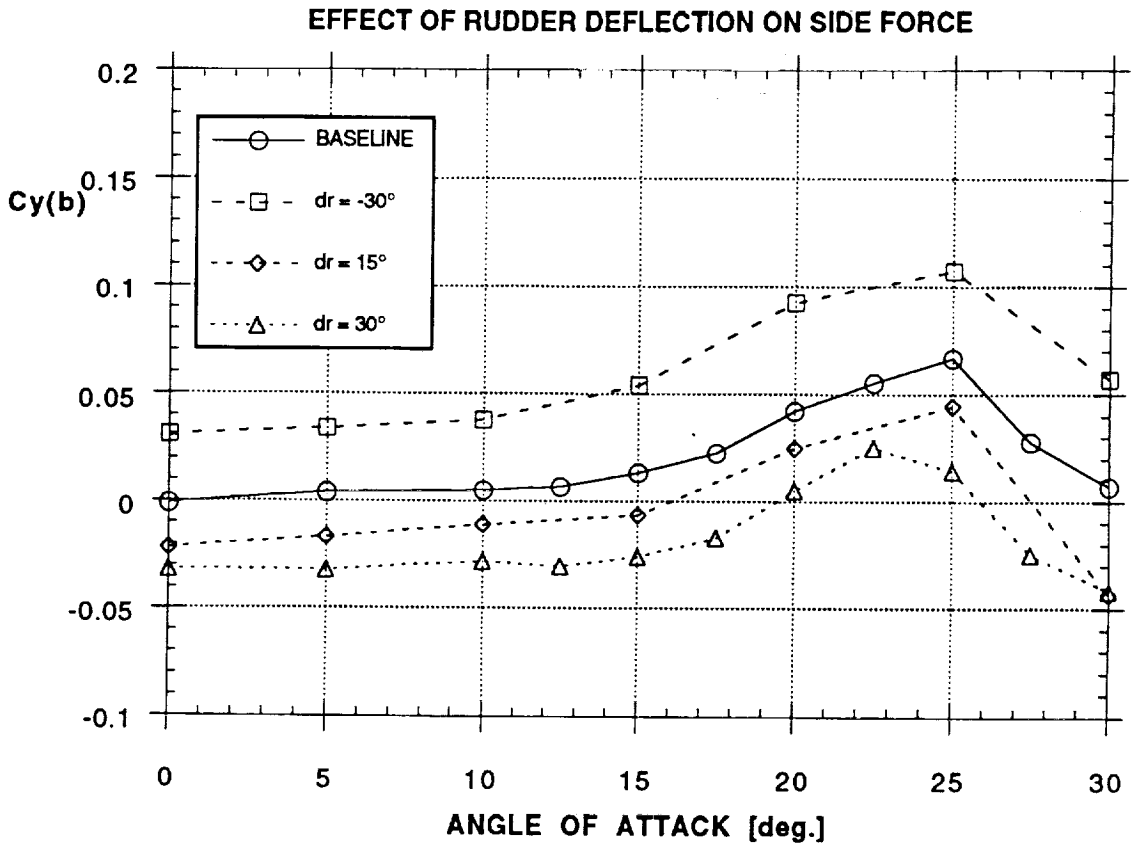

e)

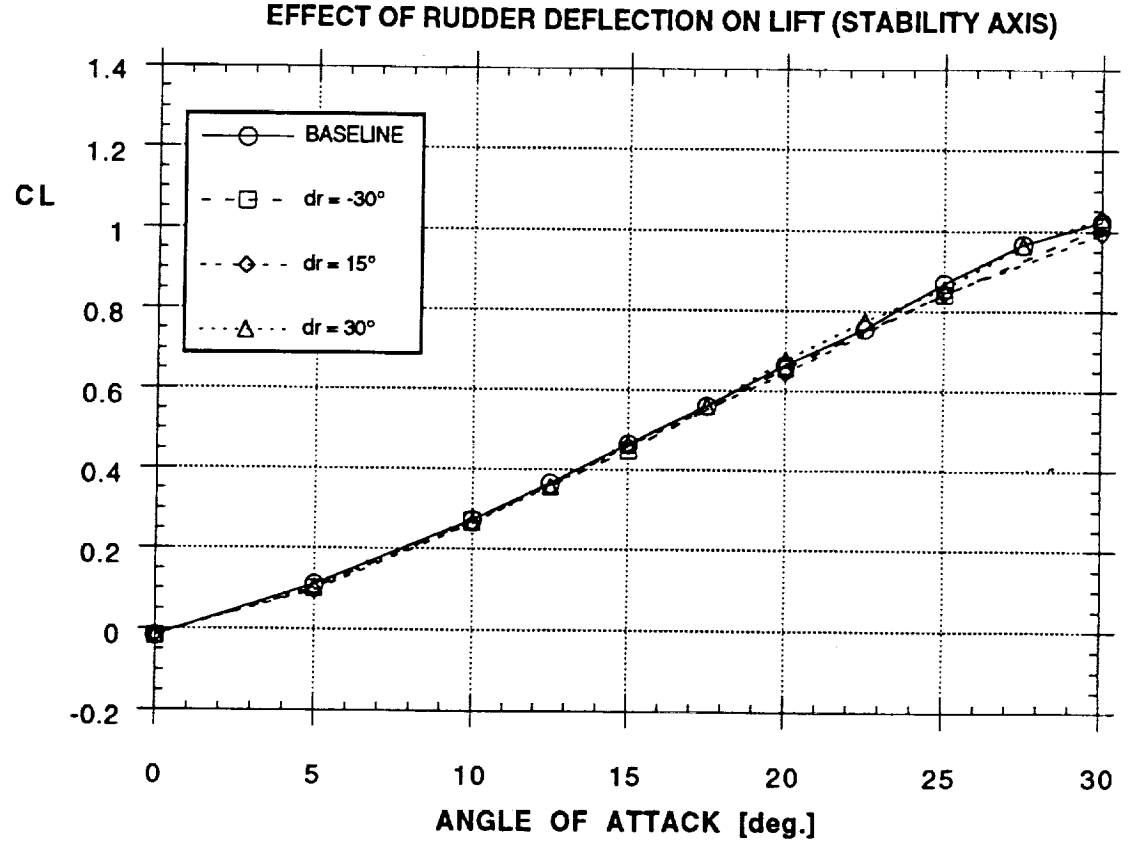

f)

Figure 10 - Concluded

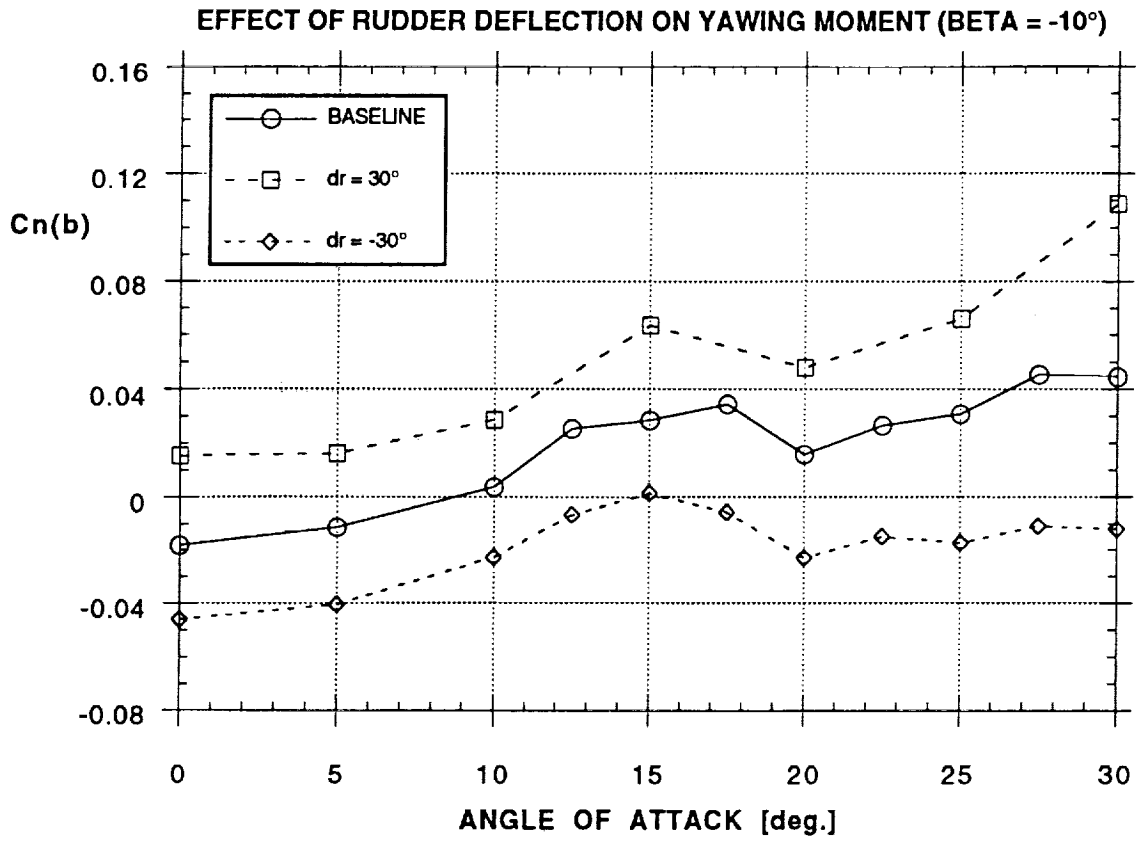

a)

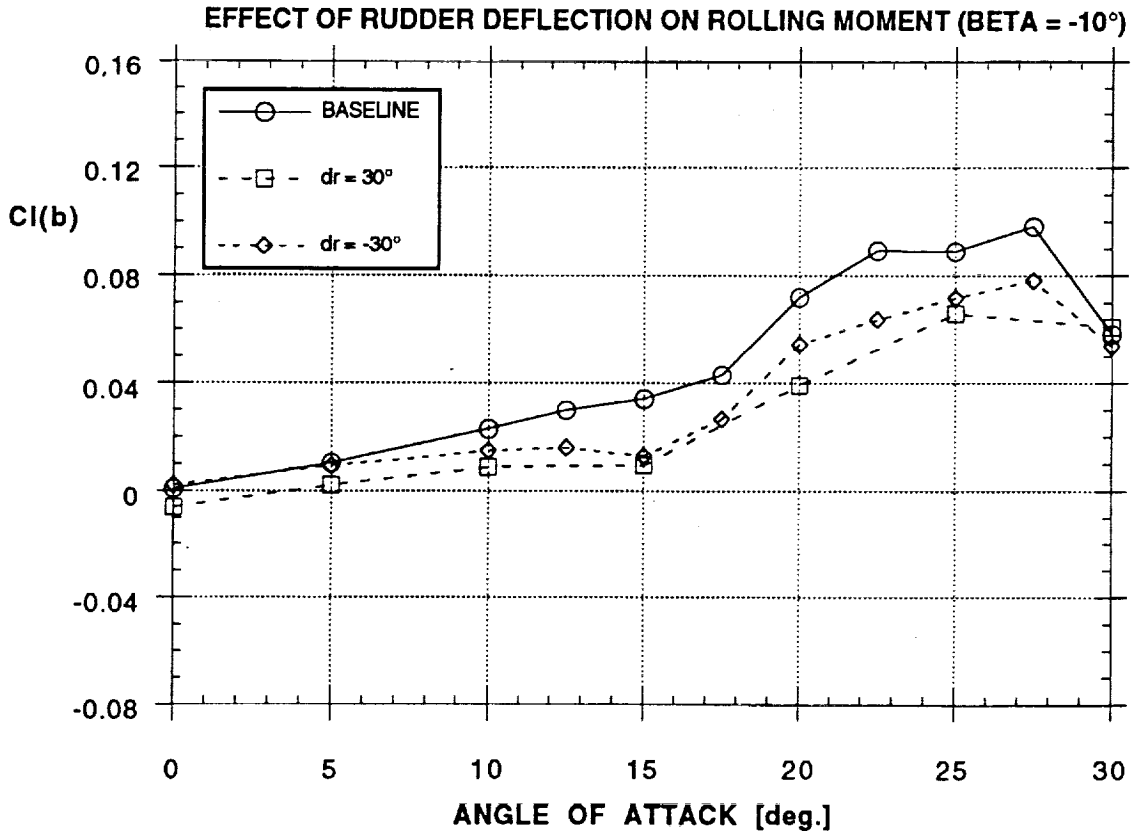

b)

Figure 11 - Effect of Rudder Deflection on Forces and Moments ($\beta = -10°$)

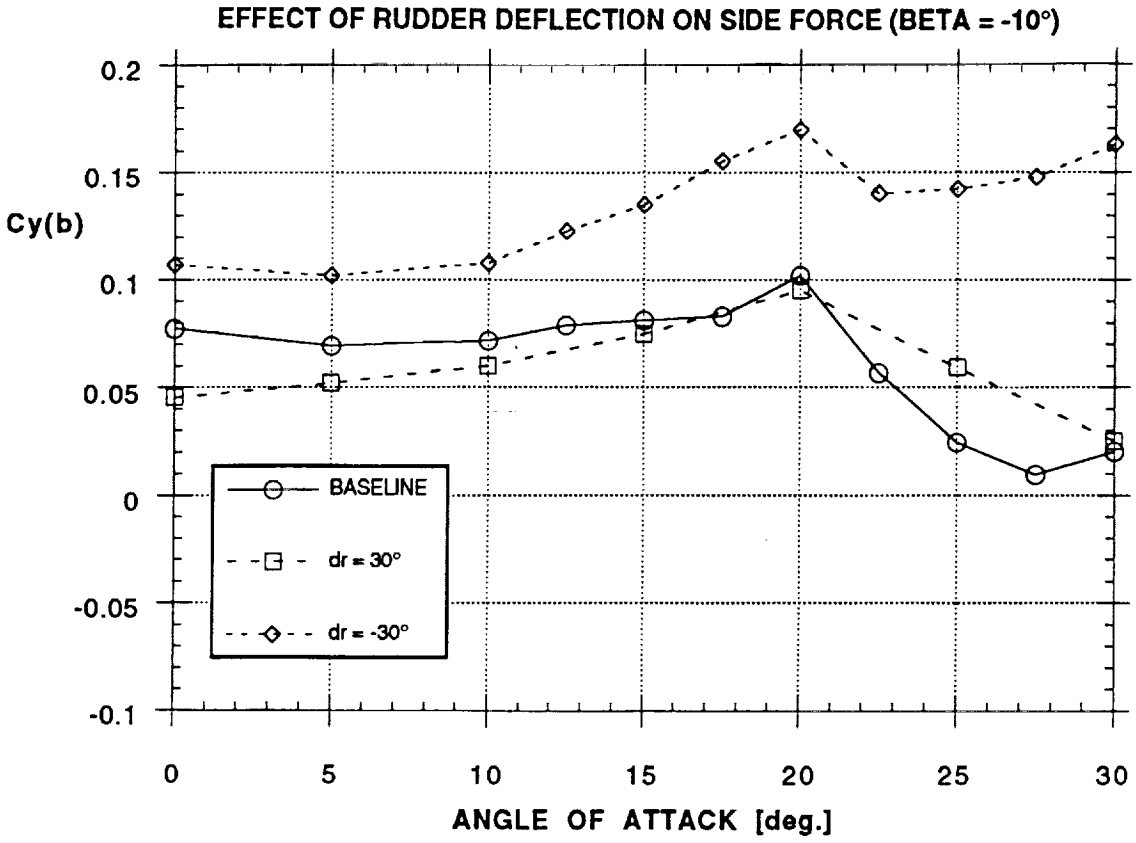

c)

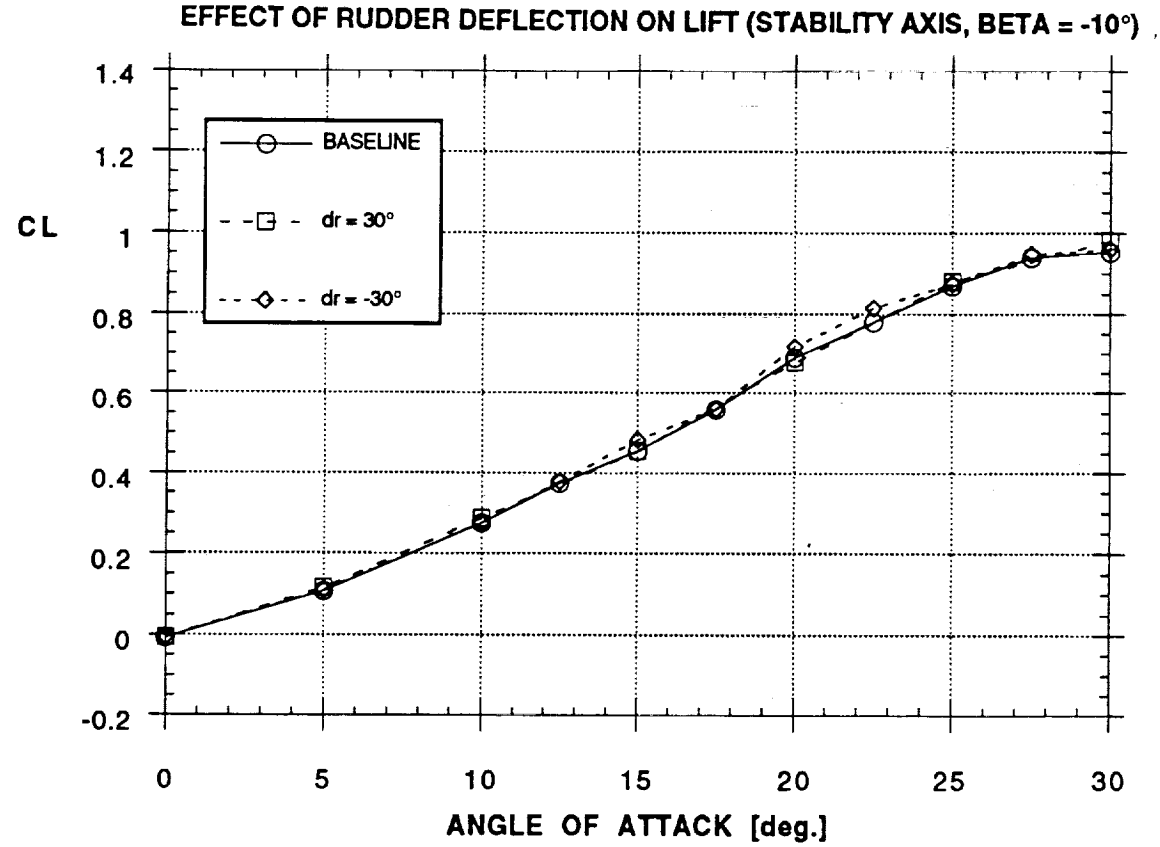

d)

Figure 11 - Concluded

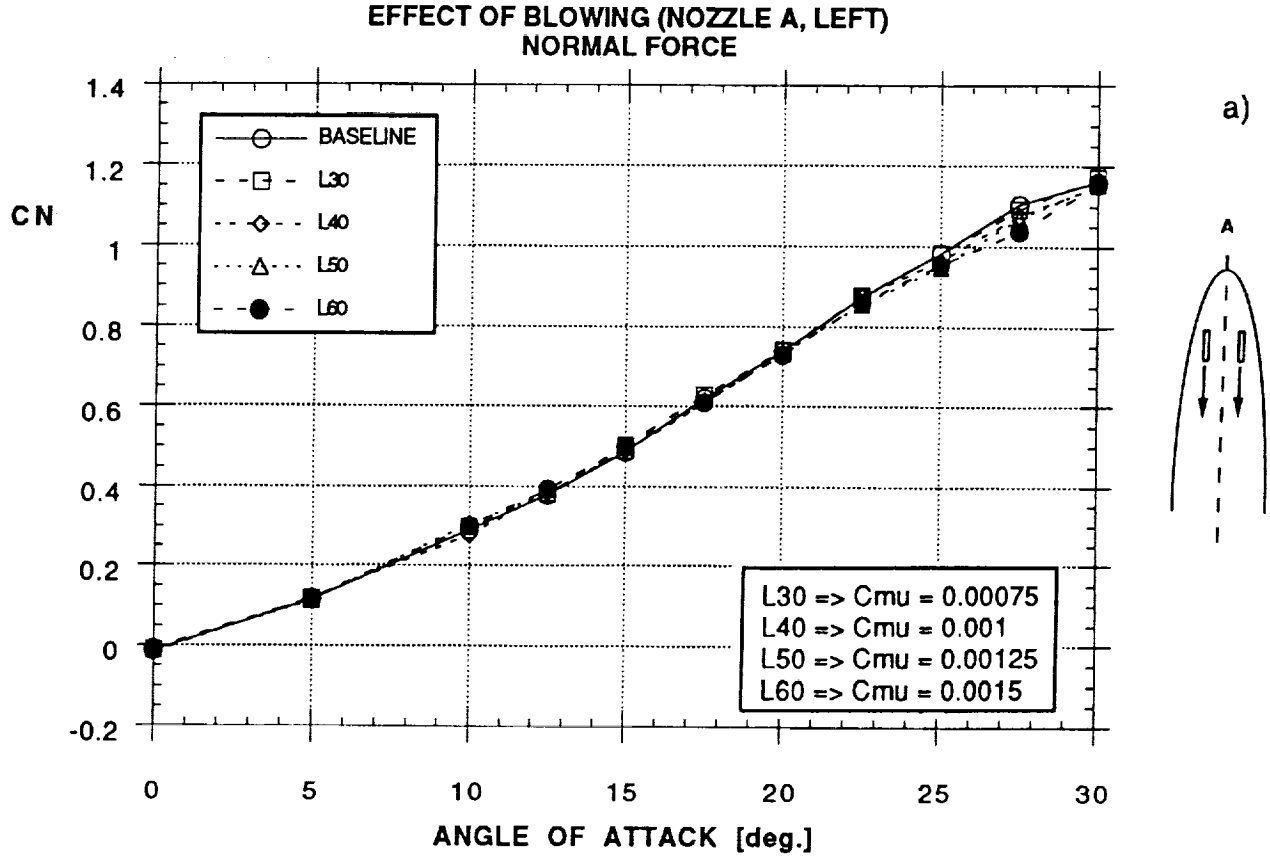

a)

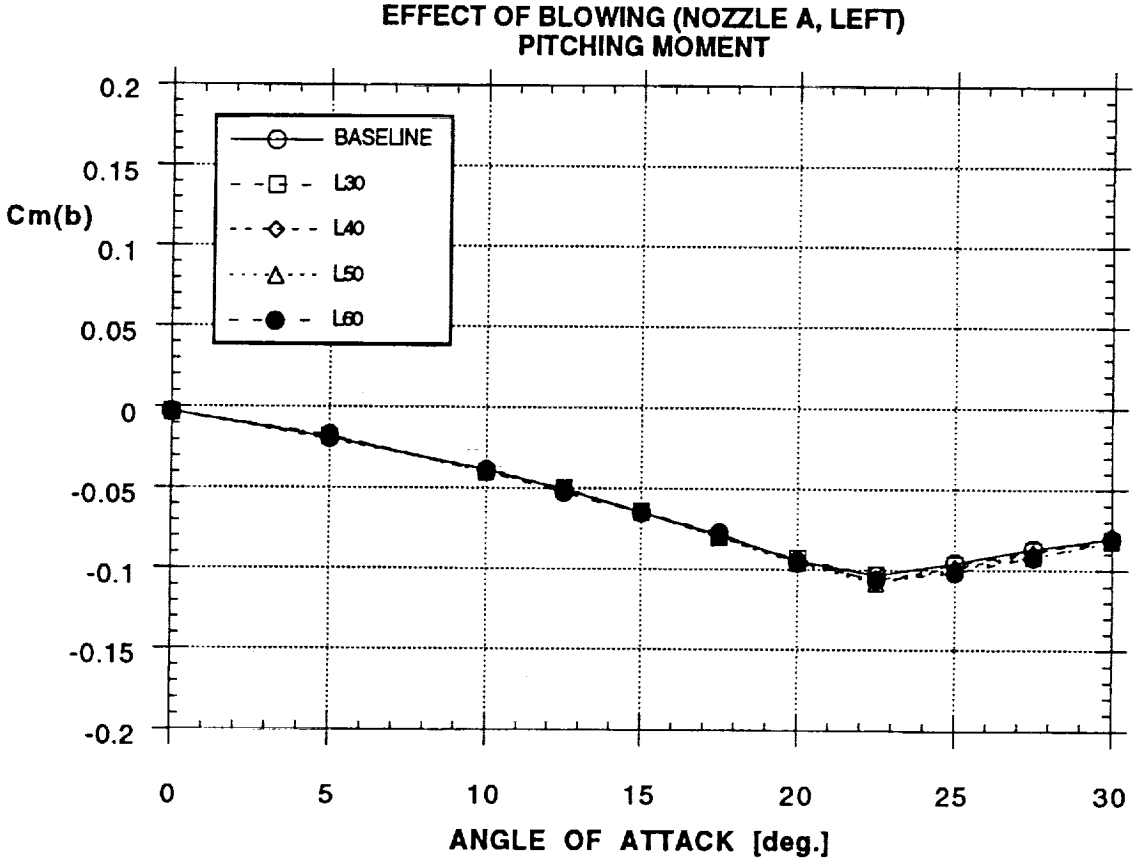

b)

Figure 12 - Effect of Aft Blowing on Forces and Moments (Nozzle A, Left Side, $\beta = 0°$)

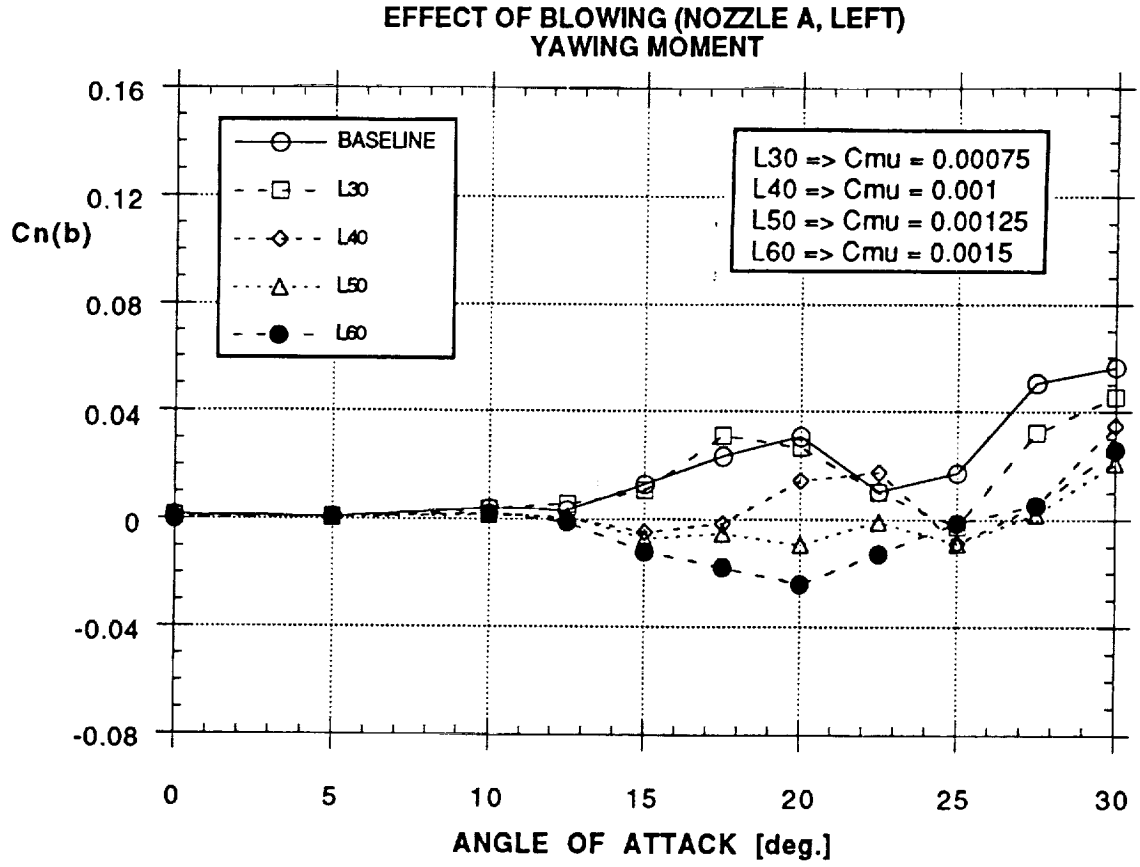

c)

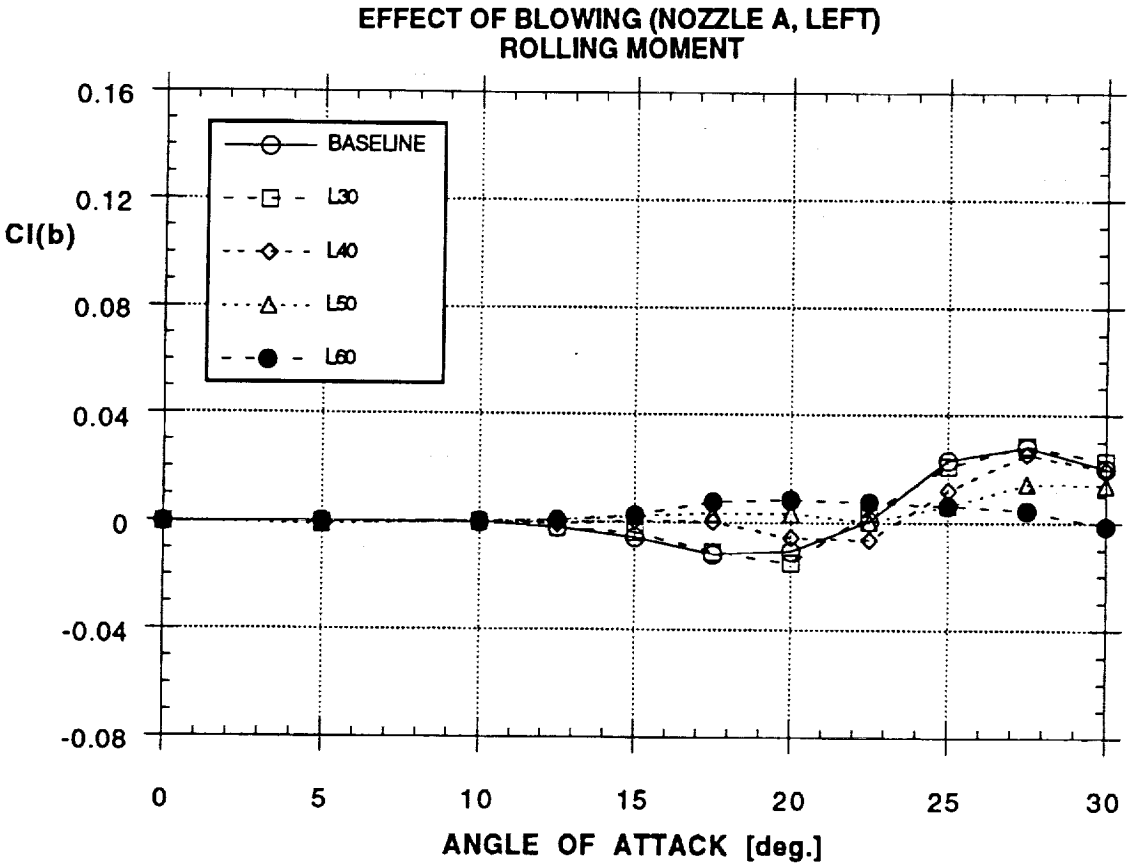

d)

Figure 12 - Continued

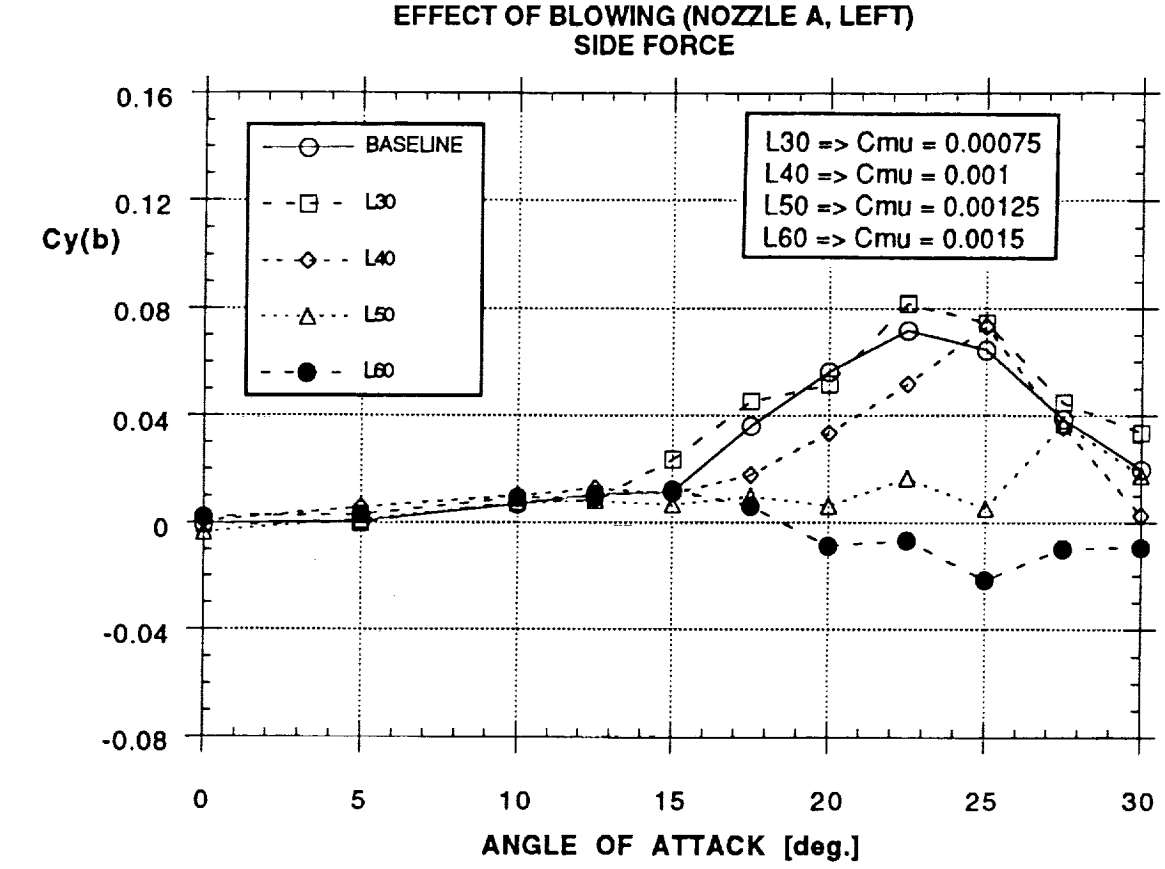

e)

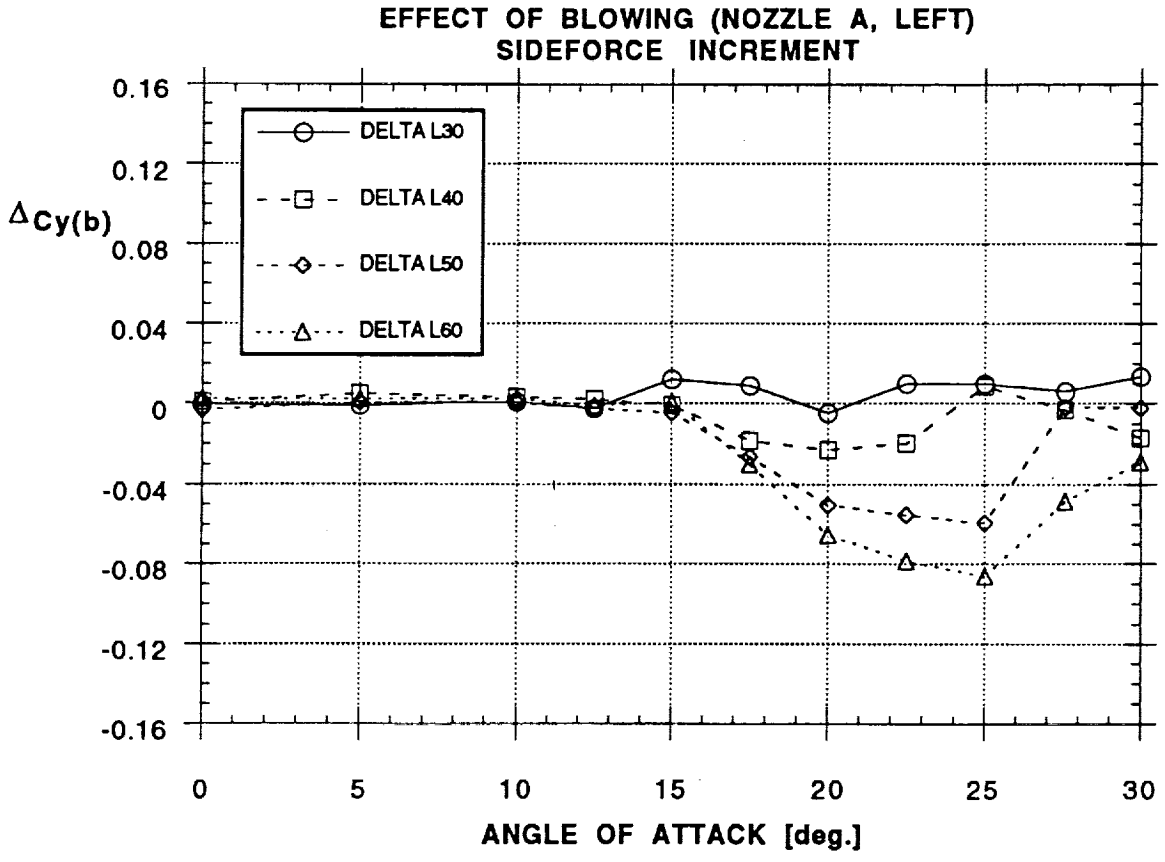

f)

Figure 12 - Continued

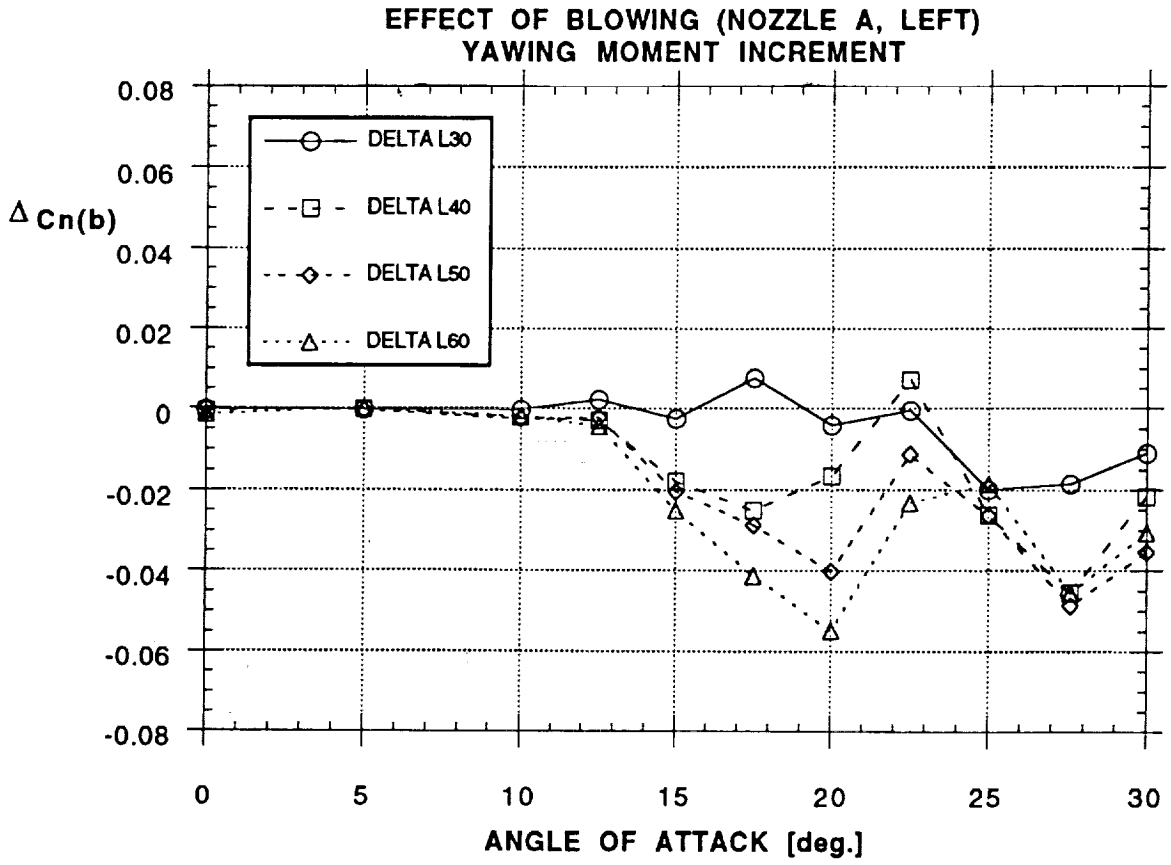

g)

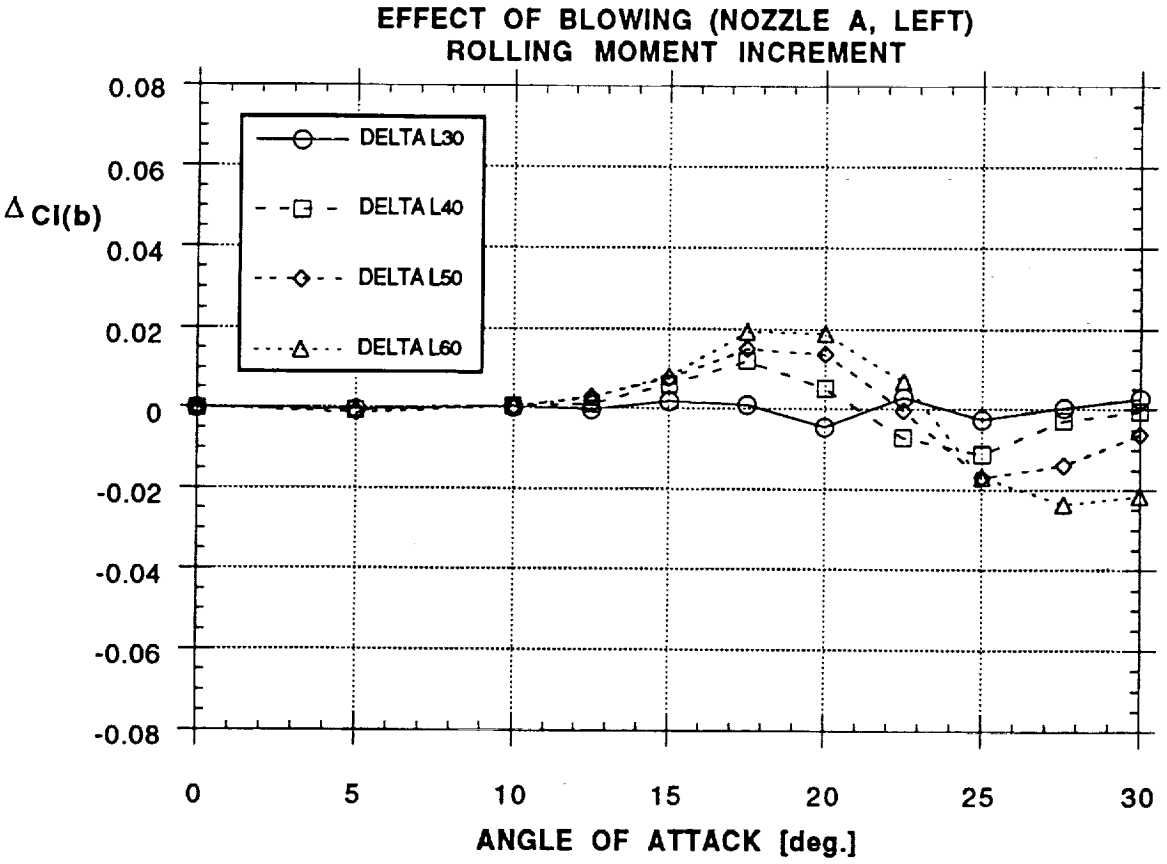

h)

Figure 12 - Concluded

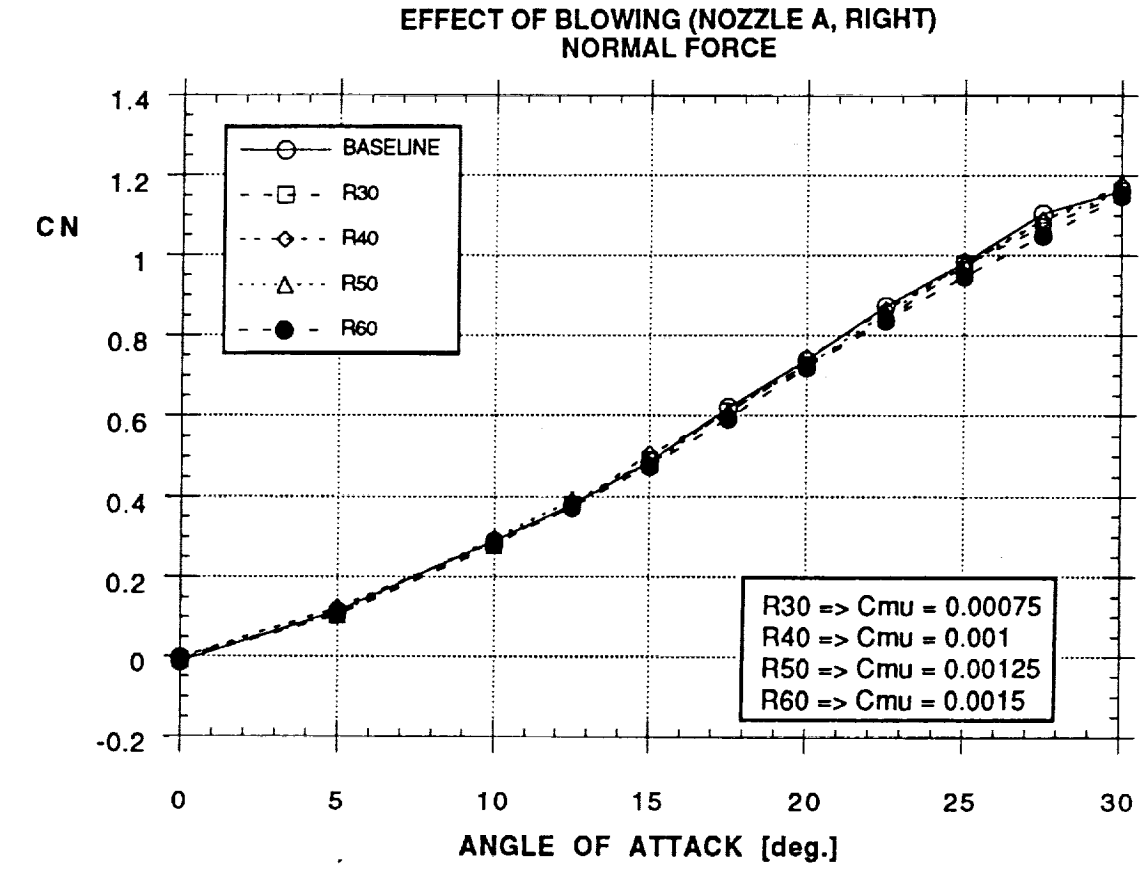

a)

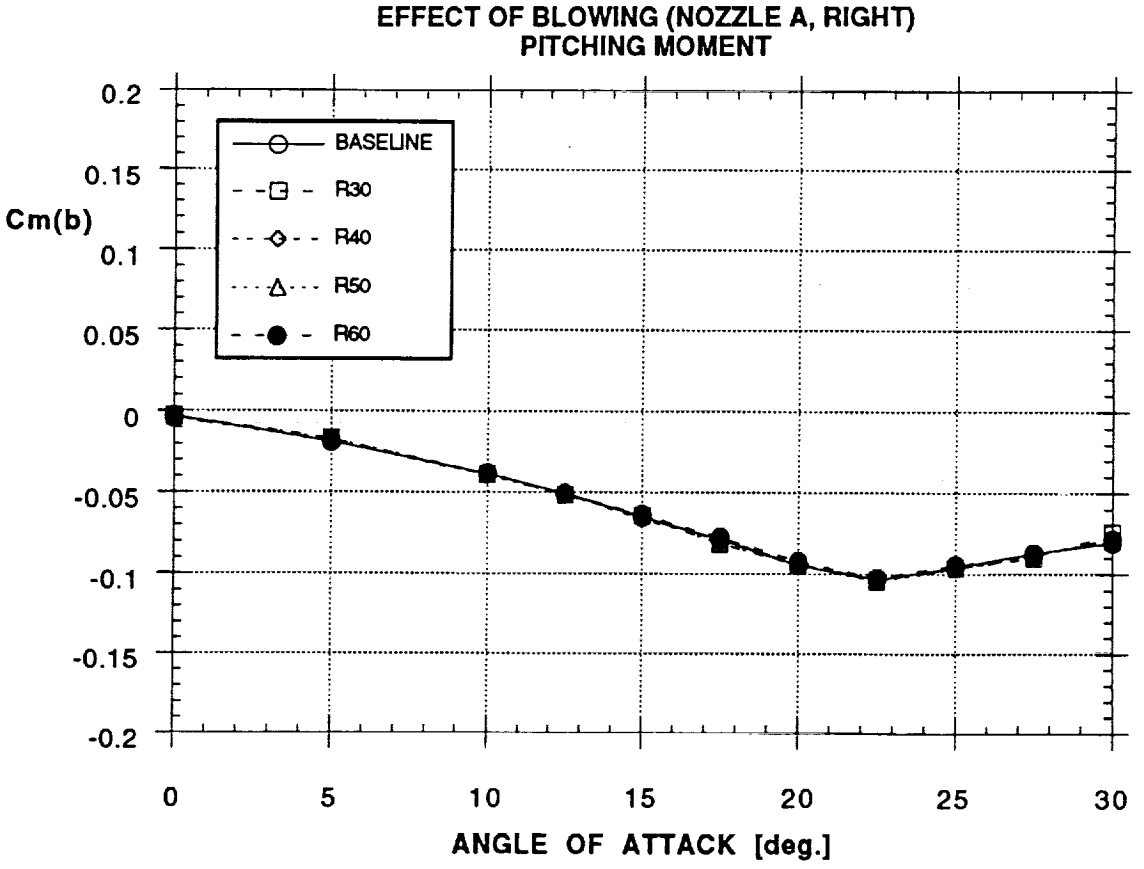

b)

Figure 13 - Effect of Aft Blowing on Forces and Moments (Nozzle A, Right Side, $\beta = 0°$)

c)

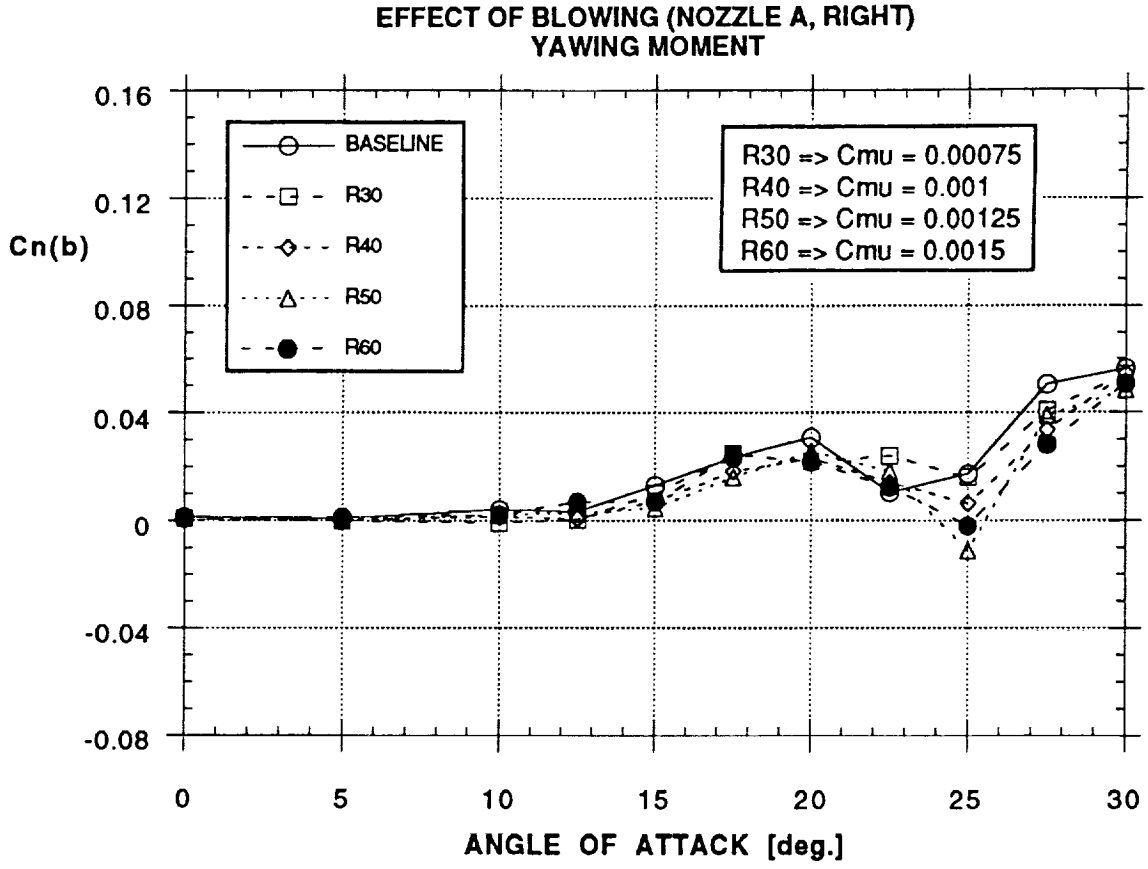

d)

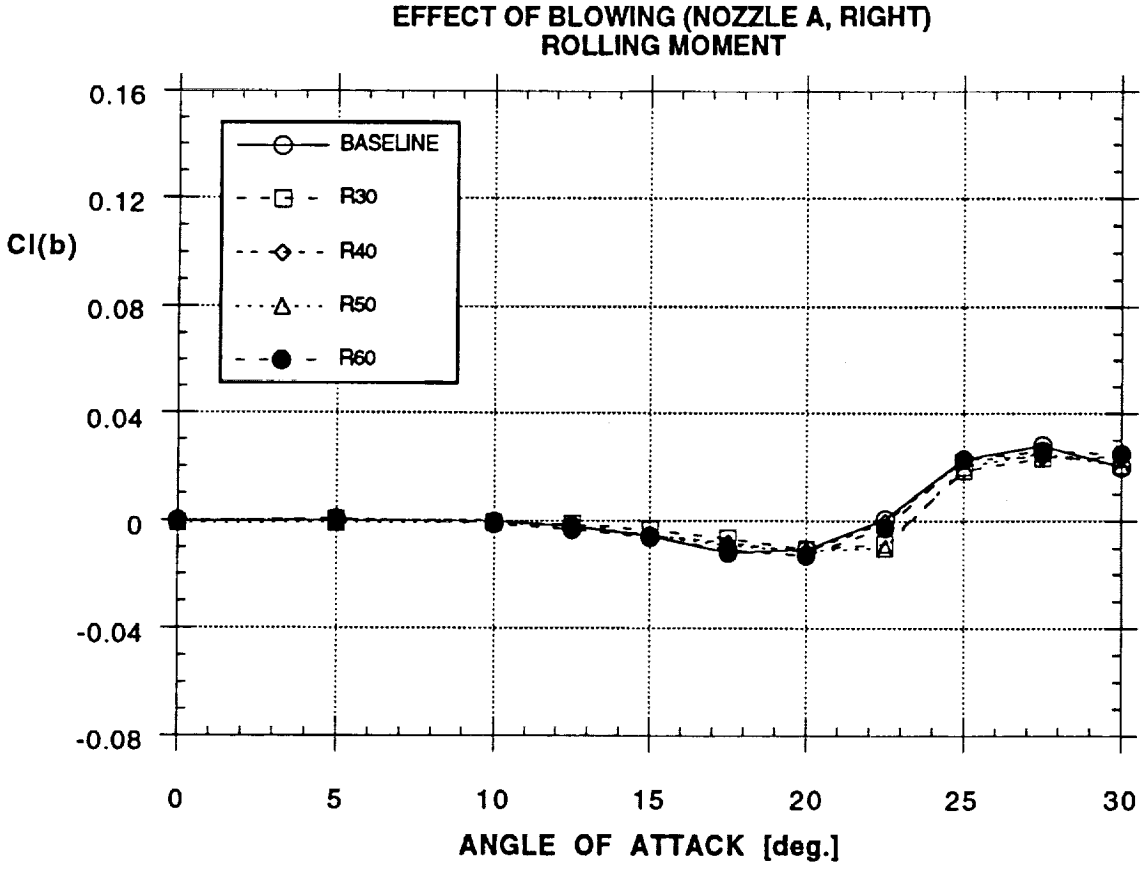

Figure 13 - Continued

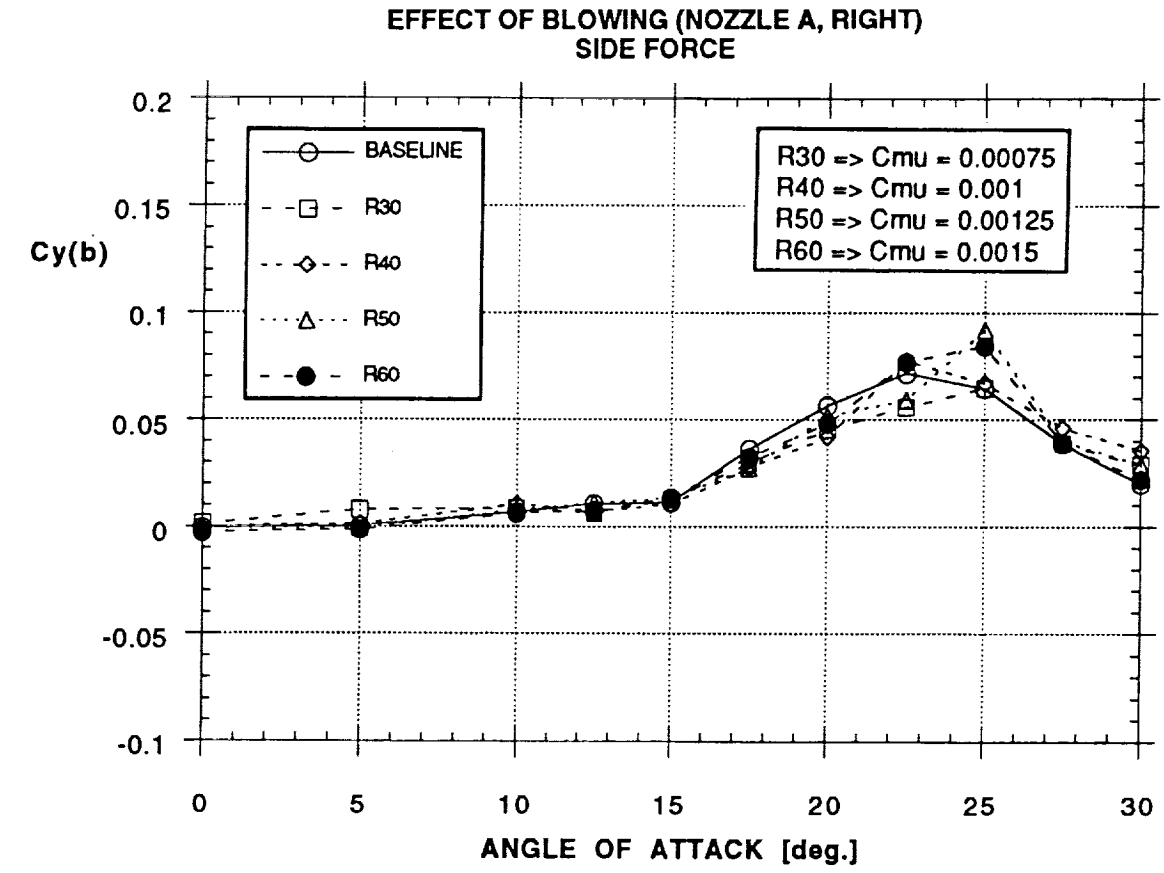

e)

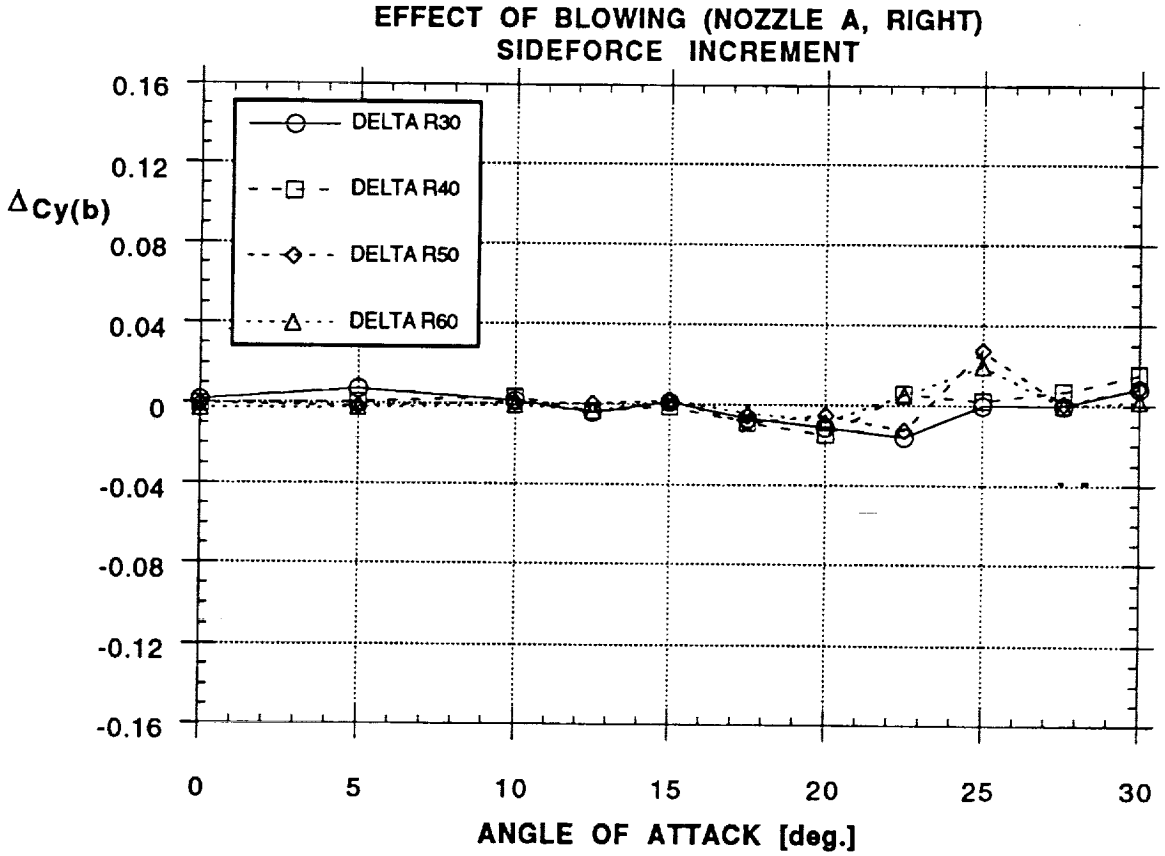

f)

Figure 13 - Continued

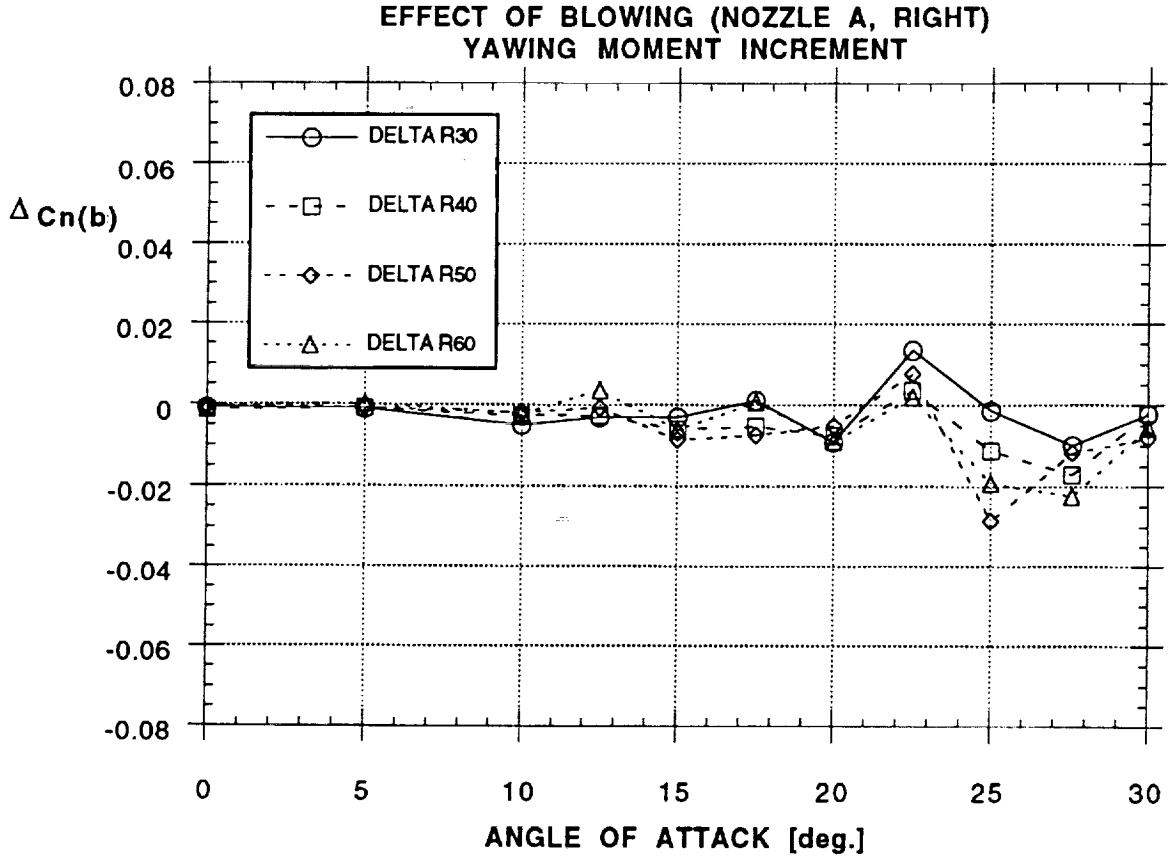

g)

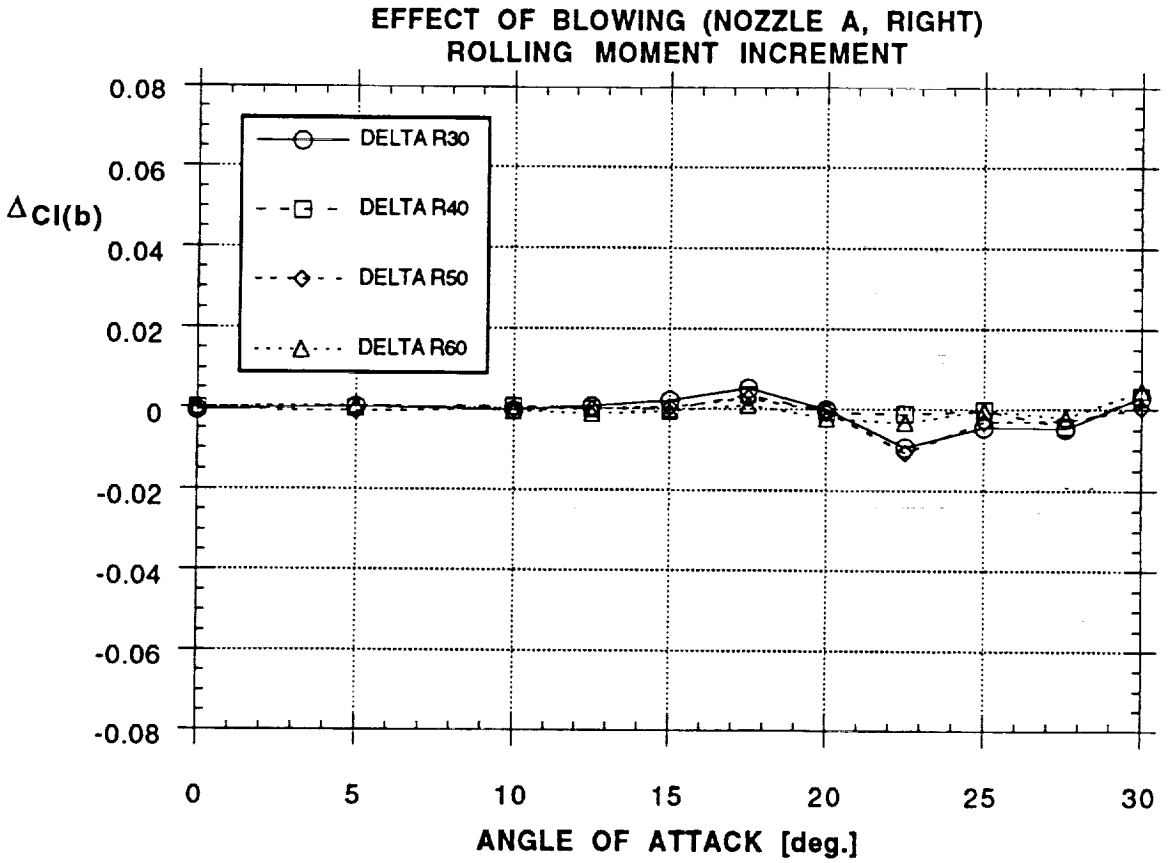

h)

Figure 13 - Concluded

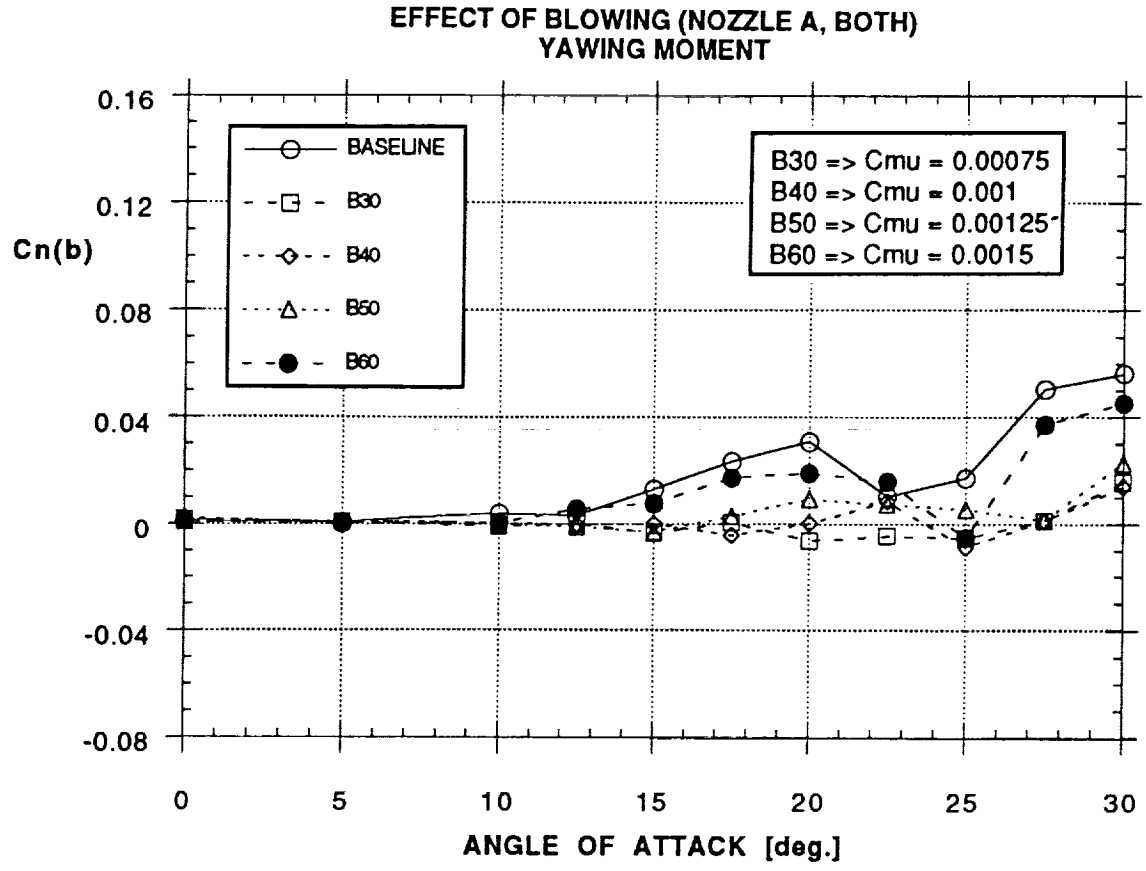

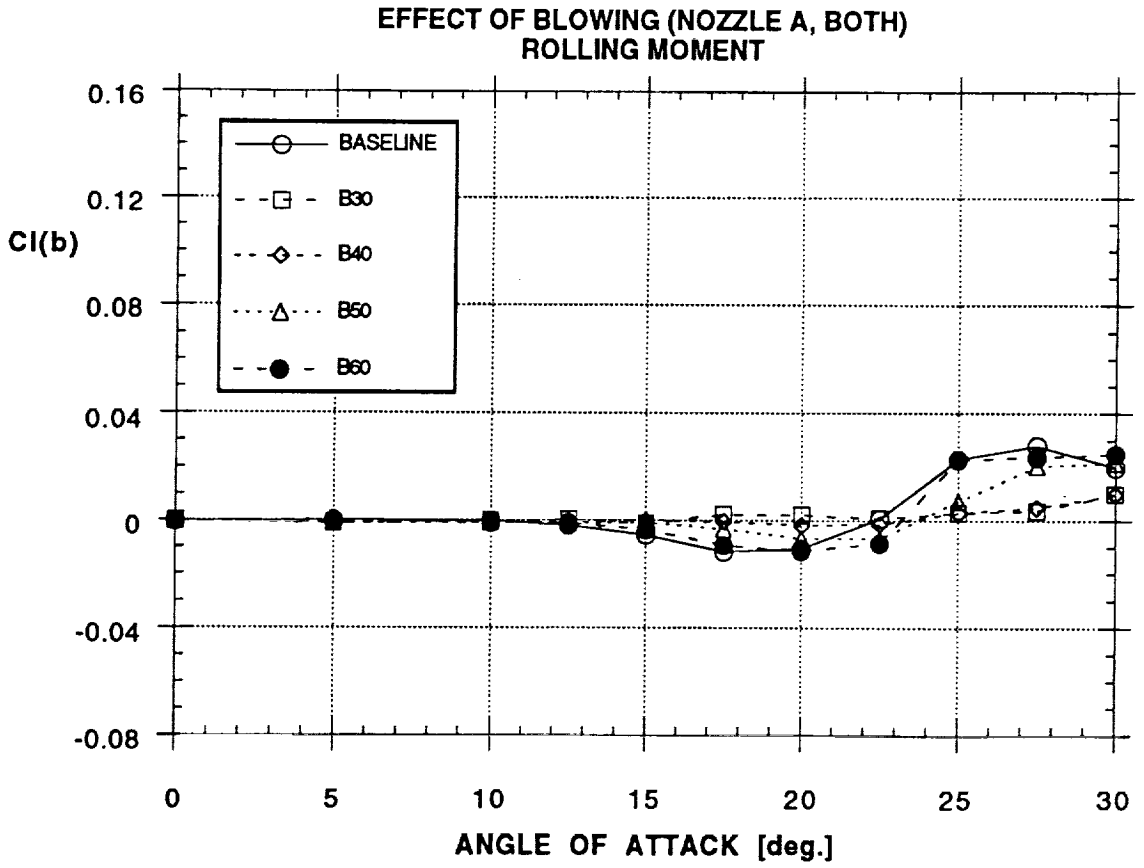

Figure 14 - Effect of Aft Blowing on Forces and Moments (Nozzle A, Both Sides, $\beta = 0°$)

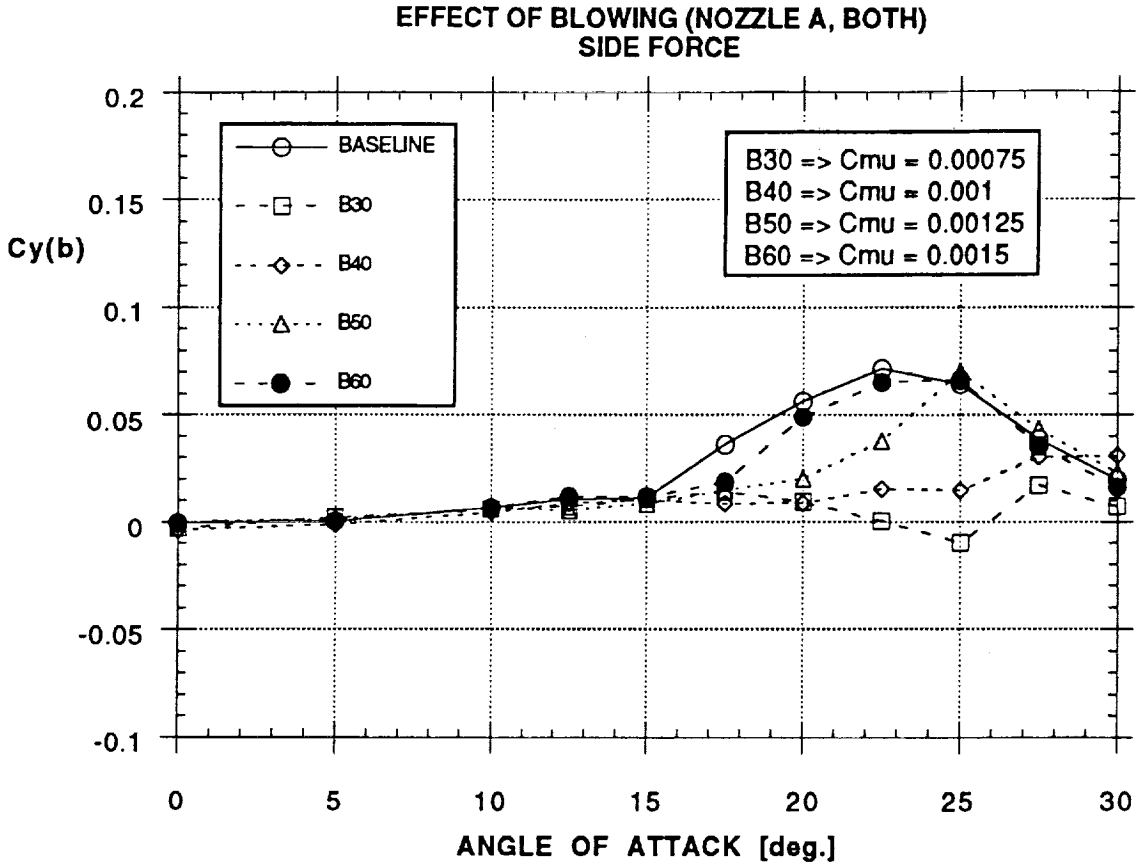

c)

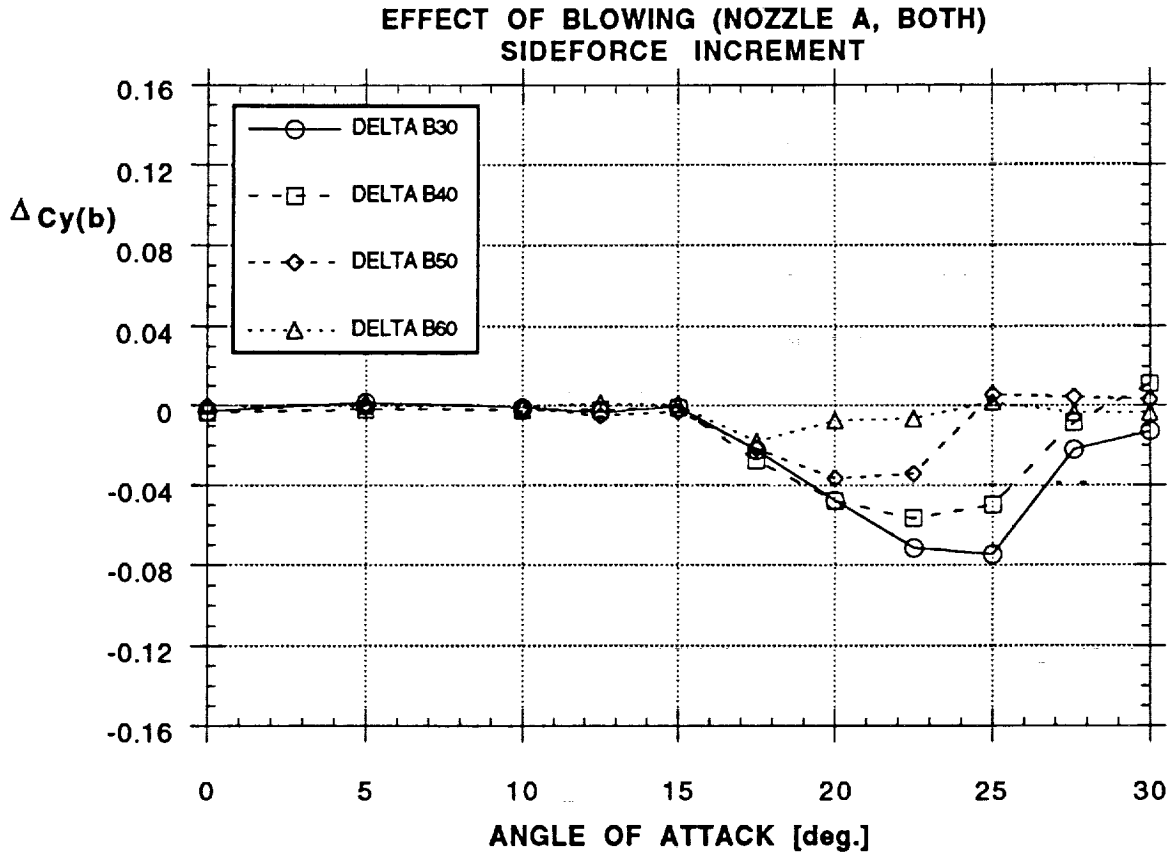

d)

Figure 14 - Continued

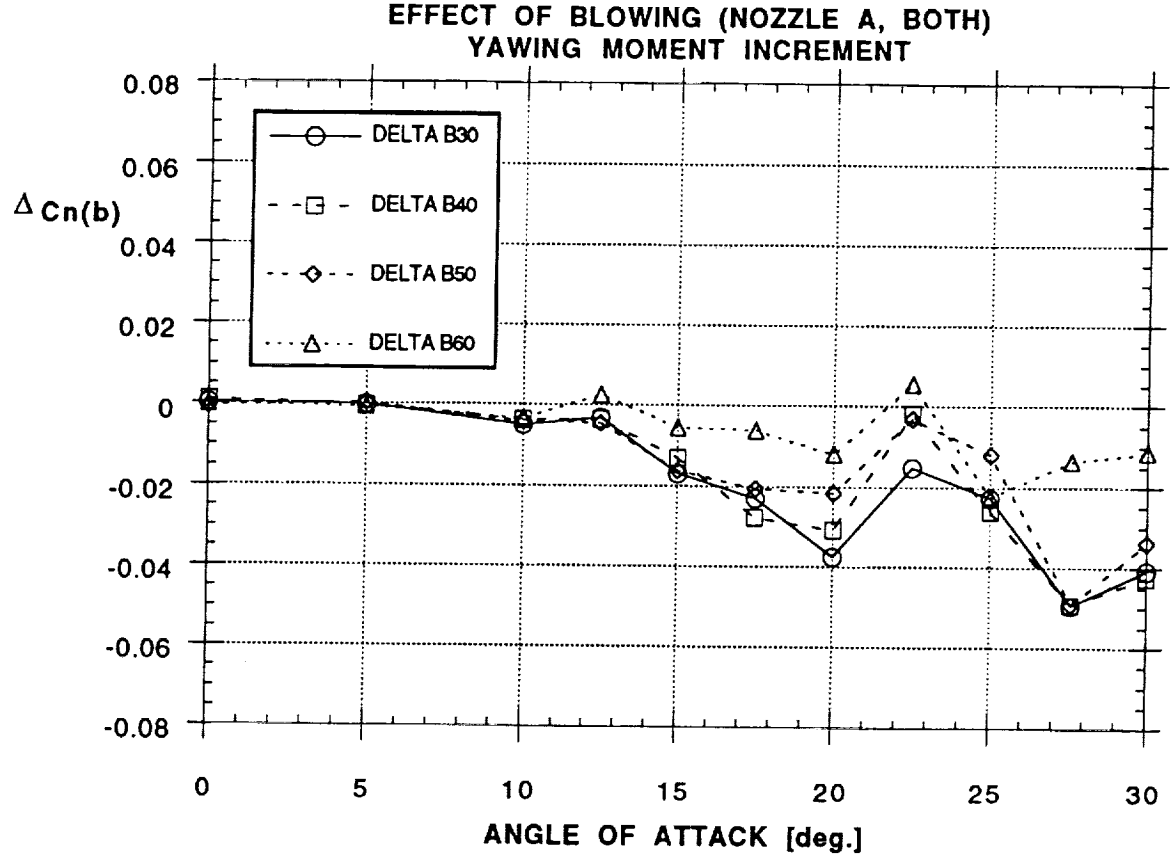

e)

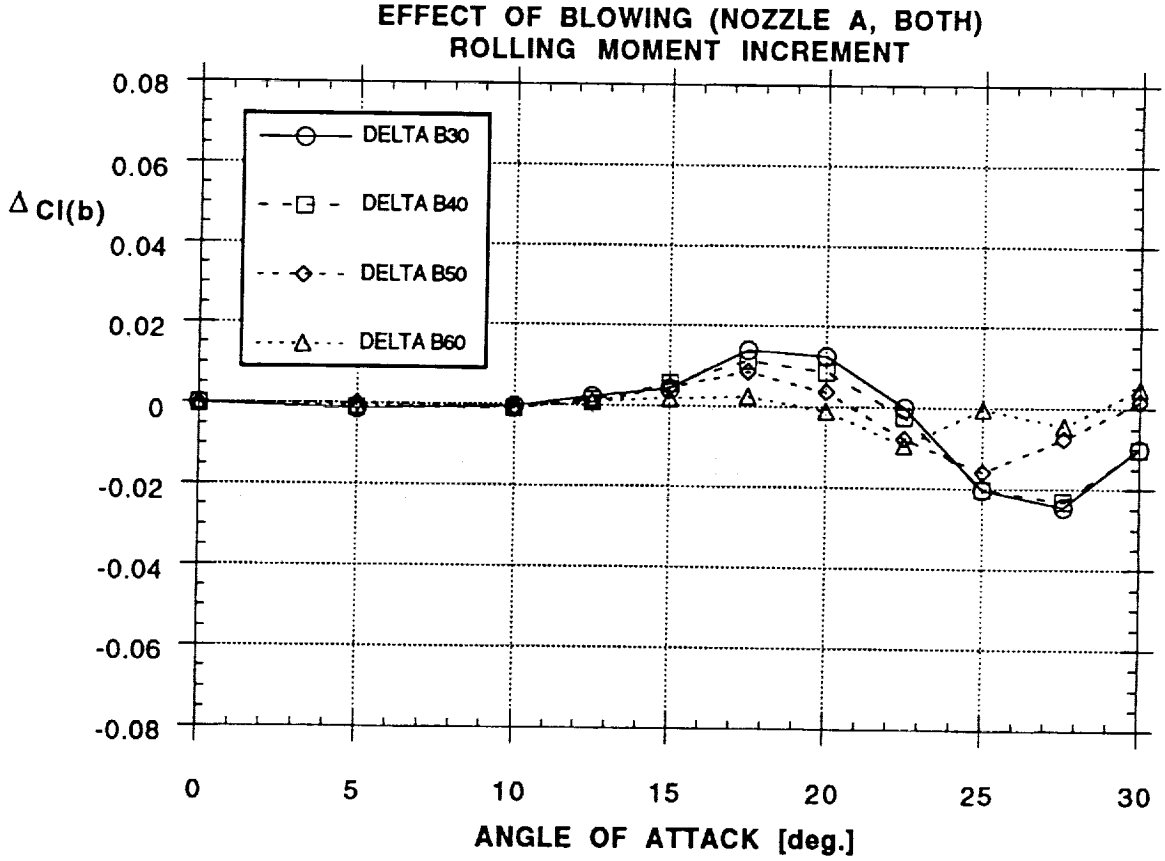

f)

Figure 14 - Concluded

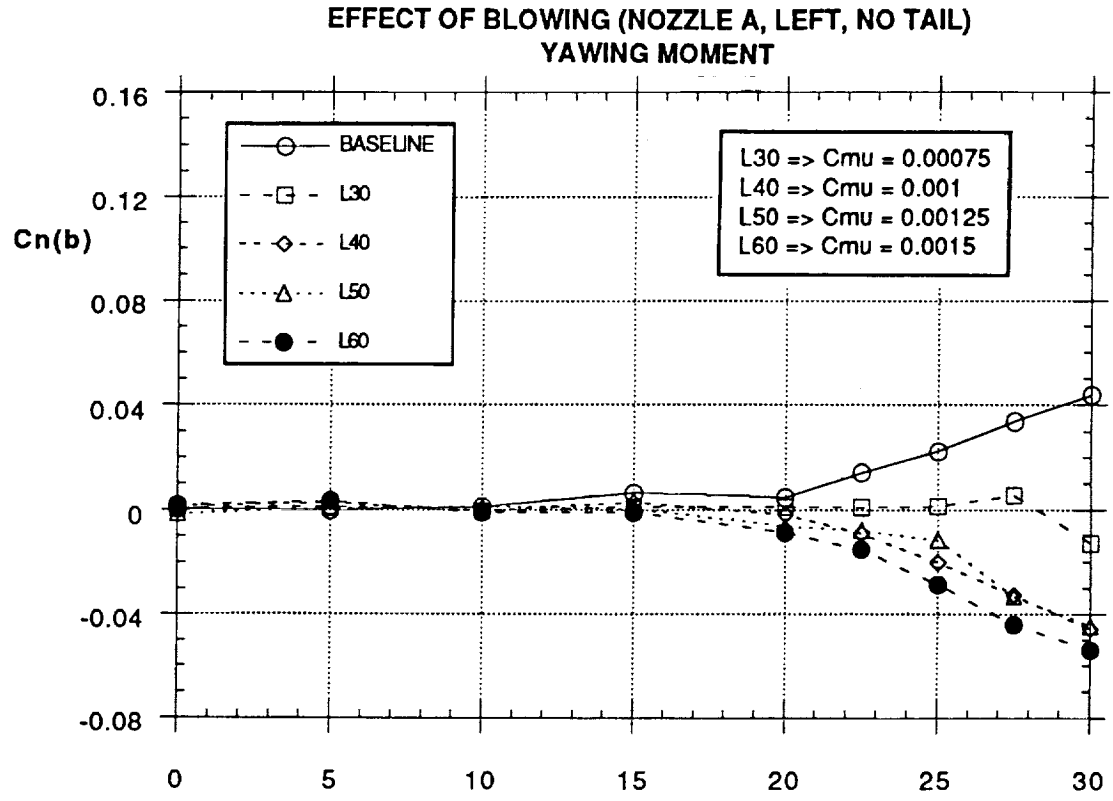

a)

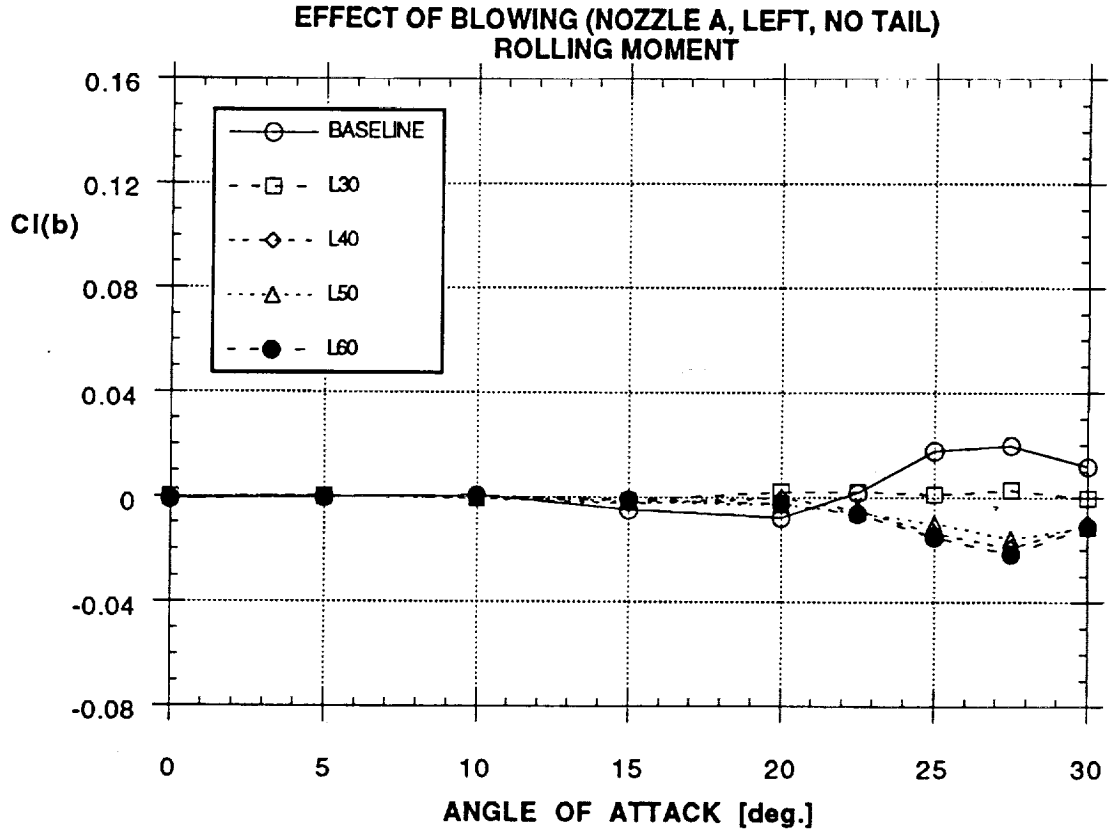

b)

Figure 15 - Effect of Aft Blowing on Forces and Moments (No Tail) (Nozzle A, Left Side, $\beta = 0°$)

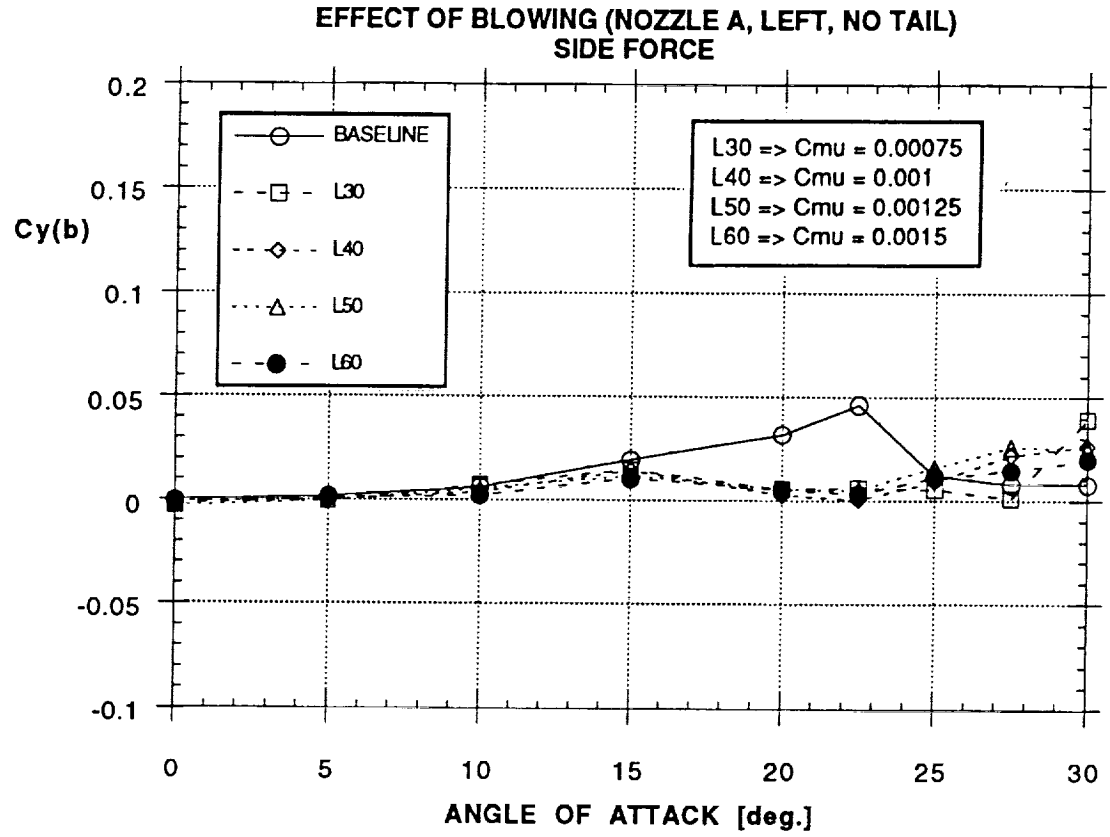

c)

Figure 15 - Concluded

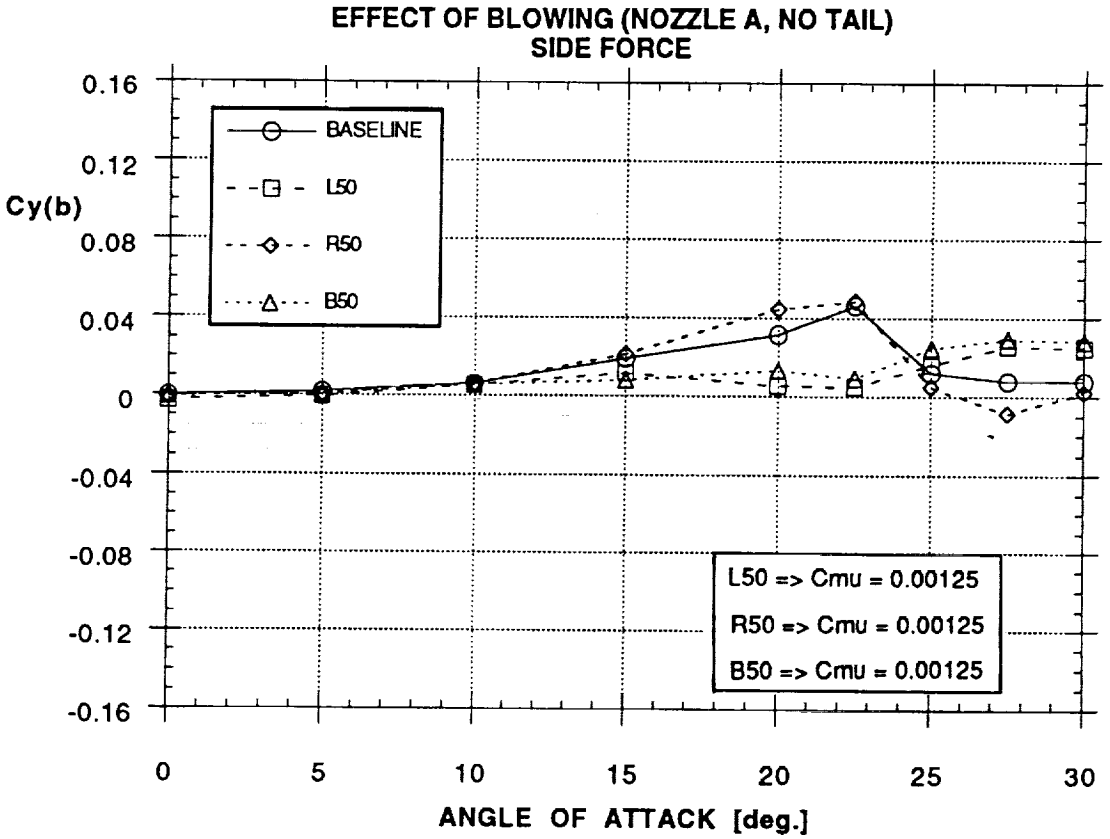

a)

Figure 16 - Effect of Aft Blowing on Forces and Moments (No Tail) (Nozzle A; Left, Right and Both Sides; $\beta = 0°$)

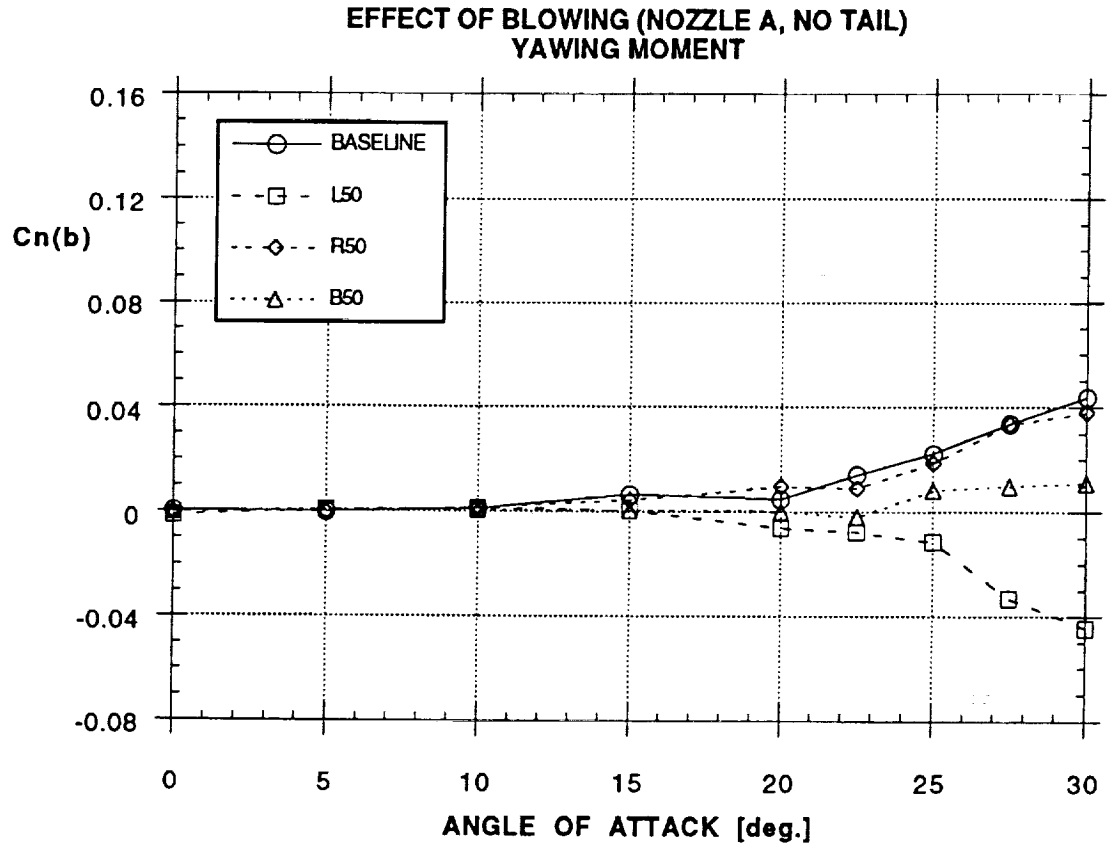

b)

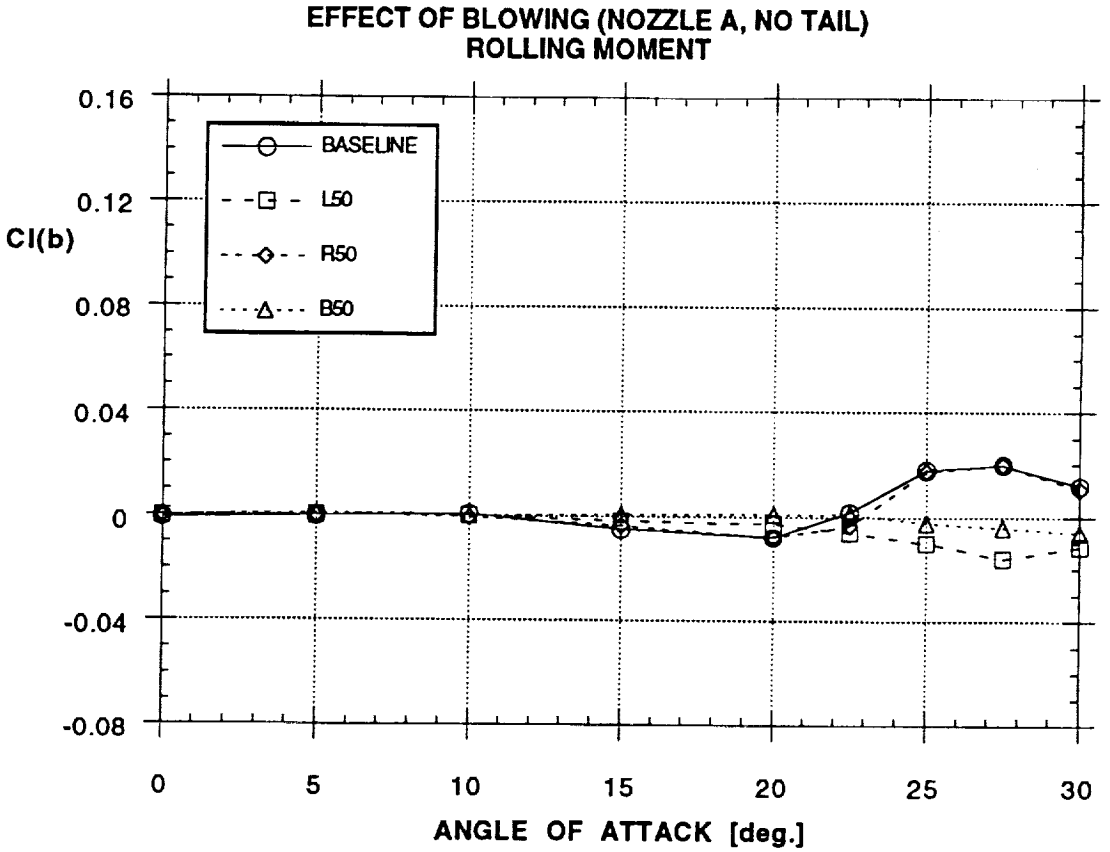

c)

Figure 16 - Concluded

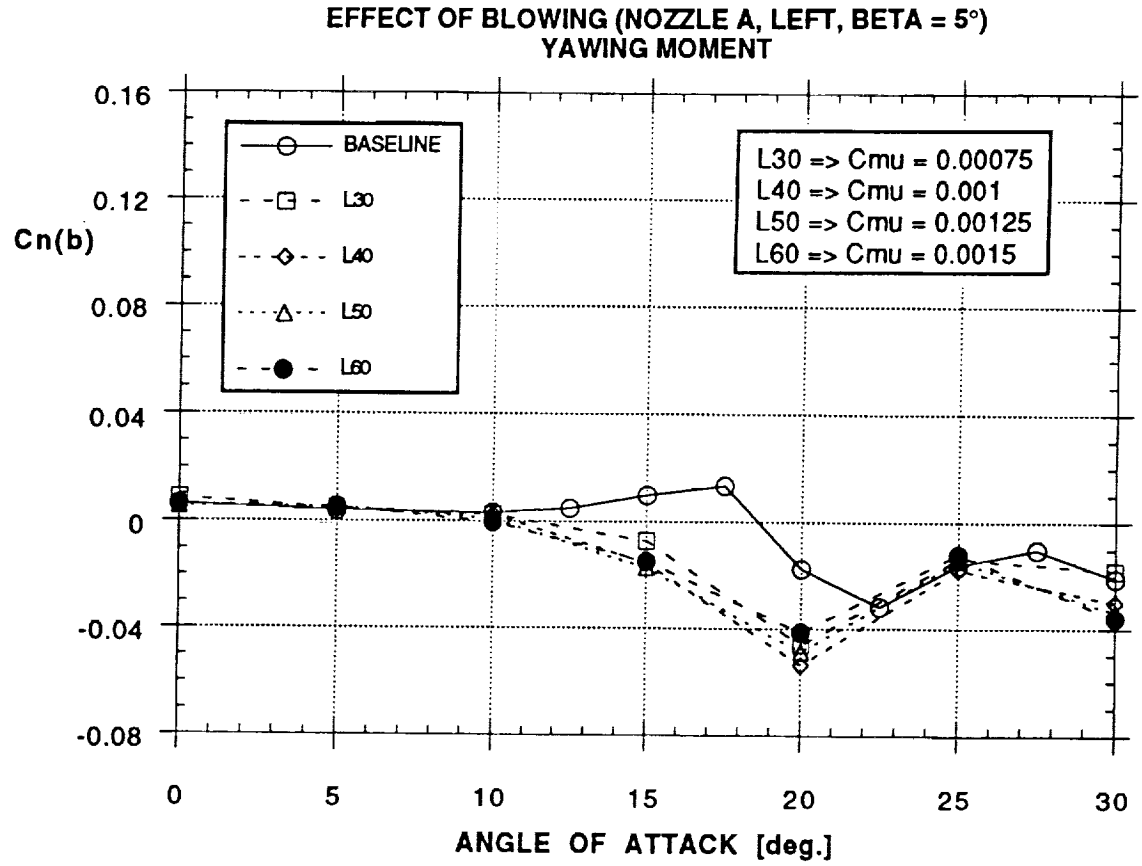

a)

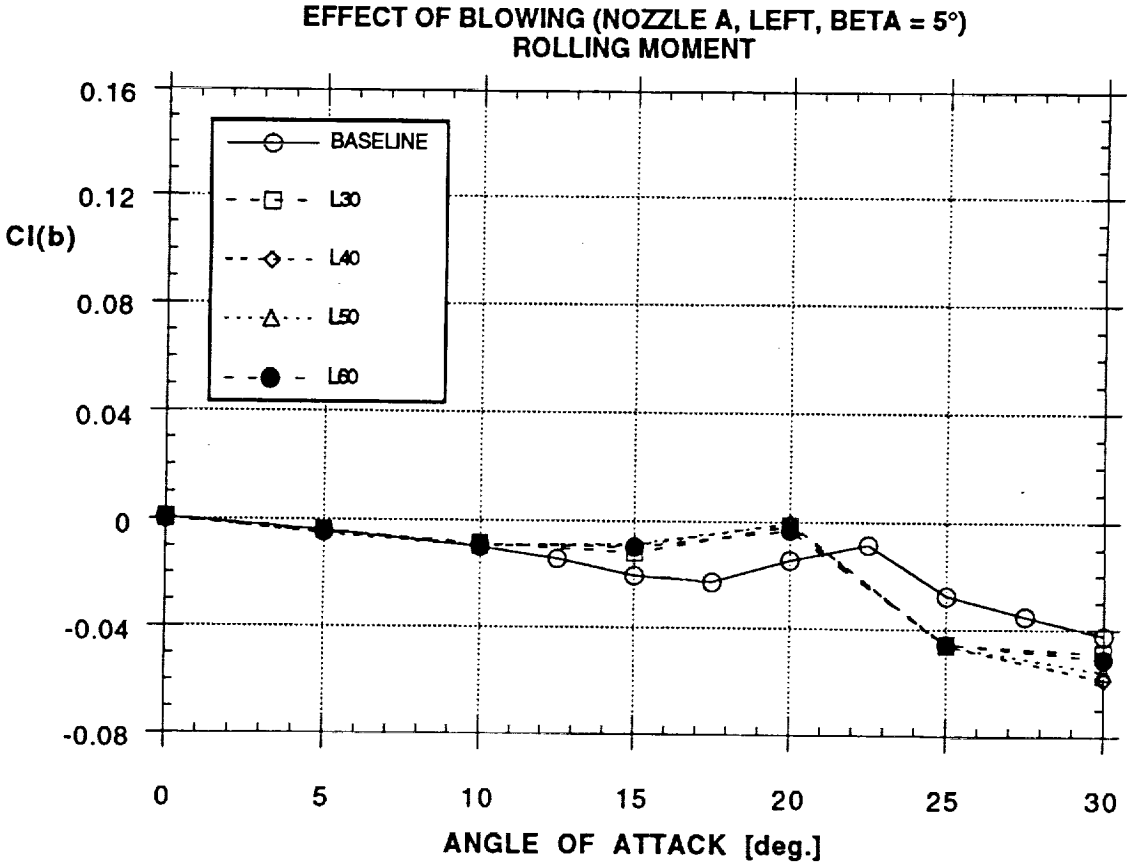

b)

Figure 17 - Effect of Aft Blowing on Forces and Moments (Nozzle A, Left and Right Sides, $\beta = 5°$)

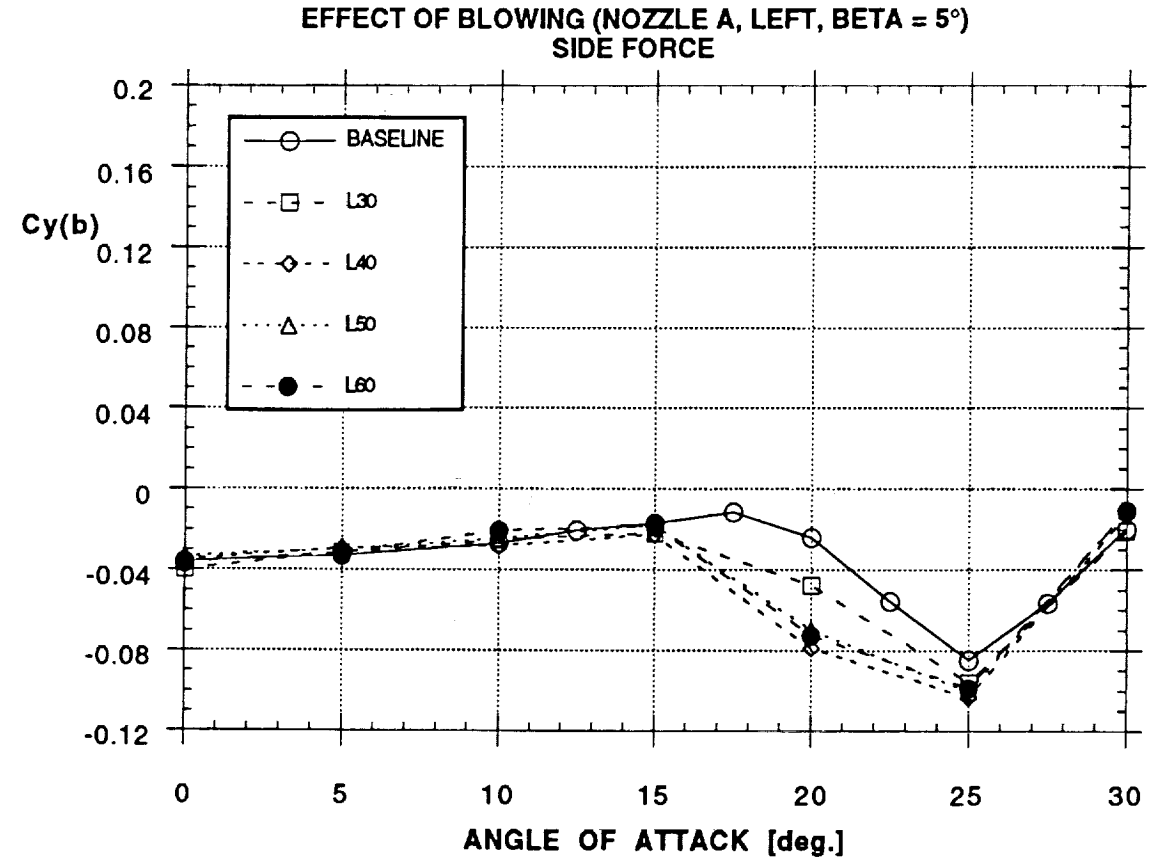

c)

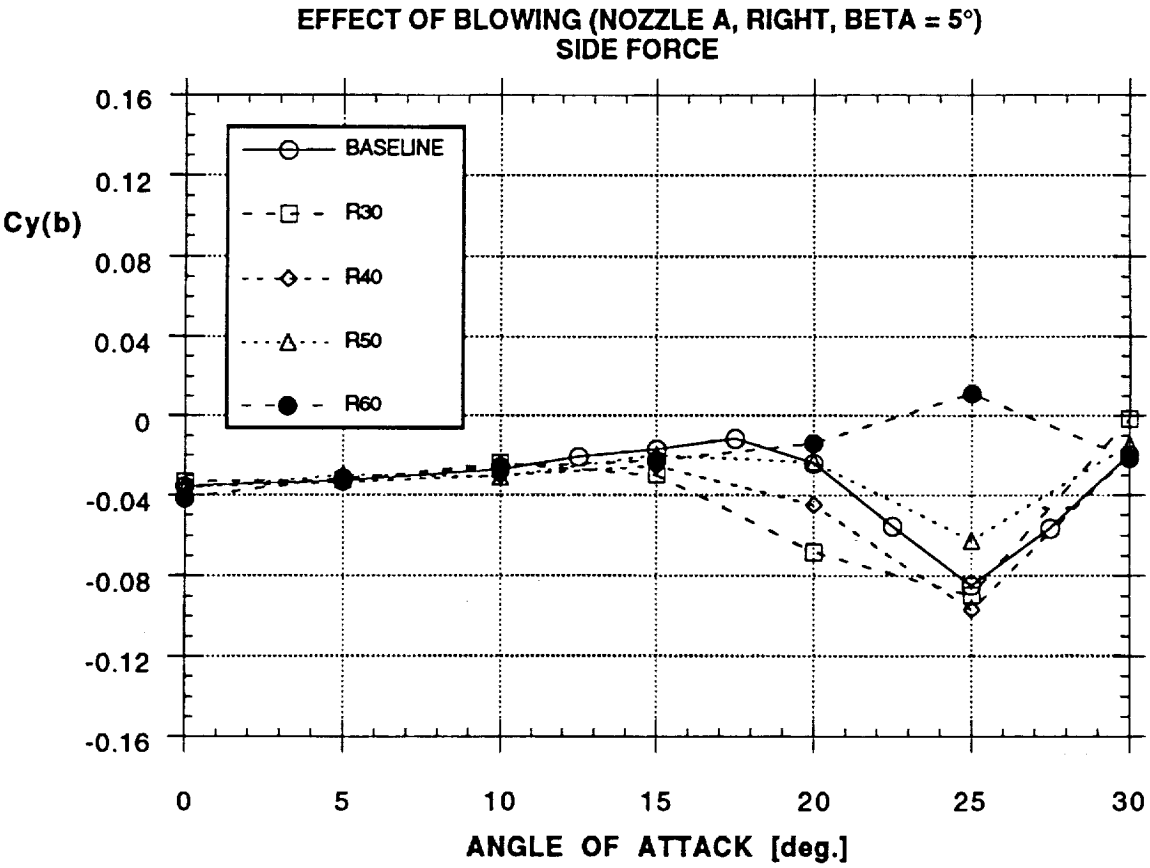

d)

Figure 17 - Continued

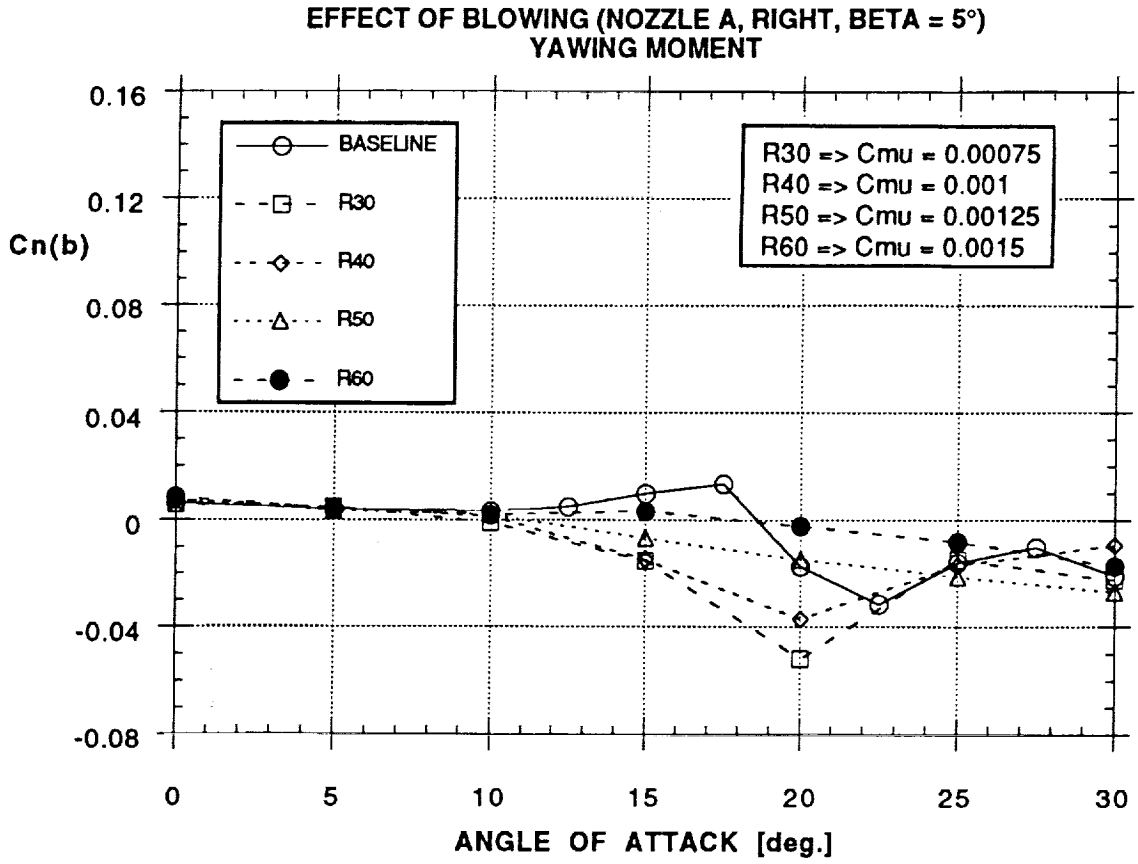

e)

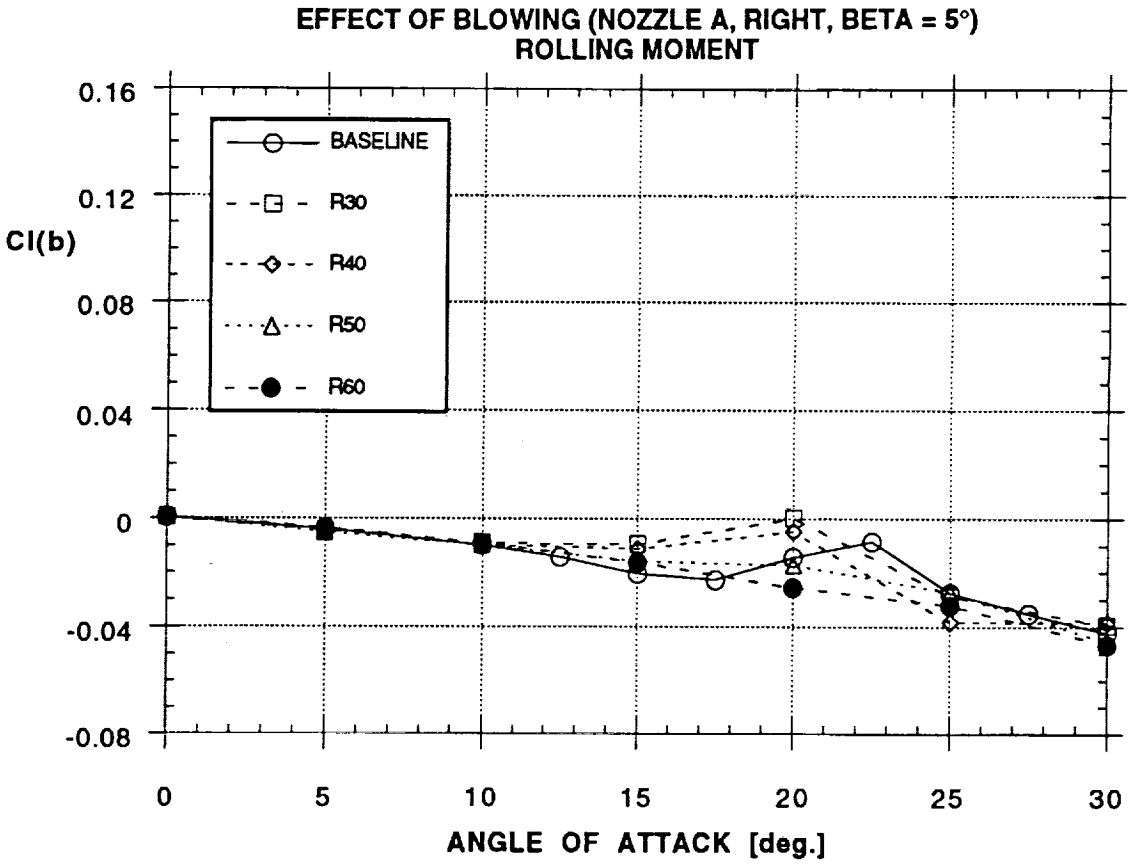

f)

Figure 17 - Concluded

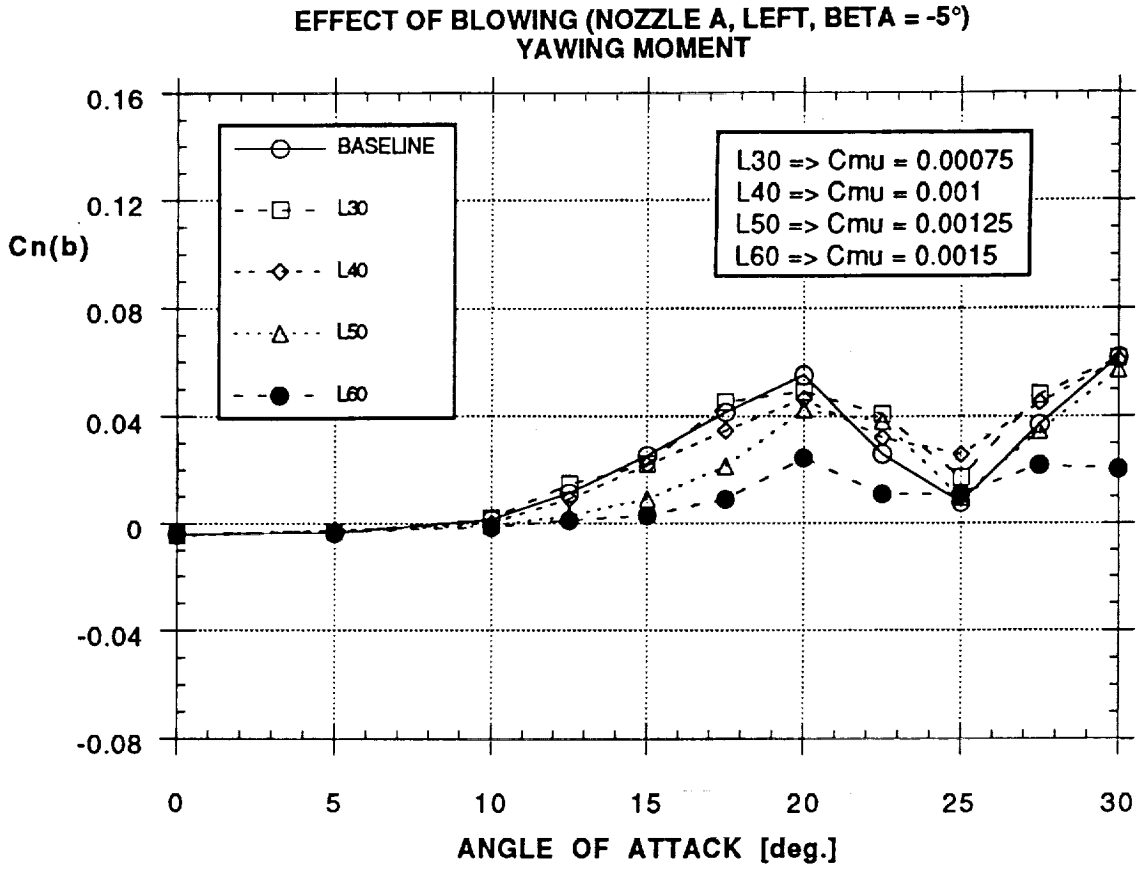

a)

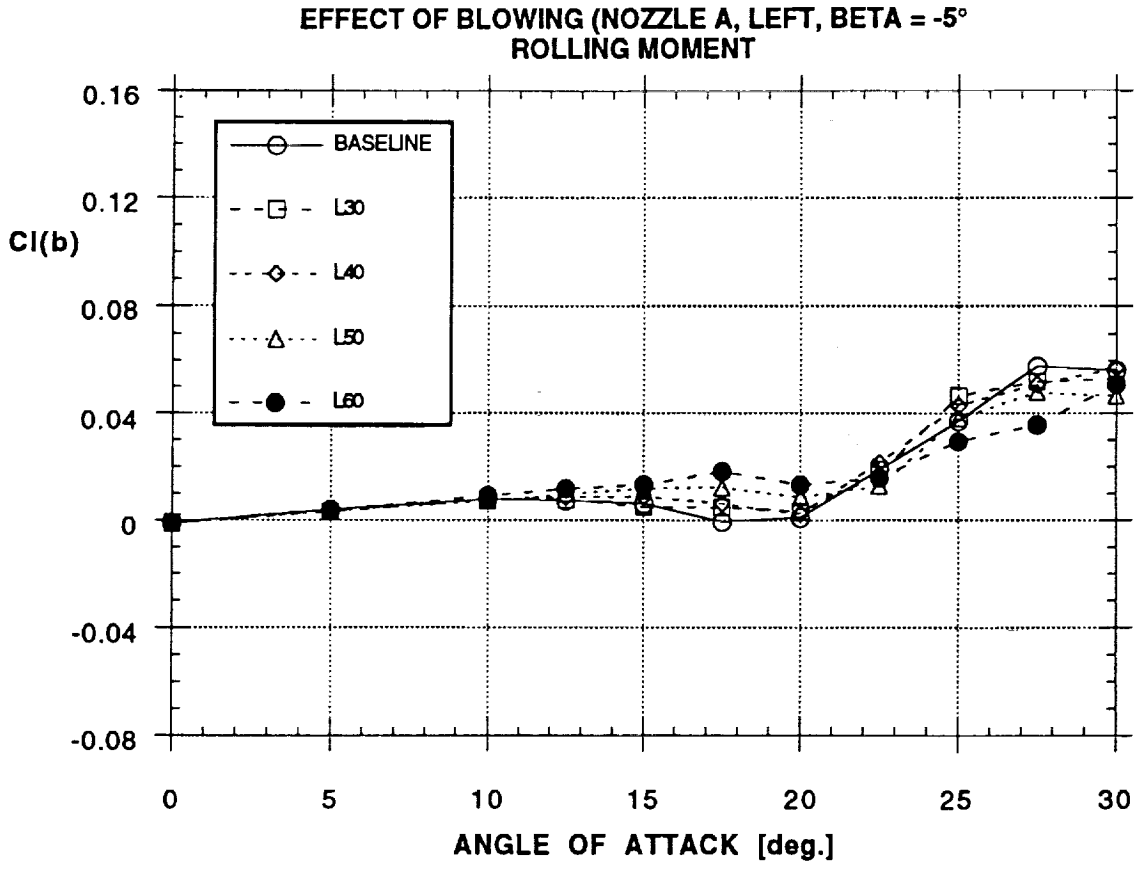

b)

Figure 18 - Effect of Aft Blowing on Forces and Moments (Nozzle A, Left and Right Sides, $\beta = -5°$)

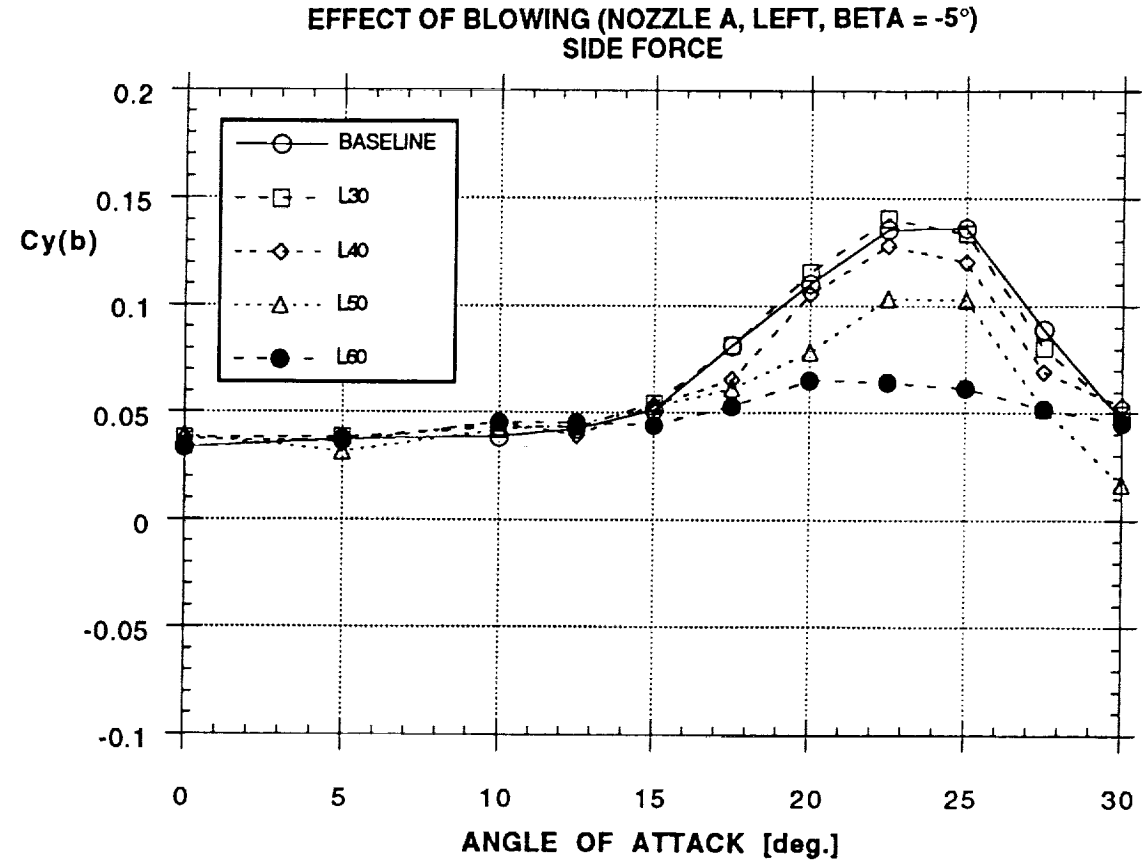

c)

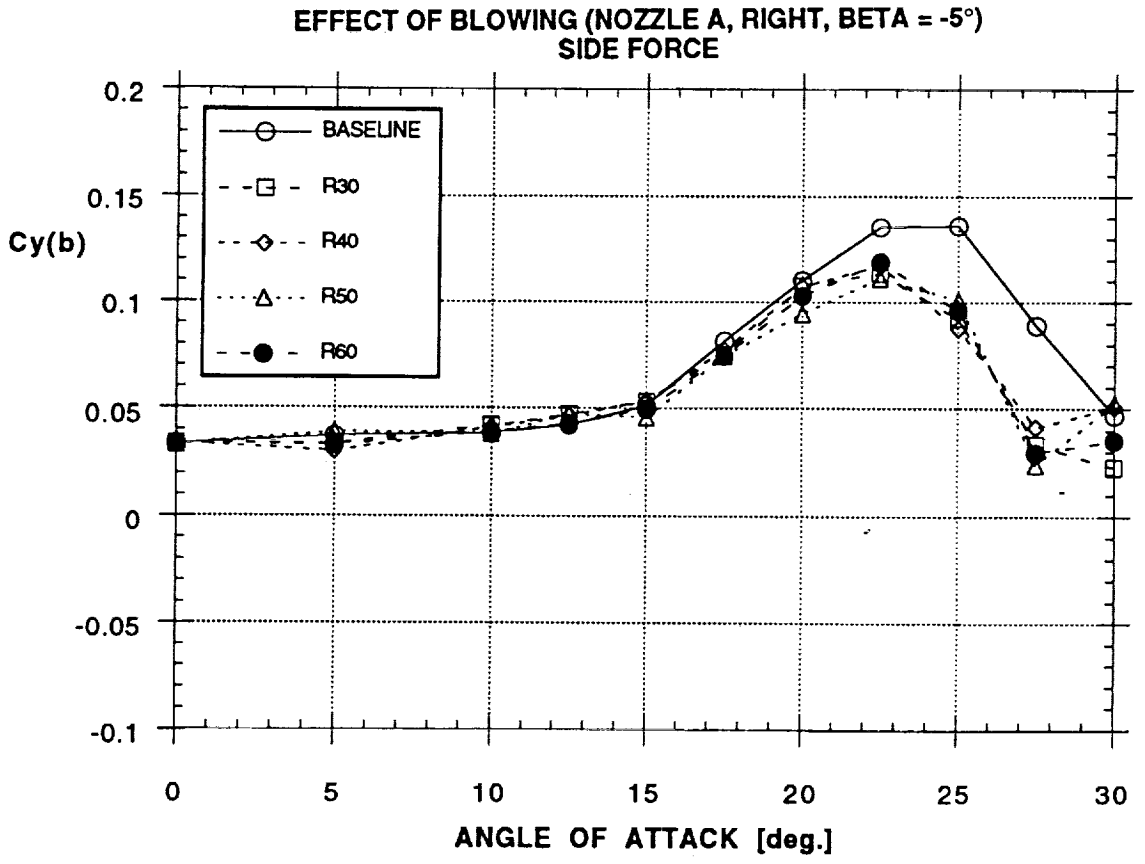

d)

Figure 18 - Continued

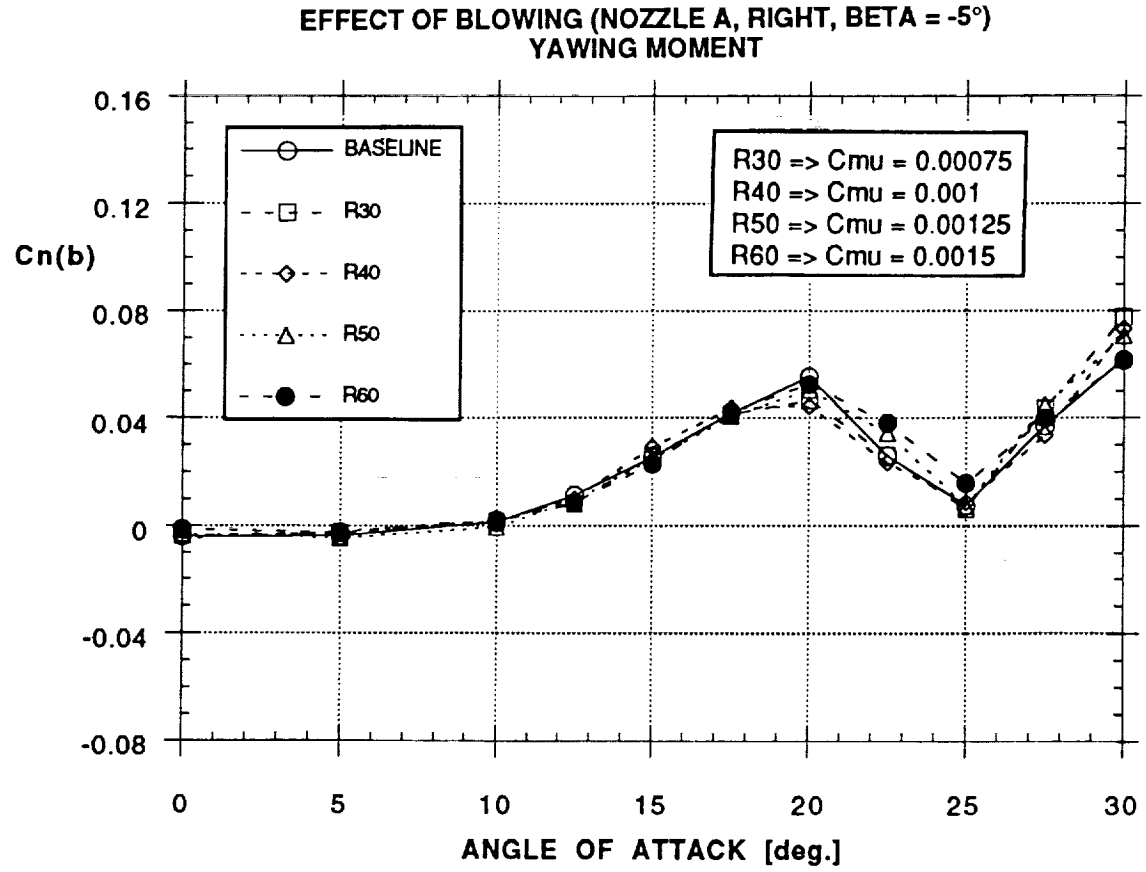

e)

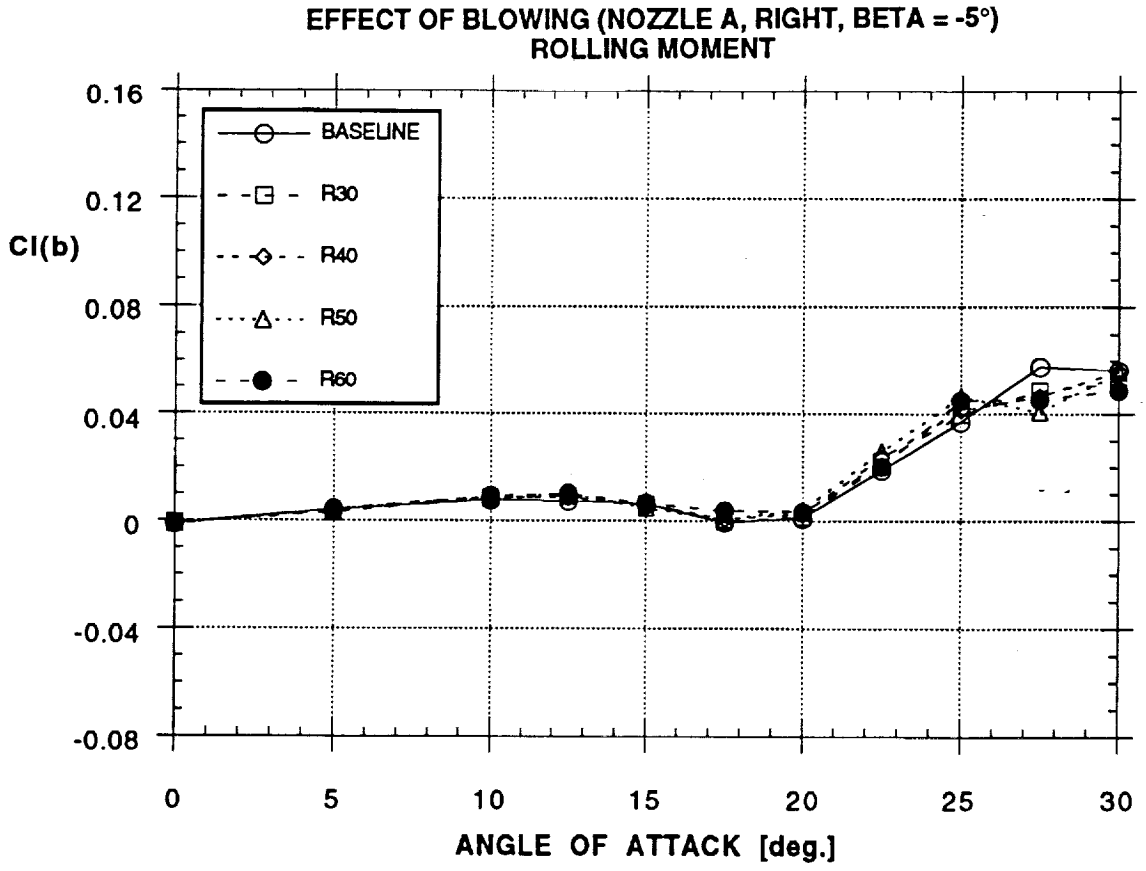

f)

Figure 18 - Concluded

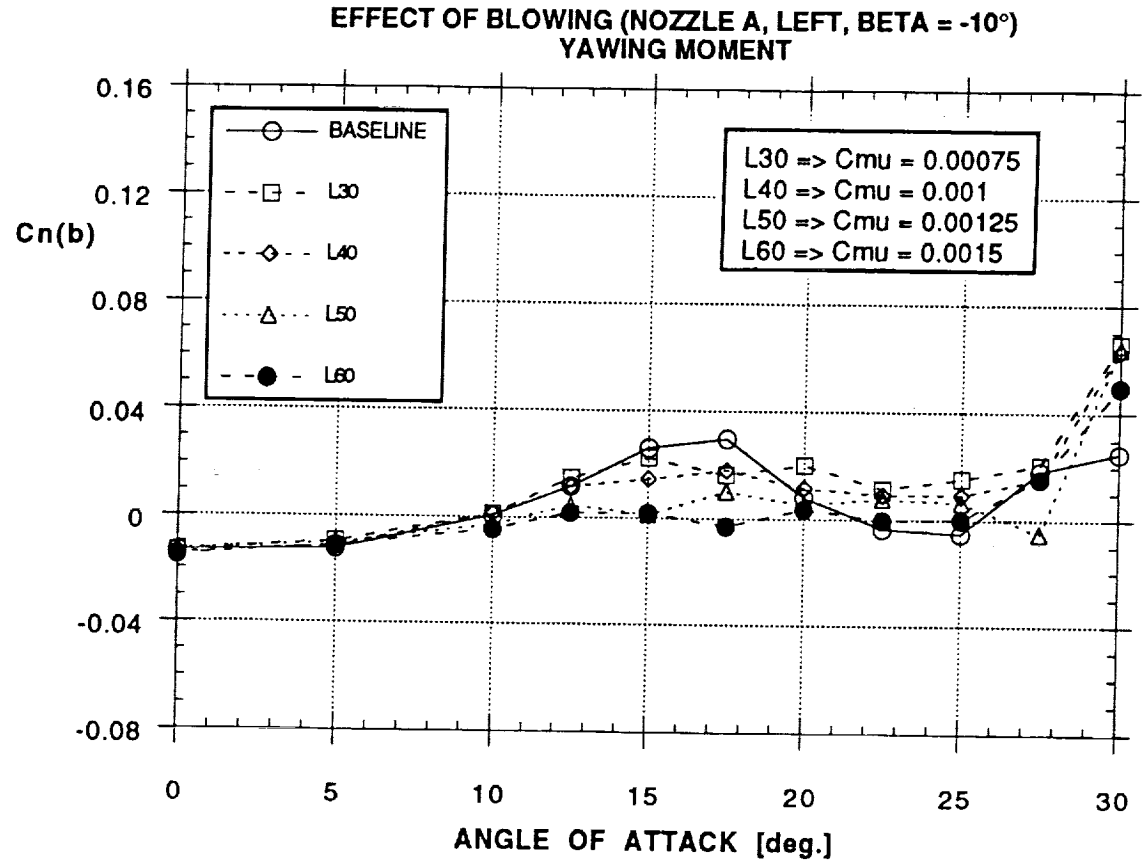

a)

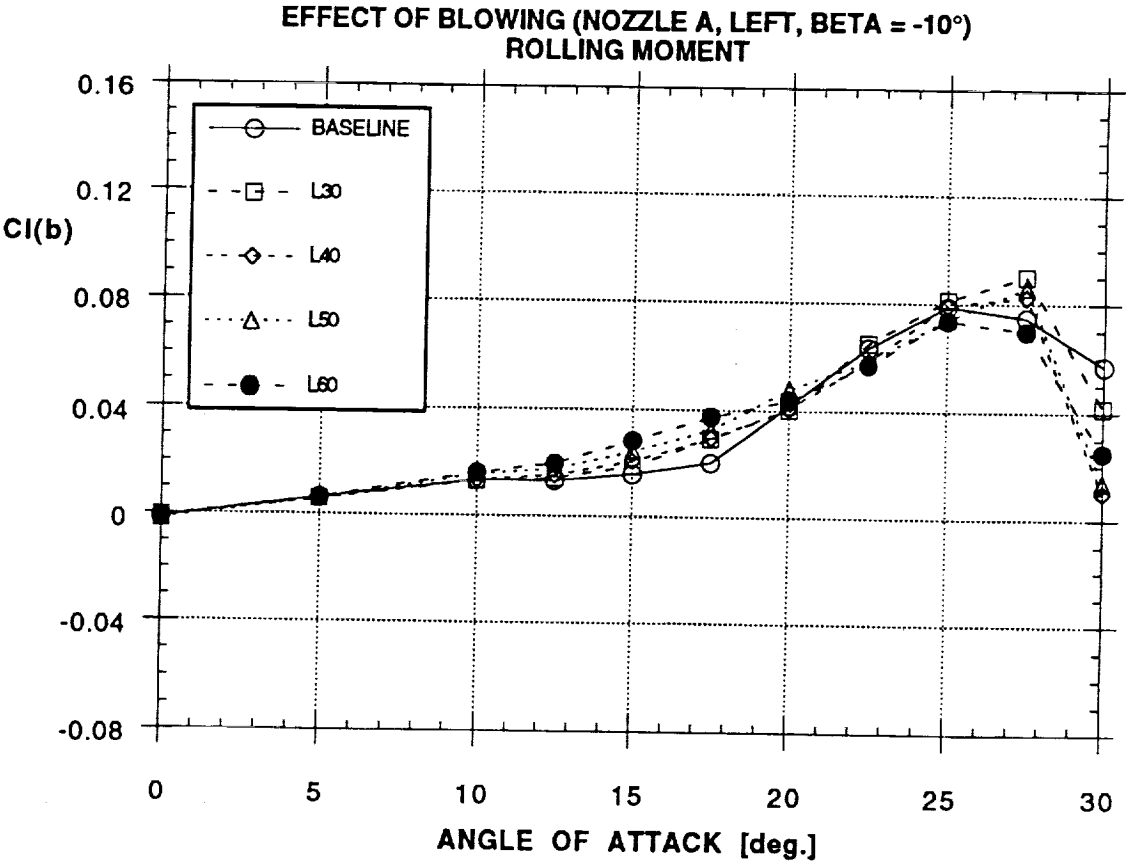

b)

Figure 19 - Effect of Aft Blowing on Forces and Moments (Nozzle A, Left and Right Sides, $\beta = -10°$)

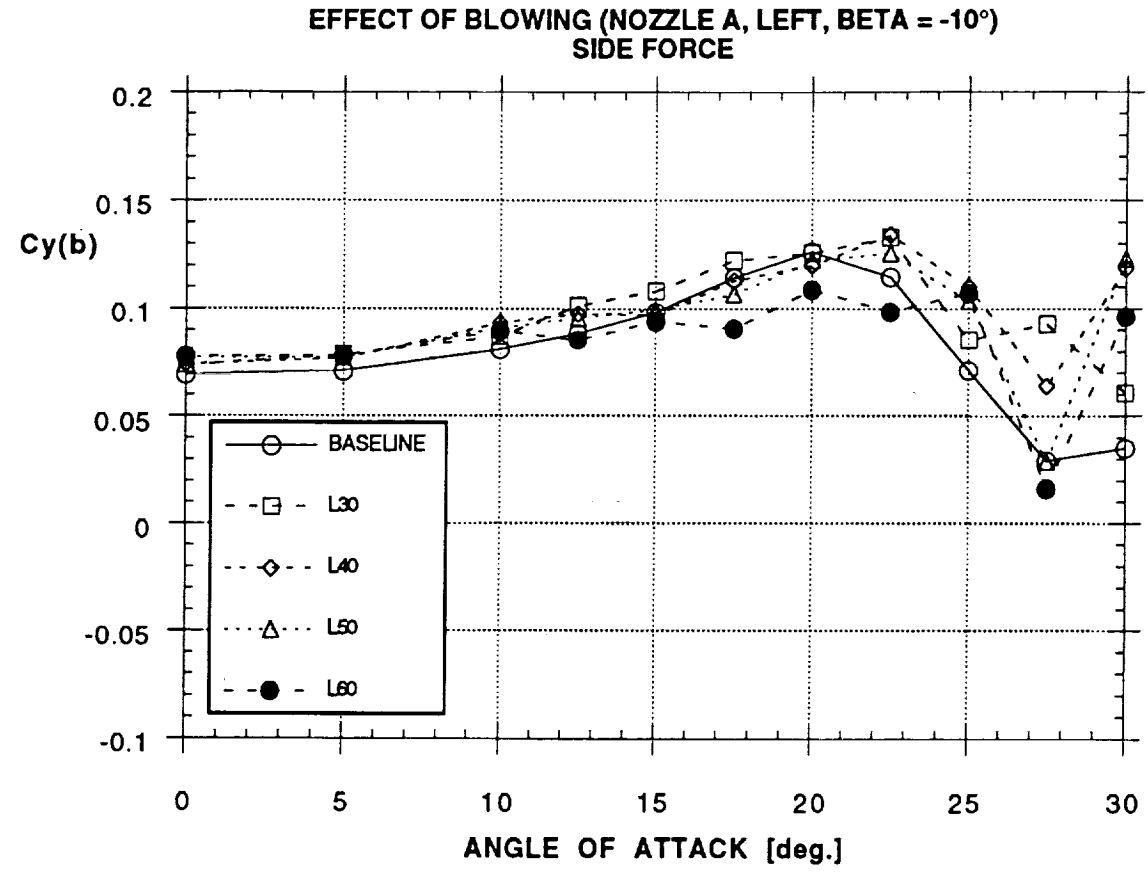

c)

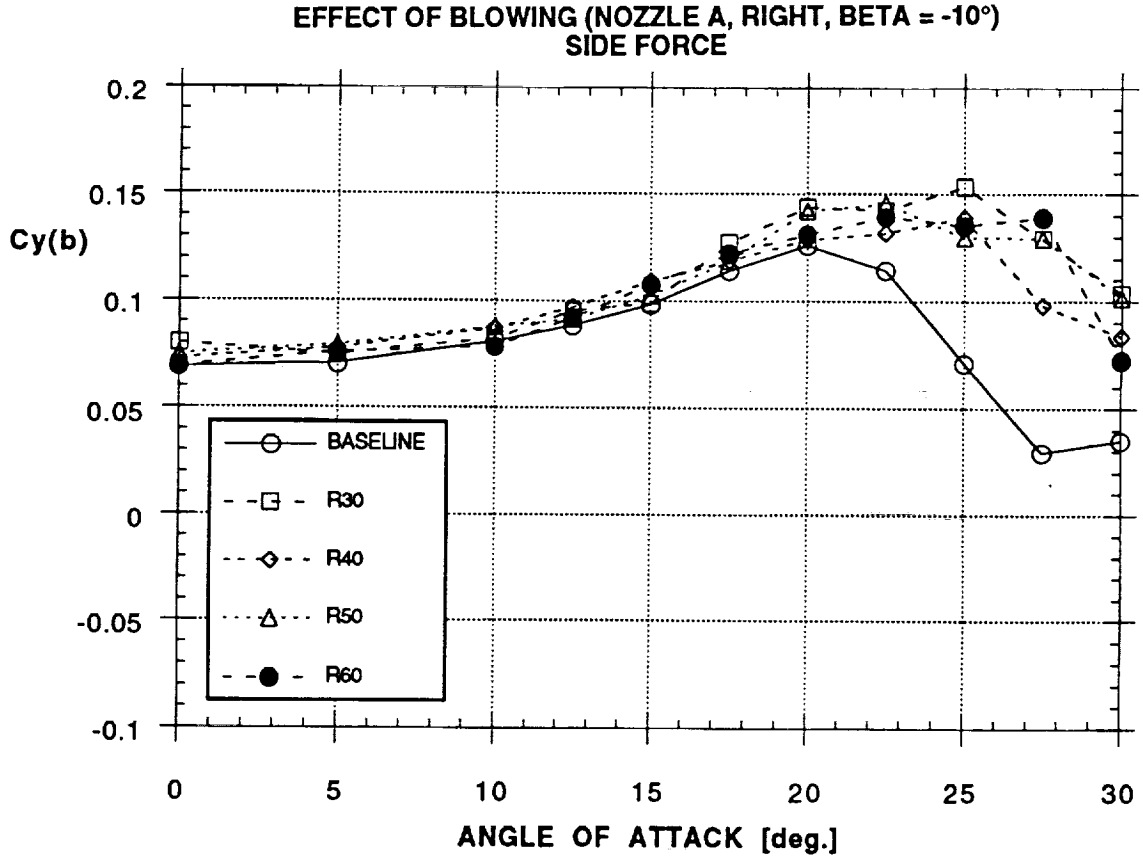

d)

Figure 19 - Continued

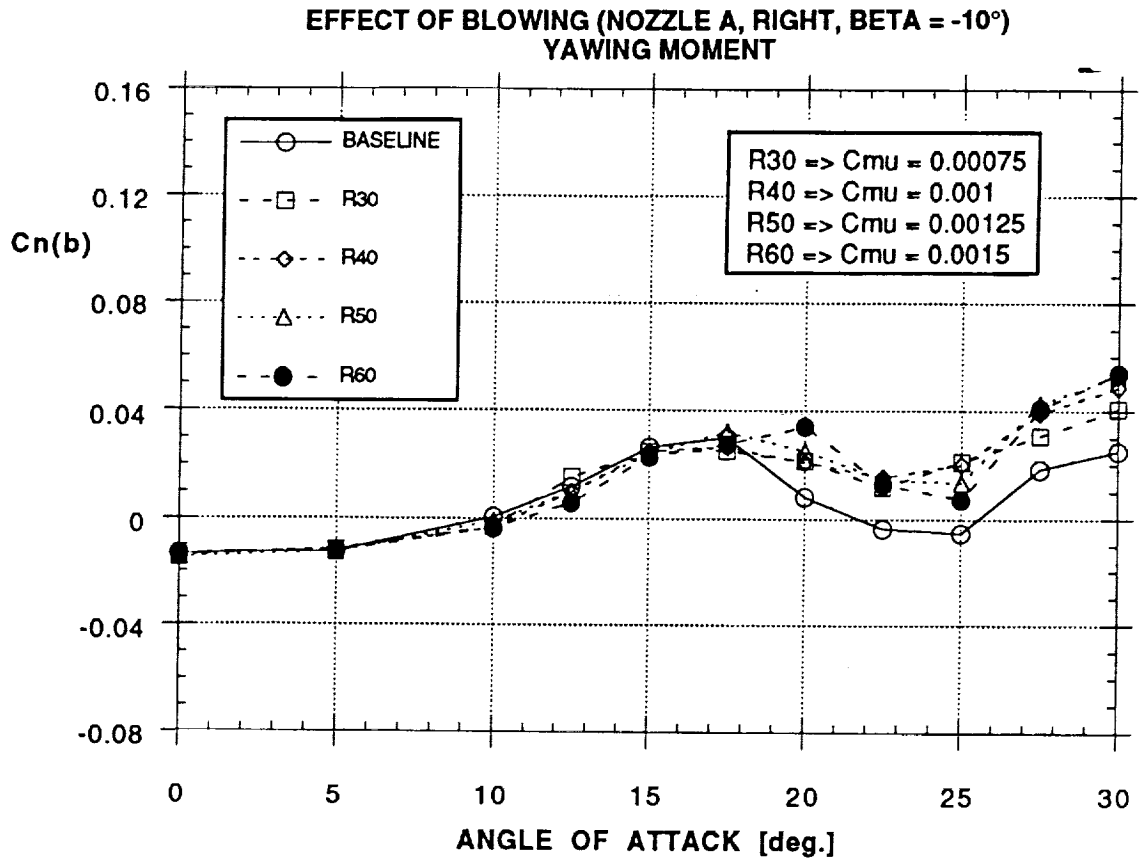

e)

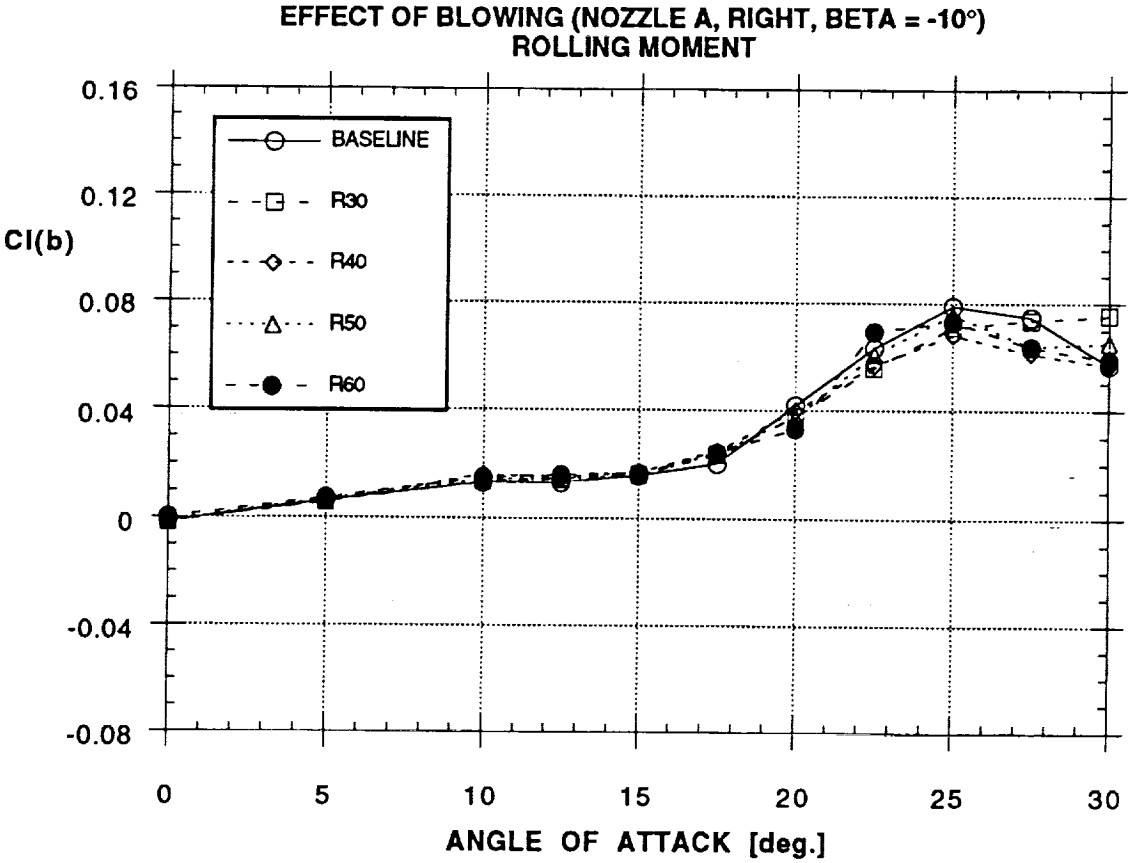

f)

Figure 19 - Concluded

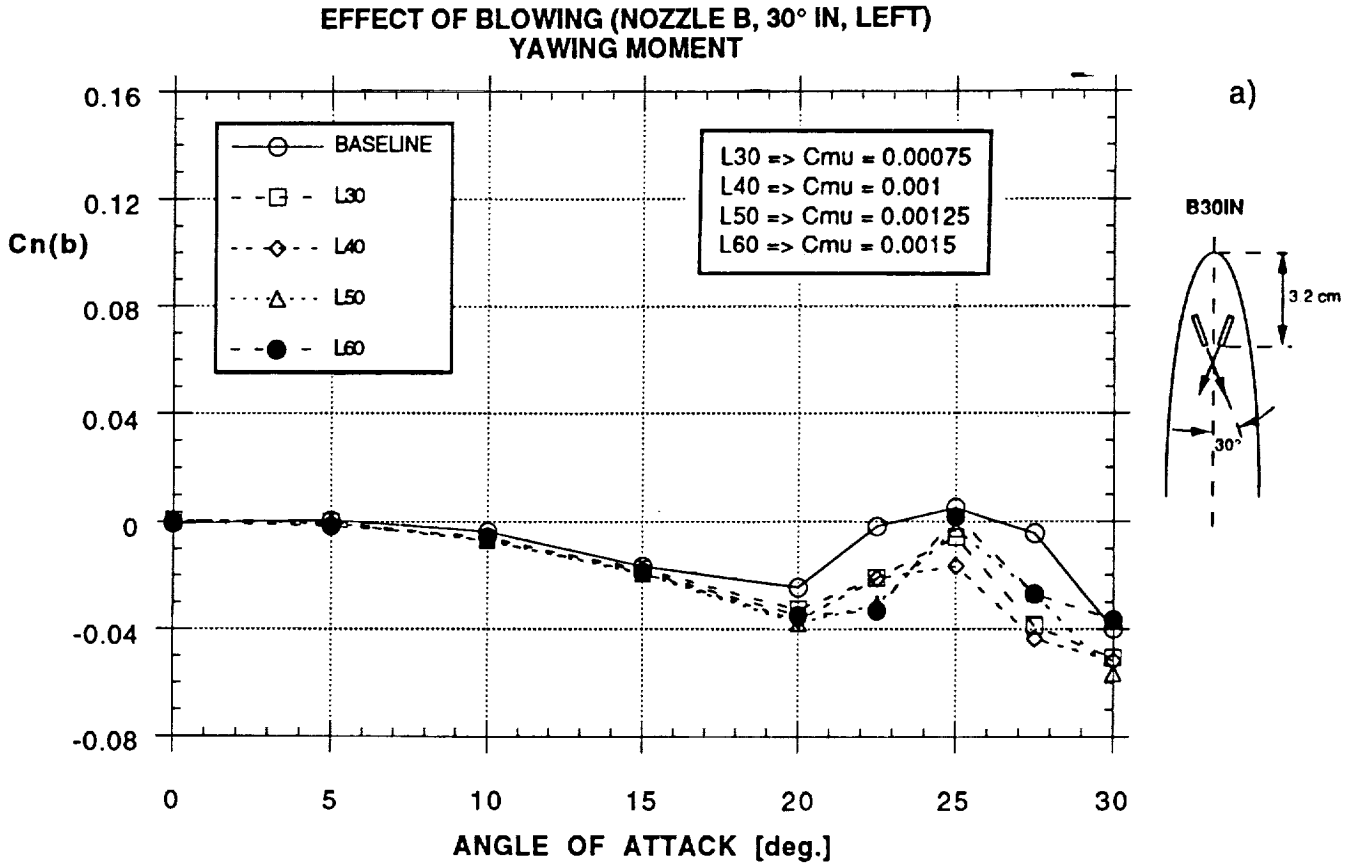

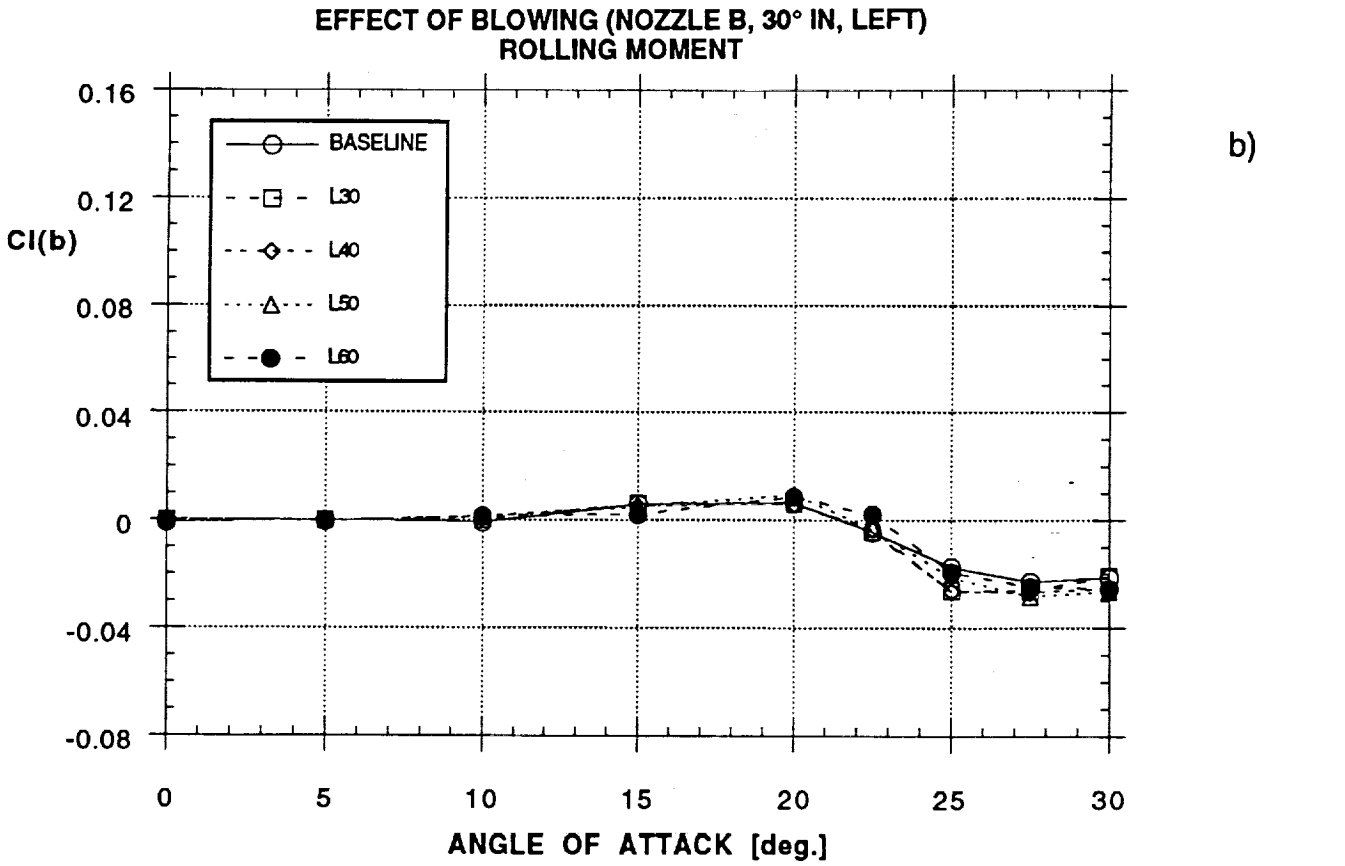

Figure 20 - Effect of Aft Blowing on Forces and Moments (Nozzle B30IN, Left and Right Sides, $\beta = 0°$)

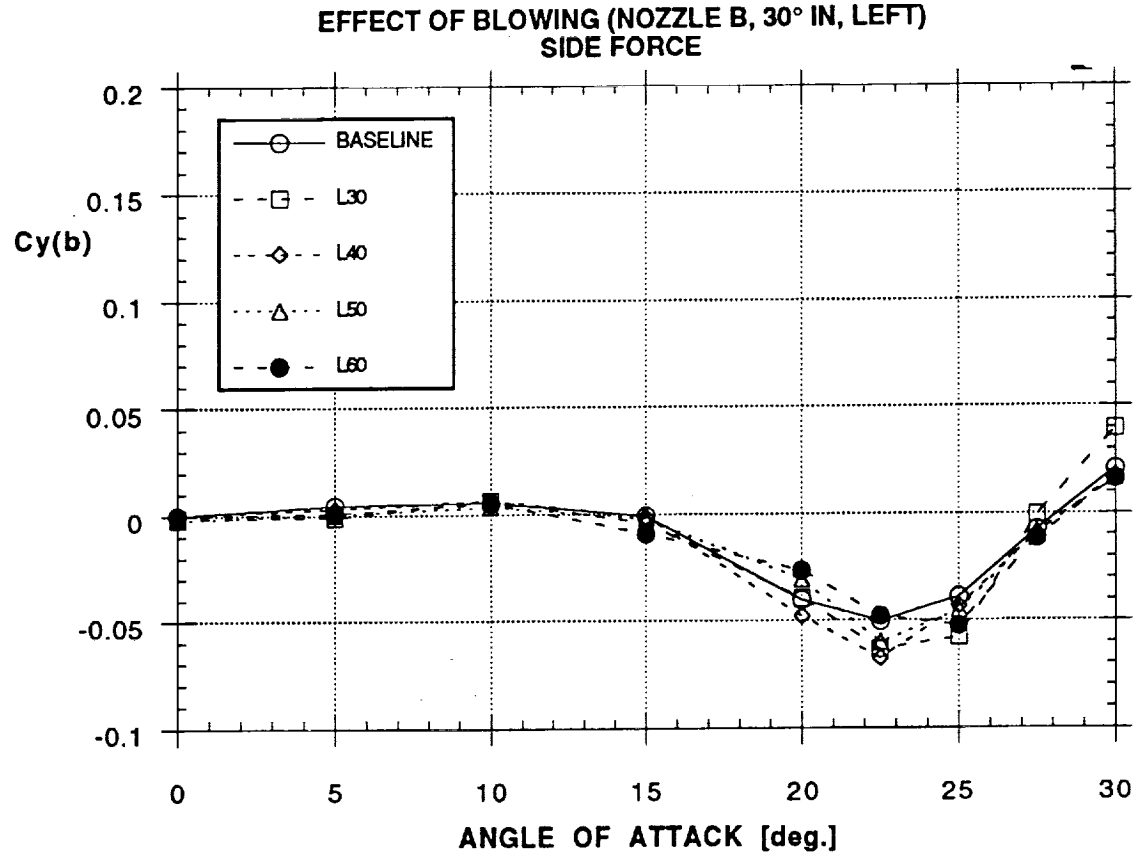

c)

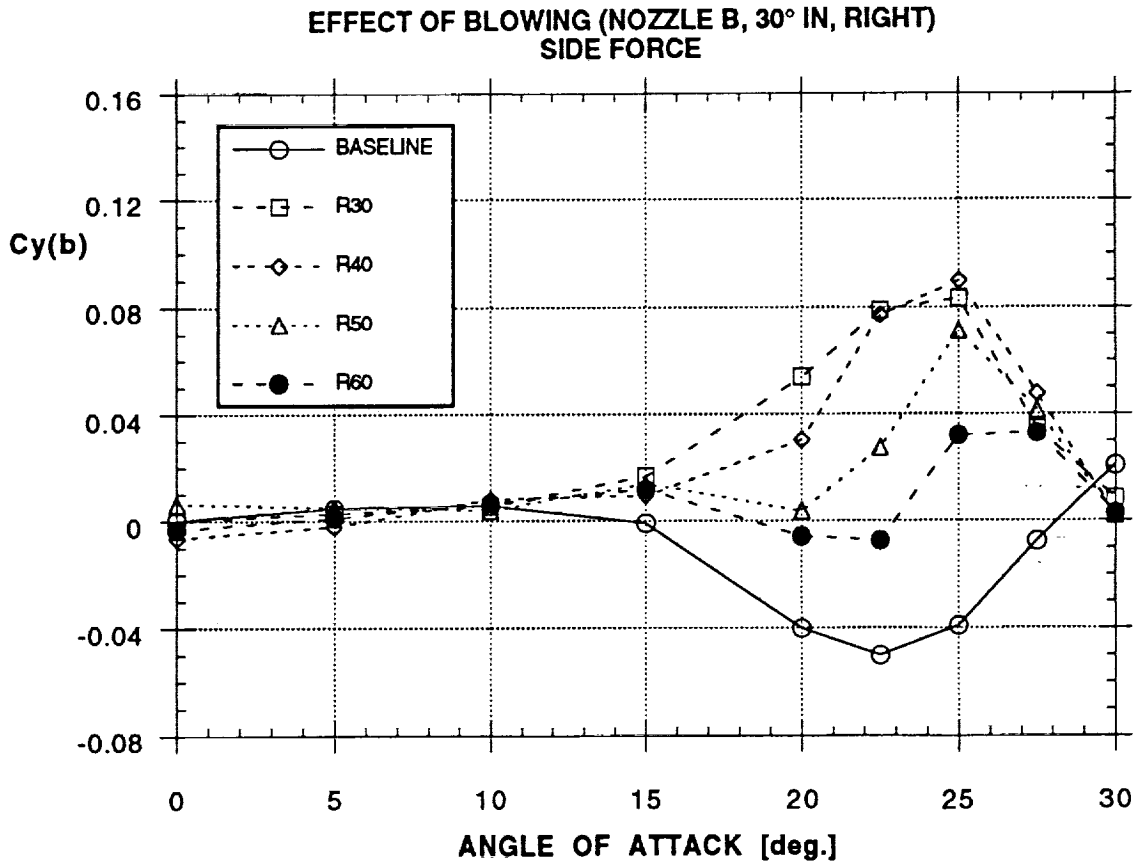

d)

Figure 20 - Continued

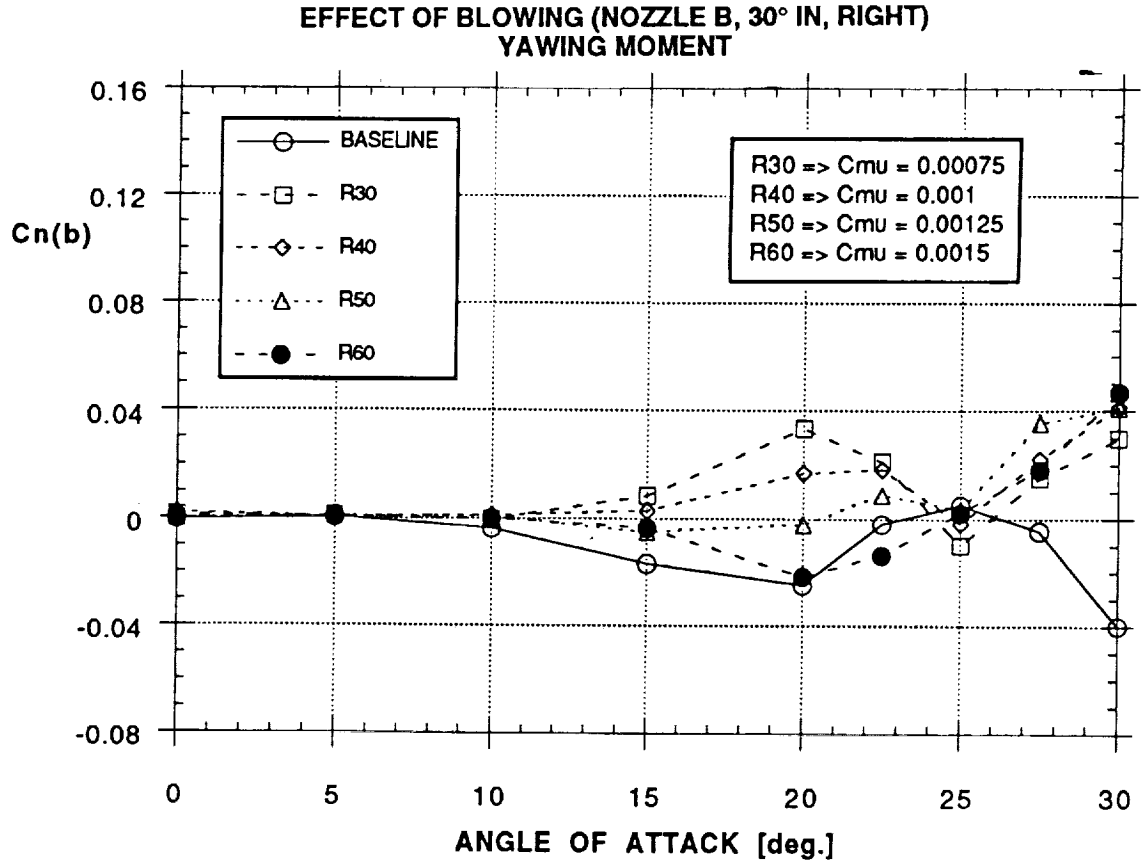

e)

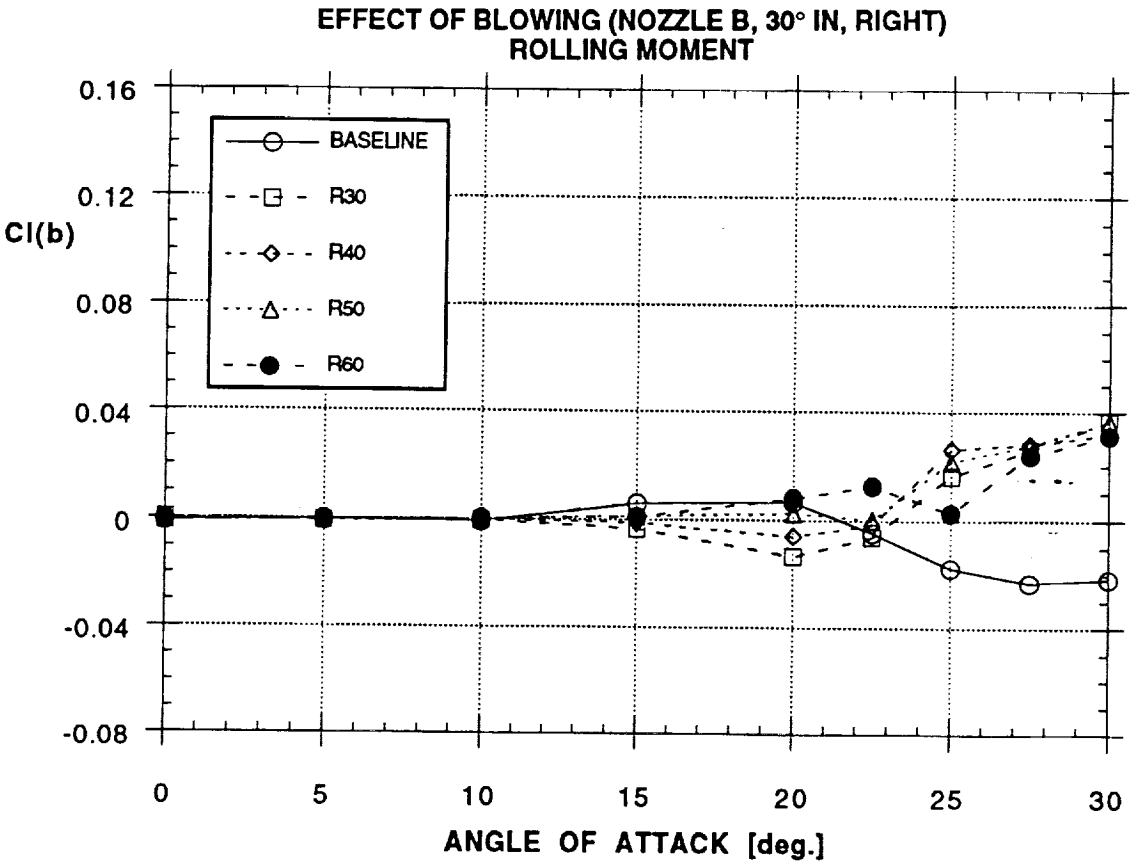

f)

Figure 20 - Concluded

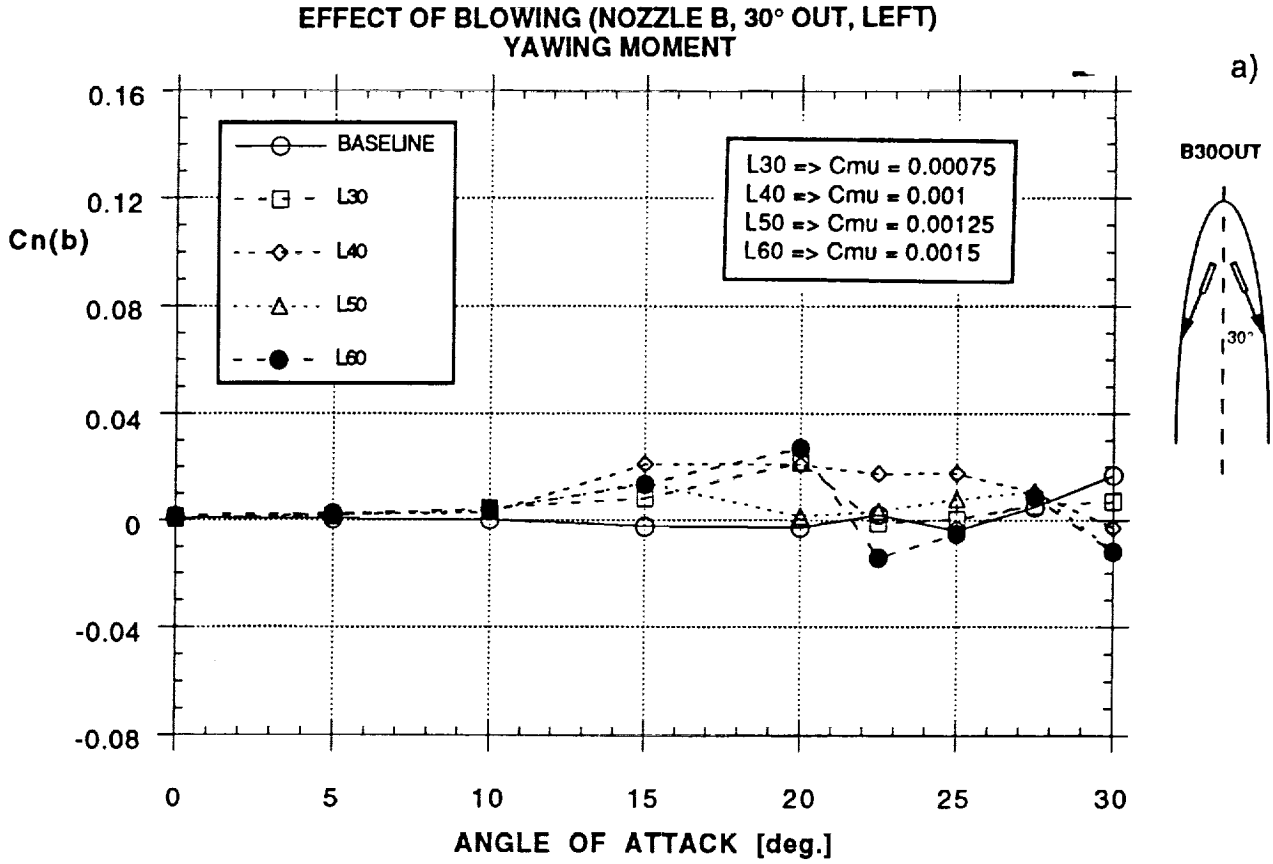

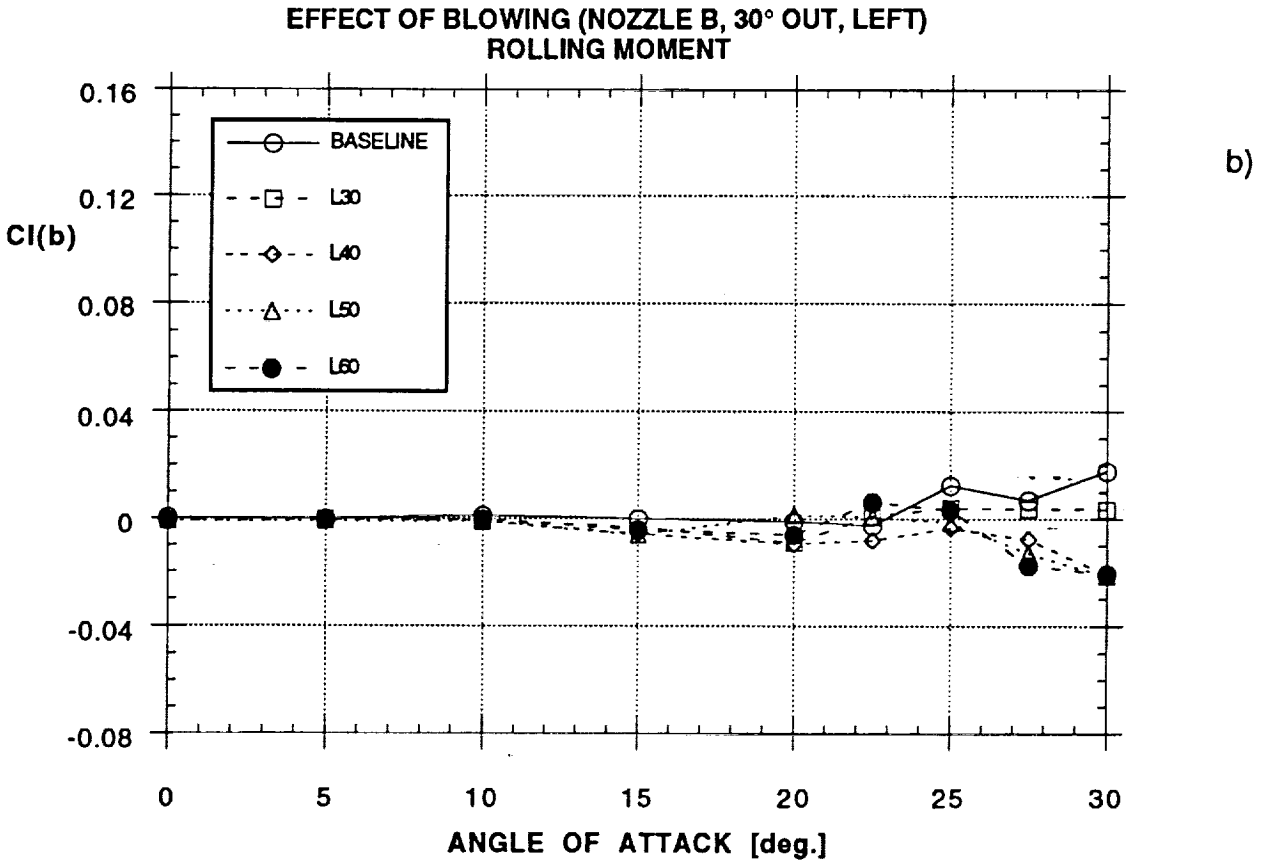

Figure 21 - Effect of Aft Blowing on Forces and Moments (Nozzle B30OUT, Left and Right Sides, $\beta = 0°$)

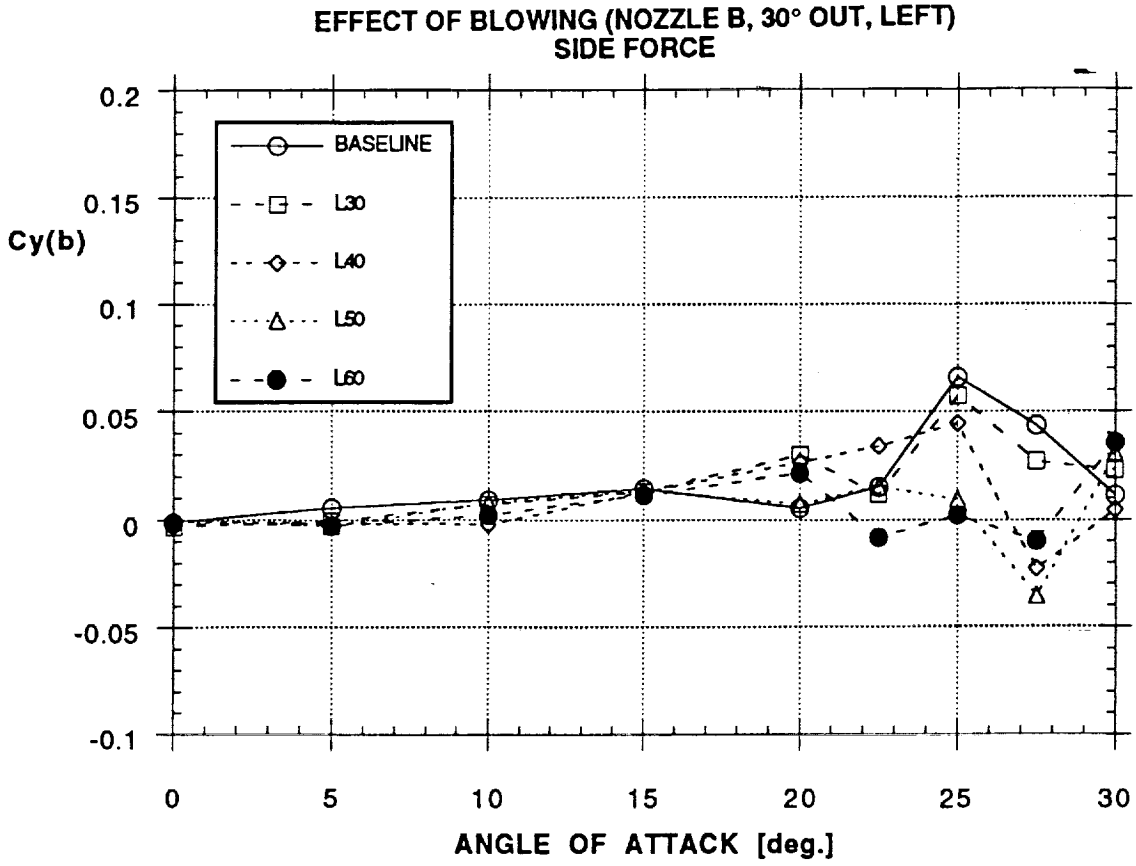

c)

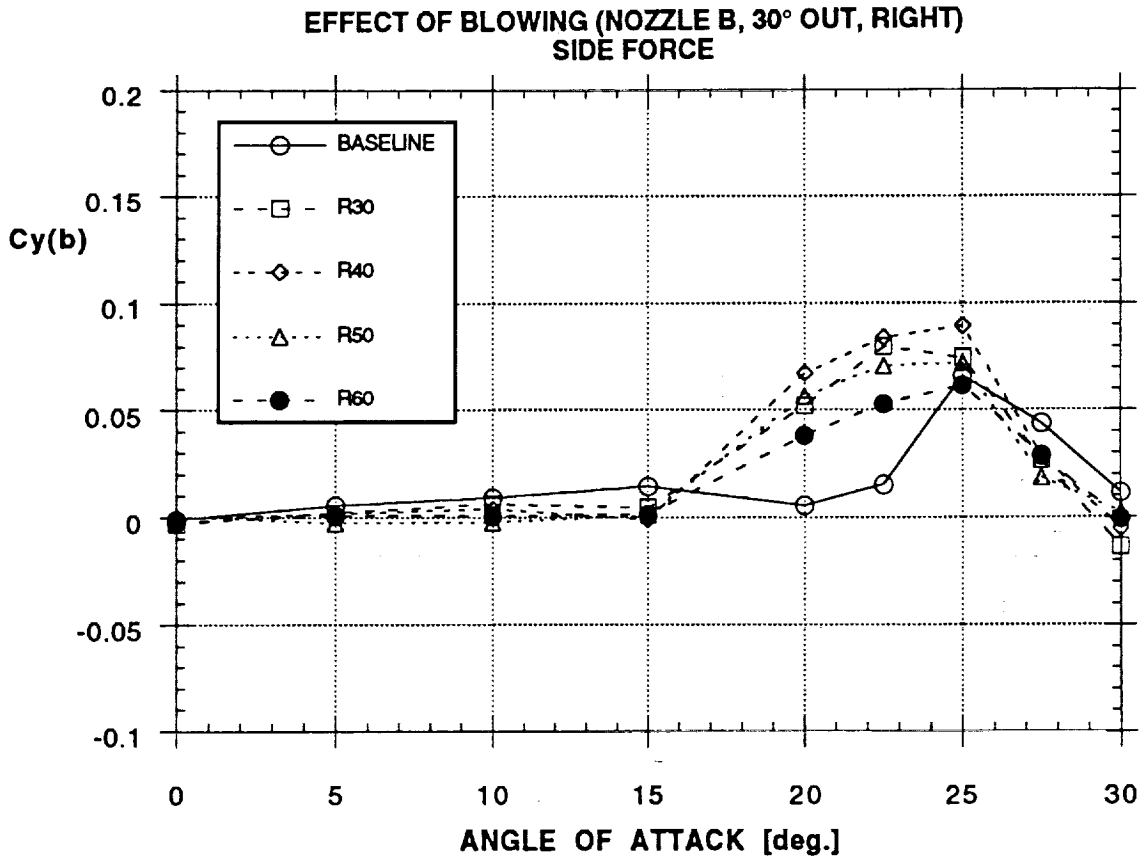

d)

Figure 21 - Continued

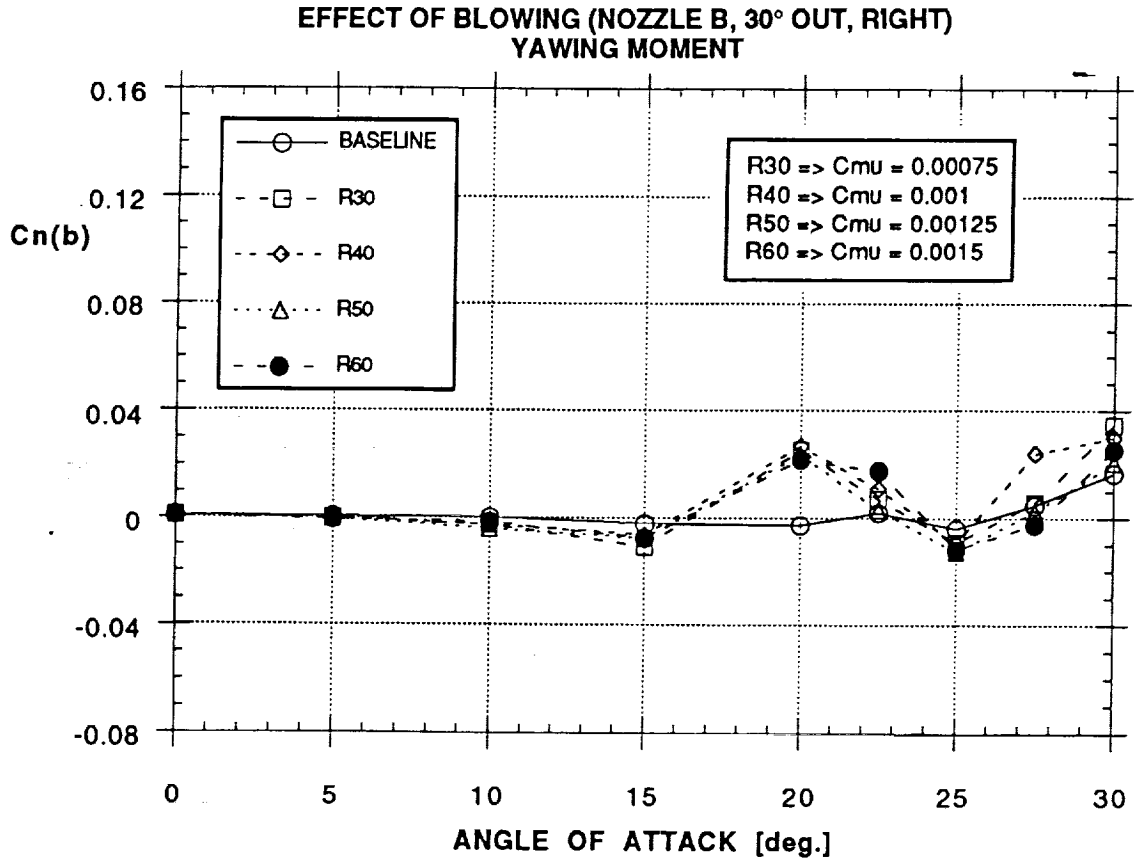

e)

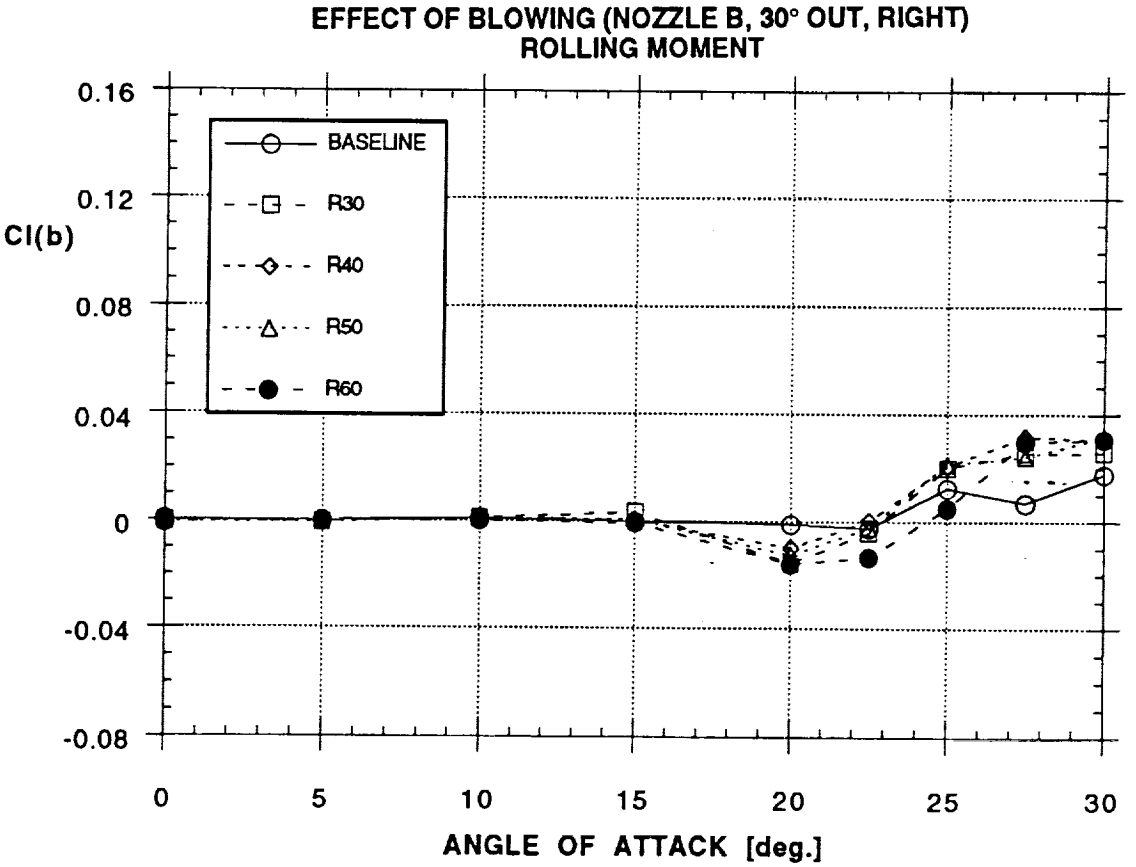

f)

Figure 21 - Concluded

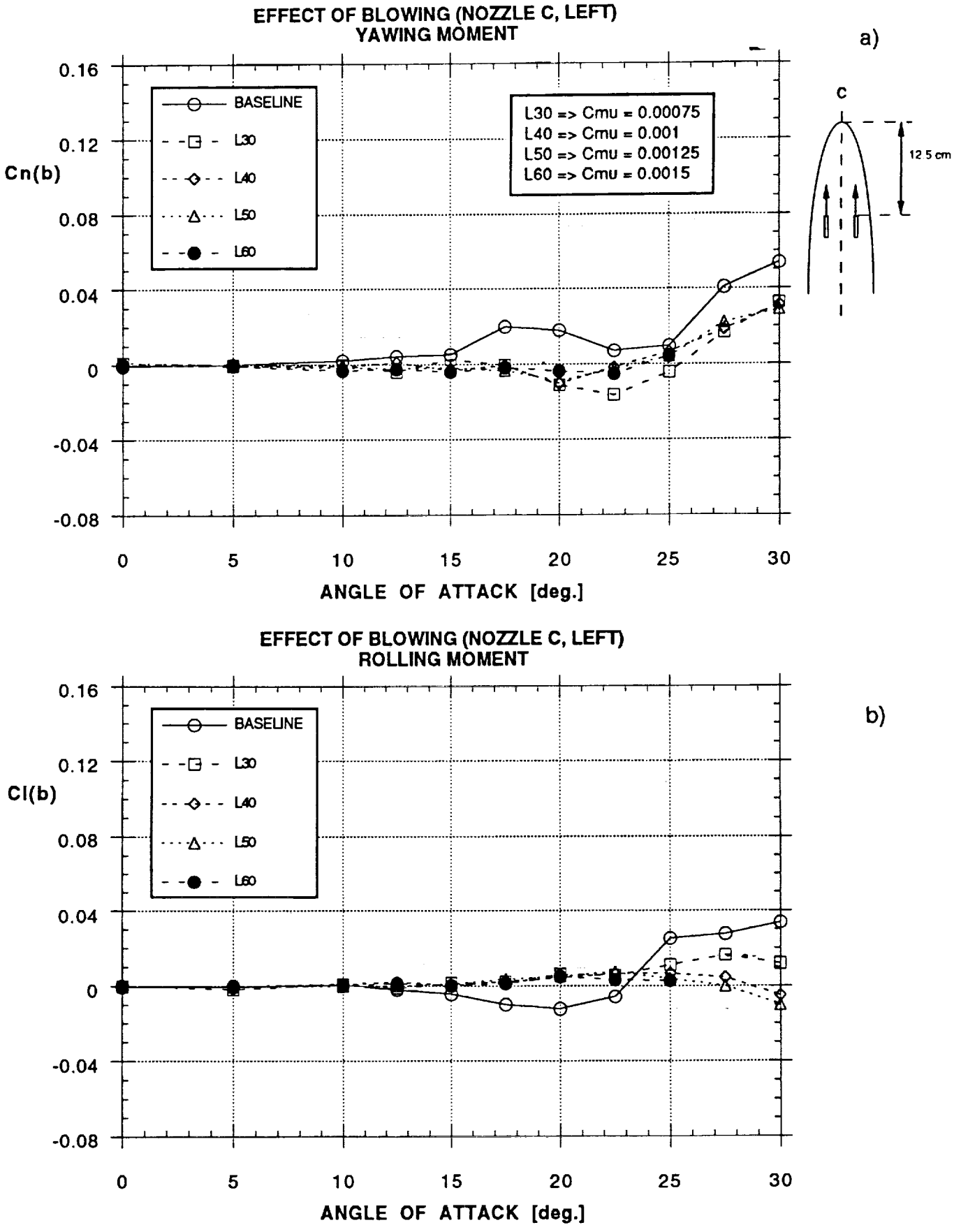

Figure 22 - Effect of Forward Blowing on Forces and Moments (Nozzle C; Left , Right and Both Sides, $\beta = 0°$)

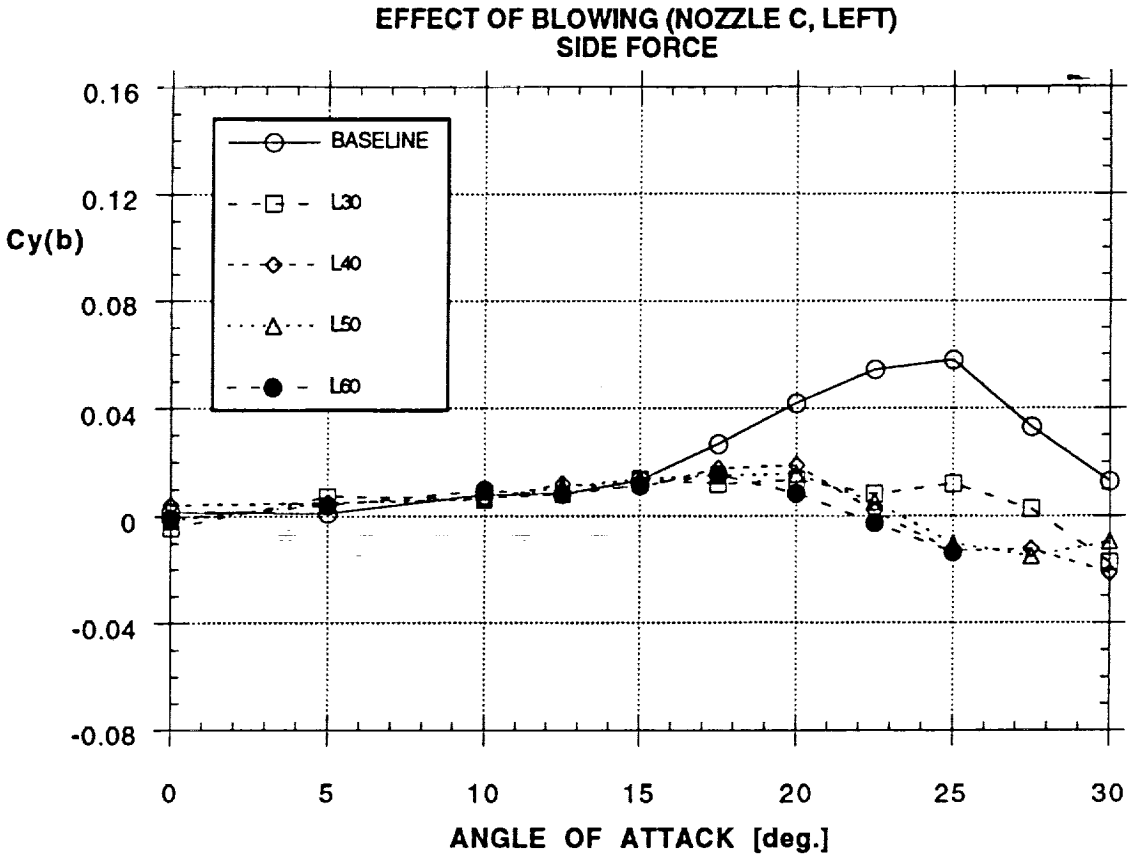

c)

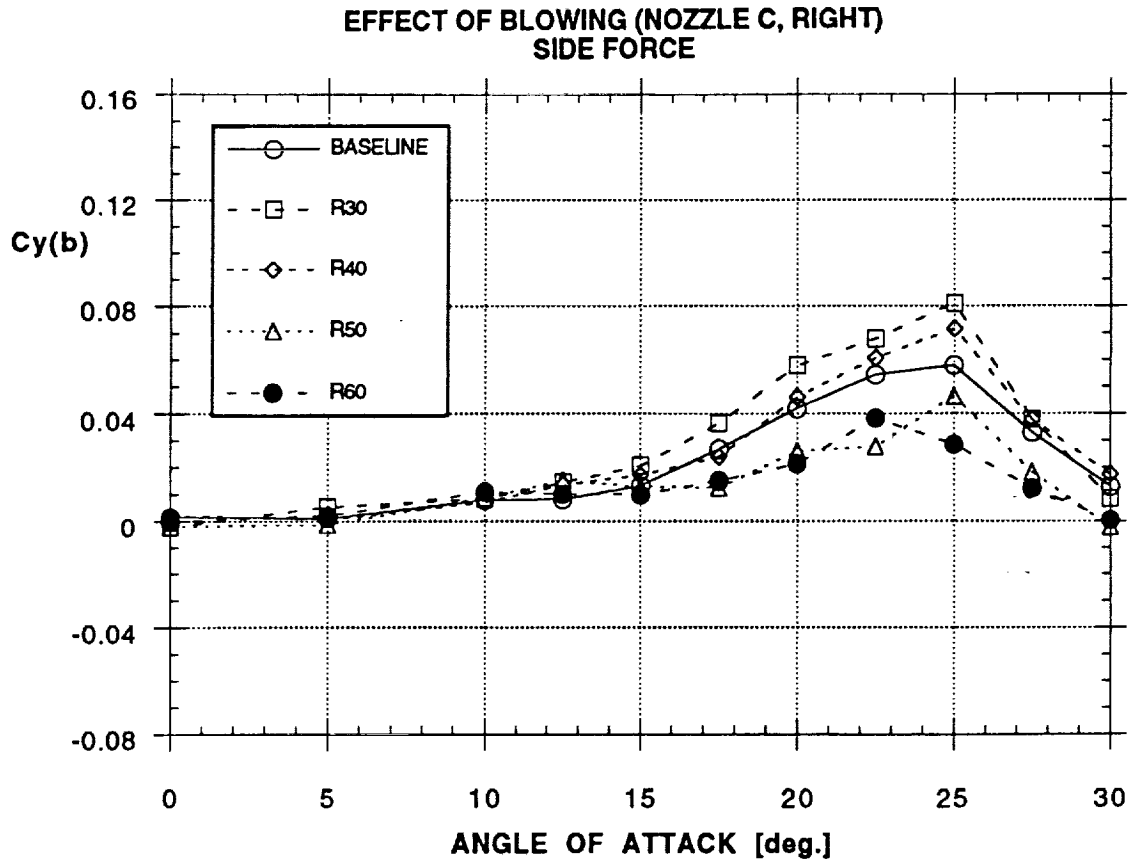

d)

Figure 22 - Continued

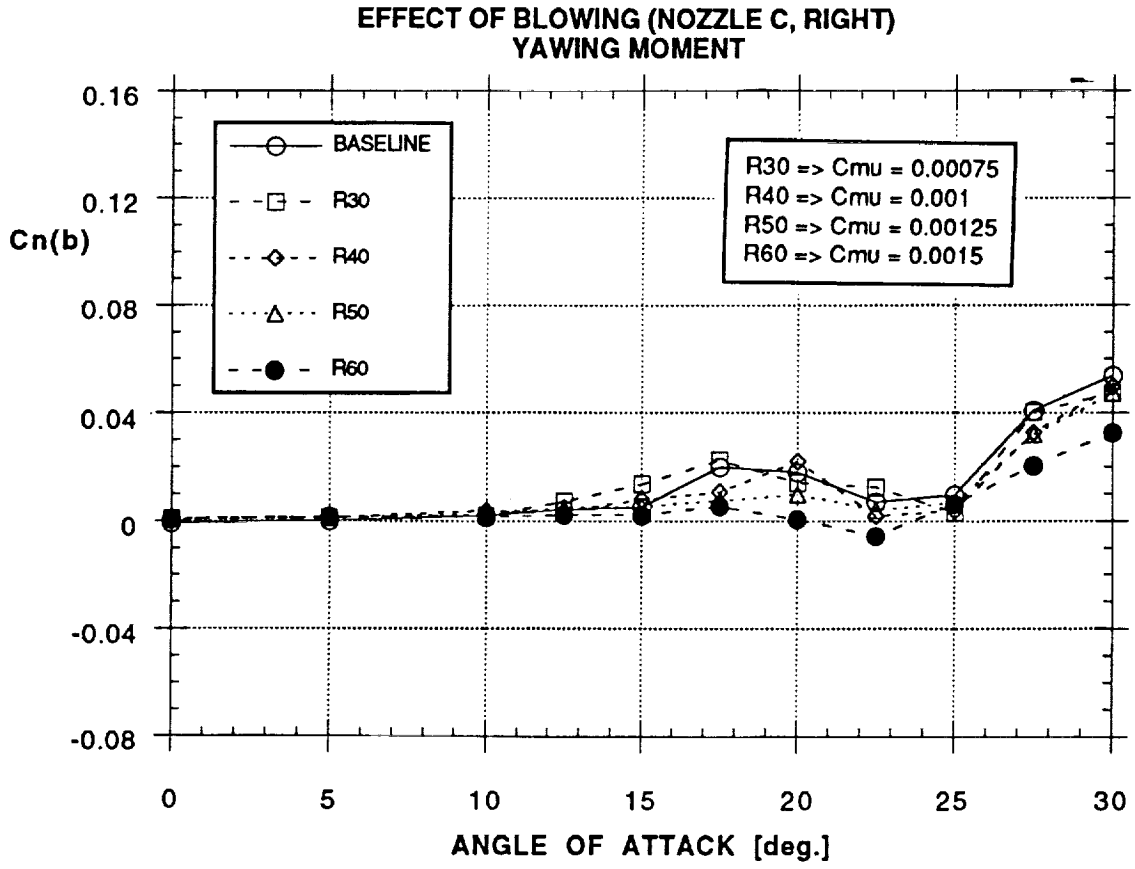

e)

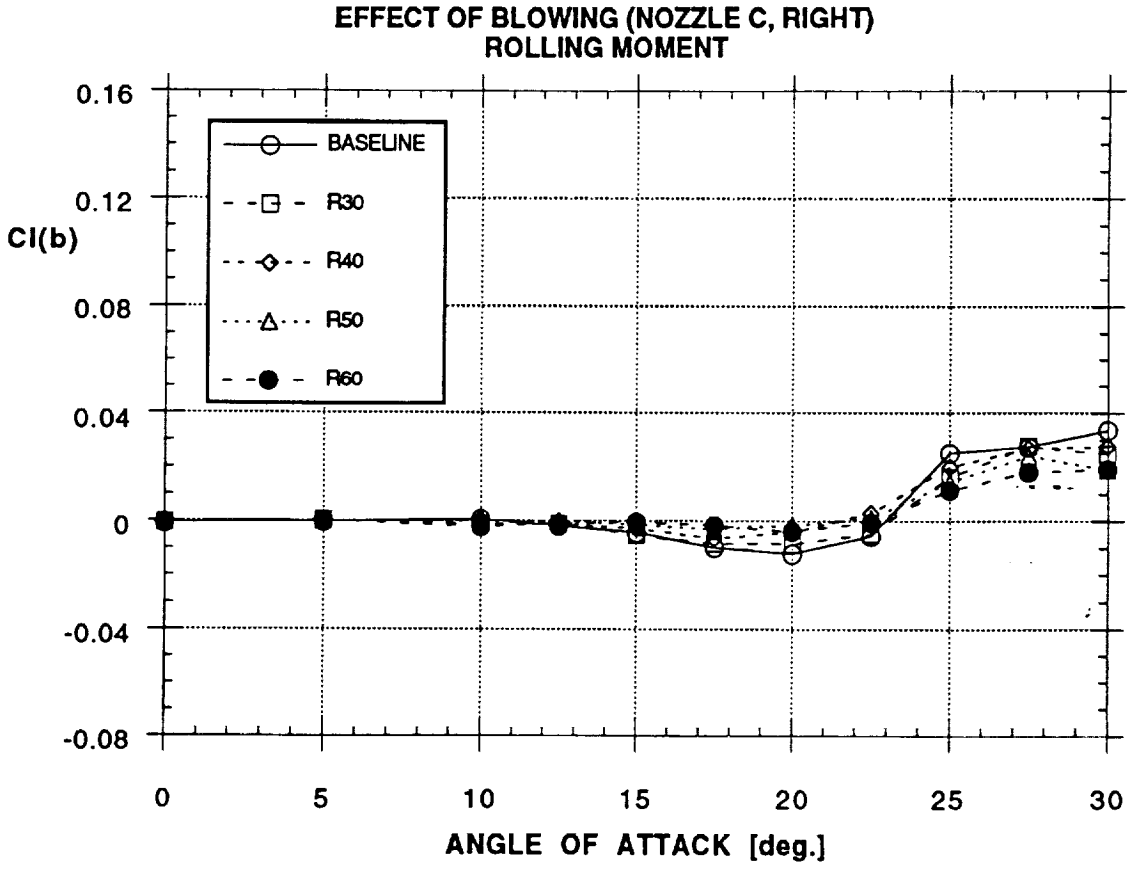

f)

Figure 22 - Continued

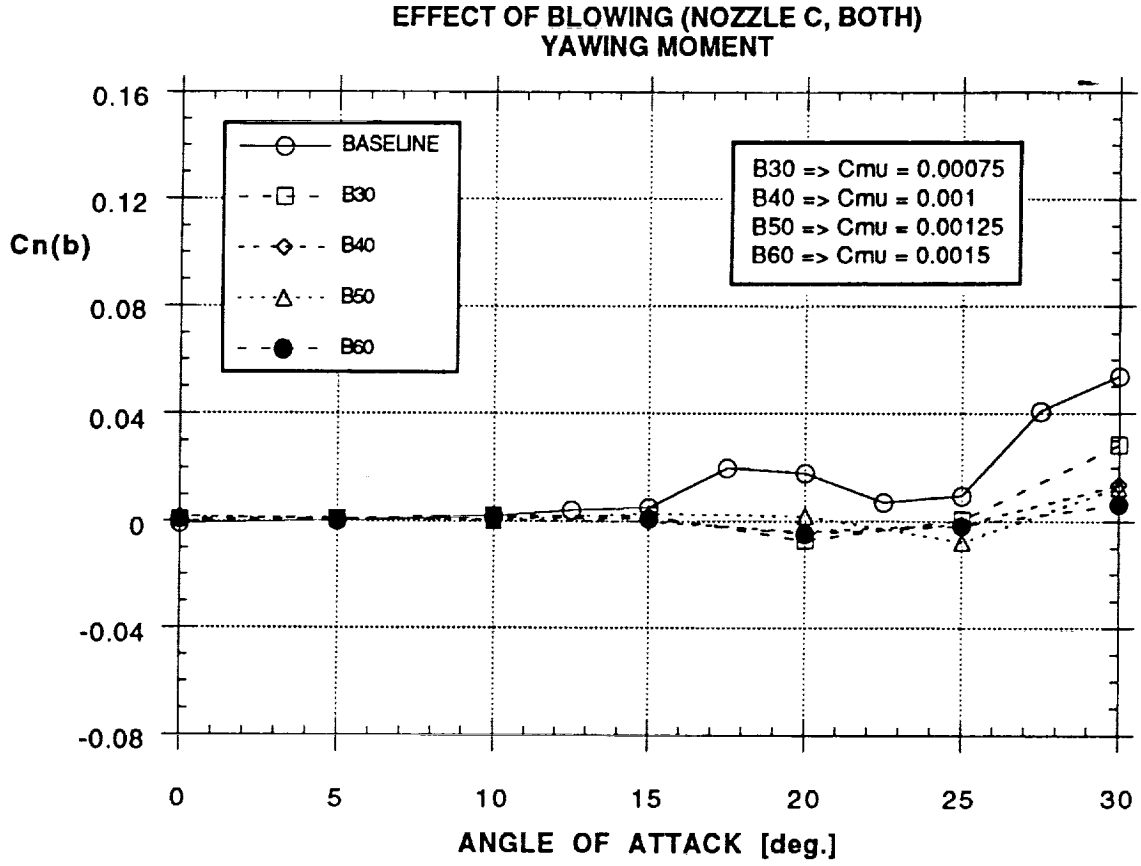

g)

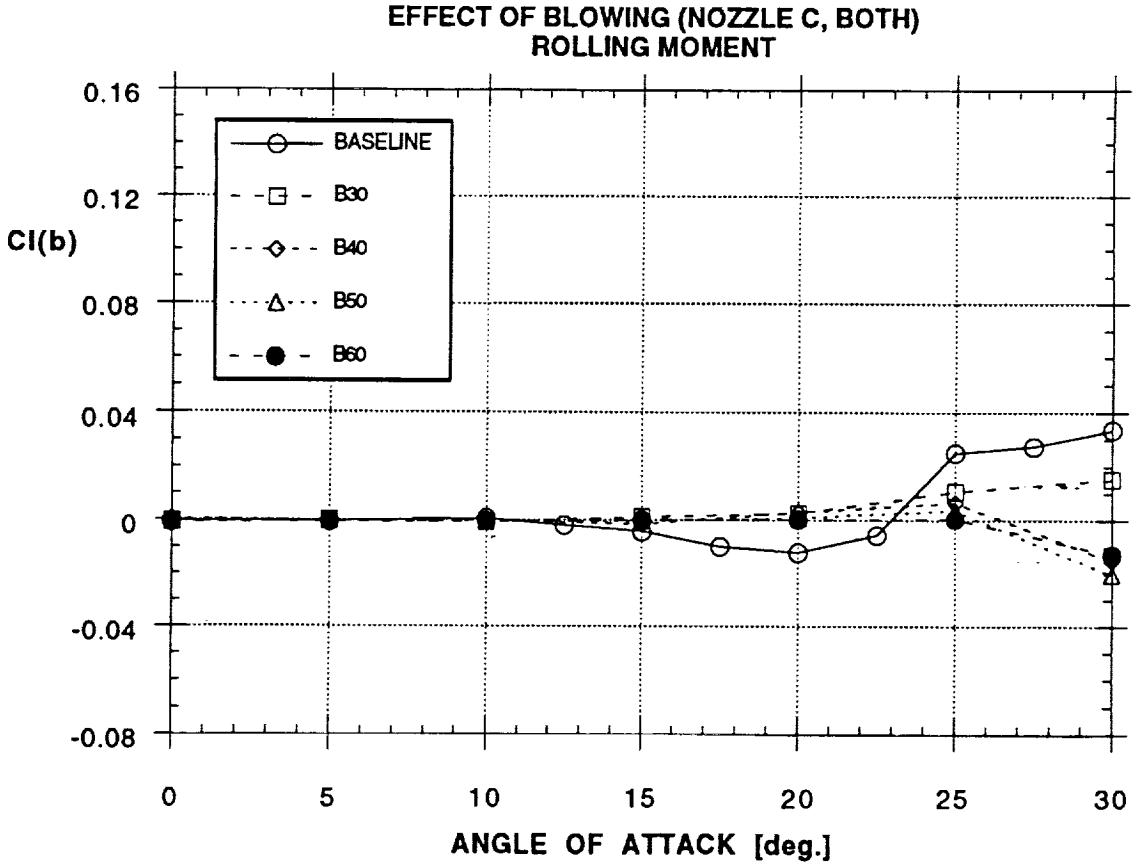

h)

Figure 22 - Concluded

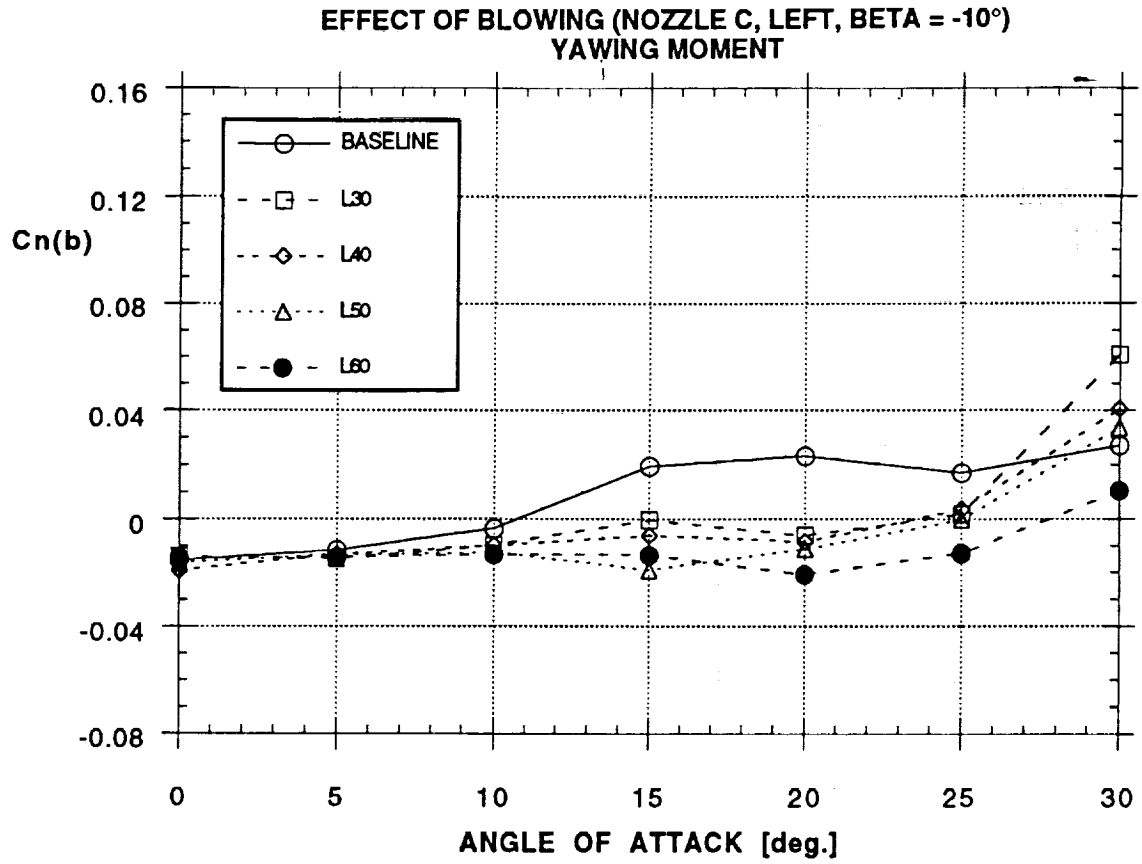

a)

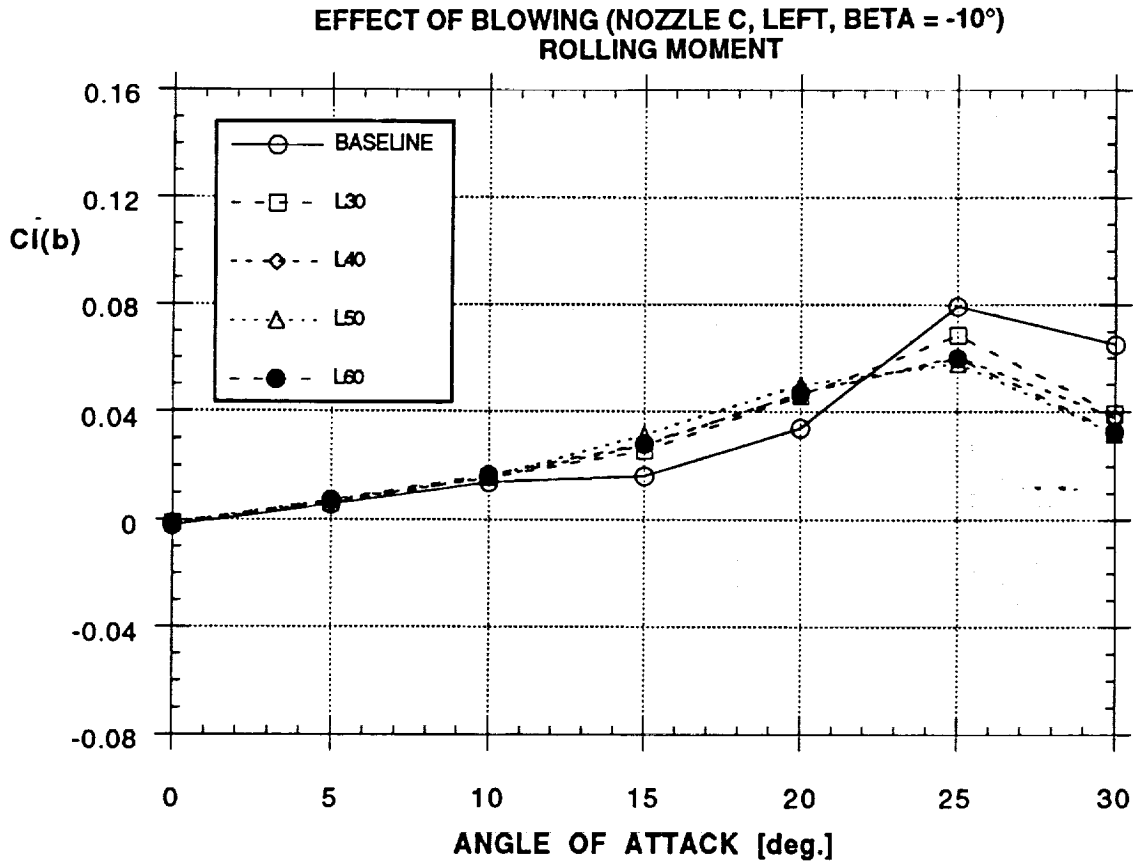

b)

Figure 23 - Effect of Forward Blowing on Forces and Moments (Nozzle C, Left and Right Sides, β = -10°)

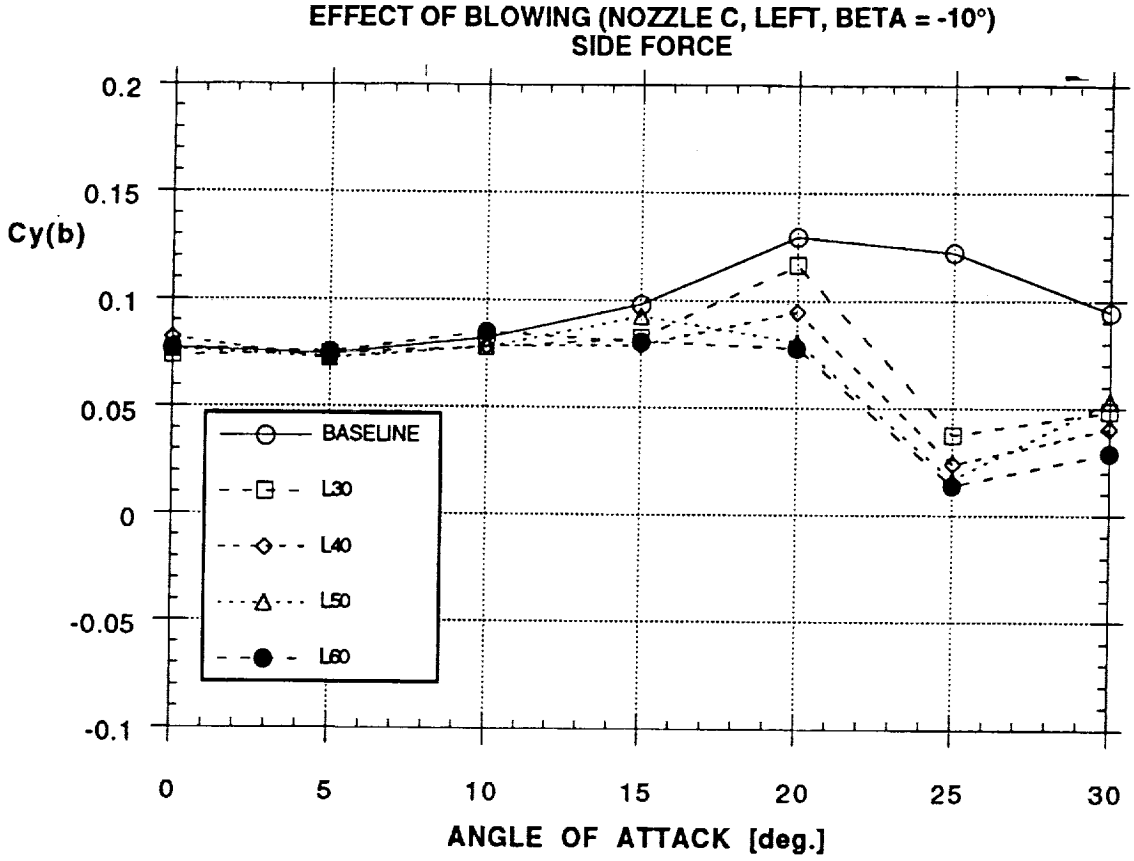

c)

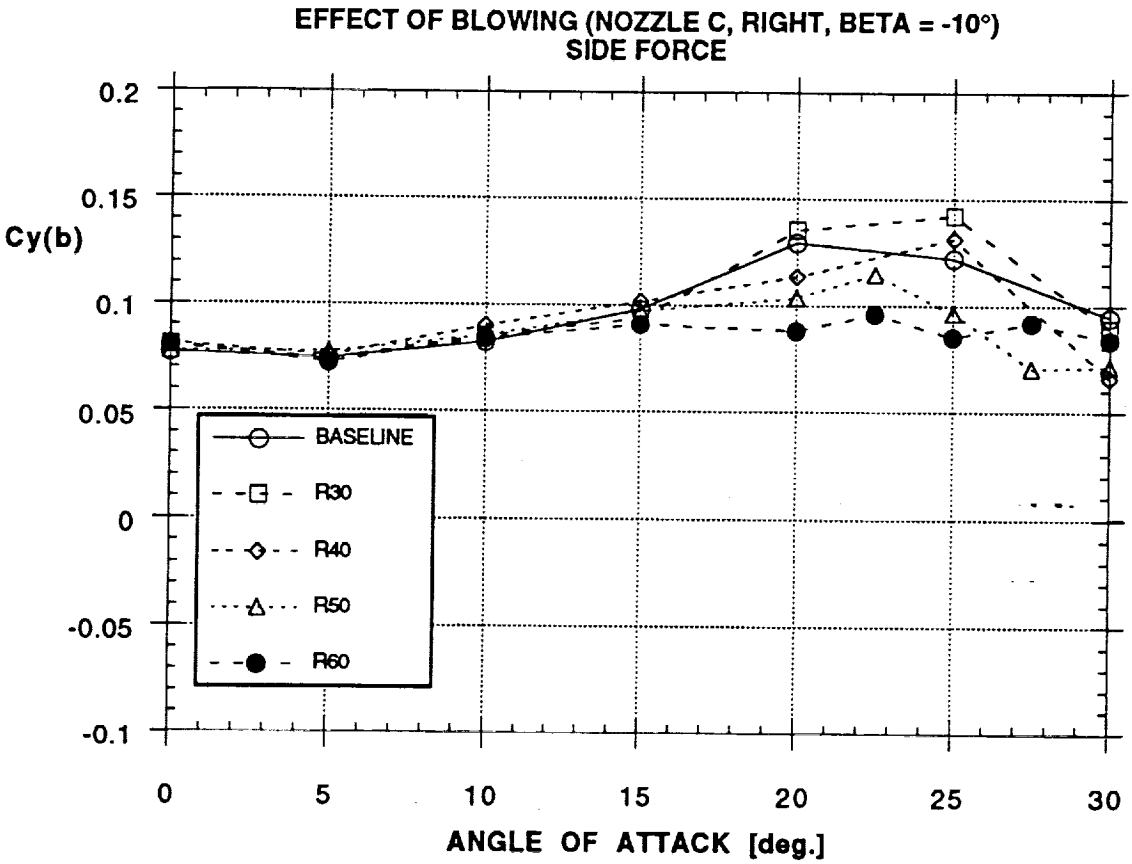

d)

Figure 23 - Continued

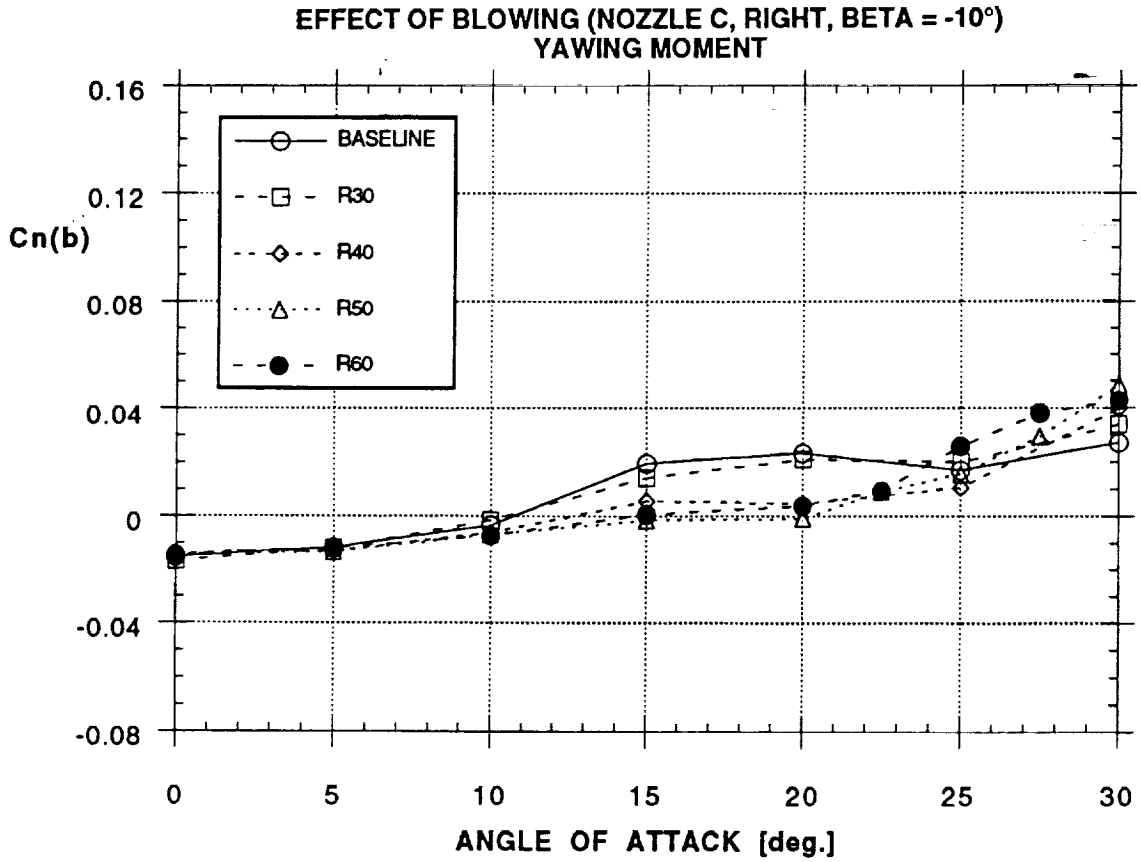

e)

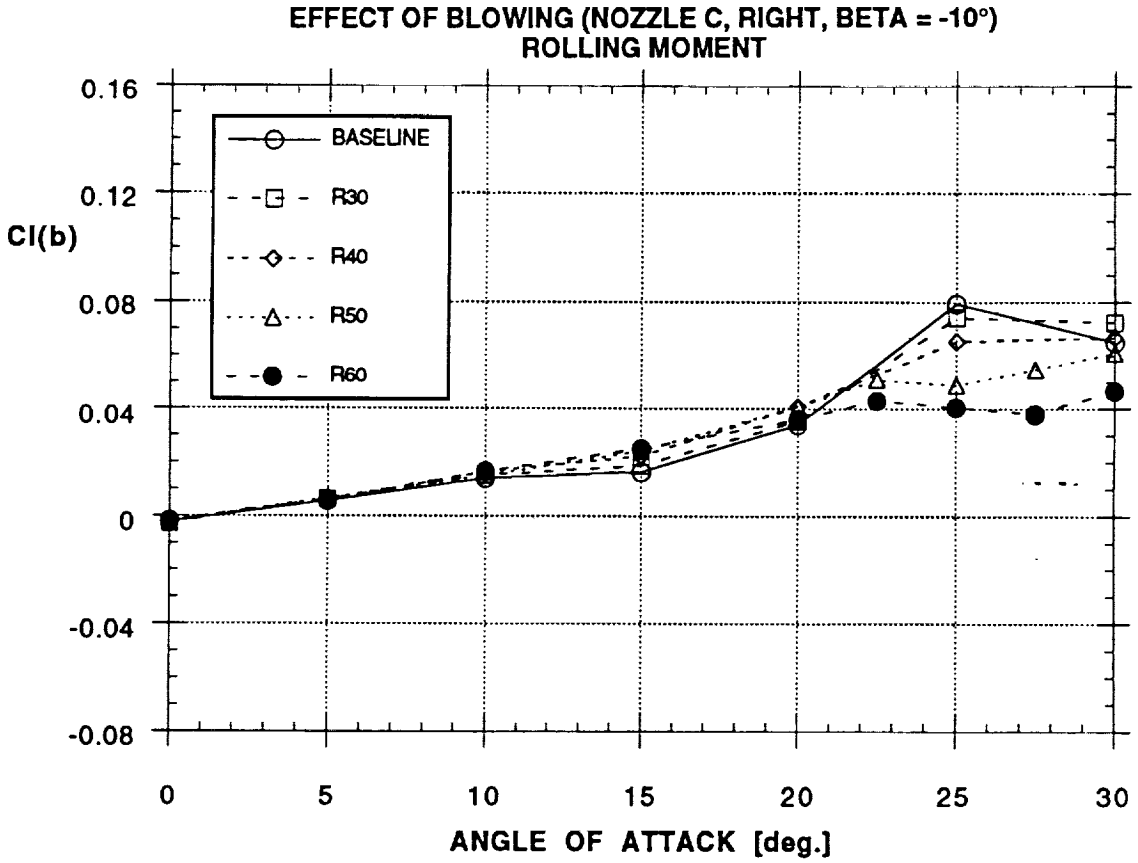

f)

Figure 23 - Concluded

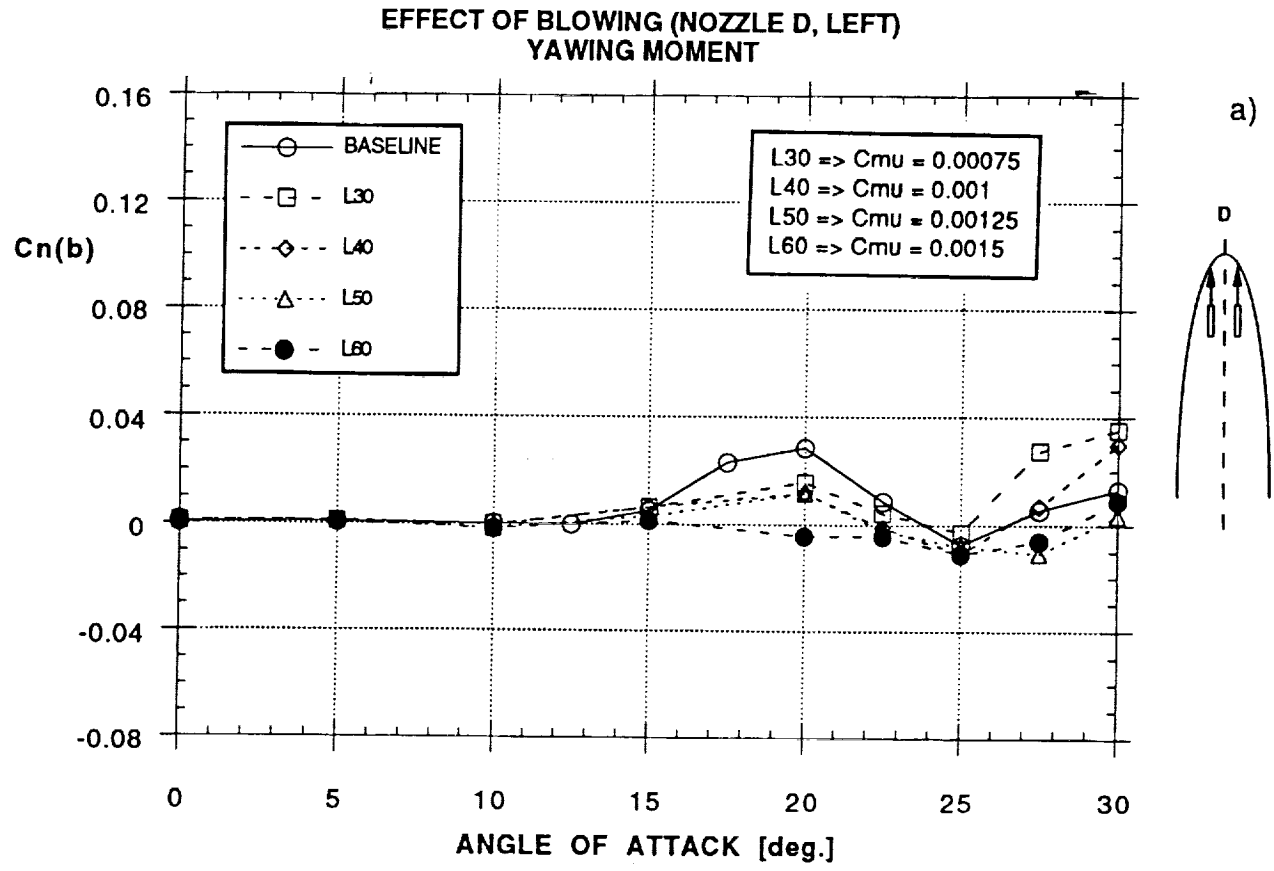

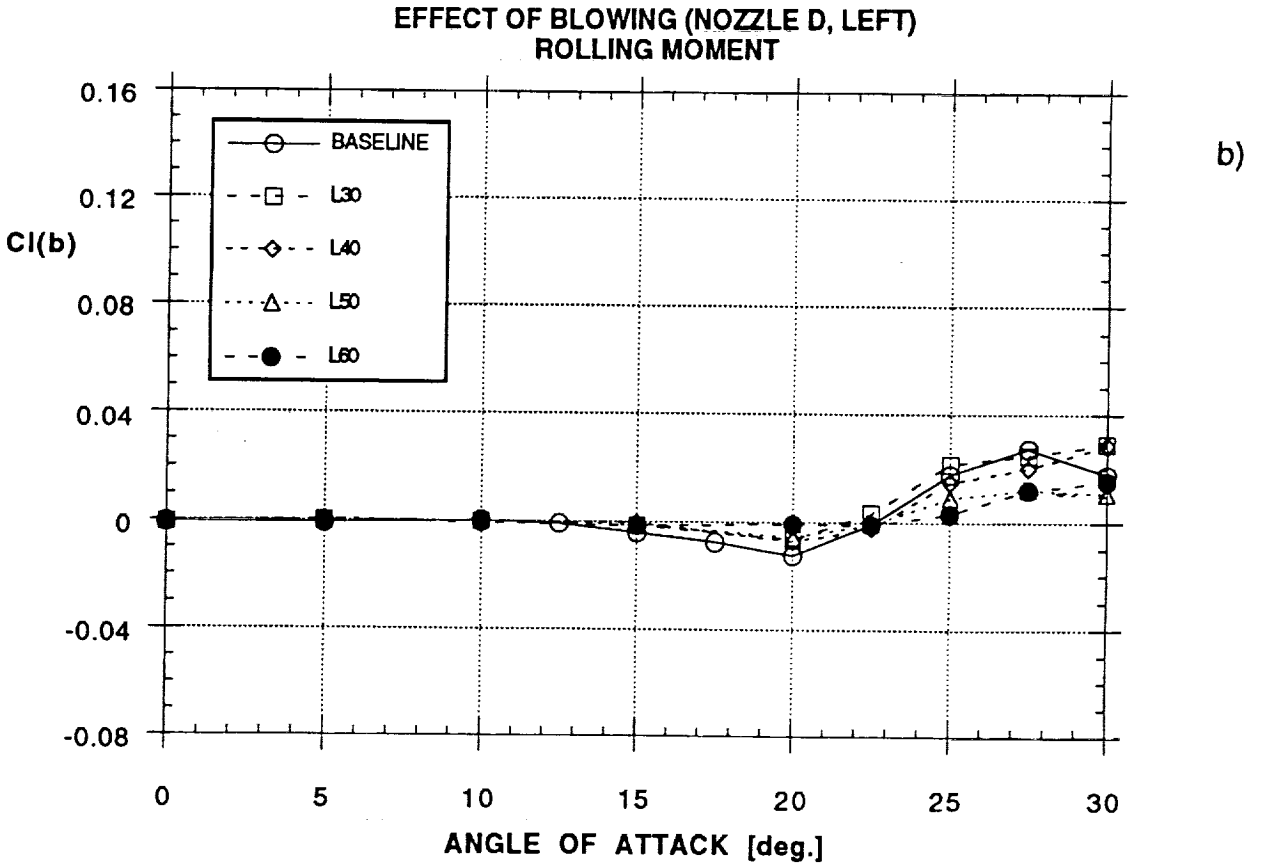

Figure 24 - Effect of Forward Blowing on Forces and Moments (Nozzle D, Left and Right Sides, $\beta = 0°$)

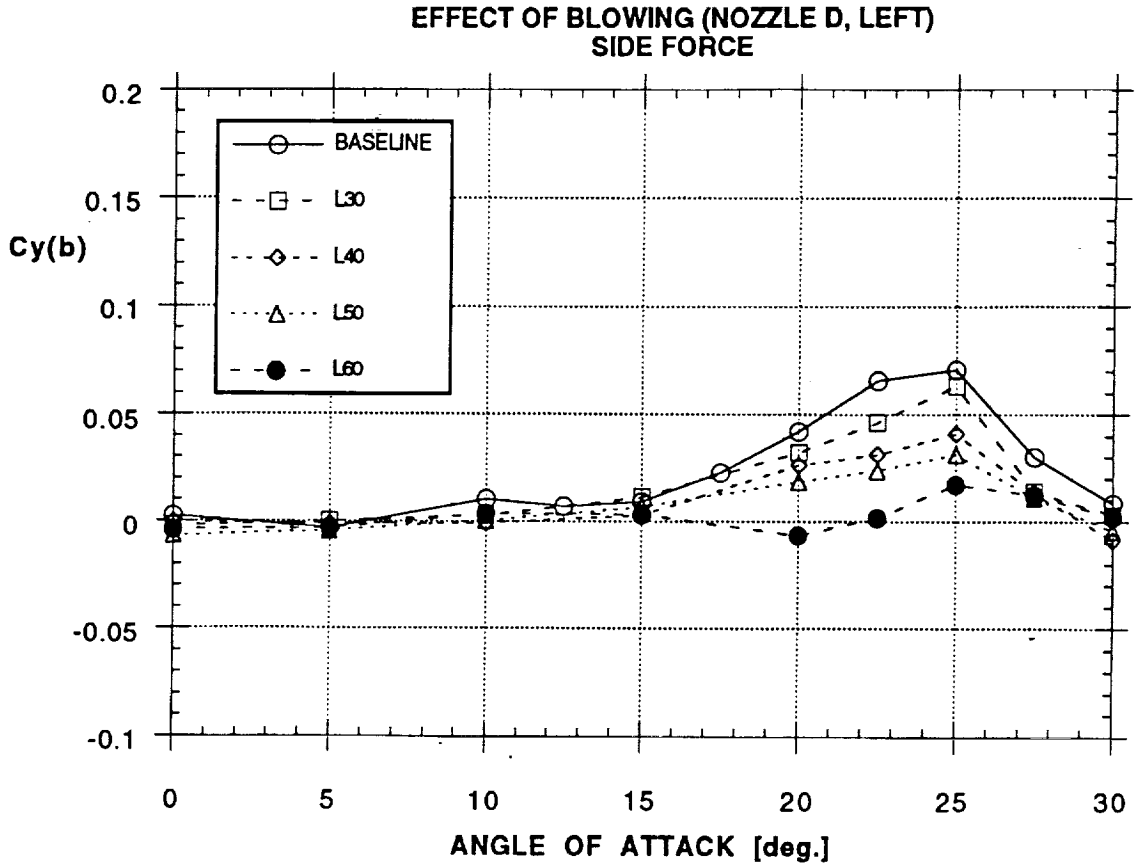

c)

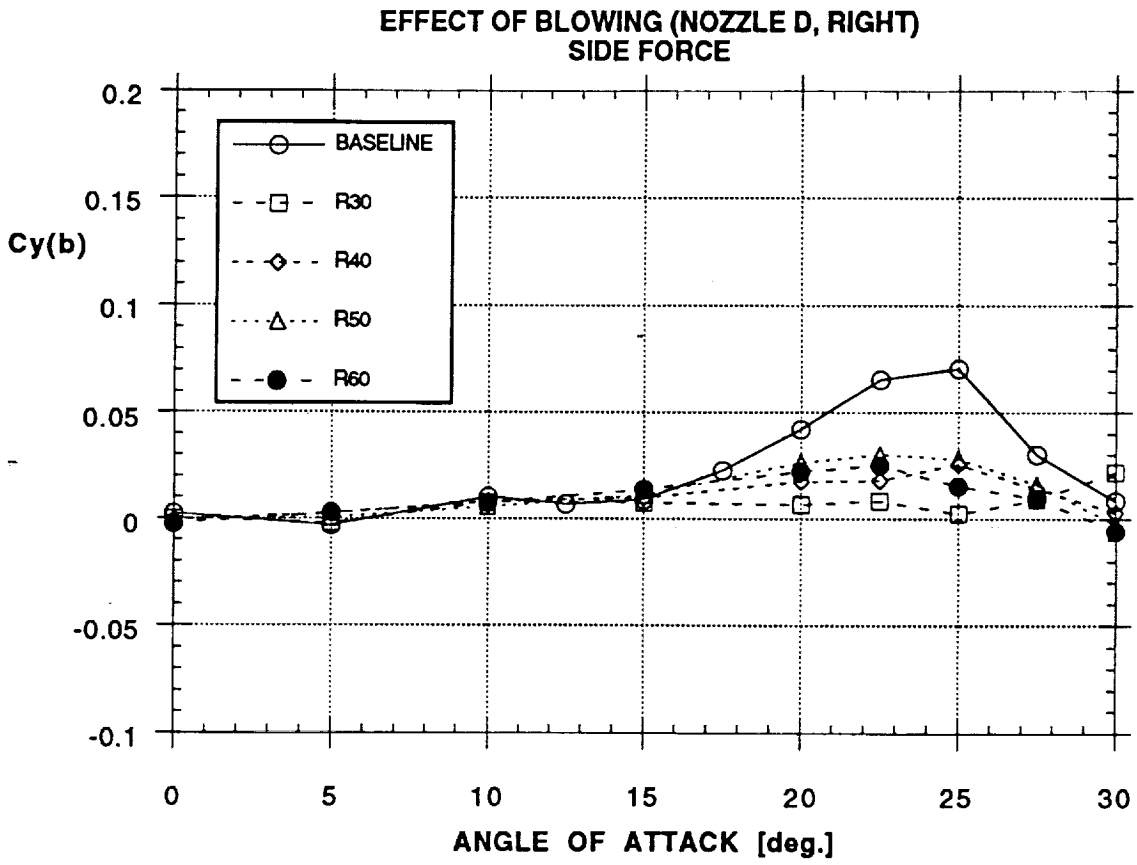

d)

Figure 24 - Continued

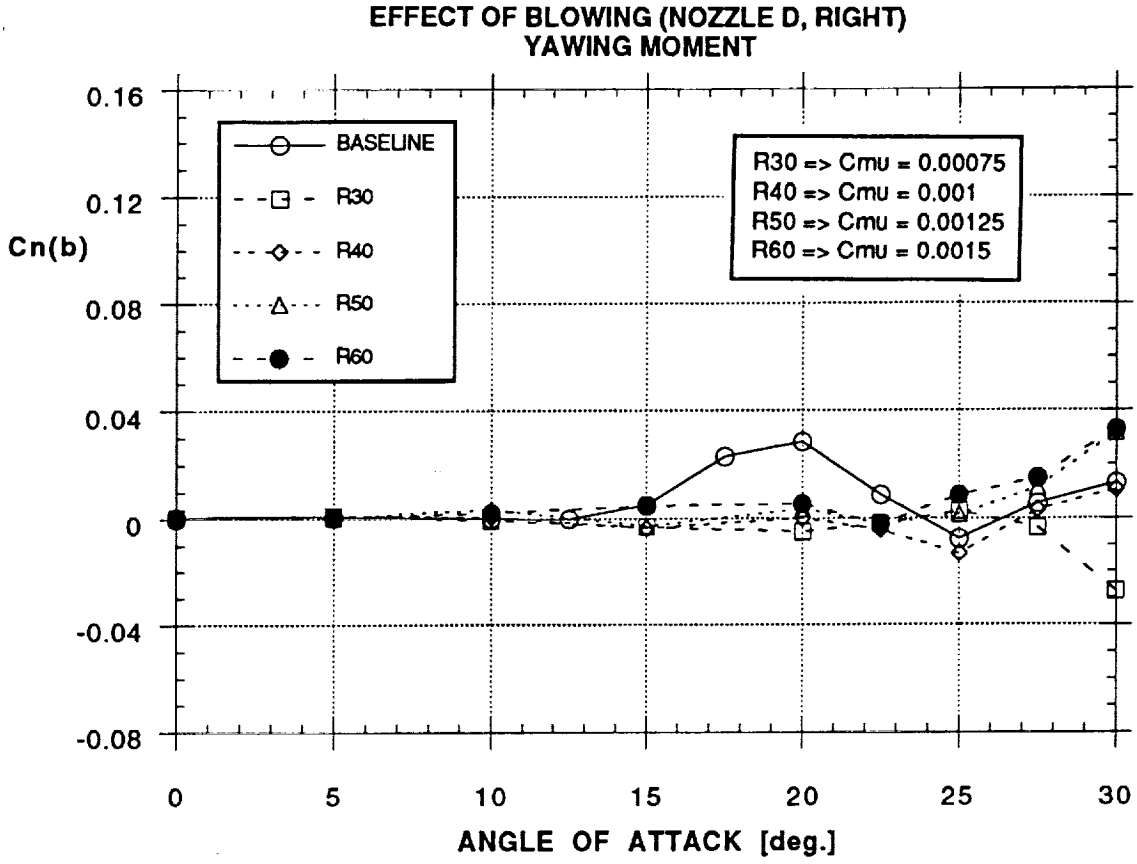

e)

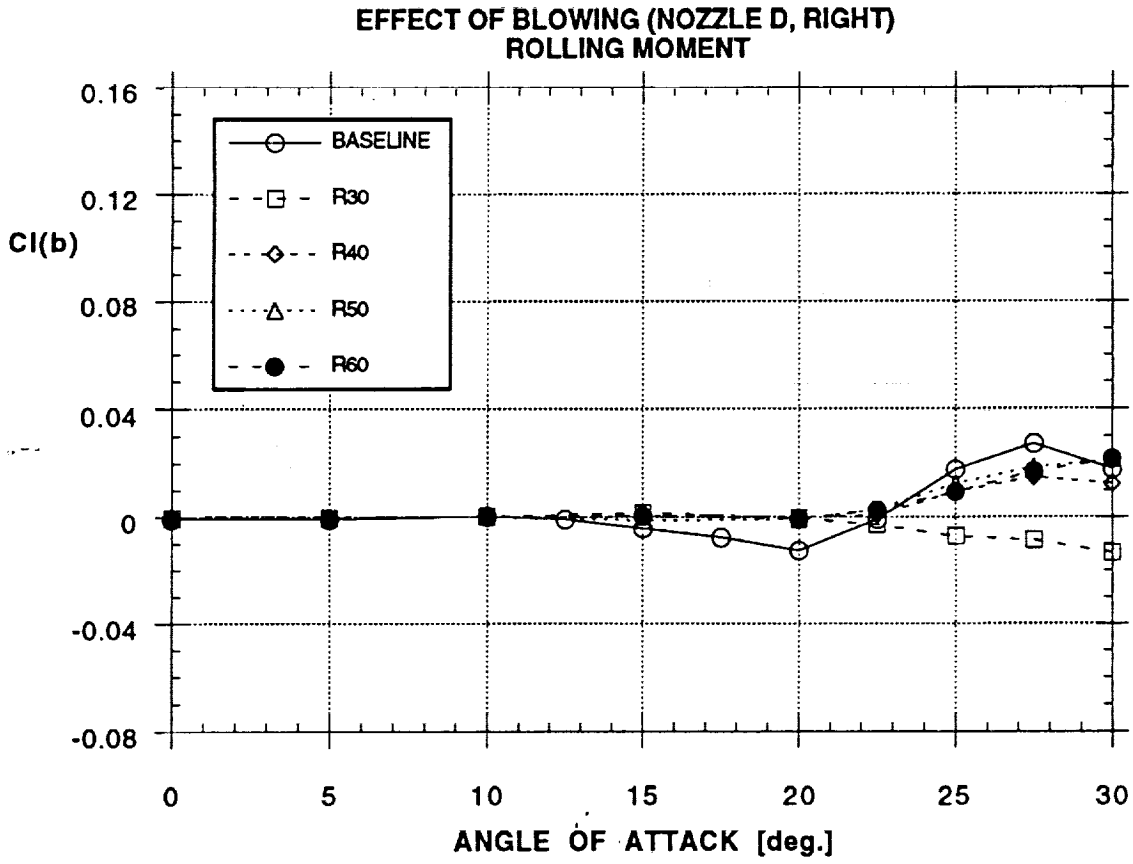

f)

Figure 24 - Concluded

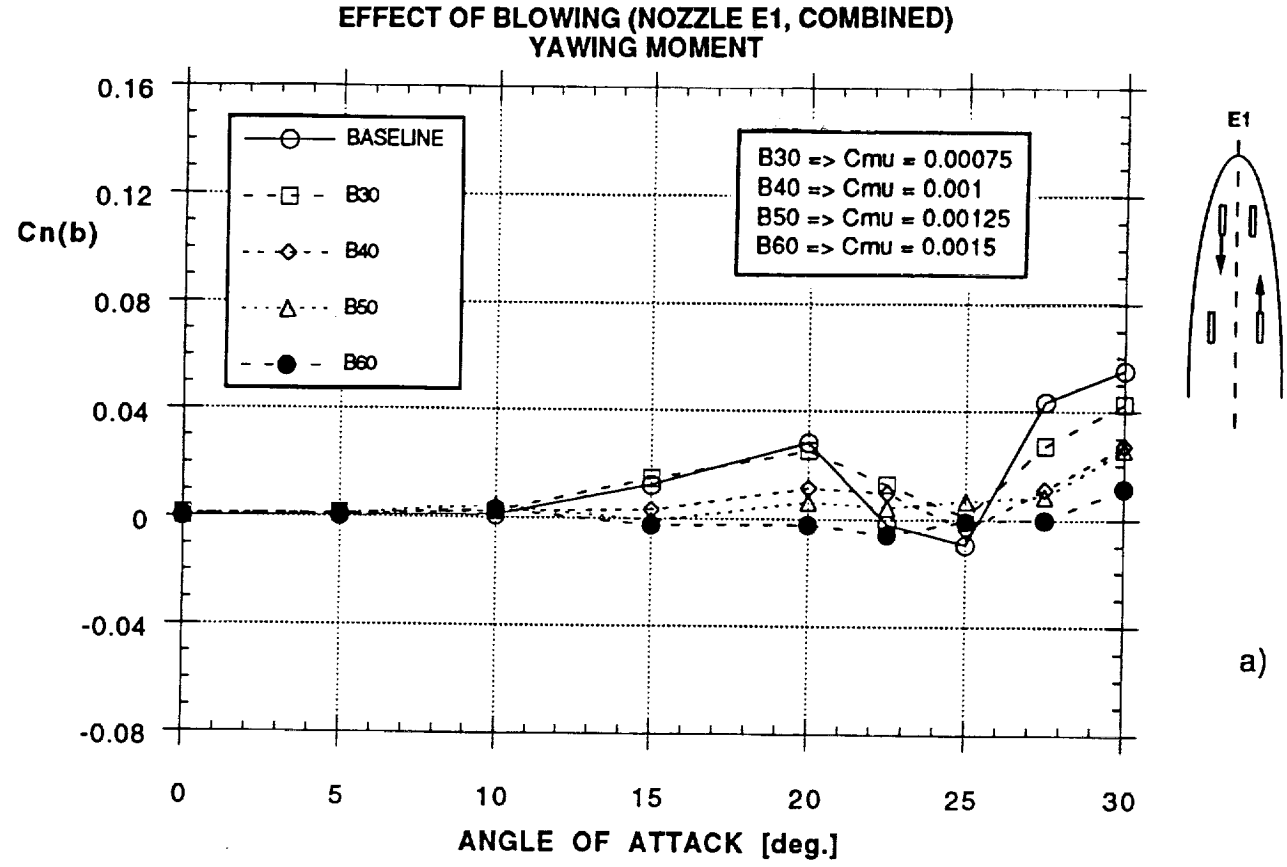

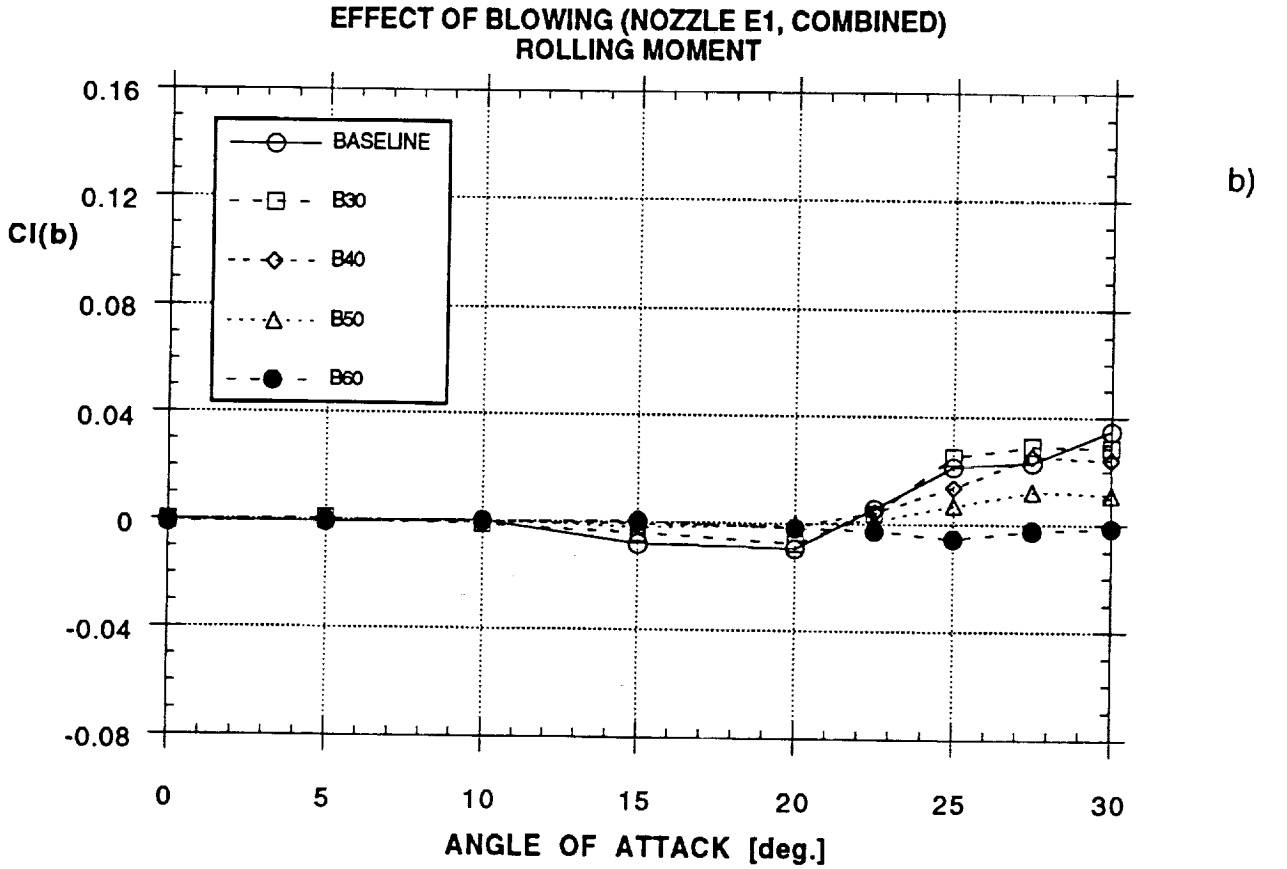

Figure 25 - Effect of Combined Blowing on Forces and Moments (Nozzle E1, $\beta = 0°$)

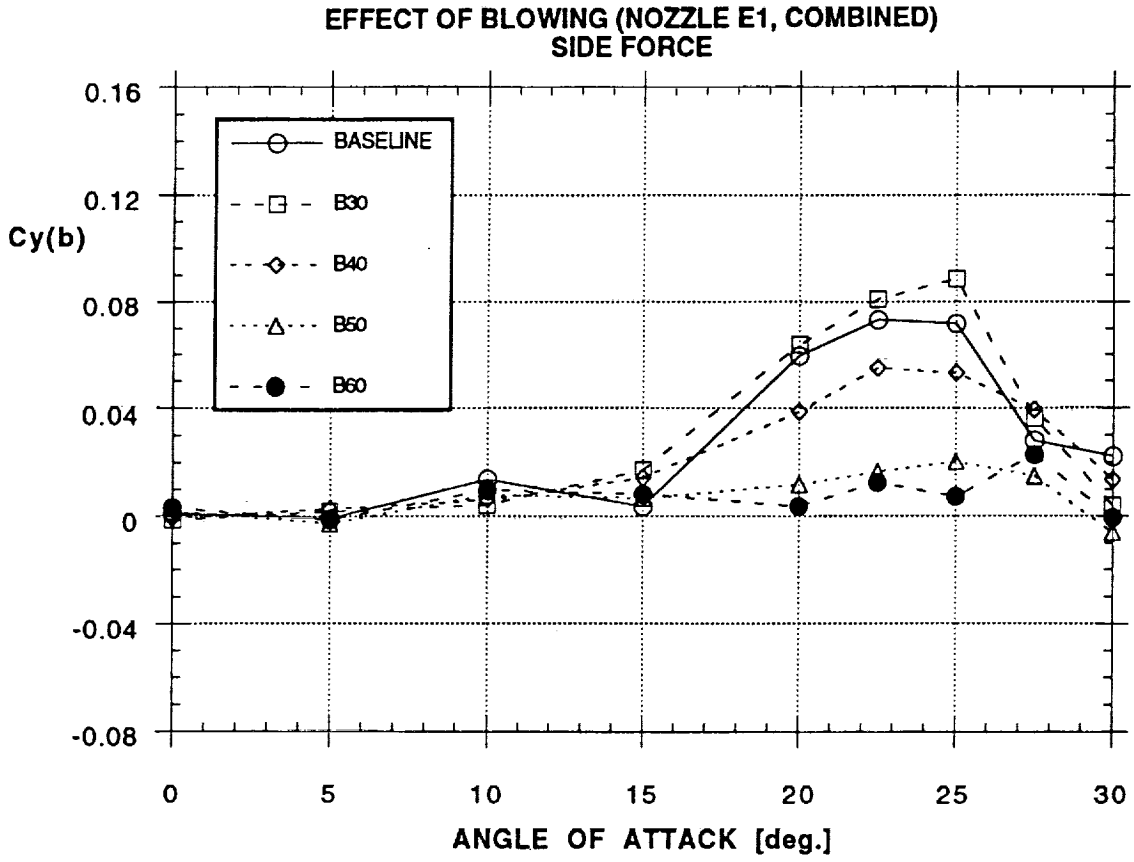

c)

Figure 25 - Concluded

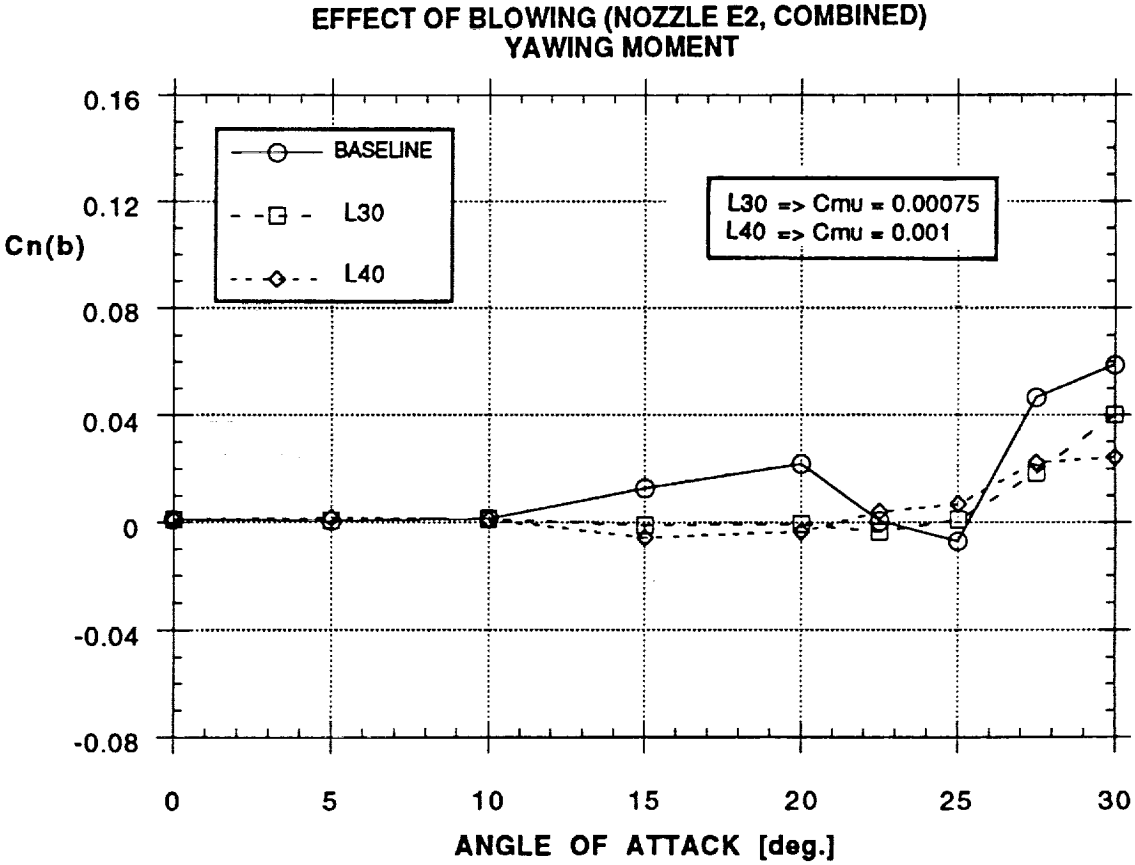

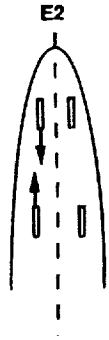

a)

Figure 26 - Effect of Combined Blowing on Forces and Moments (Nozzle E2, Left Side, $\beta = 0°$)

b)

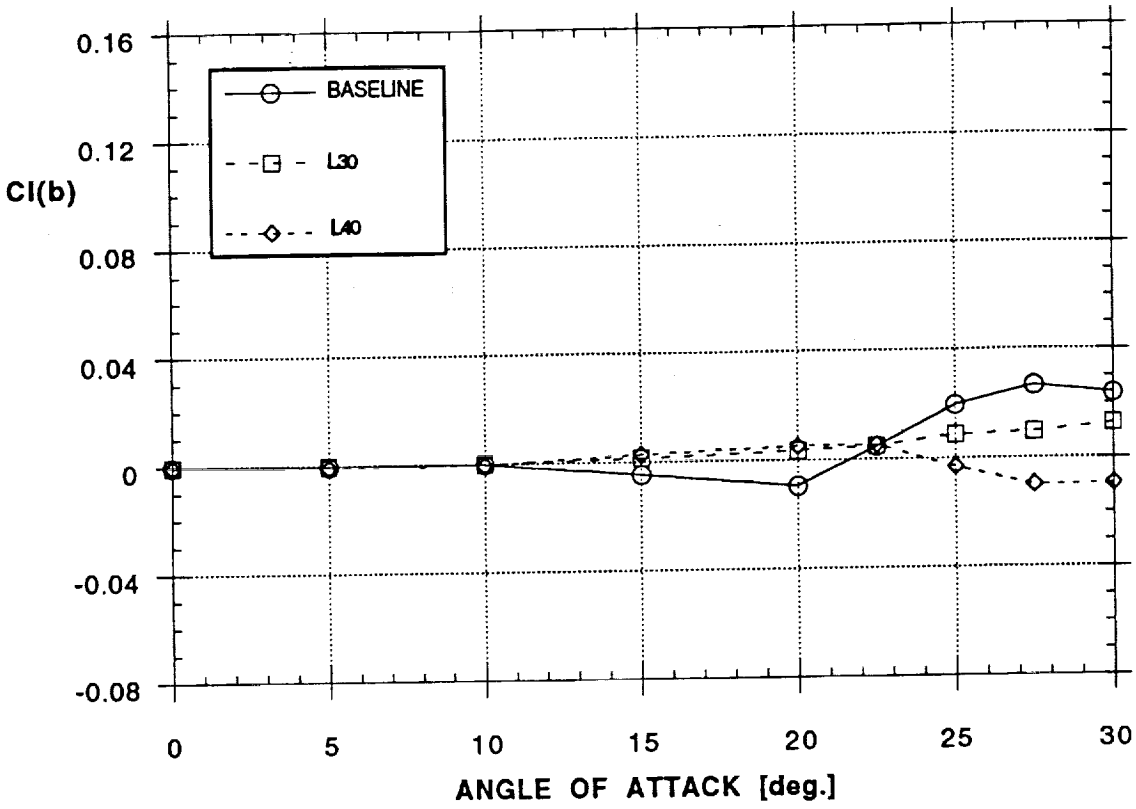

c)

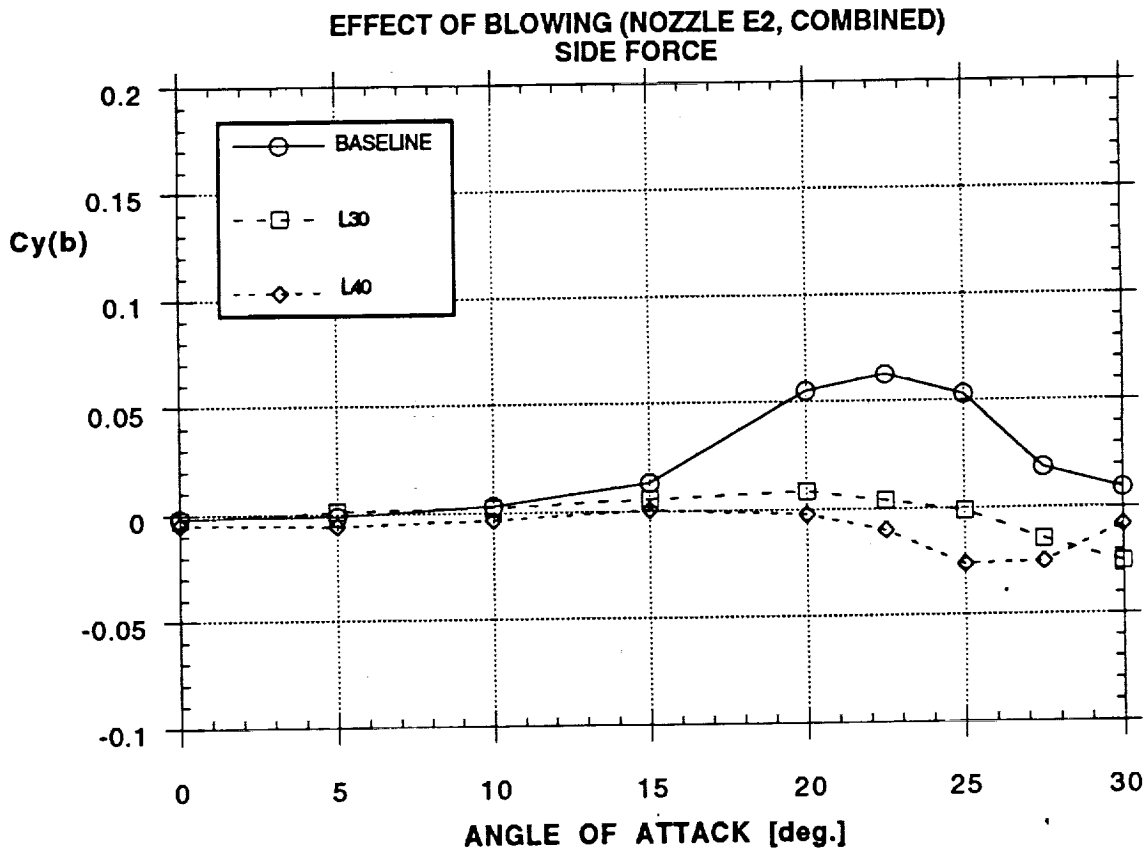

Figure 26 - Concluded

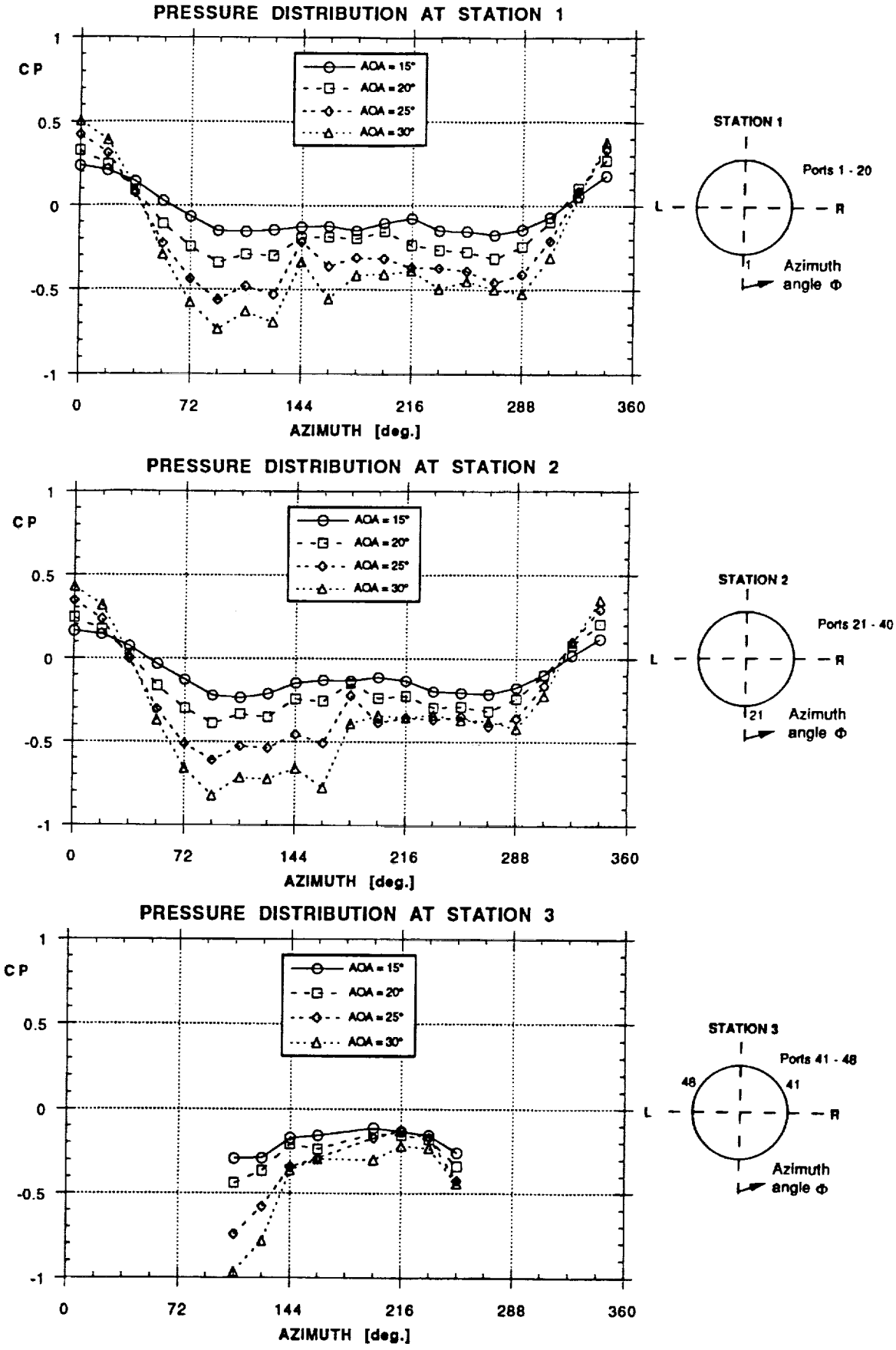

Figure 27 - Forebody Pressure Distribution at Different Angles of Attack ($\beta = 0°$)

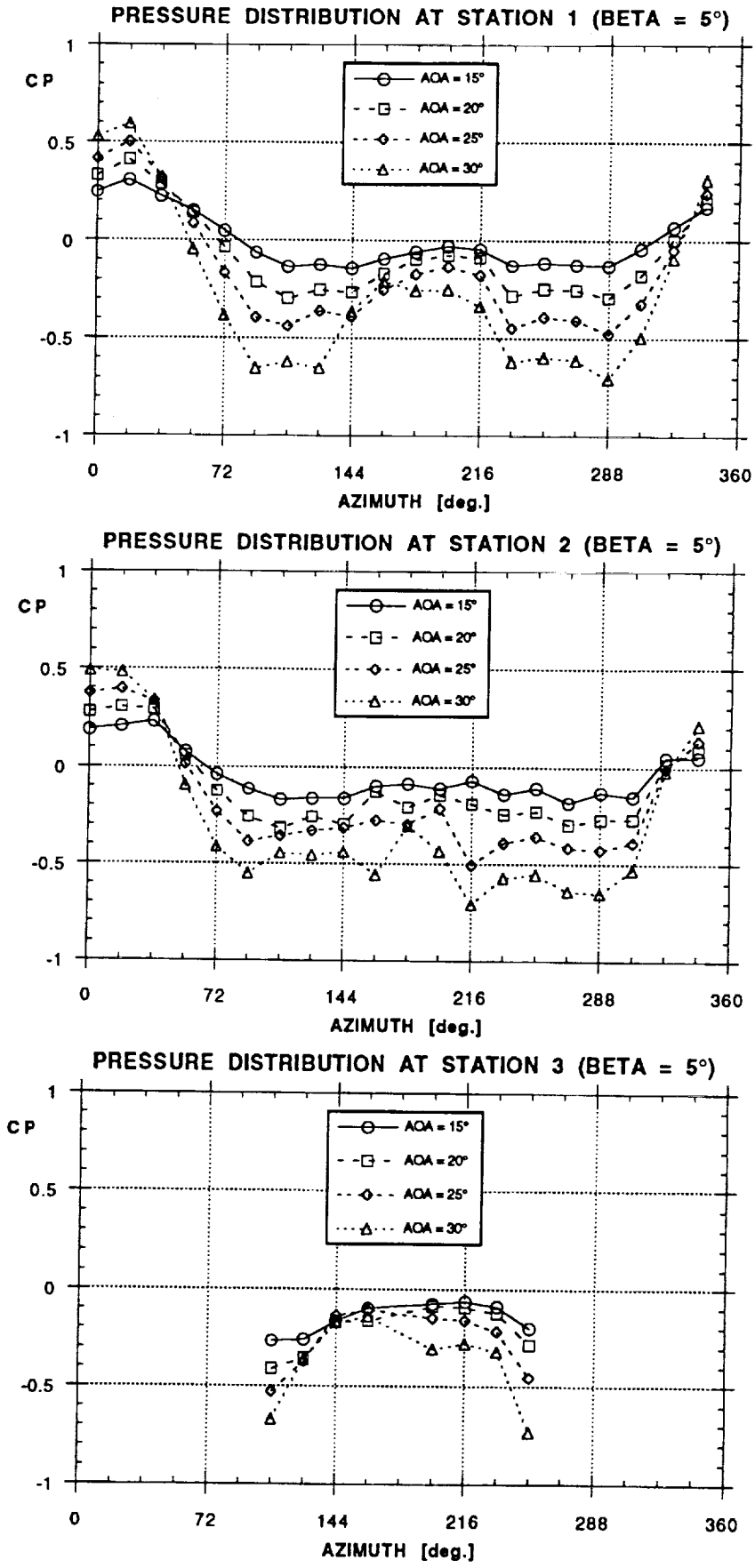

Figure 28 - Forebody Pressure Distribution at Different Angles of Attack ($\beta = 5°$)

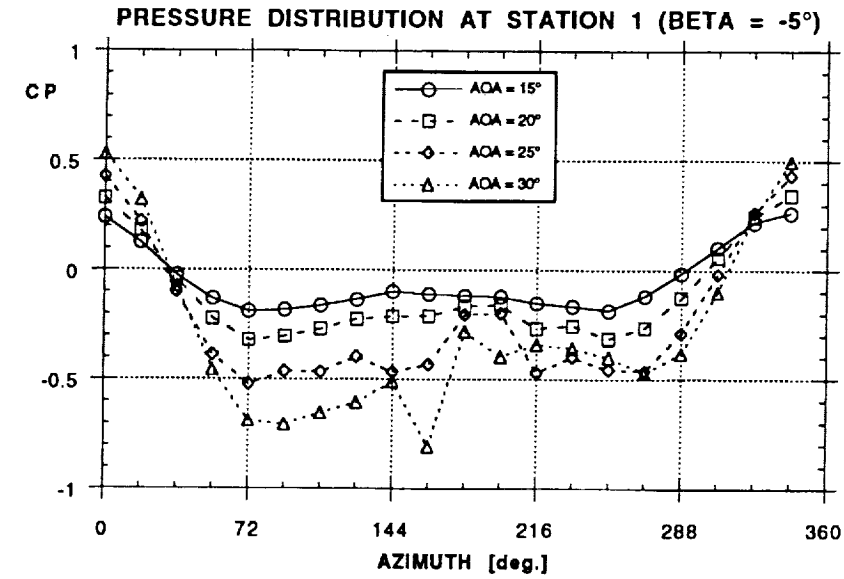

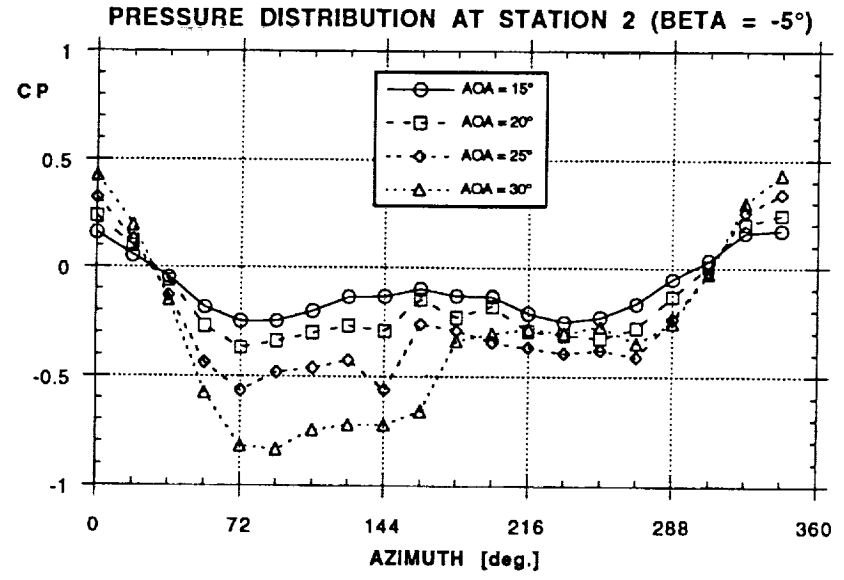

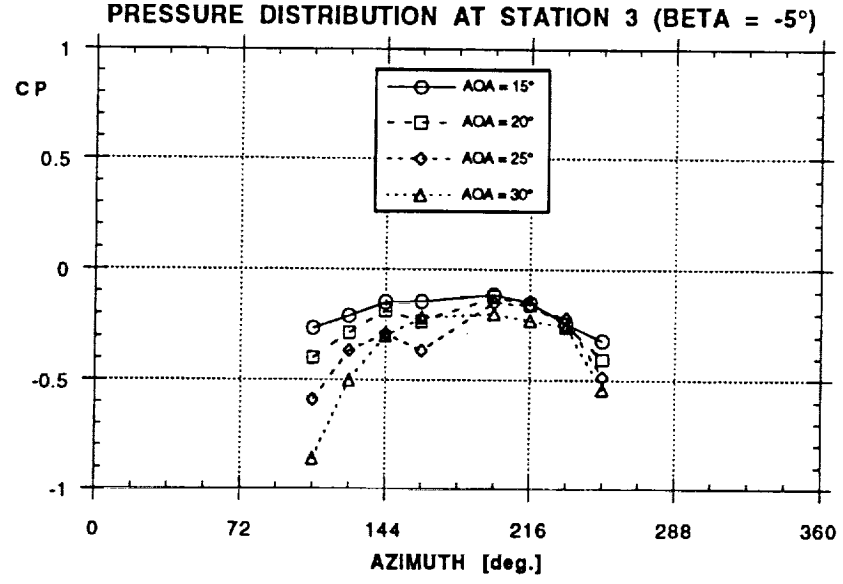

Figure 29 - Forebody Pressure Distribution at Different Angles of Attack ($\beta = -5°$)

C-2

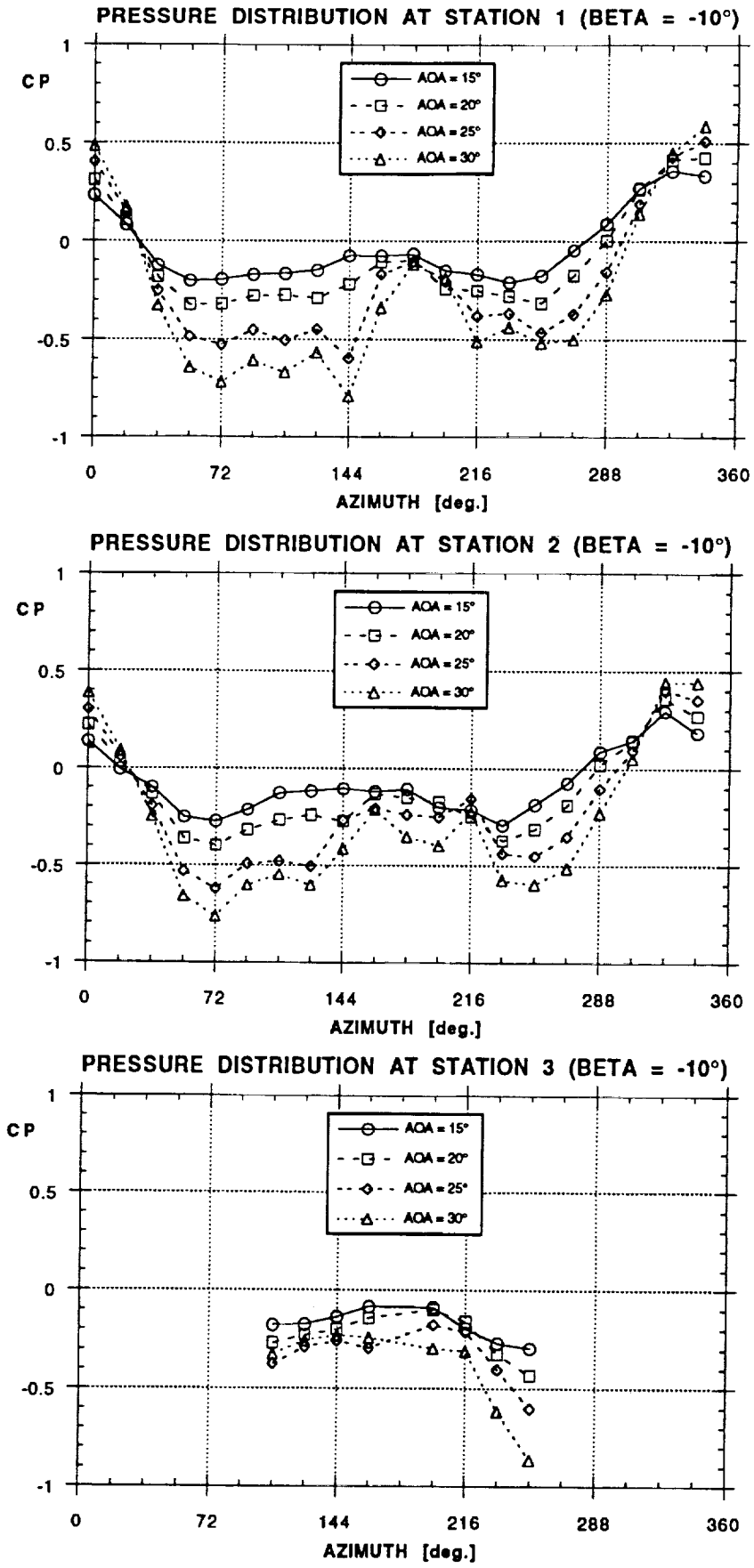

Figure 30 - Forebody Pressure Distribution at Different Angles of Attack ($\beta = -10°$)

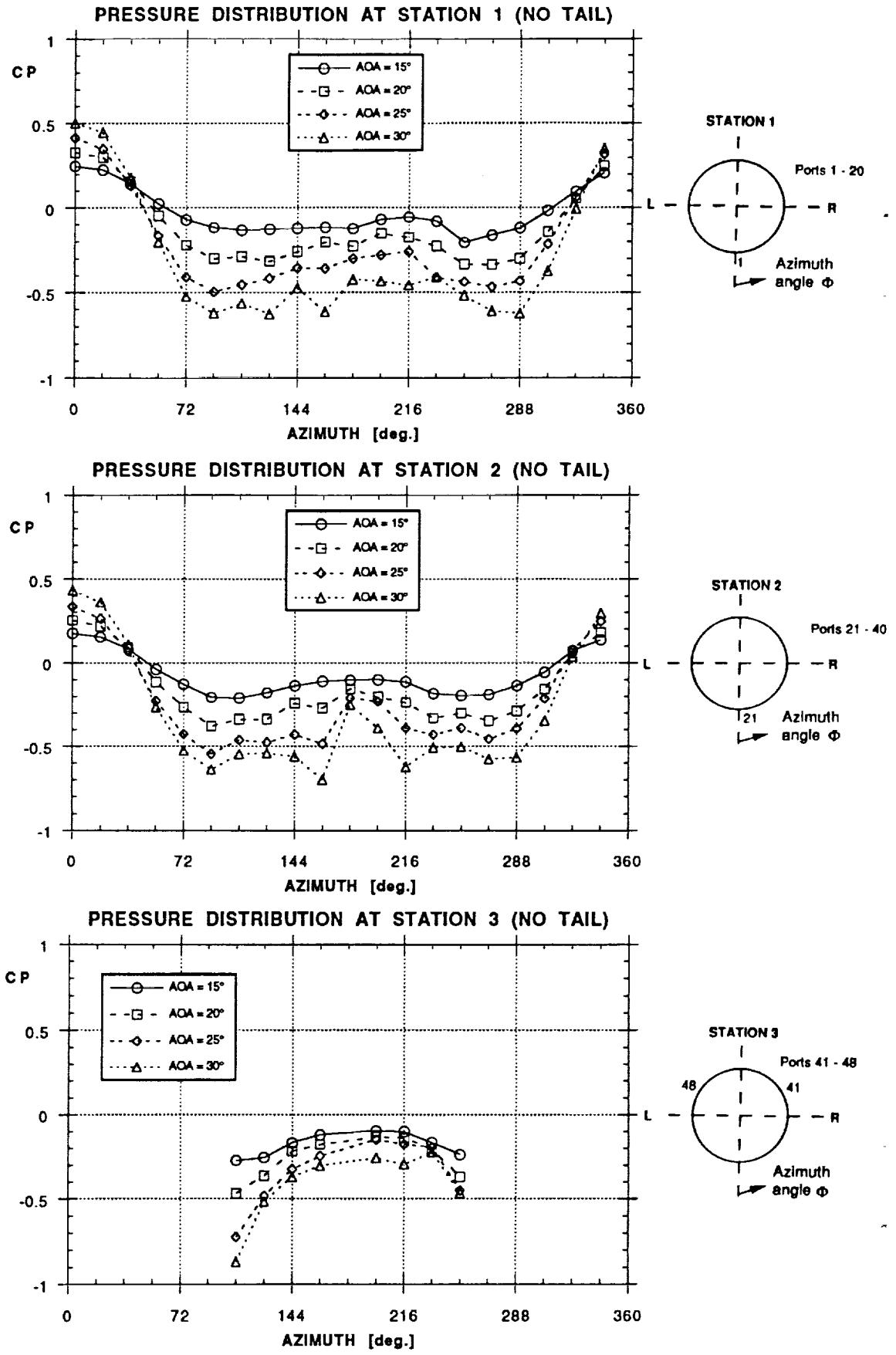

Figure 31 - Forebody Pressure Distribution at Different Angles of Attack (No Tail, $\beta = 0°$)

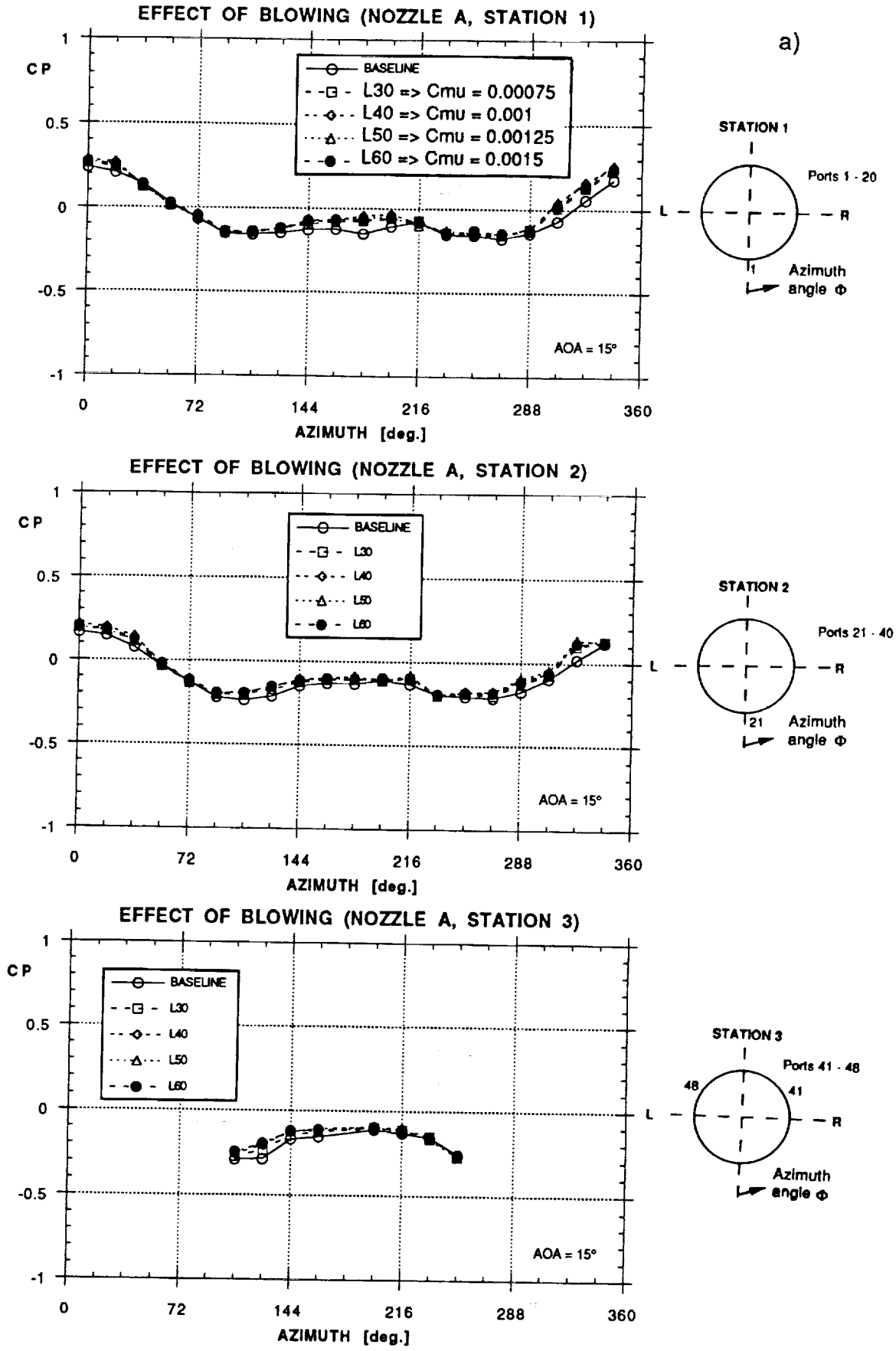

Figure 32 - Effect of Aft Blowing on Forebody Pressure Distribution (Nozzle A, $\alpha = 15°$, Left, Right and Both Sides)

b)

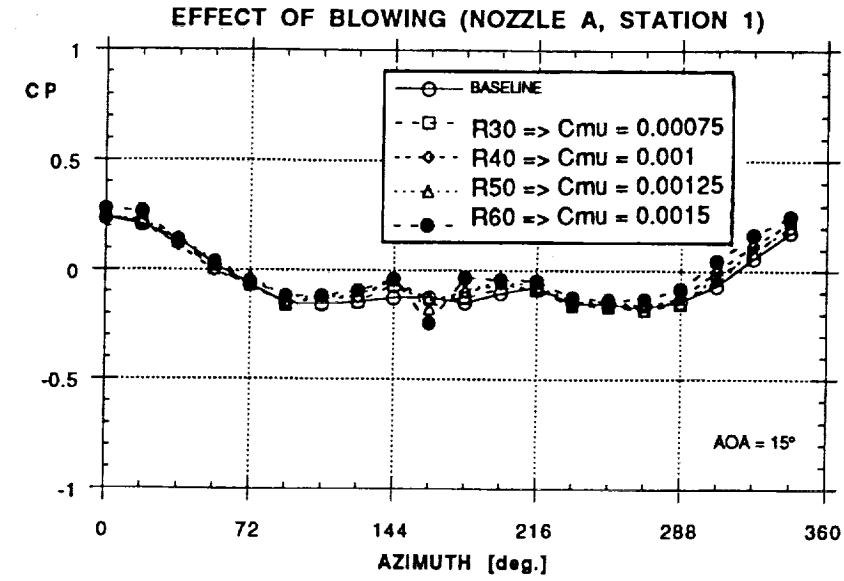

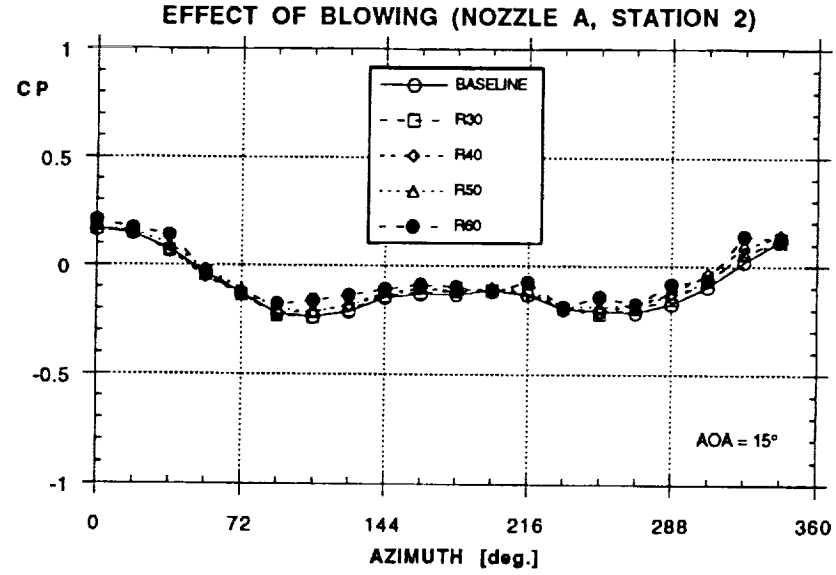

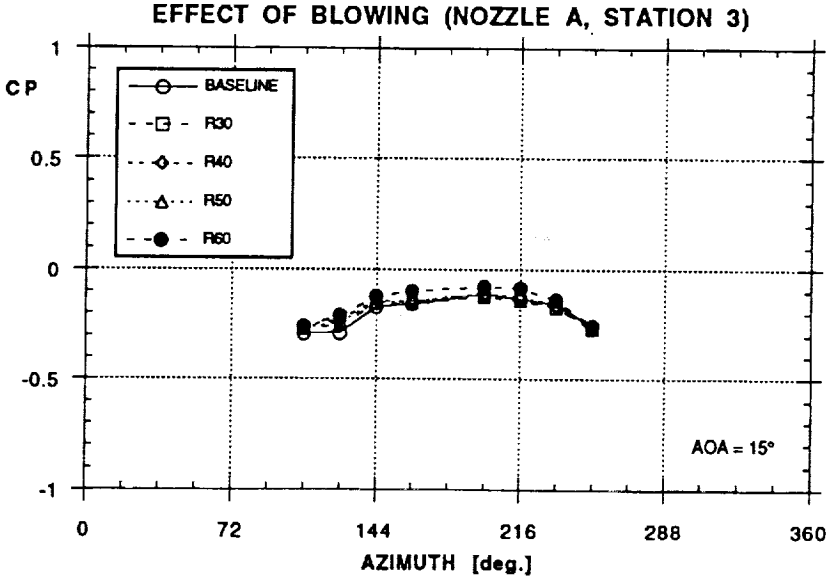

Figure 32 - Continued

c)

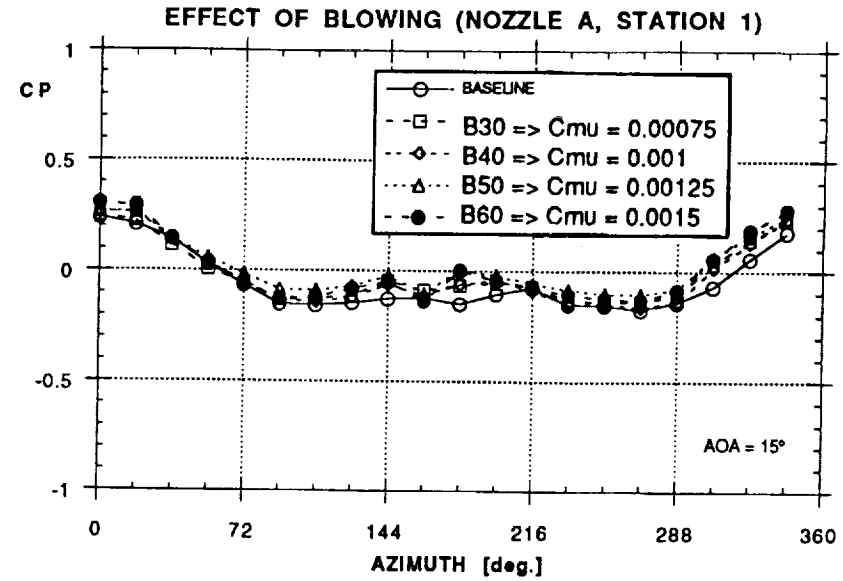

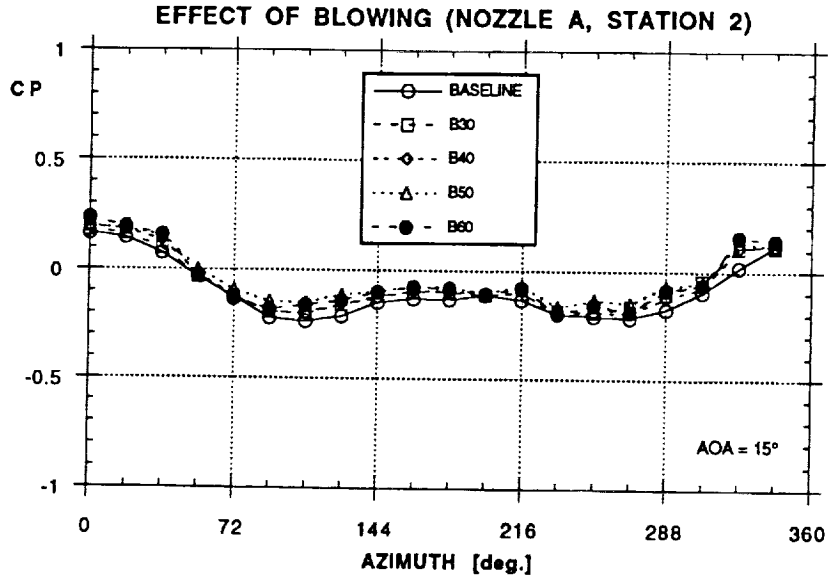

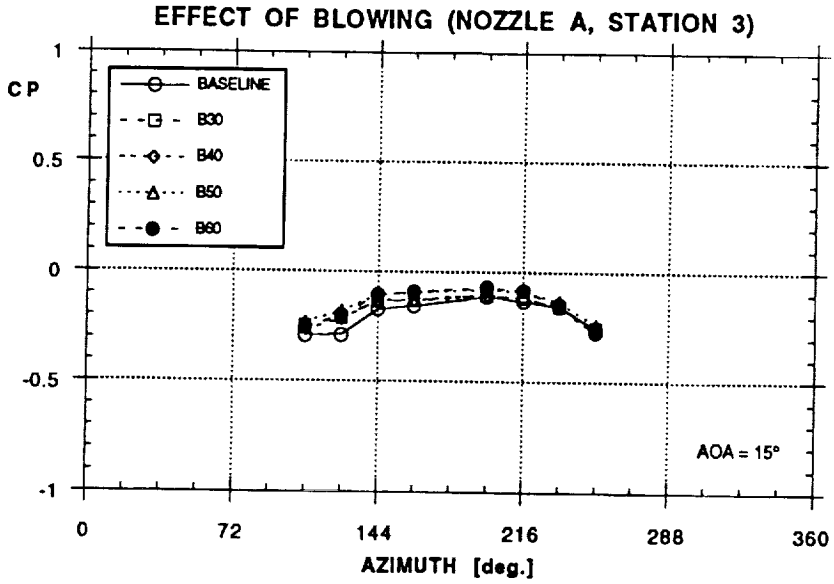

Figure 32 - Concluded

a)

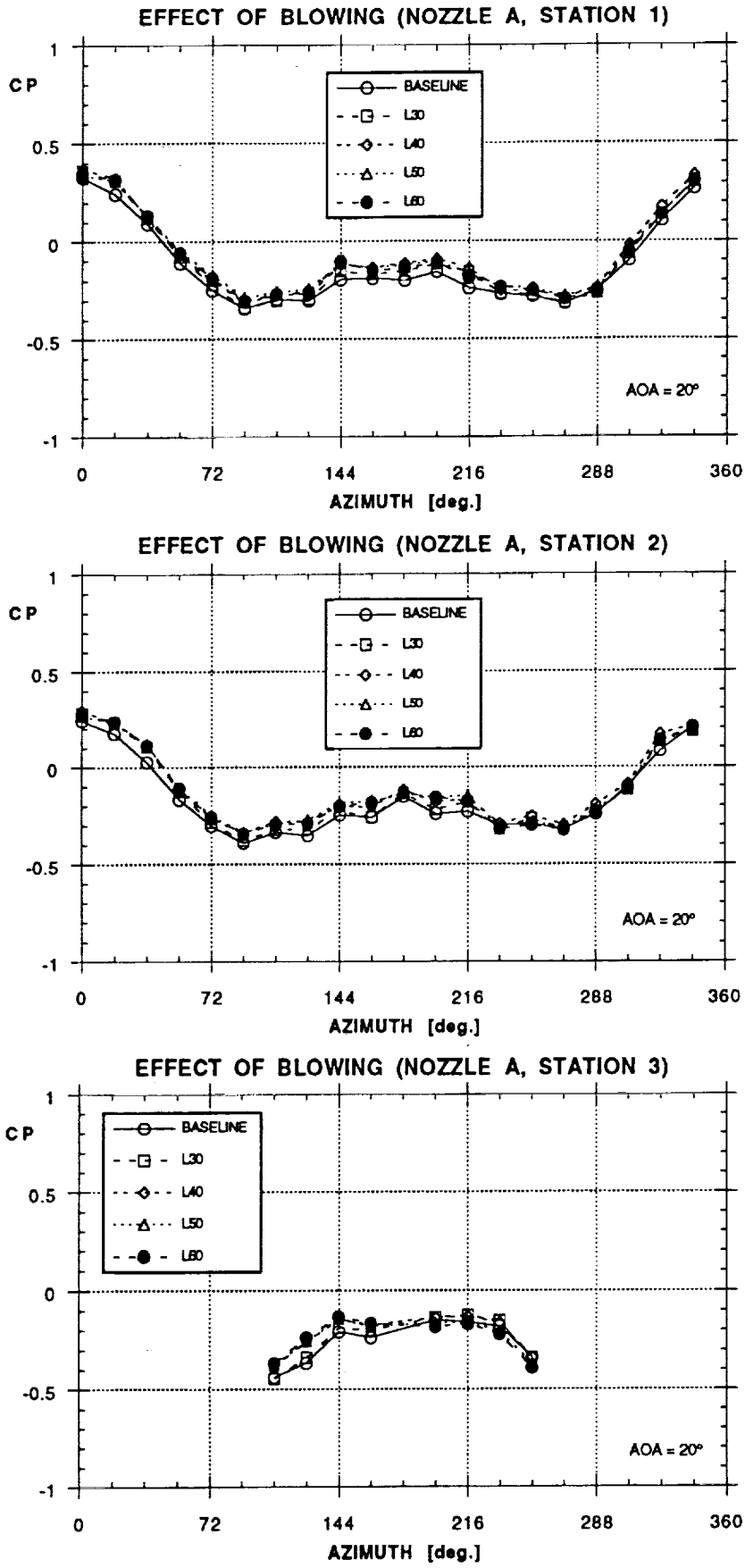

Figure 33 - Effect of Aft Blowing on Forebody Pressure Distribution (Nozzle A, $\alpha = 20°$, Left, Right and Both Sides)

b)

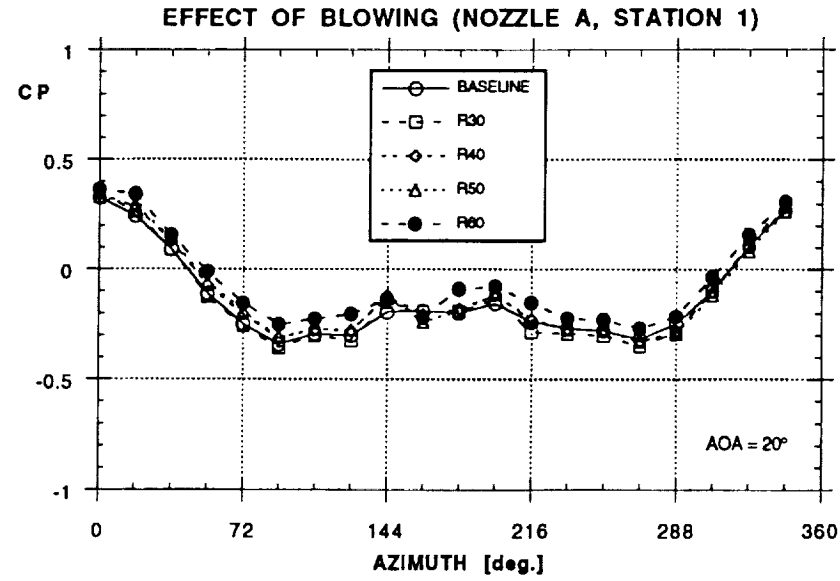

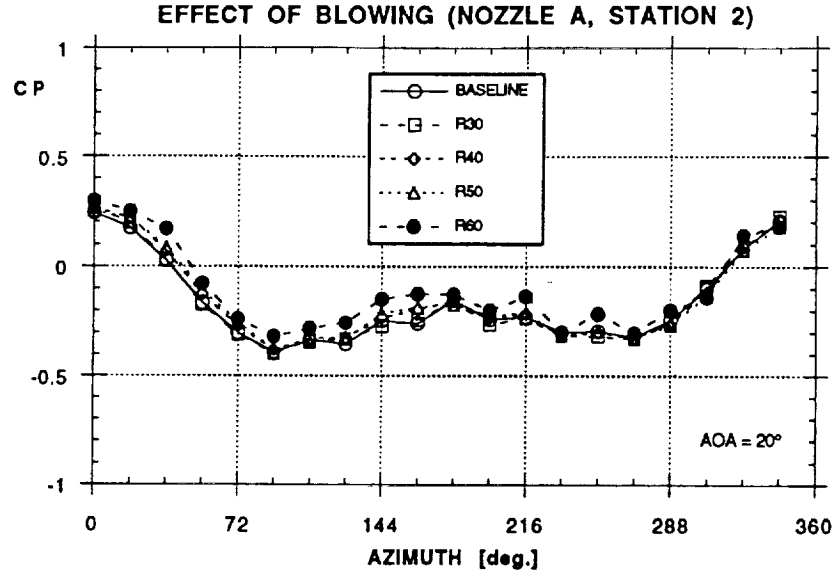

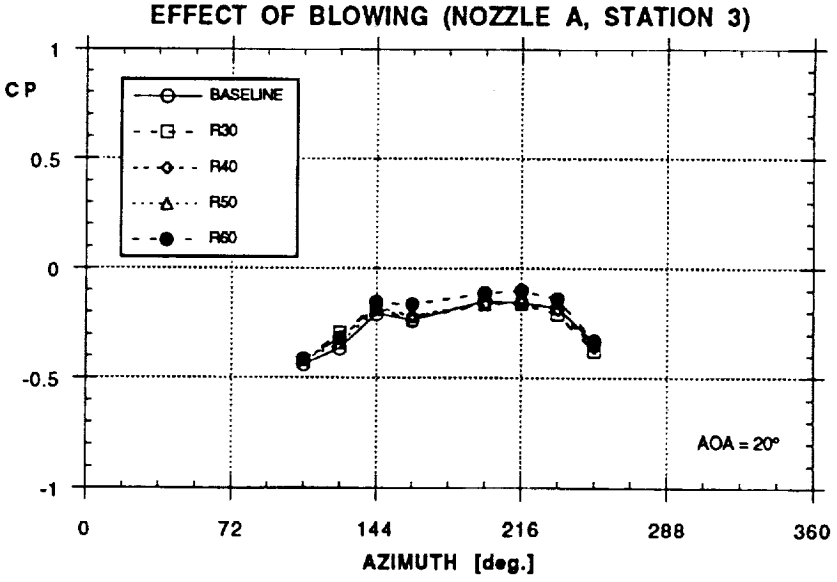

Figure 33 - Continued

c)

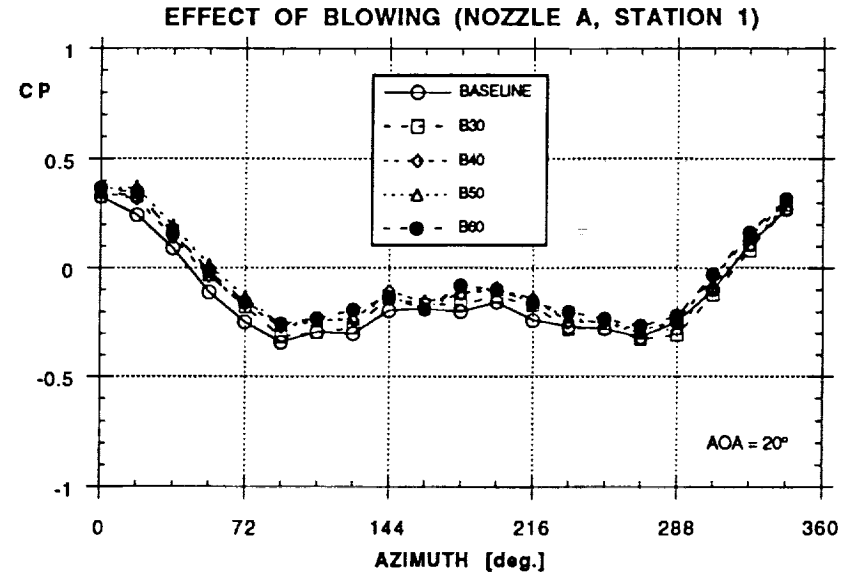

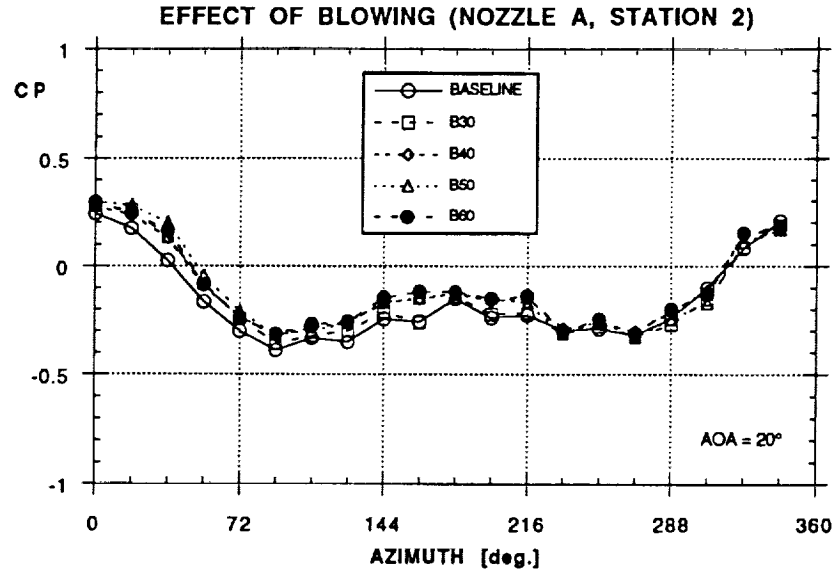

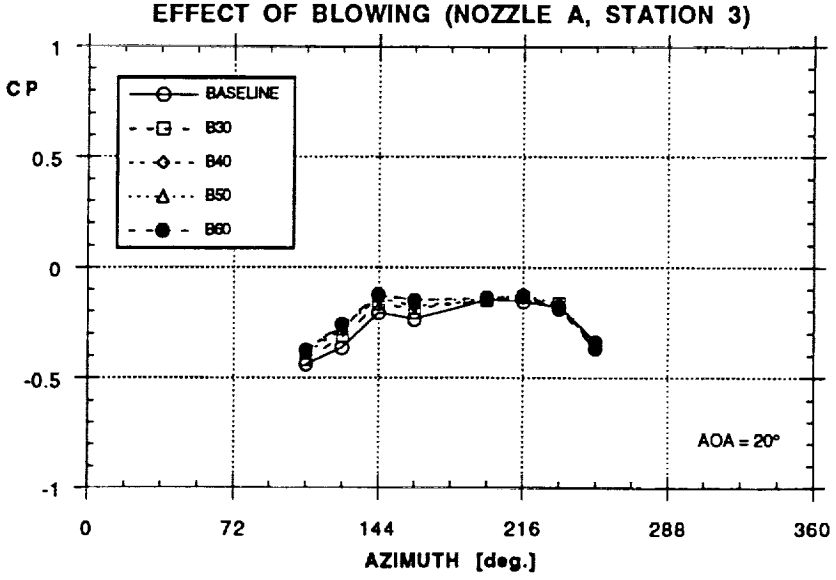

Figure 33 - Concluded

a)

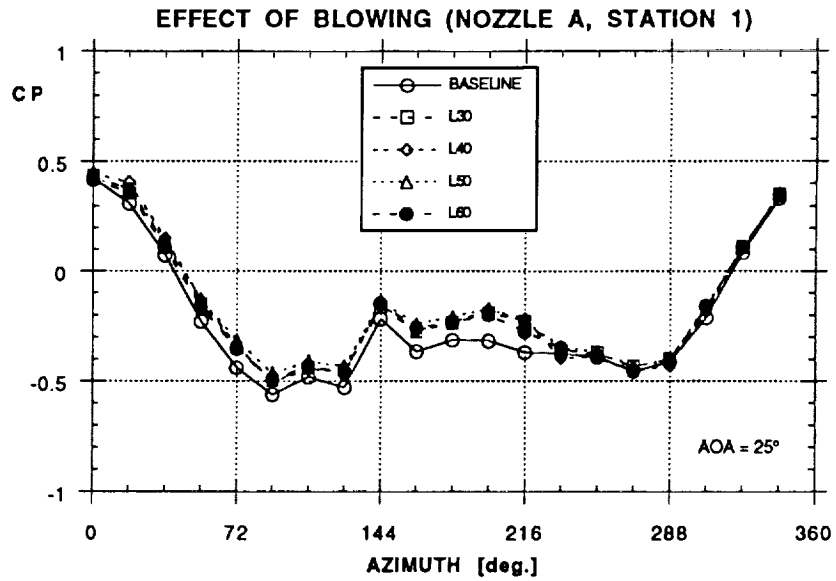

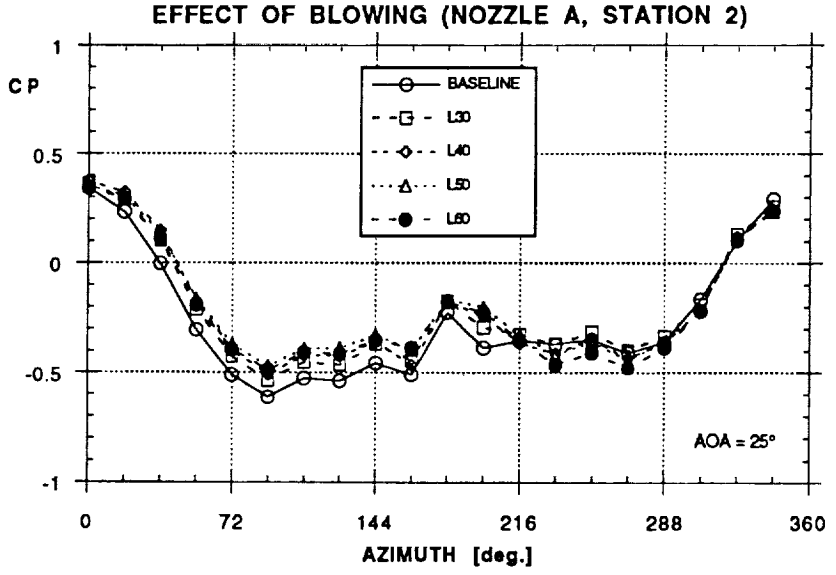

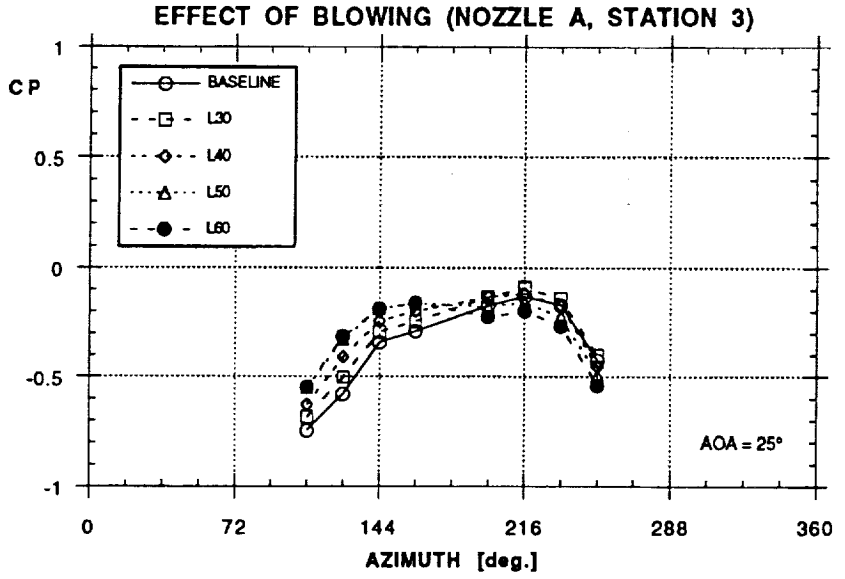

Figure 34 - Effect of Aft Blowing on Forebody Pressure Distribution (Nozzle A, $\alpha = 25°$, Left, Right and Both Sides)

b)

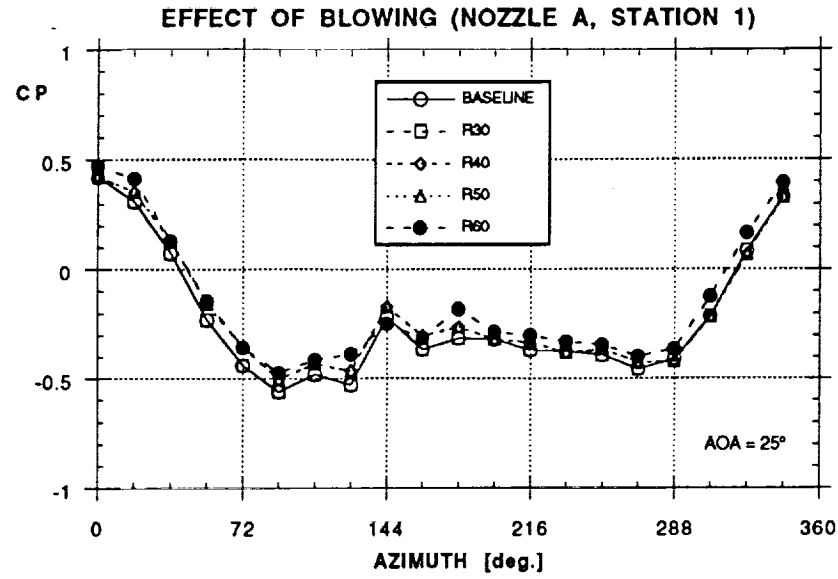

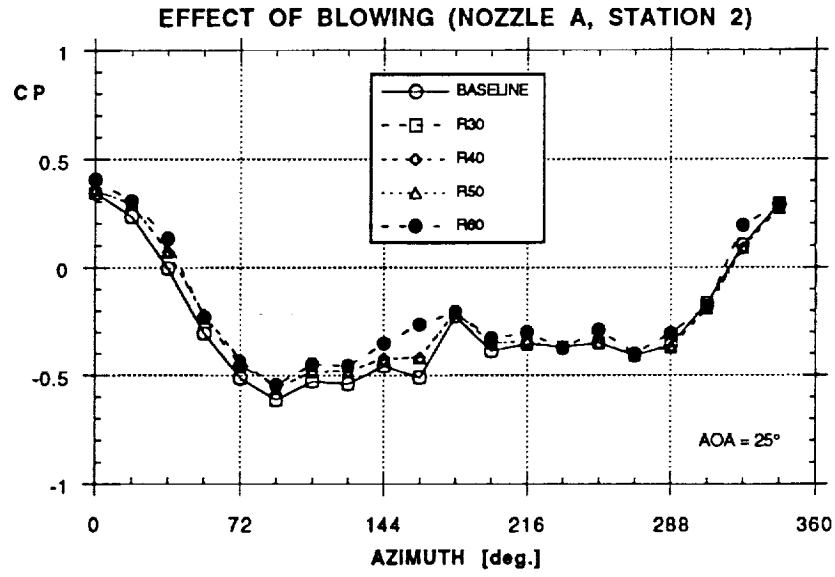

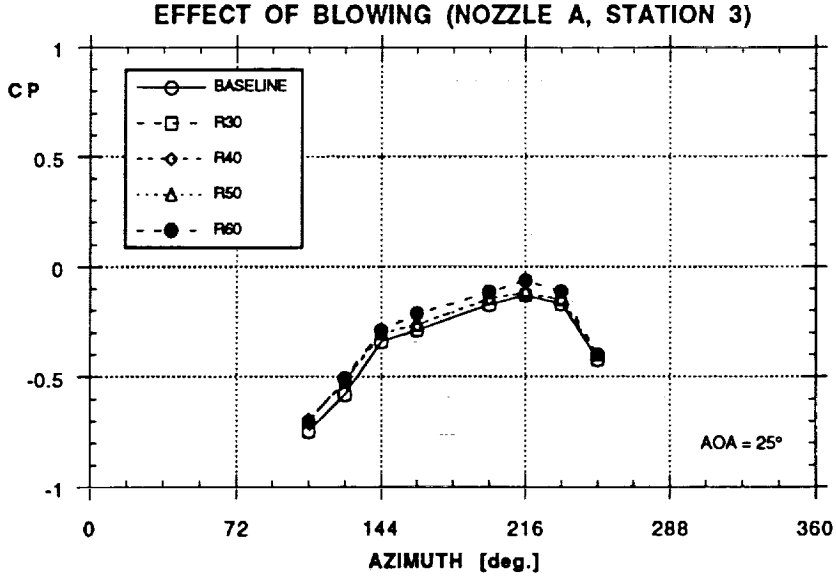

Figure 34 - Continued

c)

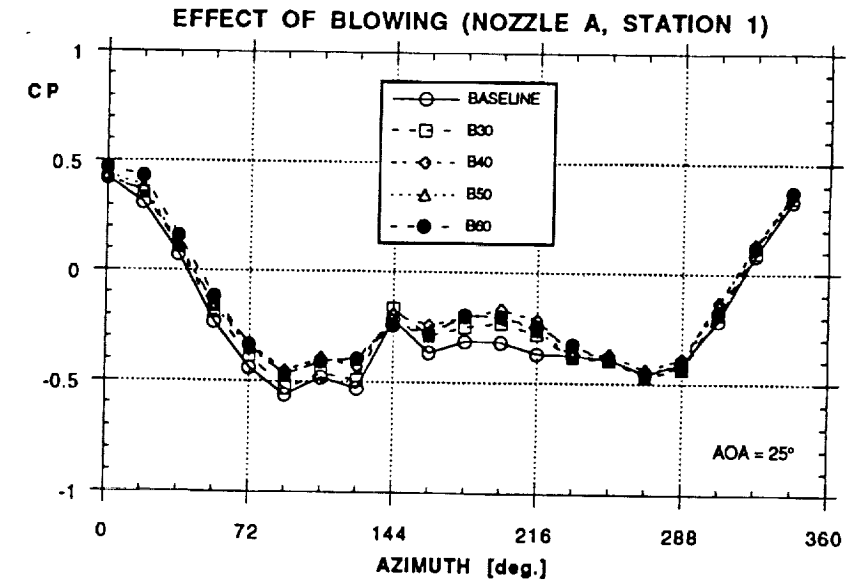

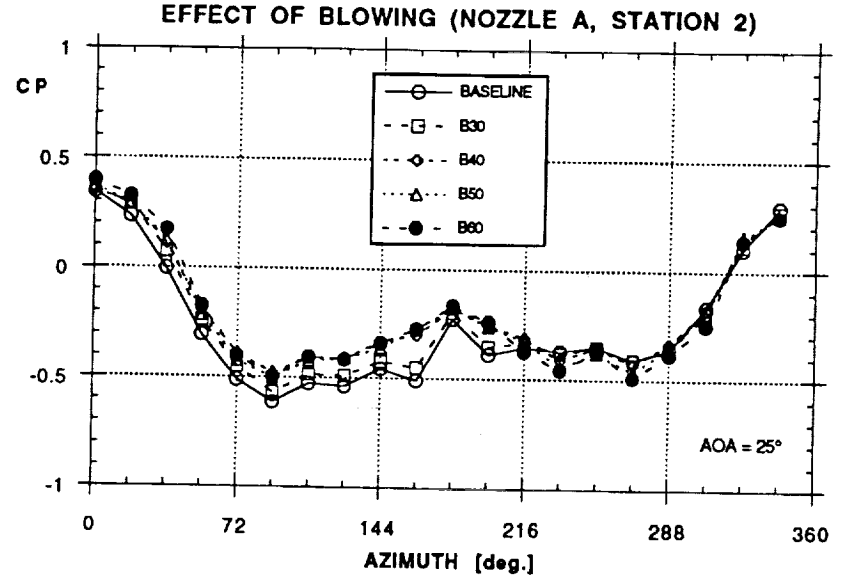

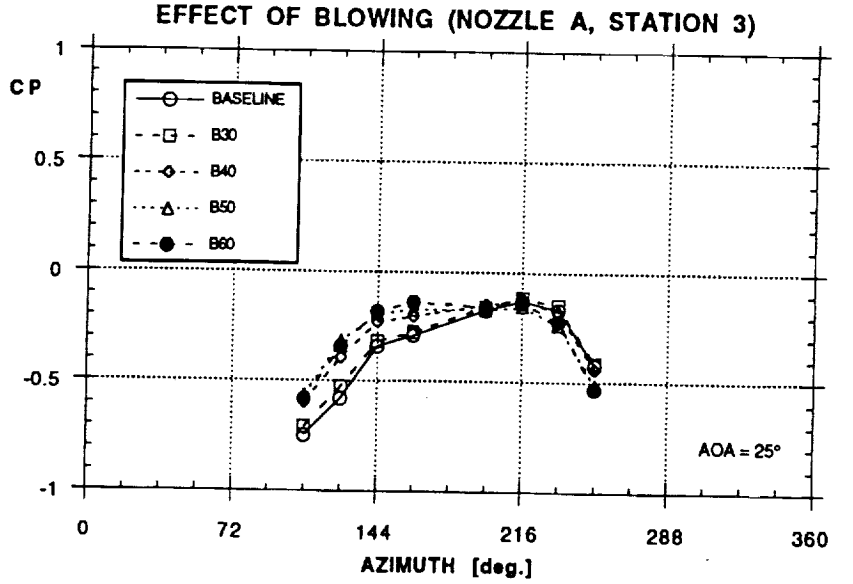

Figure 34 - Concluded

a)

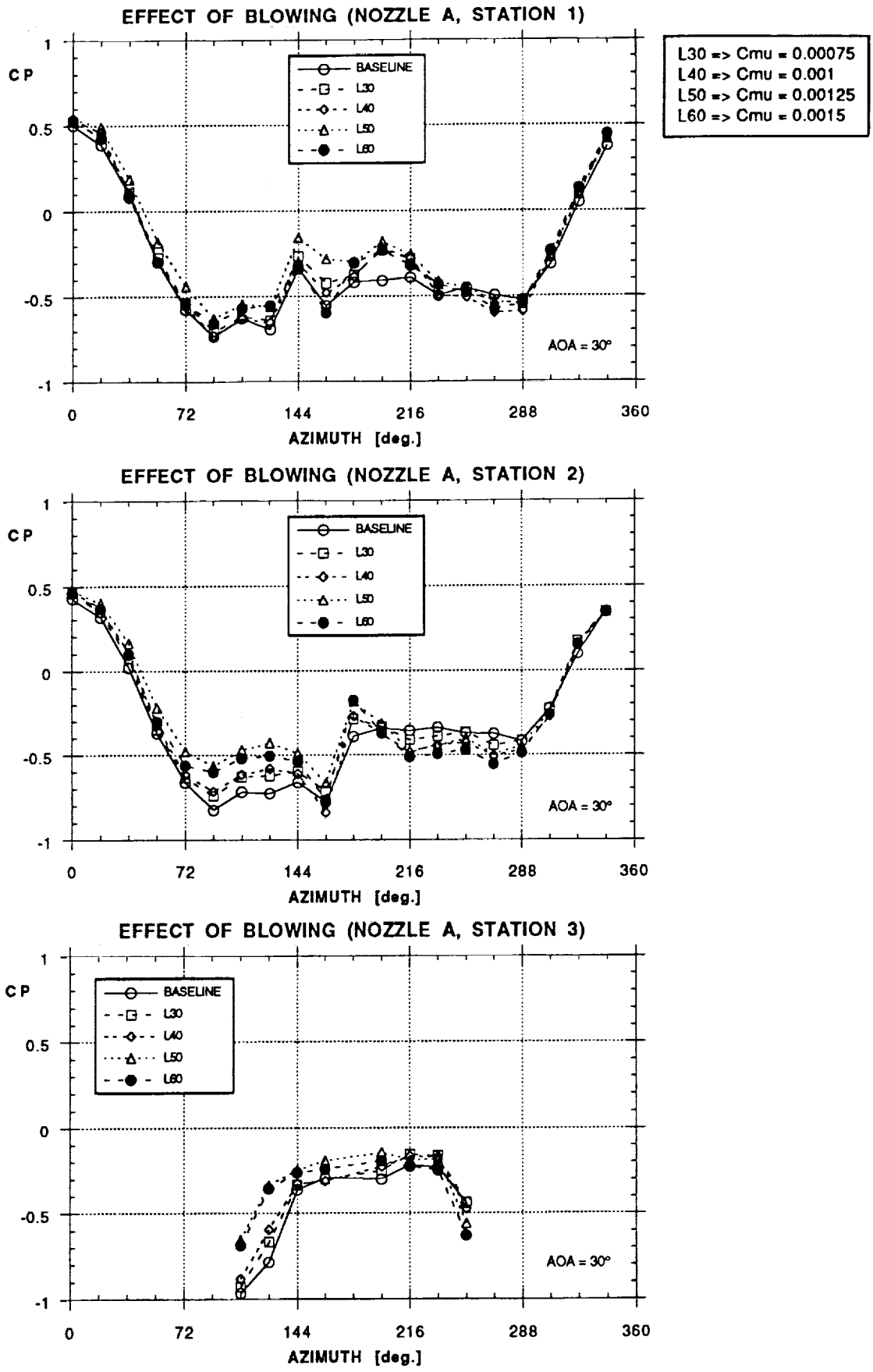

Figure 35 - Effect of Aft Blowing on Forebody Pressure Distribution (Nozzle A, $\alpha = 30°$, Left, Right and Both Sides)

b)

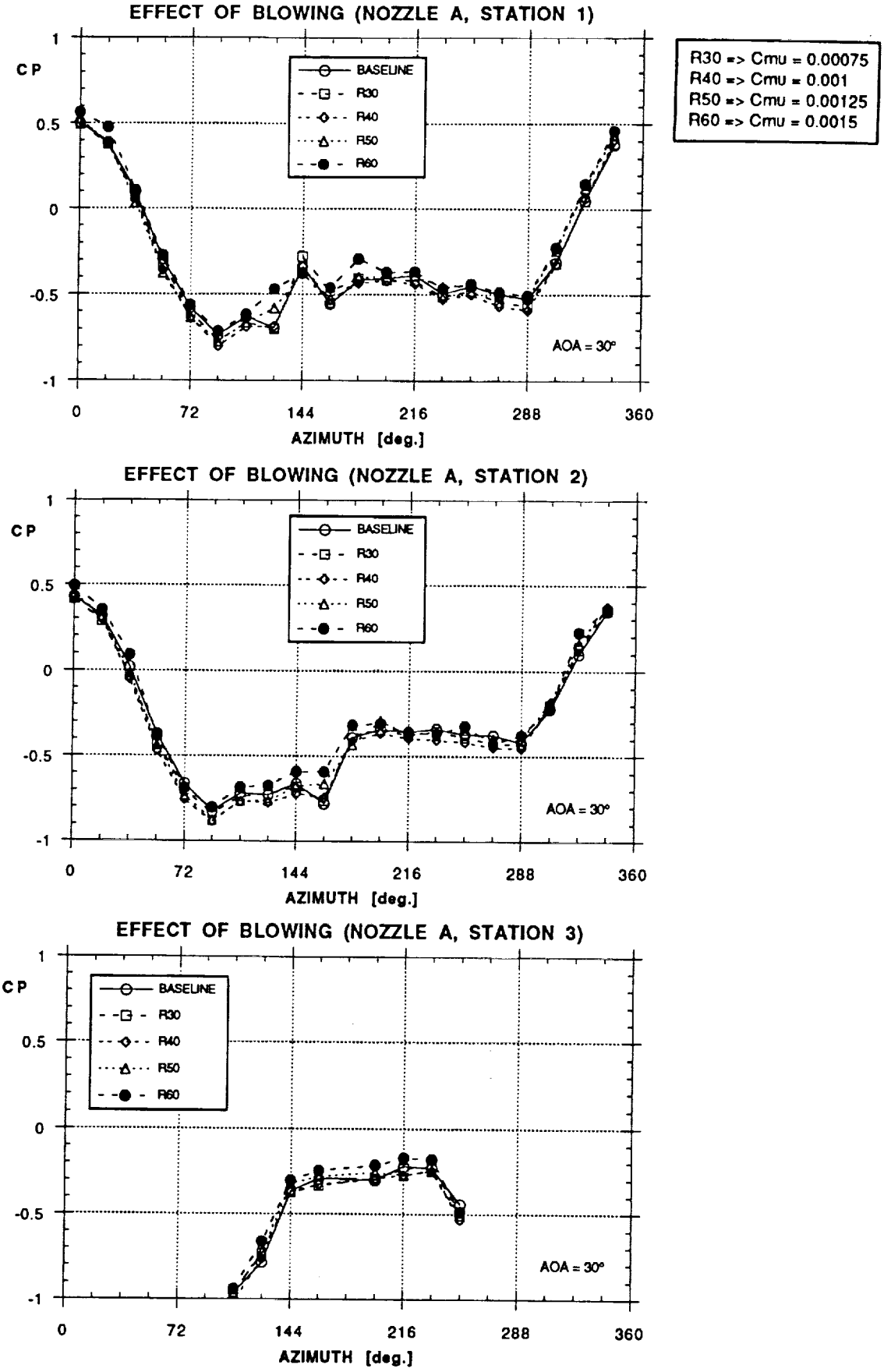

Figure 35 - Continued

c)

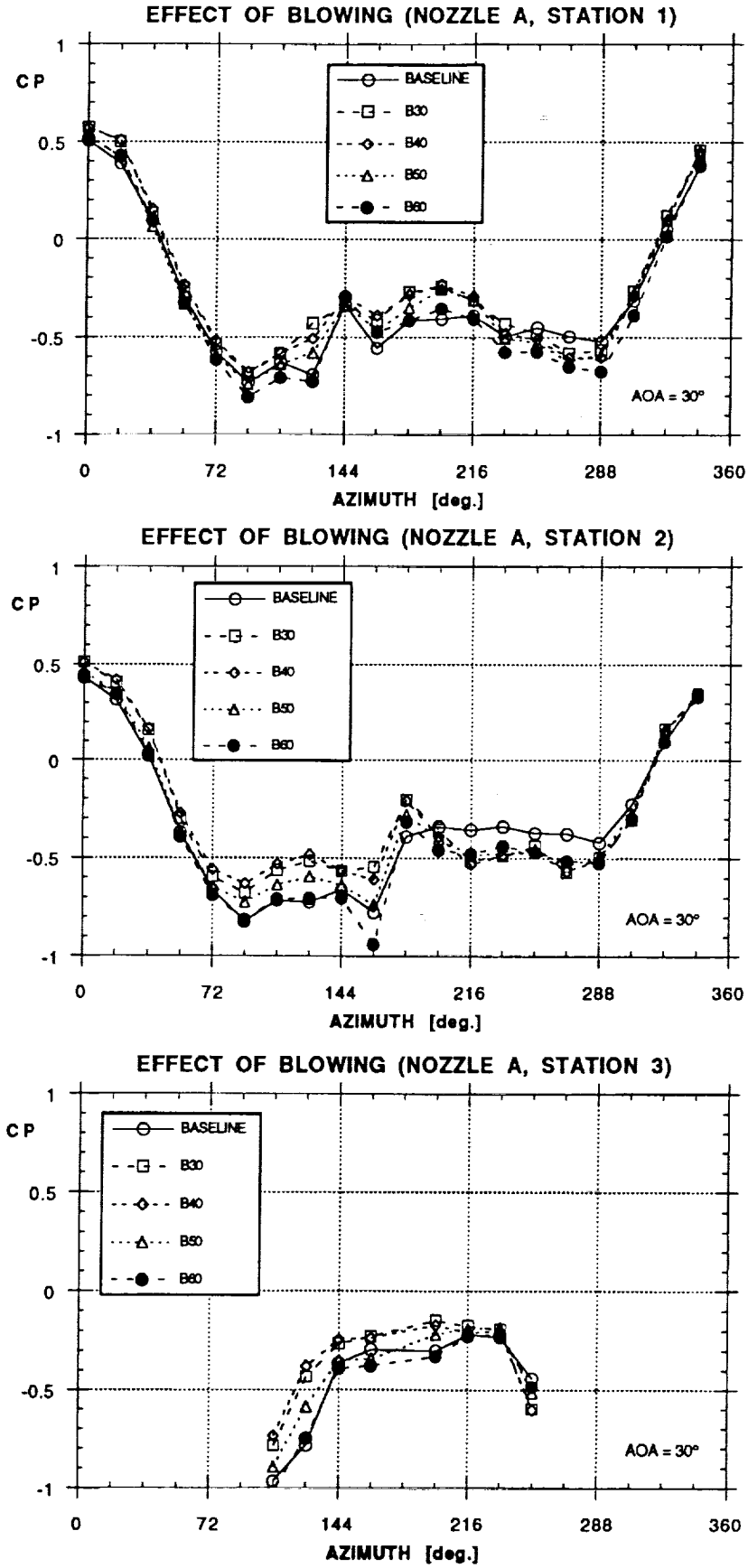

Figure 35 - Concluded

a)

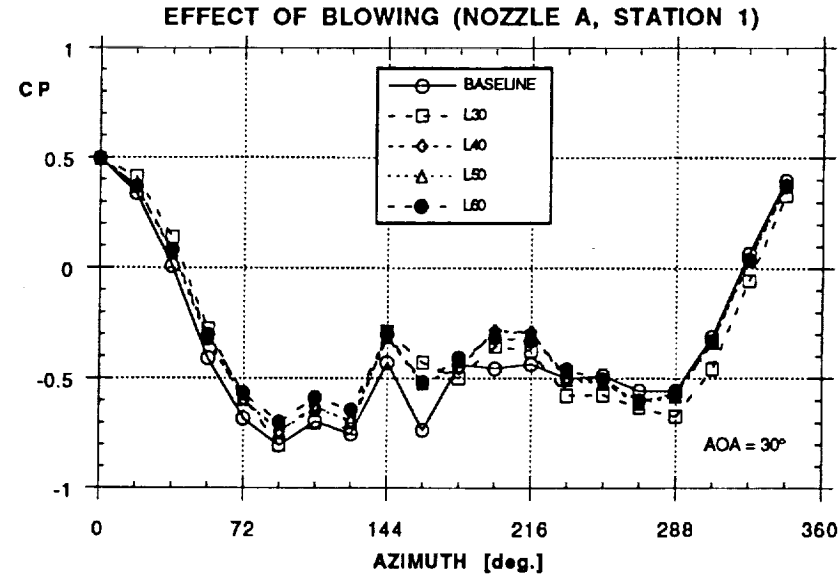

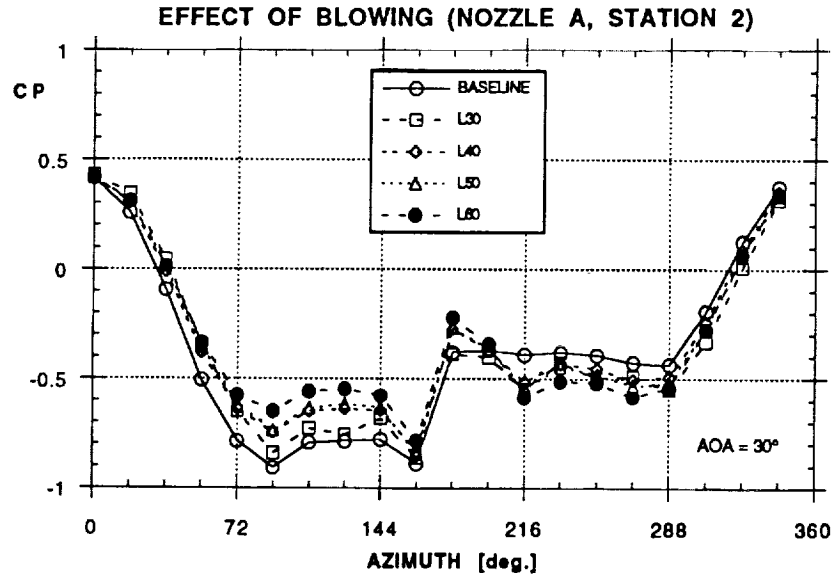

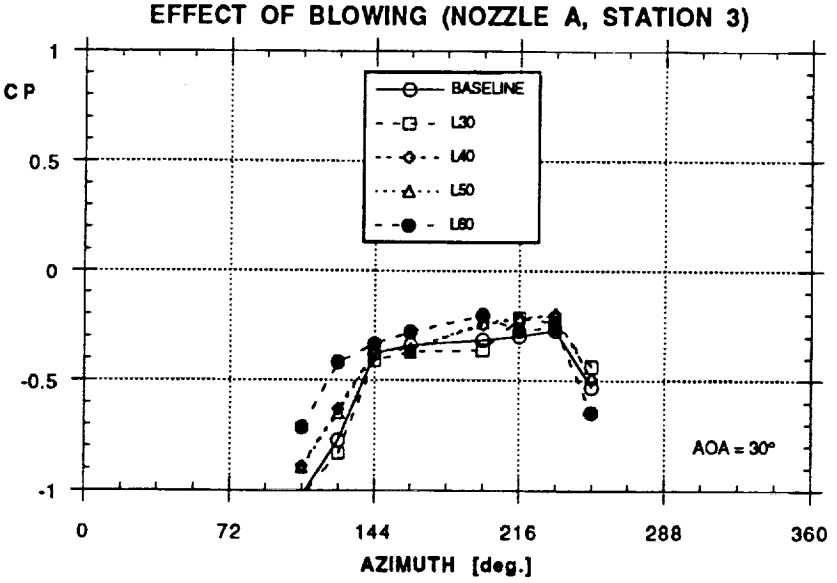

Figure 36 - Hysteresis of the Blowing Process (Nozzle A, $\alpha = 30°$, Left Side Blowing)

b)

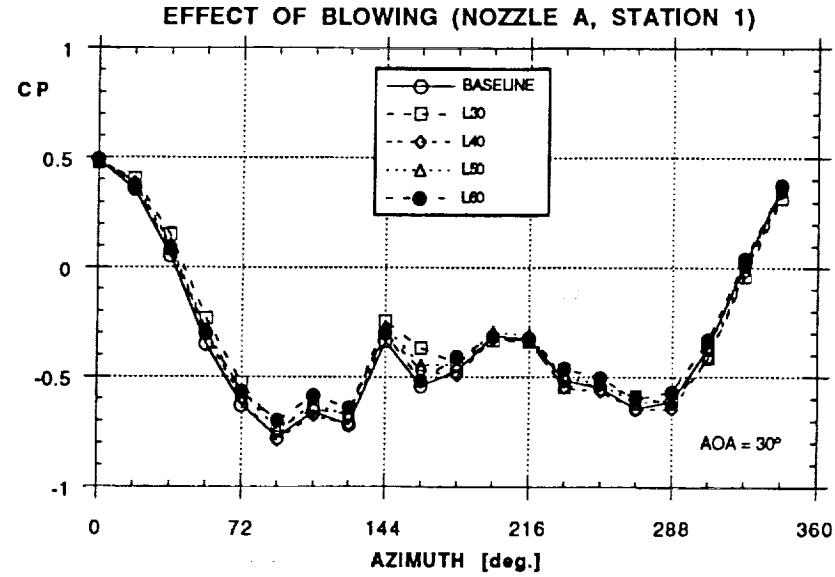

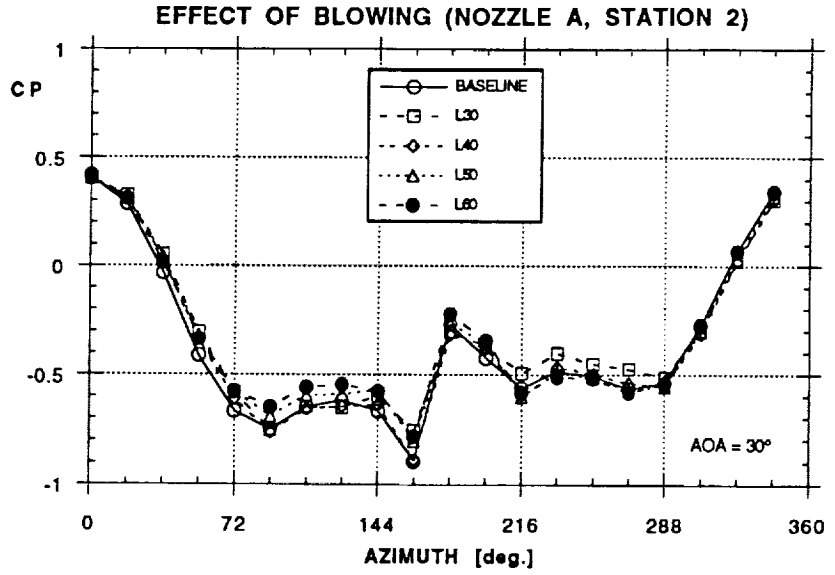

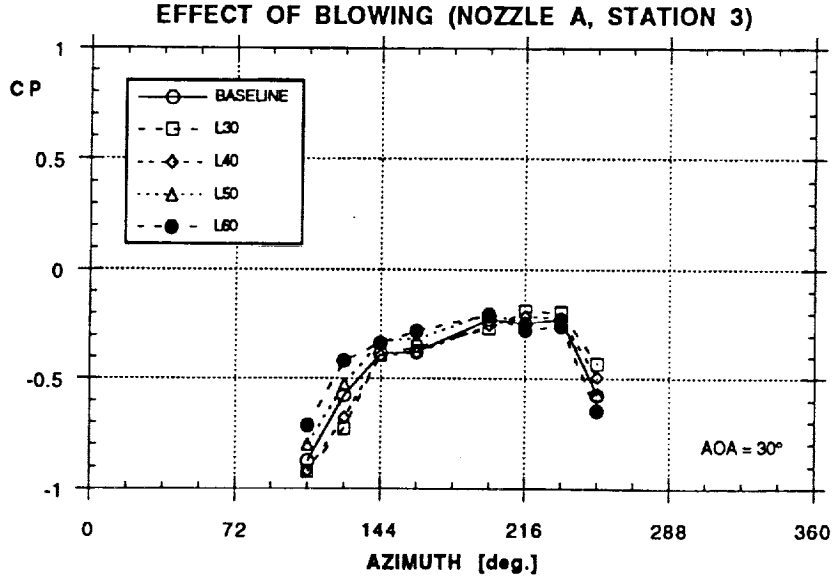

Figure 36 - Concluded

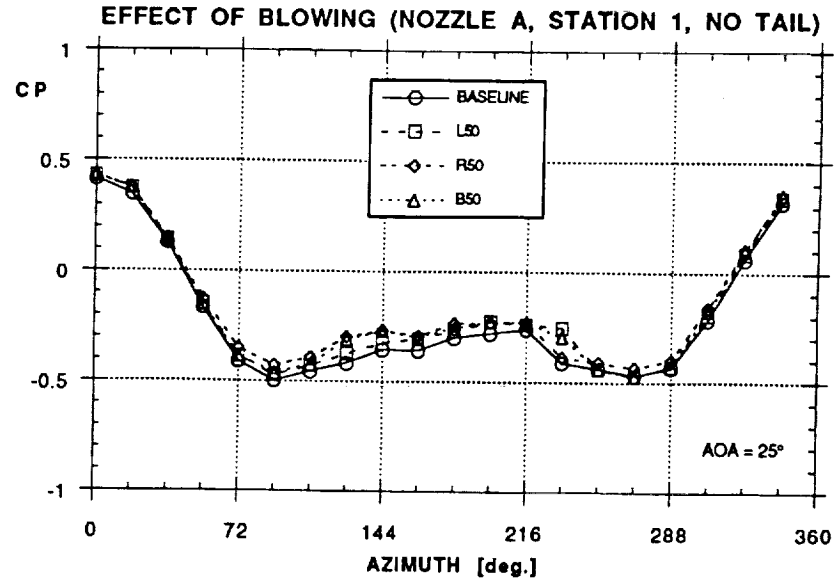

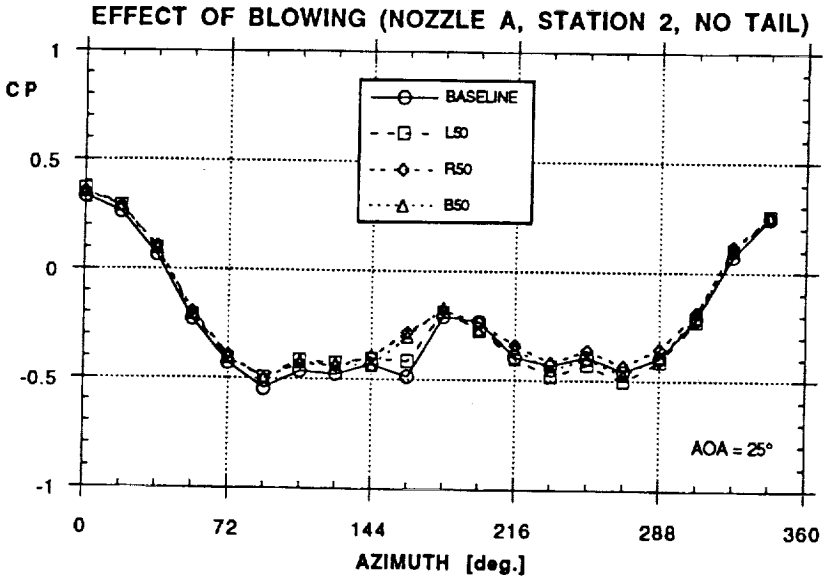

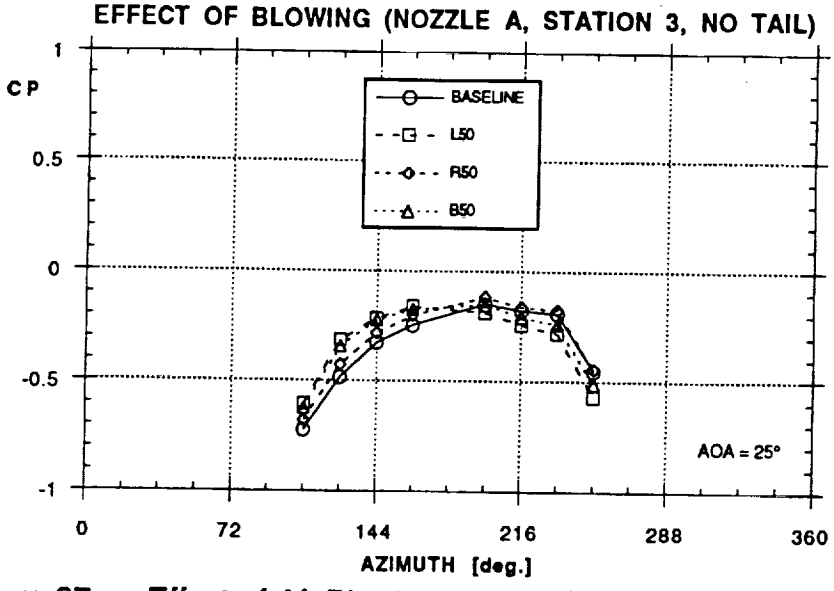

Figure 37 - Effect of Aft Blowing on Forebody Pressure Distribution (No Tail, Nozzle A, $\alpha = 25°$, Left, Right and Both Sides)

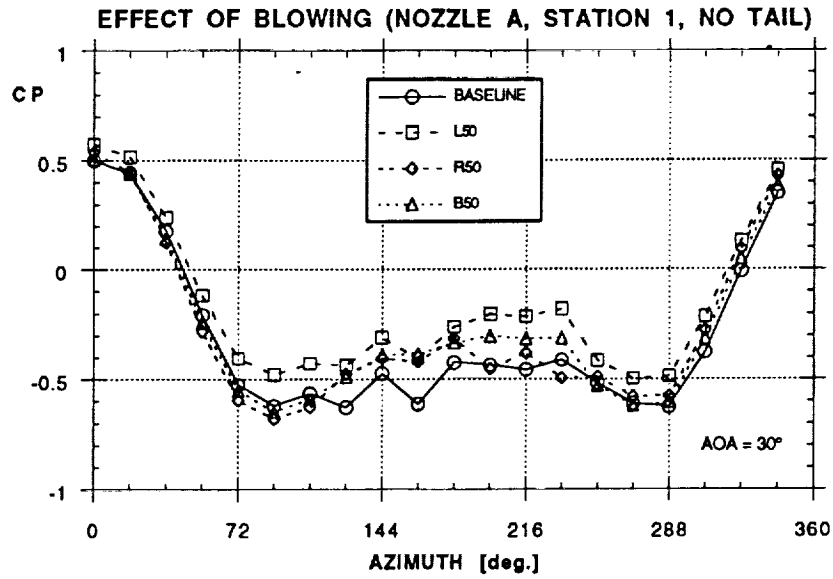

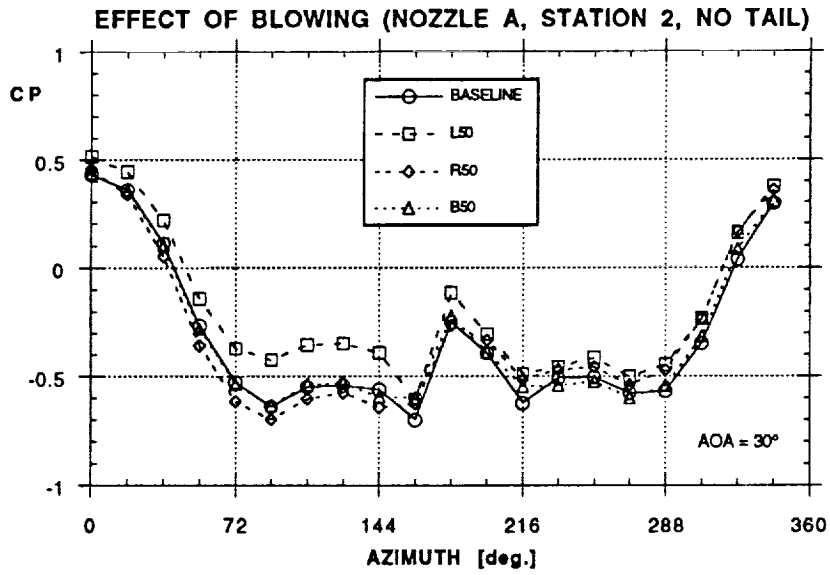

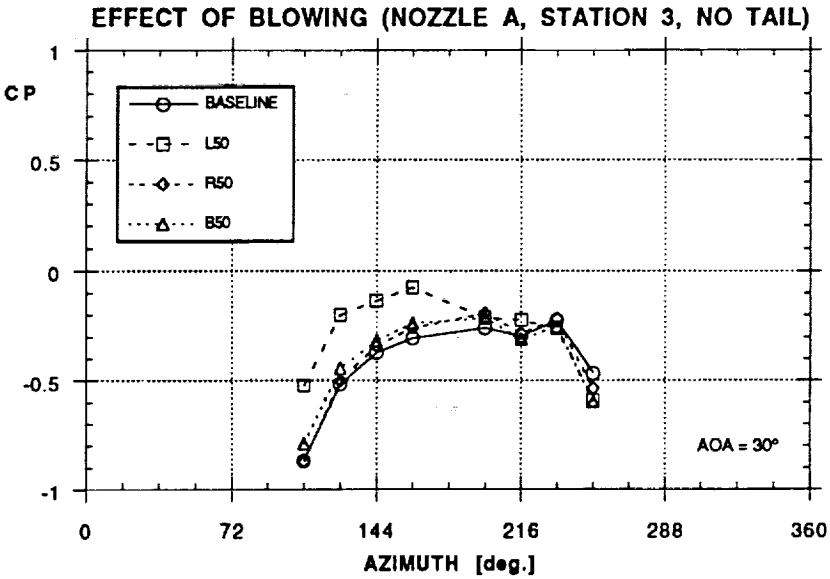

Figure 38 - Effect of Aft Blowing on Forebody Pressure Distribution (No Tail, Nozzle A, $\alpha = 30°$, Left, Right and Both Sides)

a)

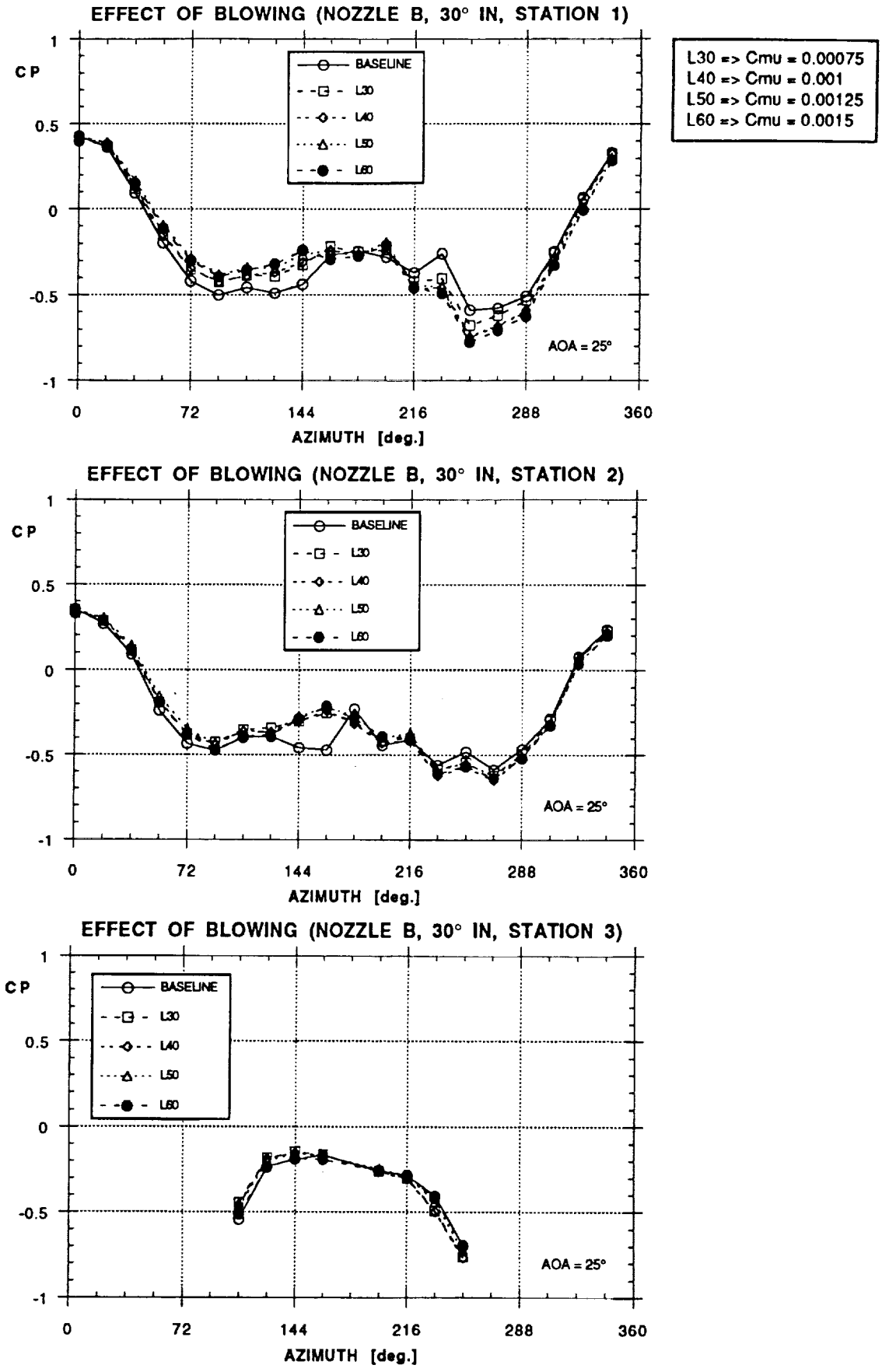

Figure 39 - Effect of Aft Blowing on Forebody Pressure Distribution (Nozzle B30IN, α = 25°, Left and Right Sides)

b)

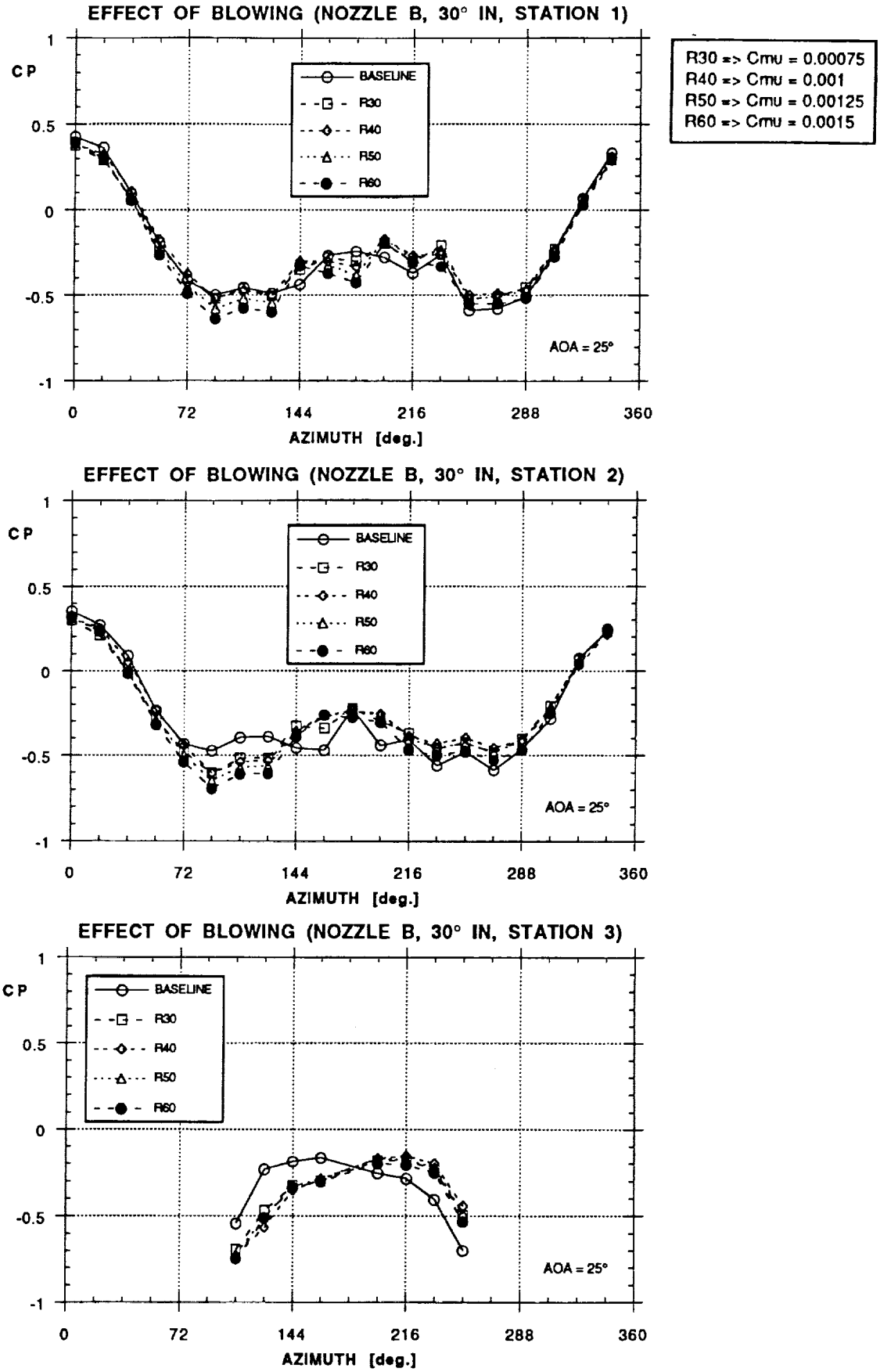

Figure 39 - Concluded

a)

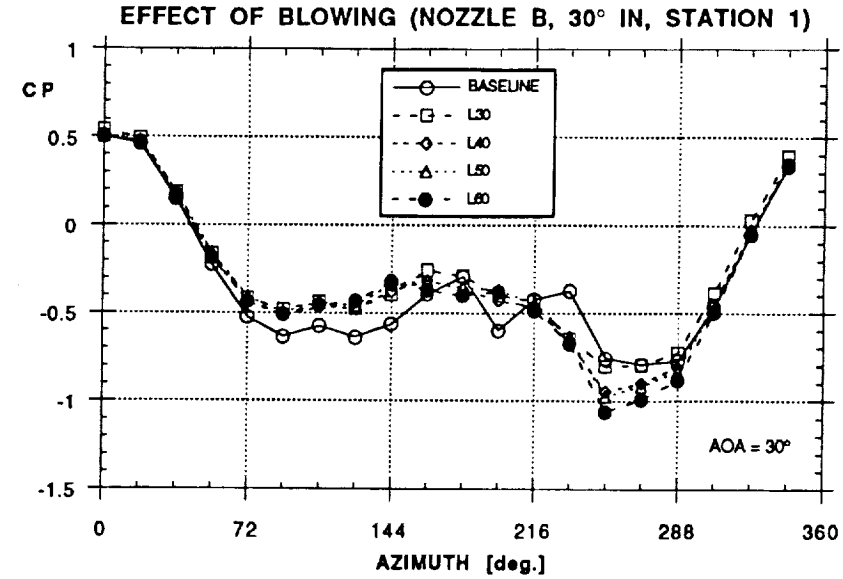

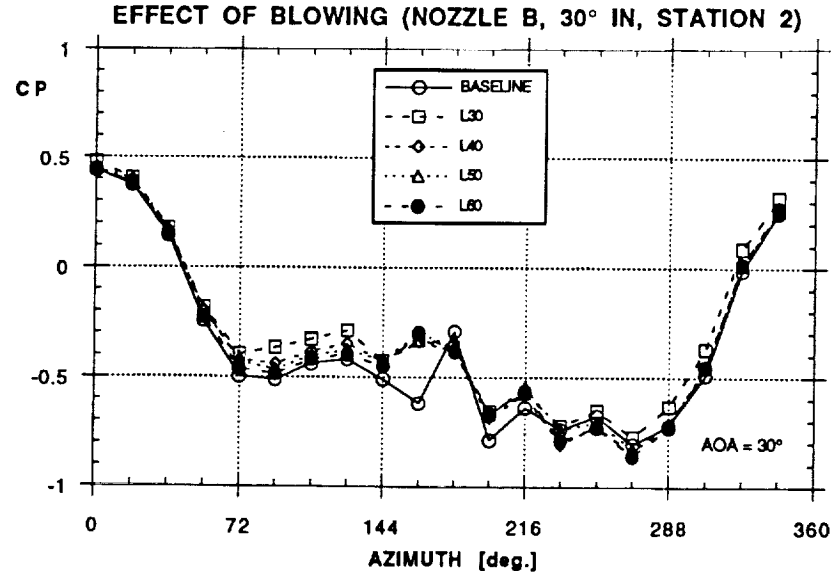

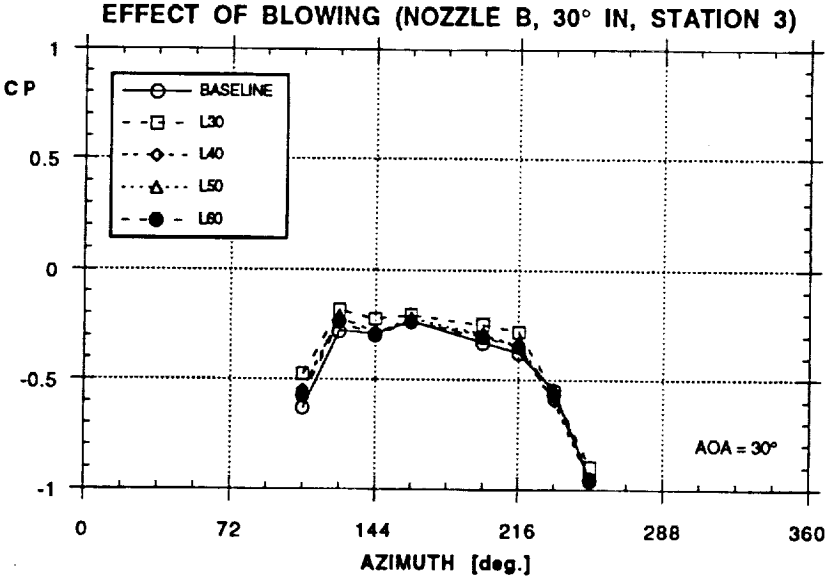

Figure 40 - Effect of Aft Blowing on Forebody Pressure Distribution (Nozzle B30IN, $\alpha = 30°$, Left and Right Sides)

b)

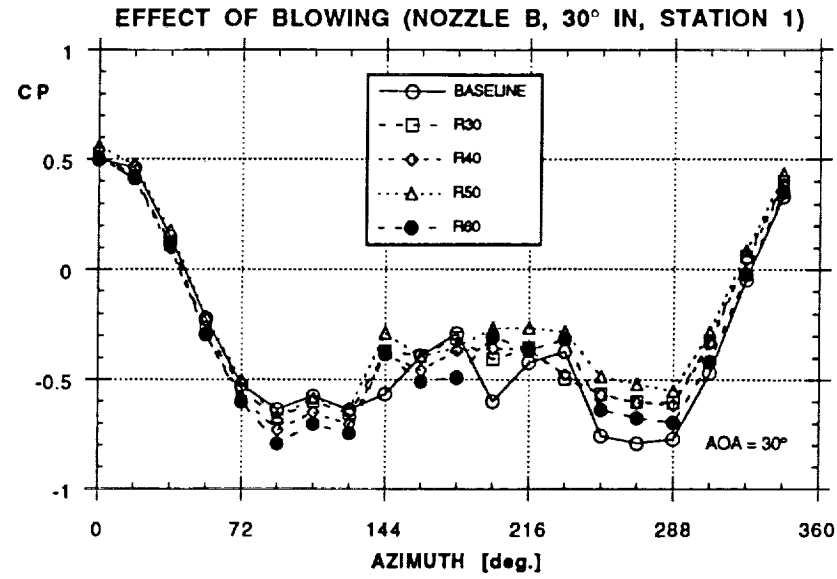

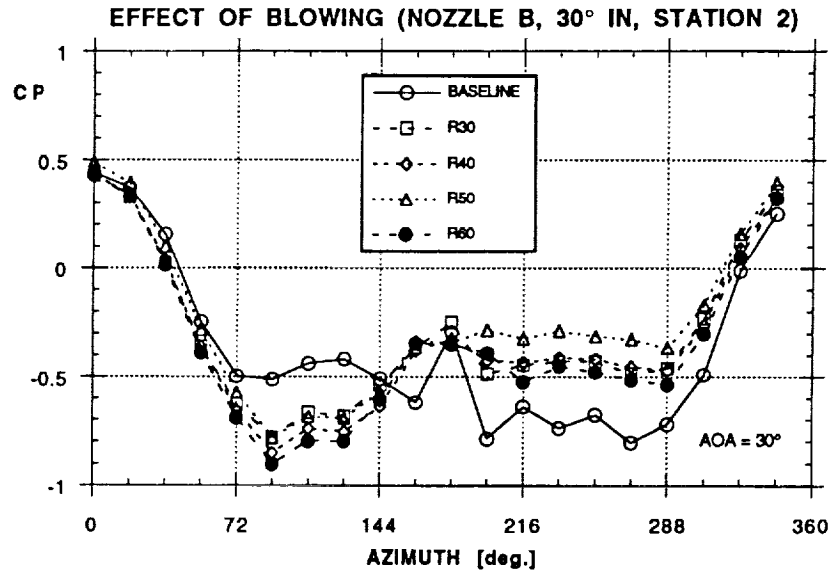

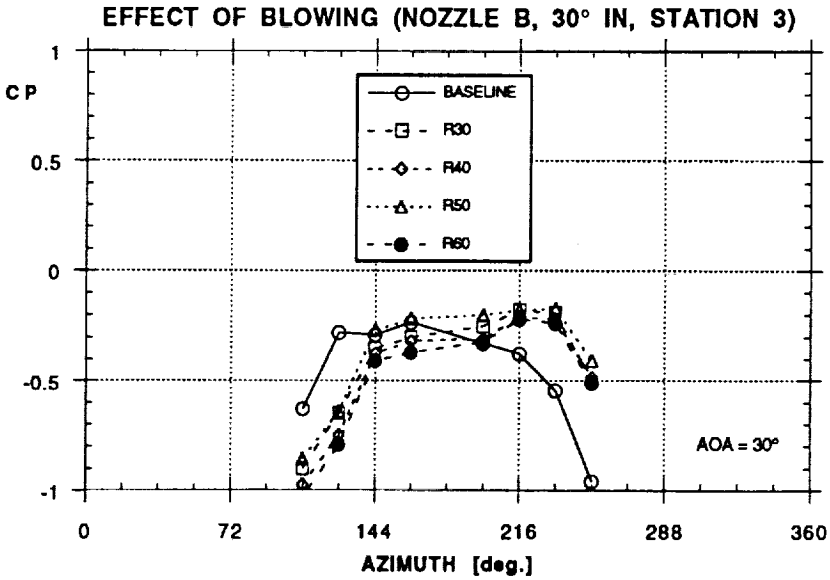

Figure 40 - Concluded

a)

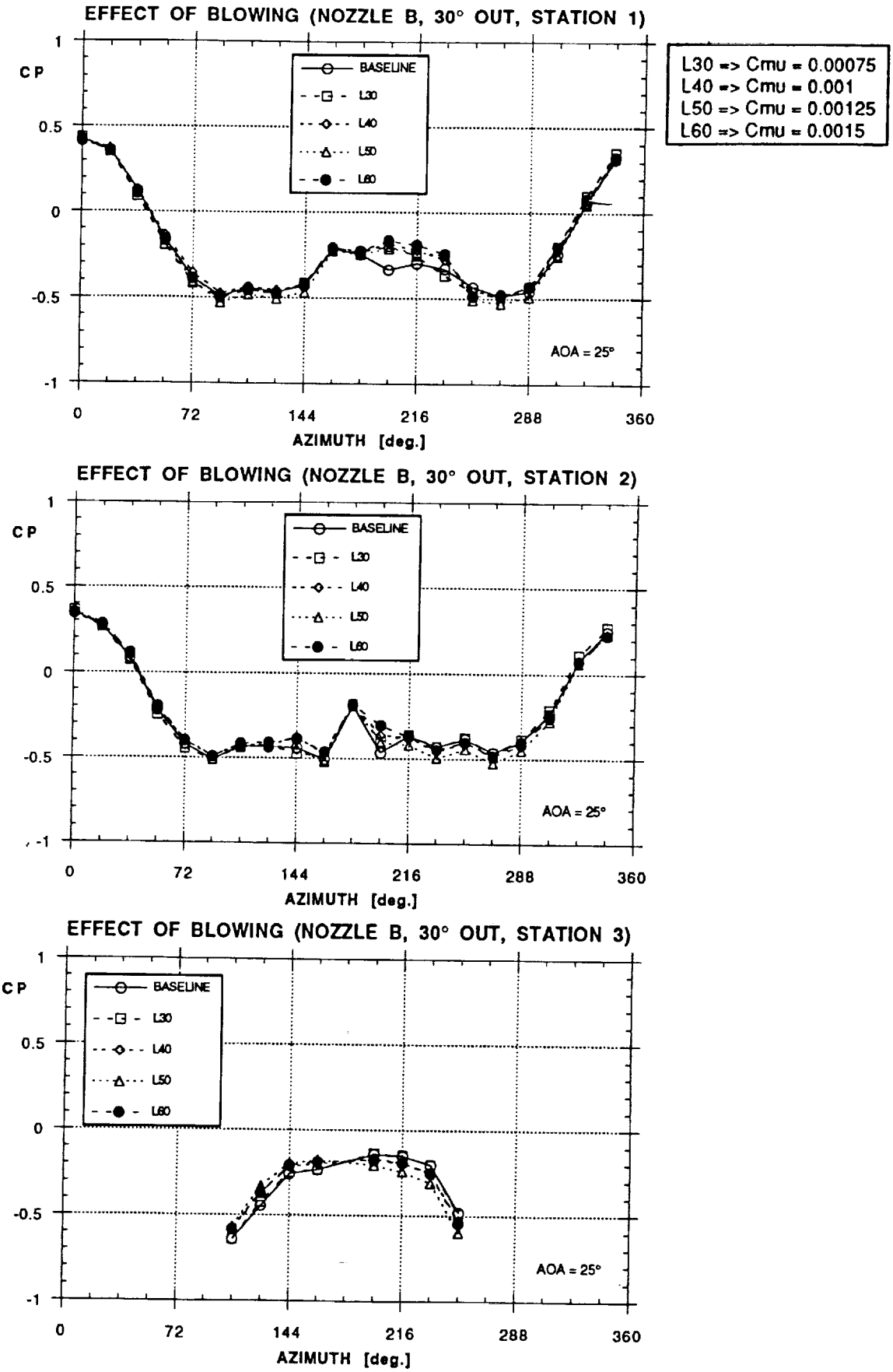

Figure 41 - Effect of Aft Blowing on Forebody Pressure Distribution (Nozzle B30OUT, $\alpha = 25°$, Left and Right Sides)

b)

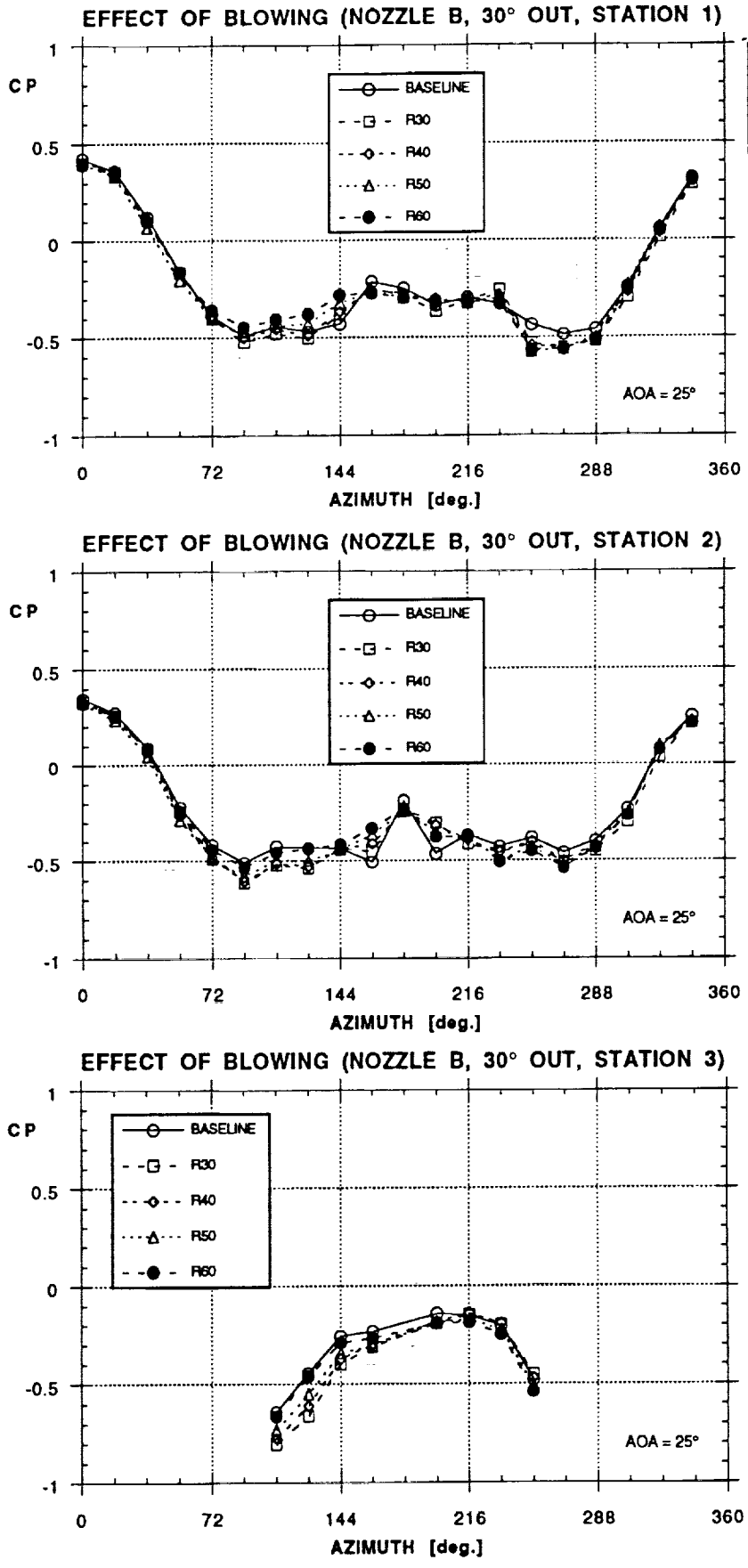

Figure 41 - Concluded

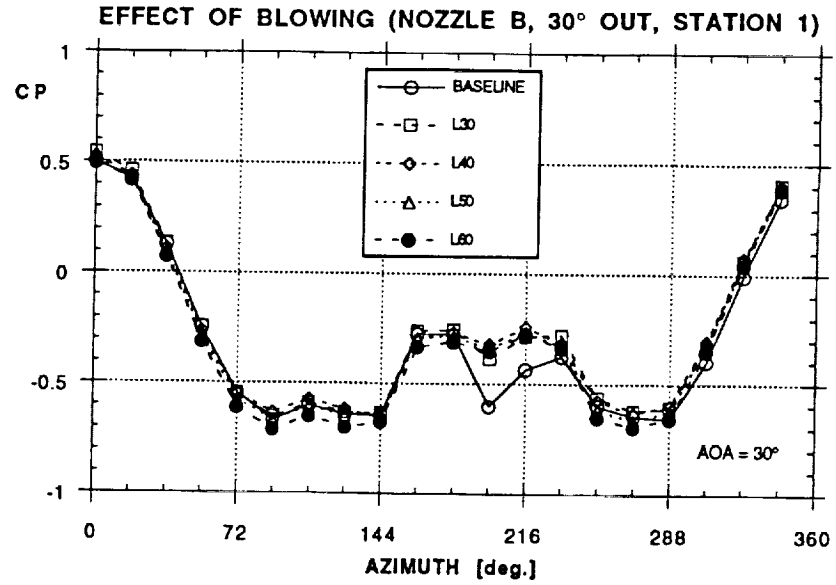

a)

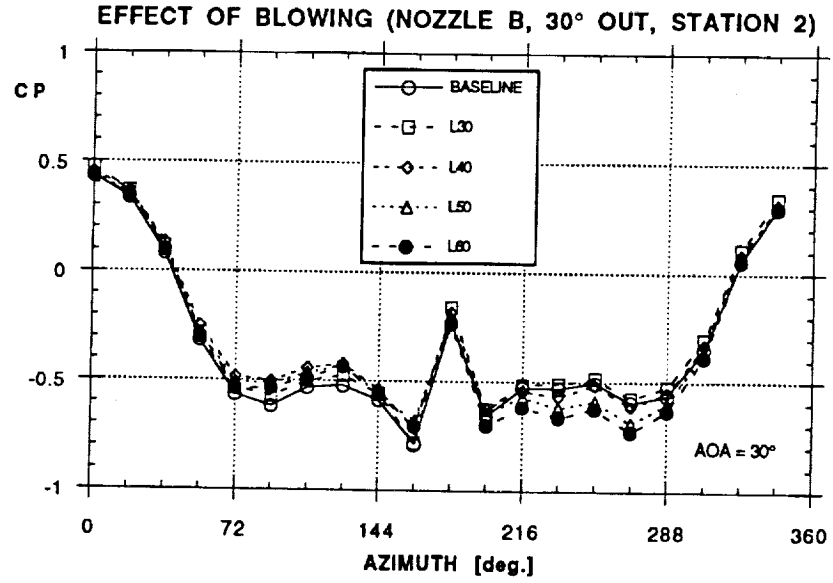

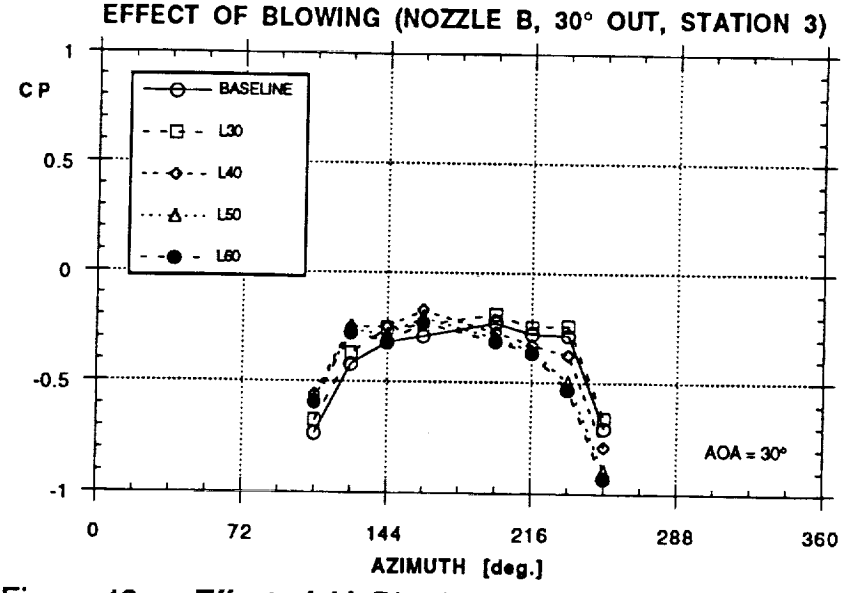

Figure 42 - Effect of Aft Blowing on Forebody Pressure Distribution (Nozzle B30OUT, $\alpha = 30°$, Left and Right Sides)

b)

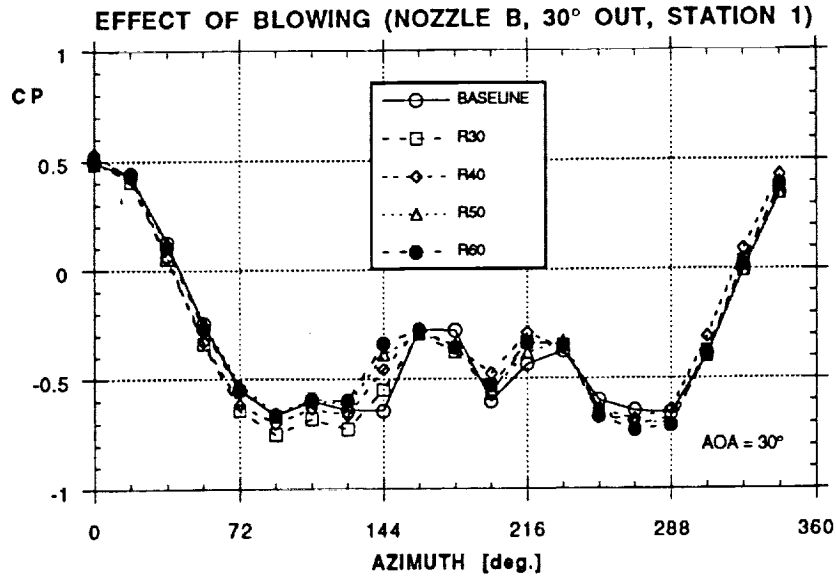

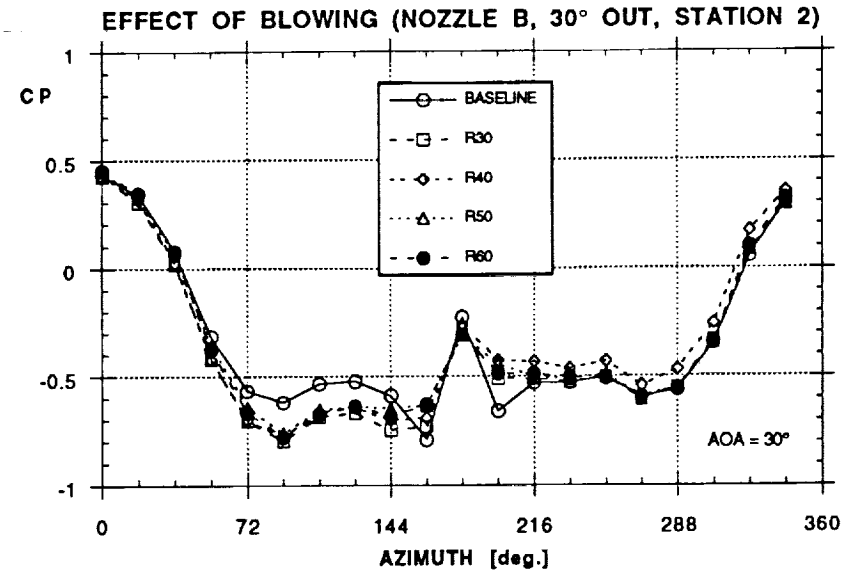

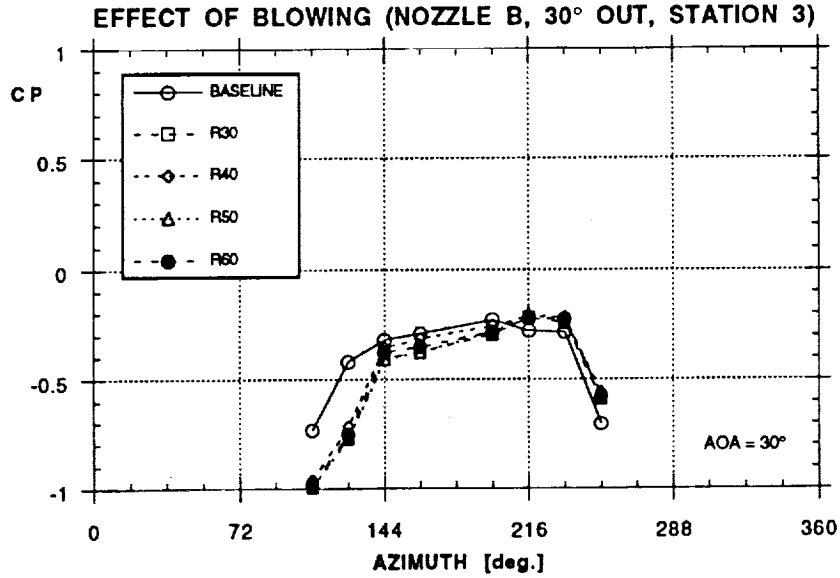

Figure 42 - Concluded

a)

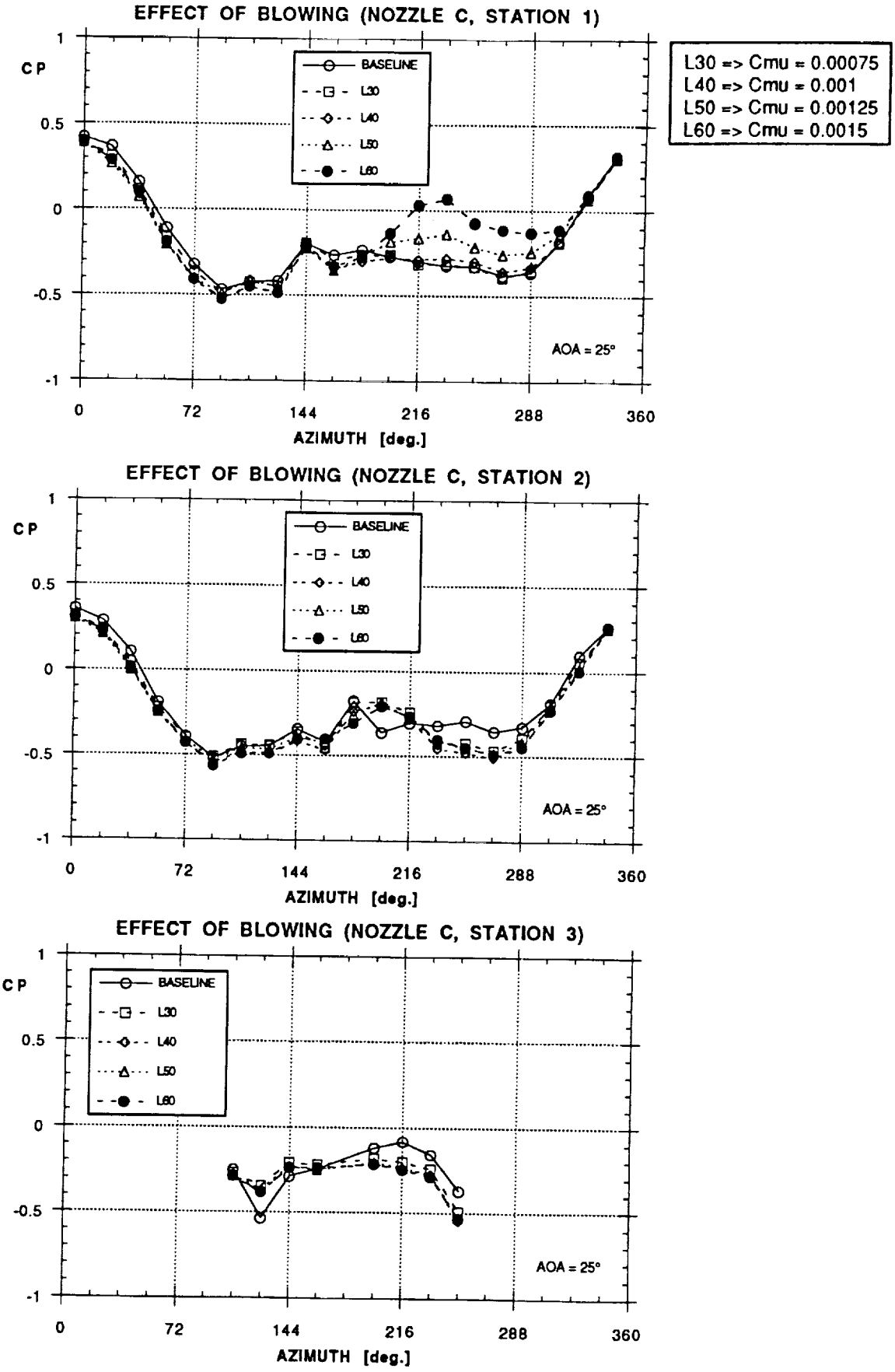

Figure 43 - Effect of Forward Blowing on Forebody Pressure Distribution (Nozzle C, $\alpha = 25°$, Left and Right Sides)

b)

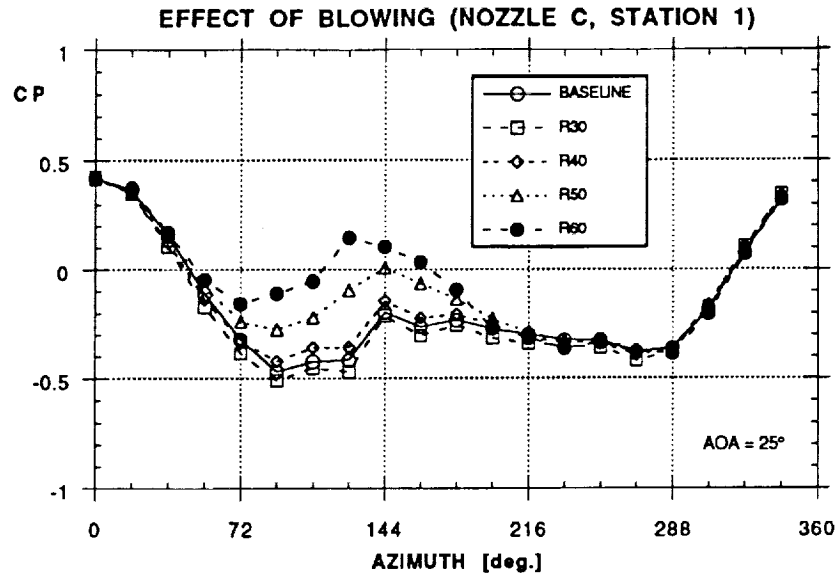

R30 => Cmu = 0.00075
R40 => Cmu = 0.001
R50 => Cmu = 0.00125
R60 => Cmu = 0.0015

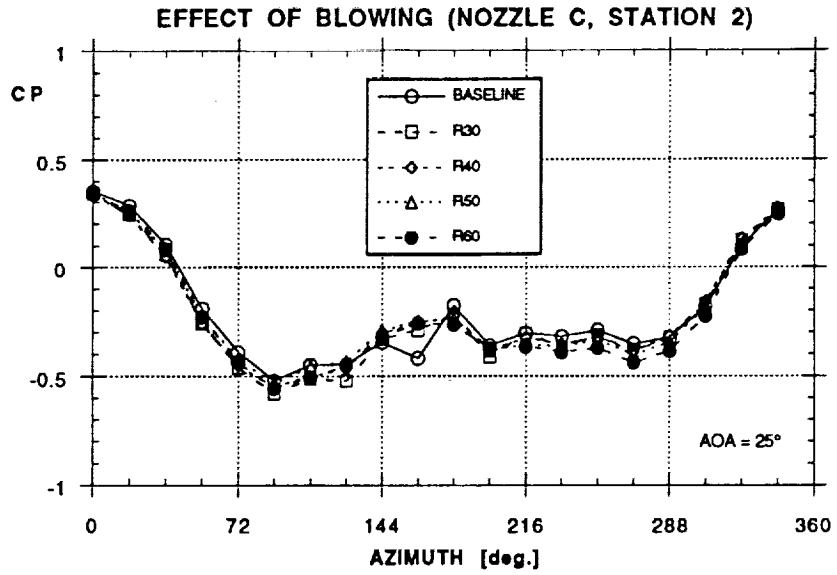

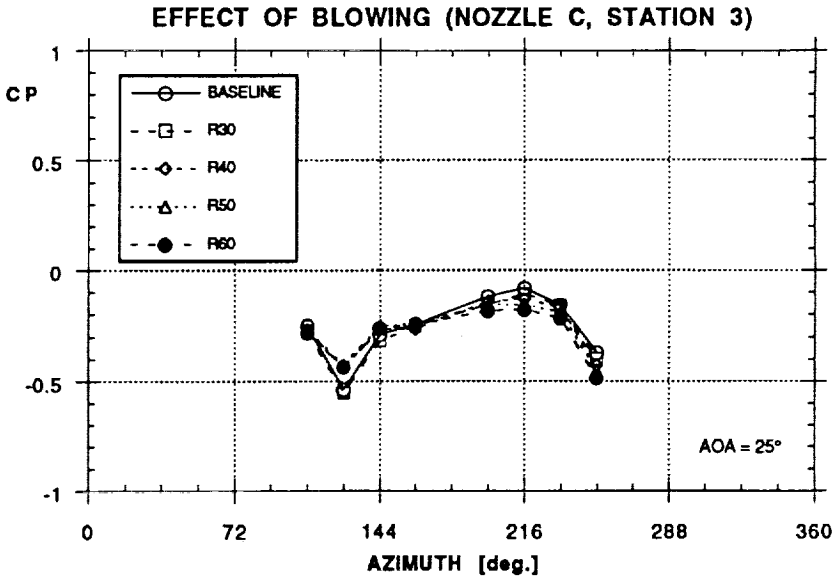

Figure 43 - Concluded

a)

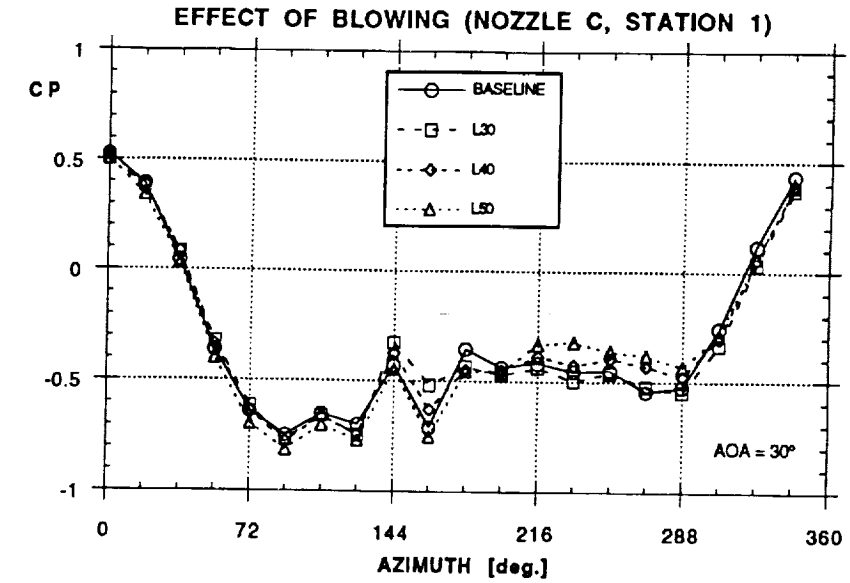

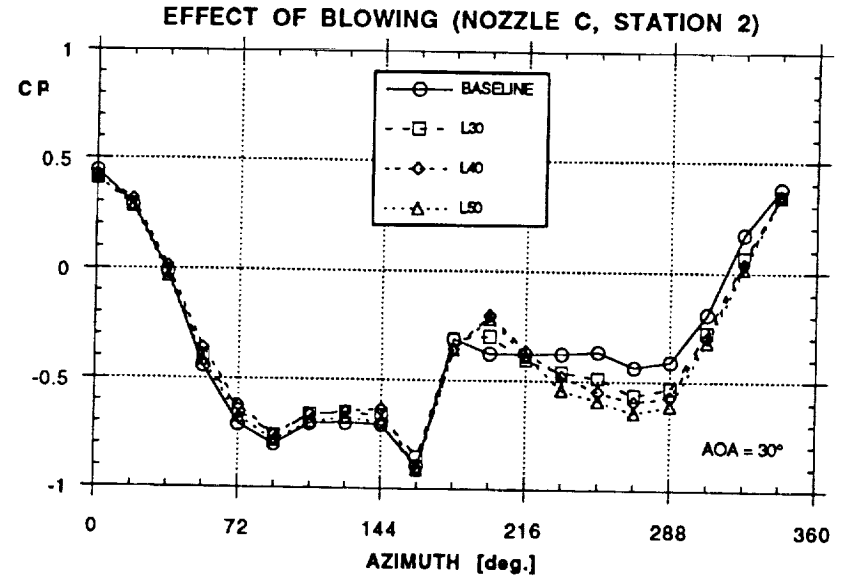

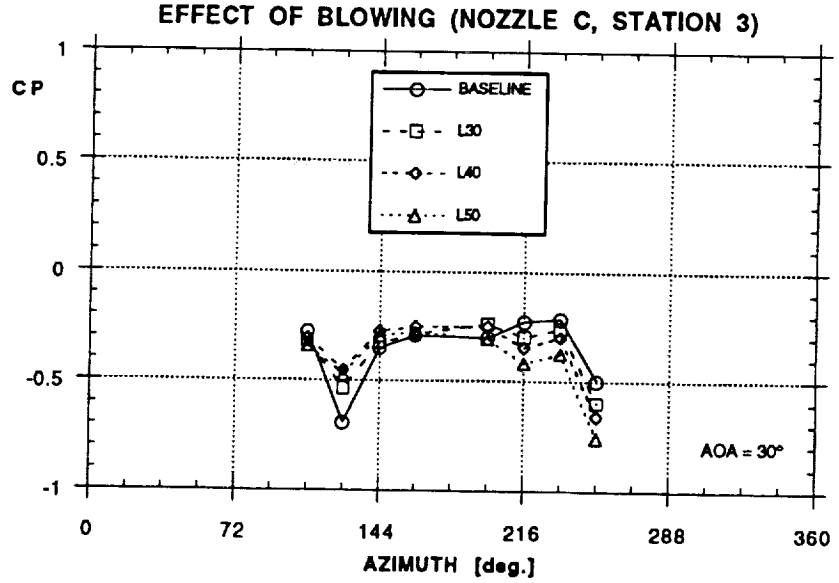

Figure 44 - Effect of Forward Blowing on Forebody Pressure Distribution (Nozzle C, α = 30°, Left and Right Sides)

b)

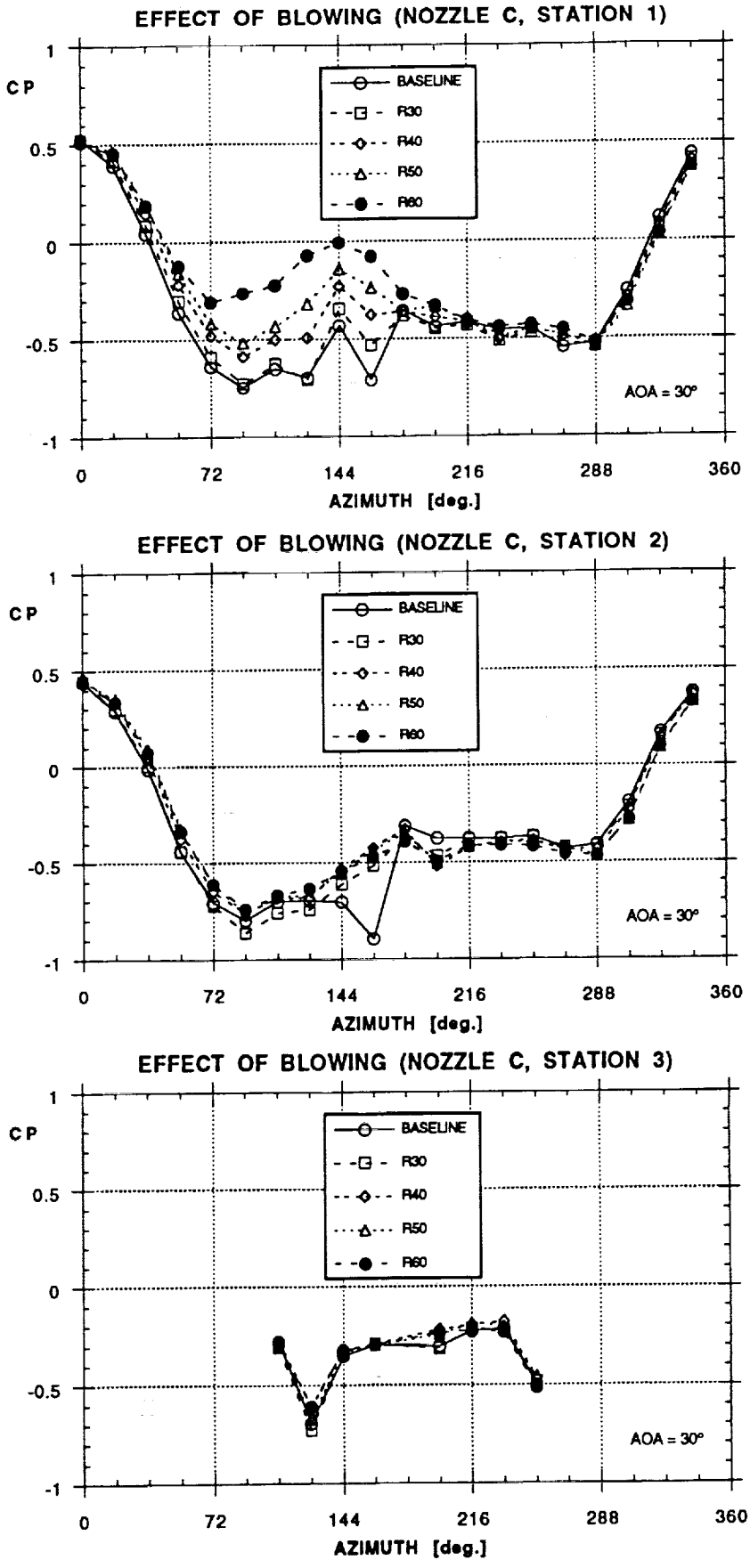

Figure 44 - Concluded

a)

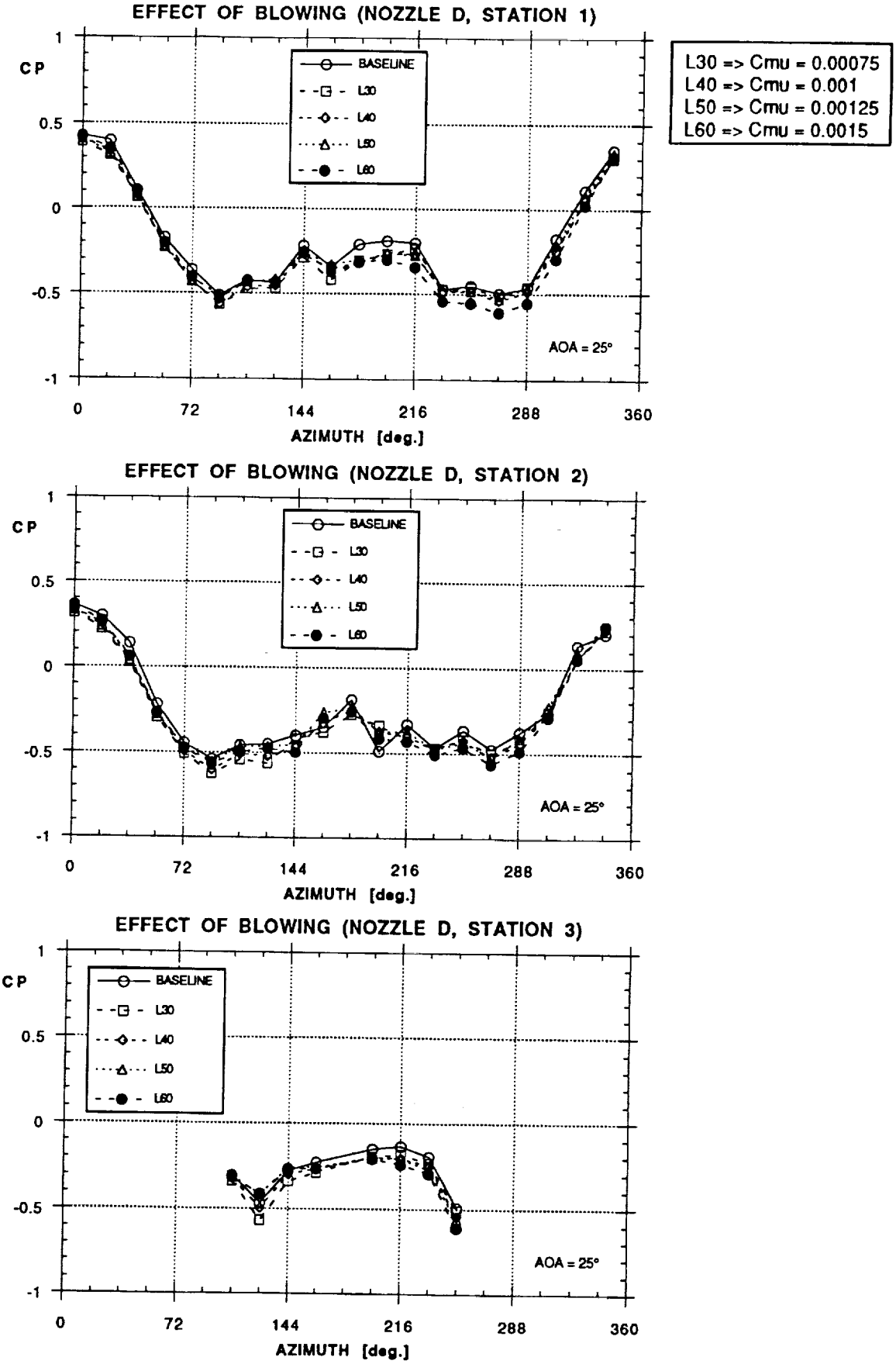

Figure 45 - Effect of Forward Blowing on Forebody Pressure Distribution (Nozzle D, $\alpha = 25°$, Left and Right Sides)

b)

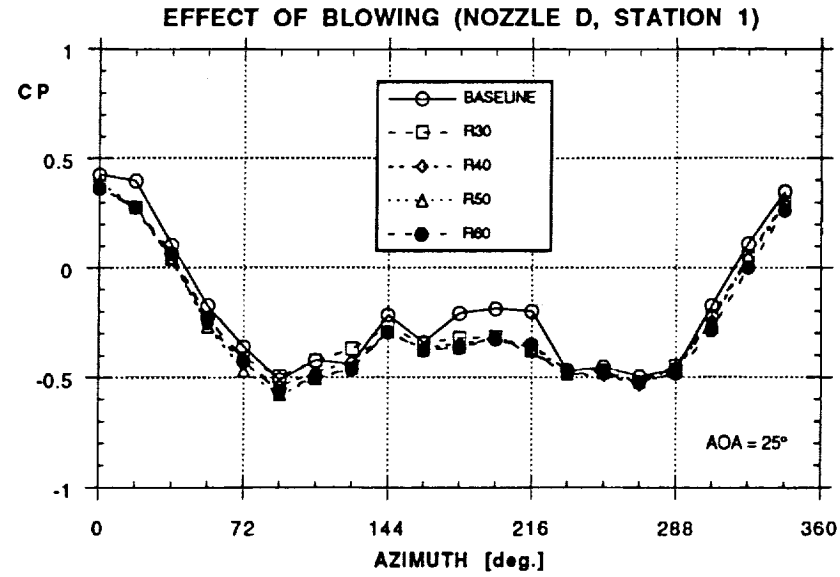

R30 => Cmu = 0.00075
R40 => Cmu = 0.001
R50 => Cmu = 0.00125
R60 => Cmu = 0.0015

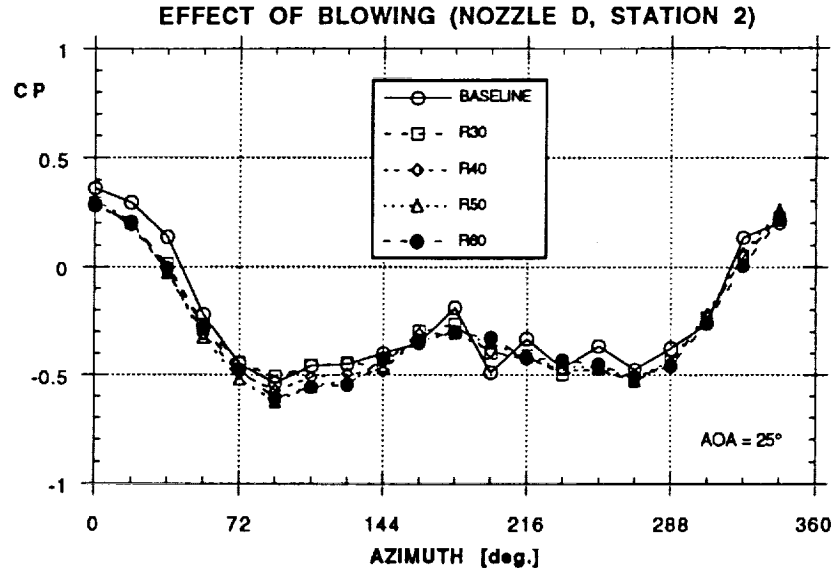

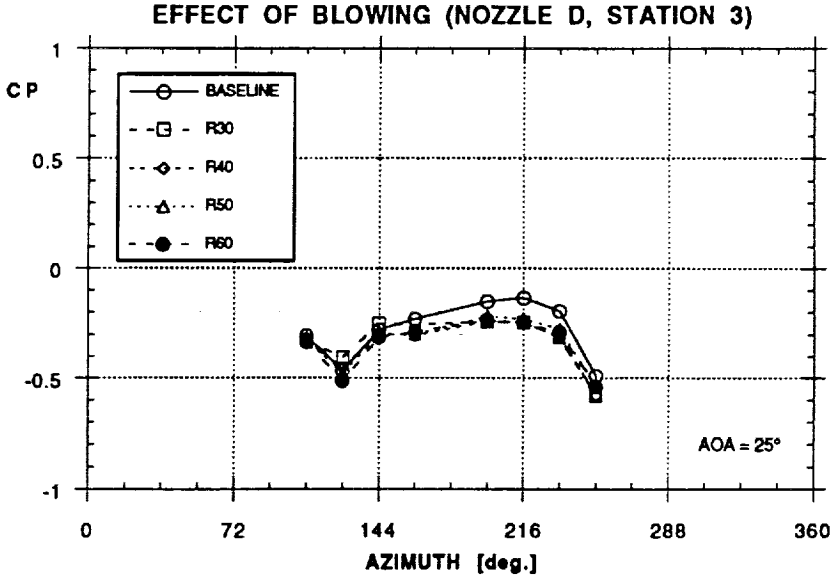

Figure 45 - Concluded

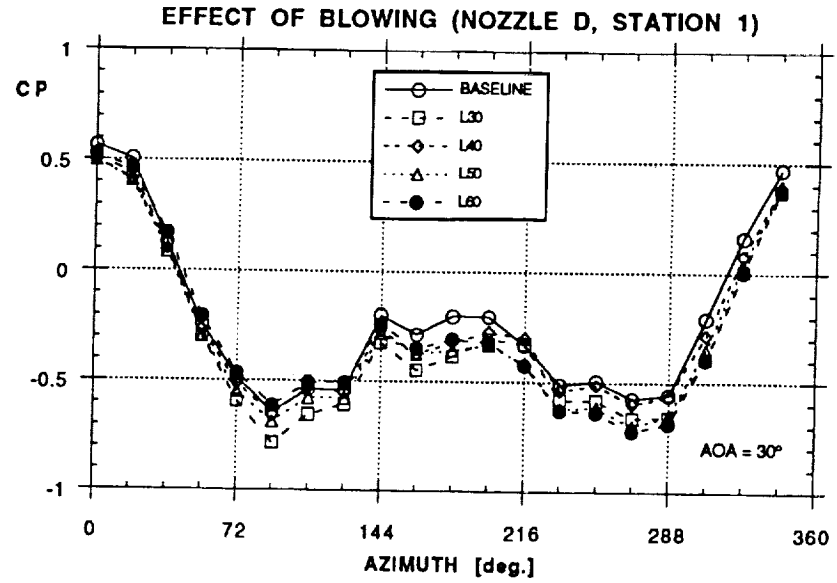

a)

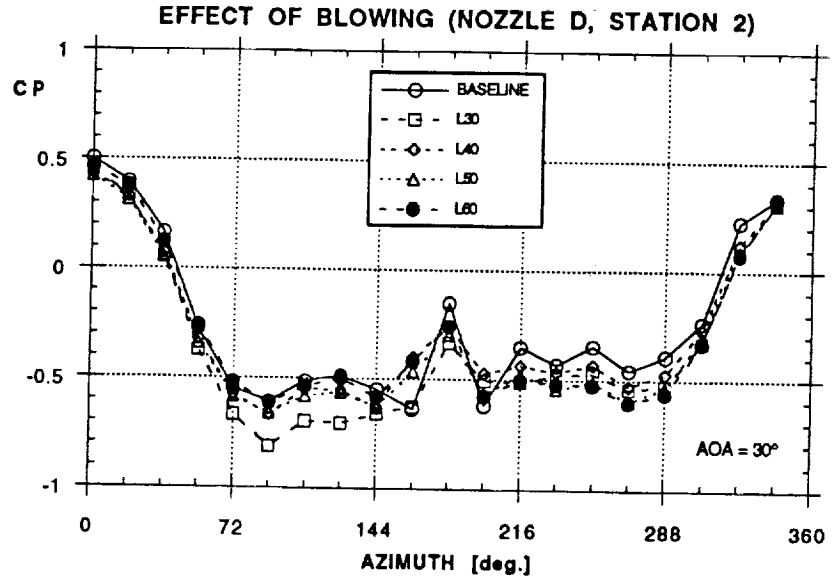

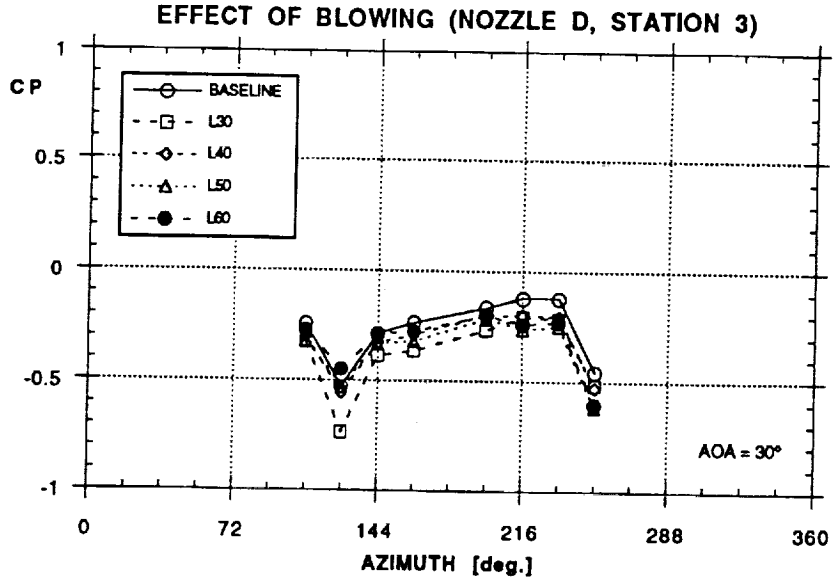

Figure 46 - Effect of Forward Blowing on Forebody Pressure Distribution (Nozzle D, $\alpha = 30°$, Left and Right Sides)

b)

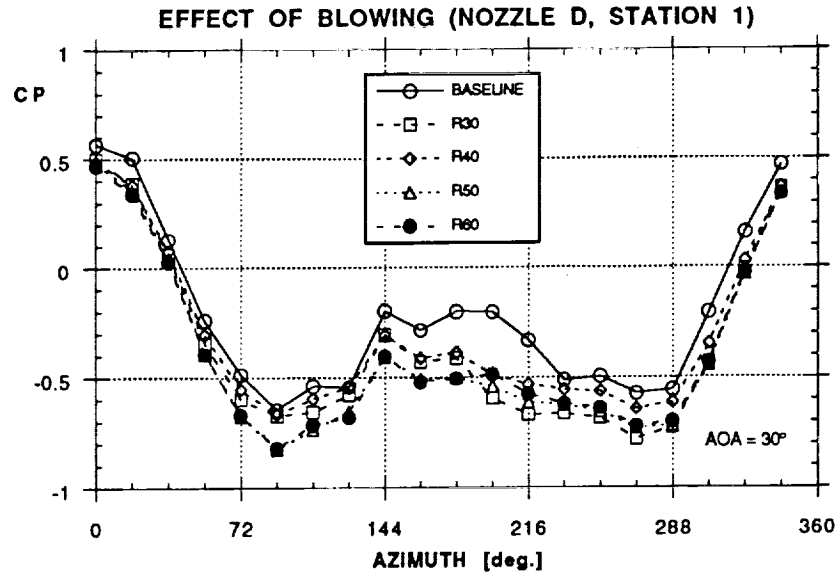

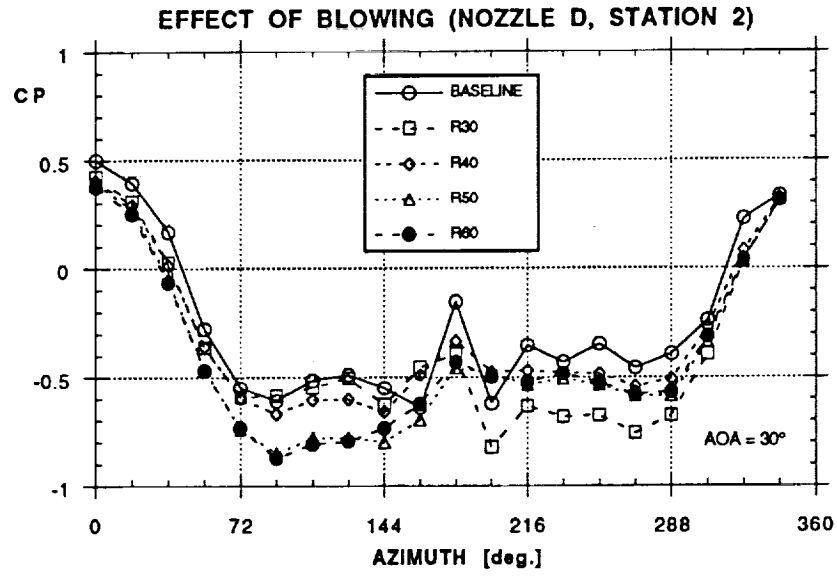

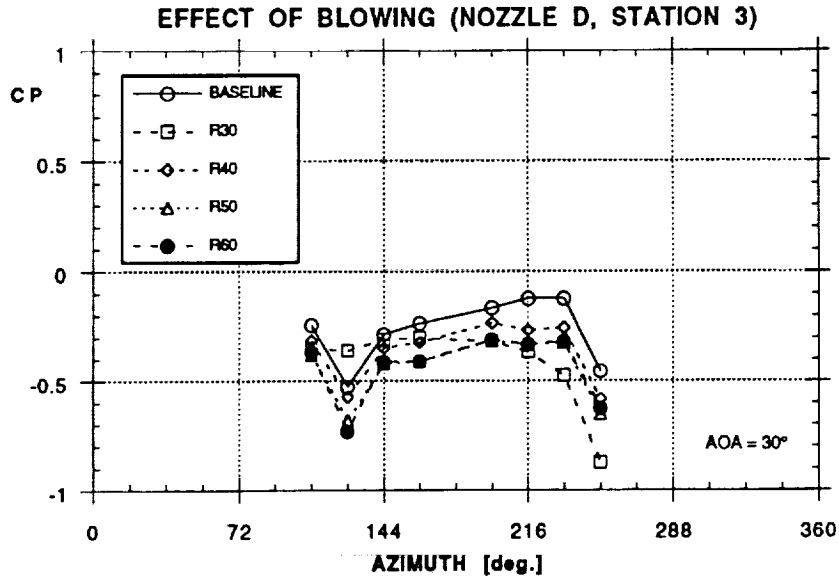

Figure 46 - Concluded

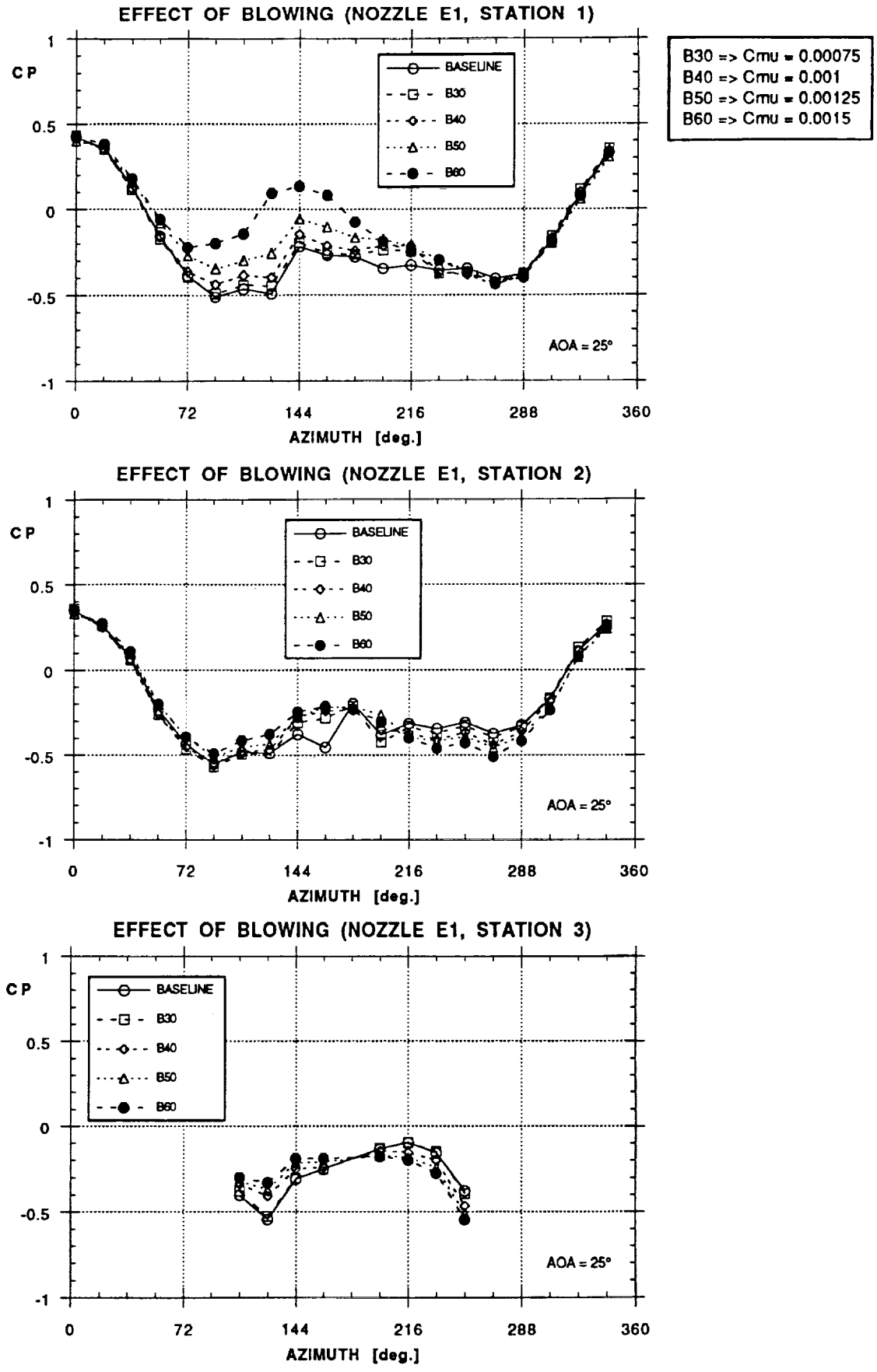

Figure 47 - Effect of Combined Blowing on Forebody Pressure Distribution (Nozzle E1, $\alpha = 25°$)

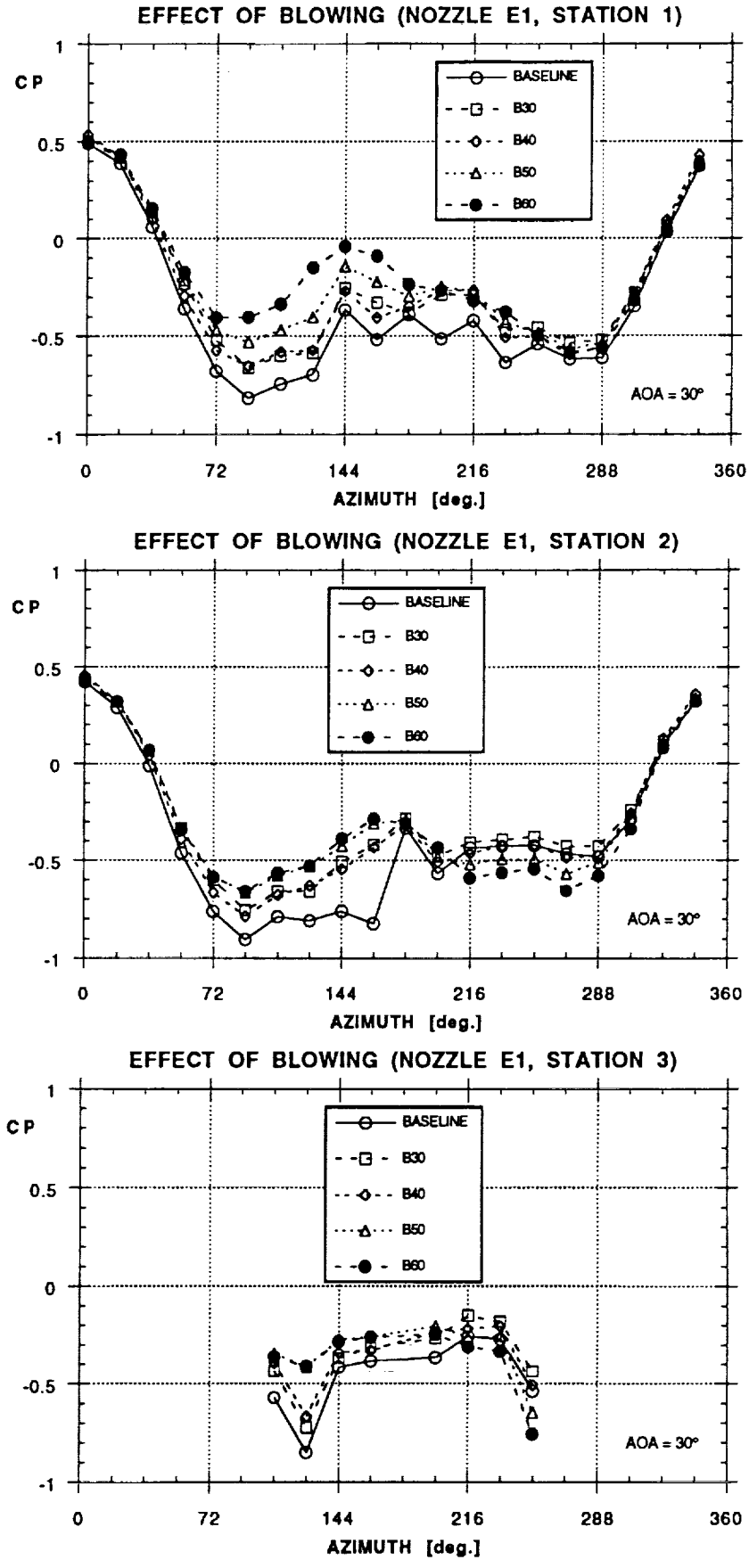

Figure 48 - Effect of Combined Blowing on Forebody Pressure Distribution (Nozzle E1, $\alpha = 30°$)

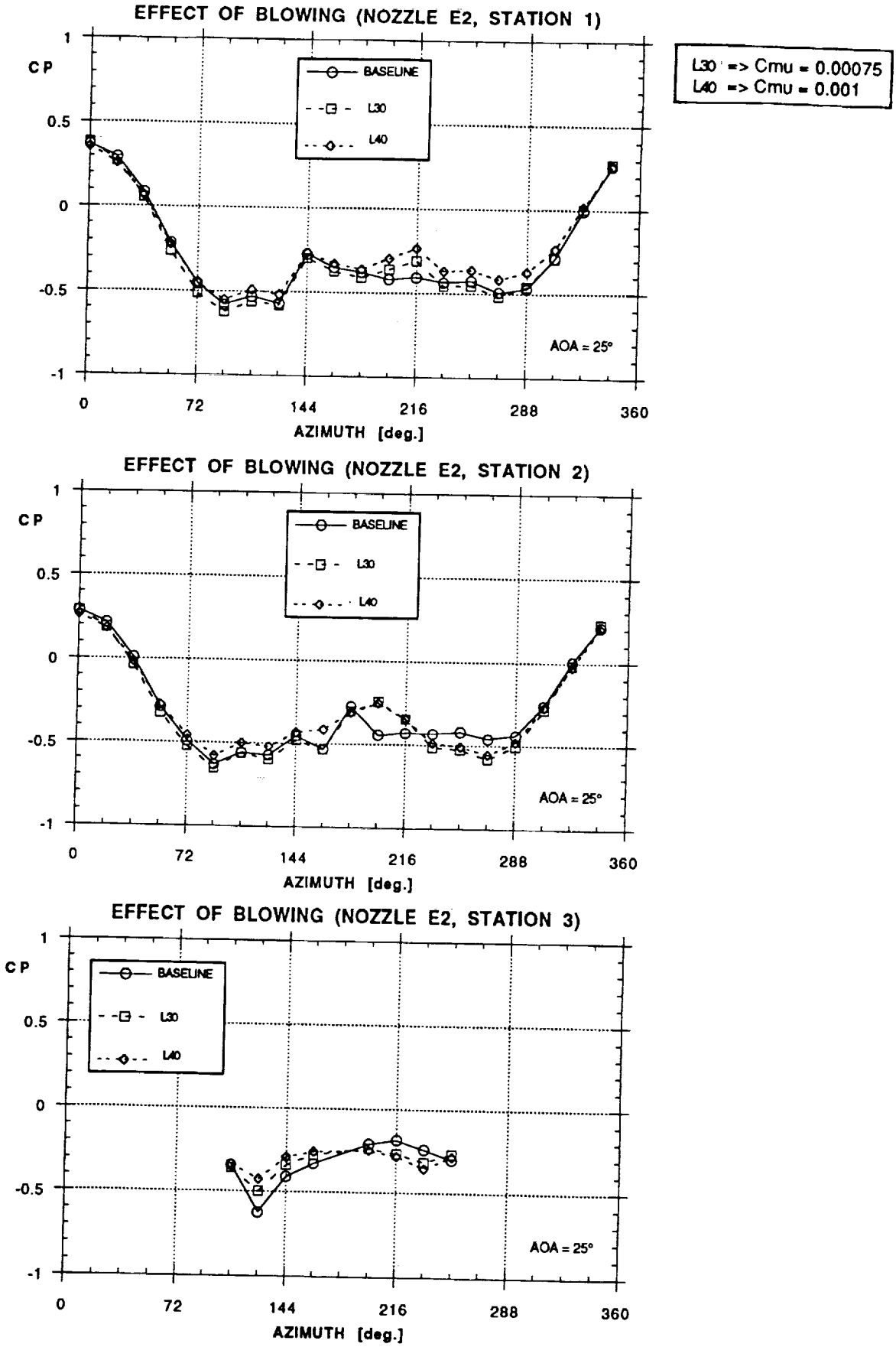

Figure 49 - Effect of Combined Blowing on Forebody Pressure Distribution (Nozzle E2, α = 25°, Left Side Blowing)

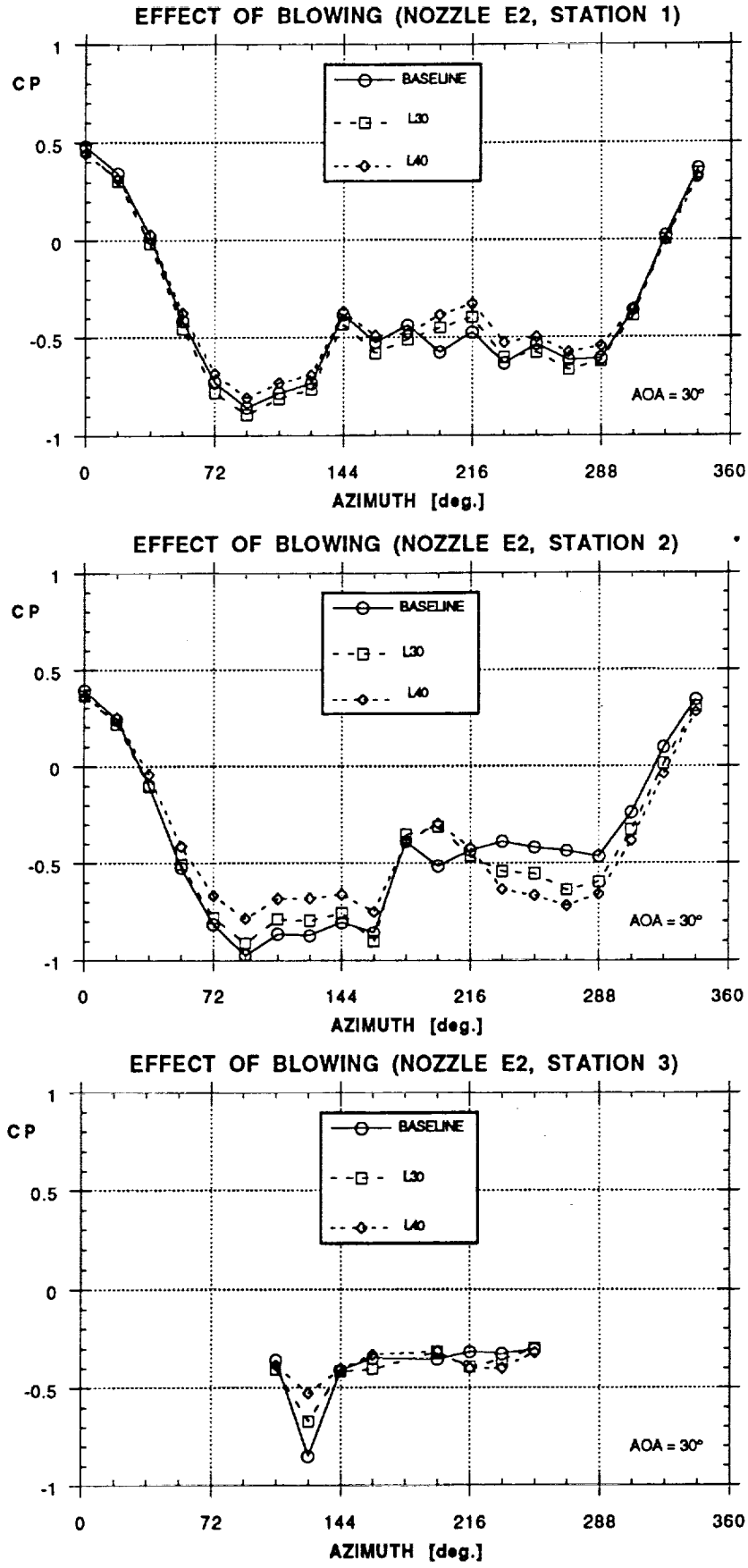

Figure 50 - Effect of Combined Blowing on Forebody Pressure Distribution (Nozzle E2, $\alpha = 30°$)

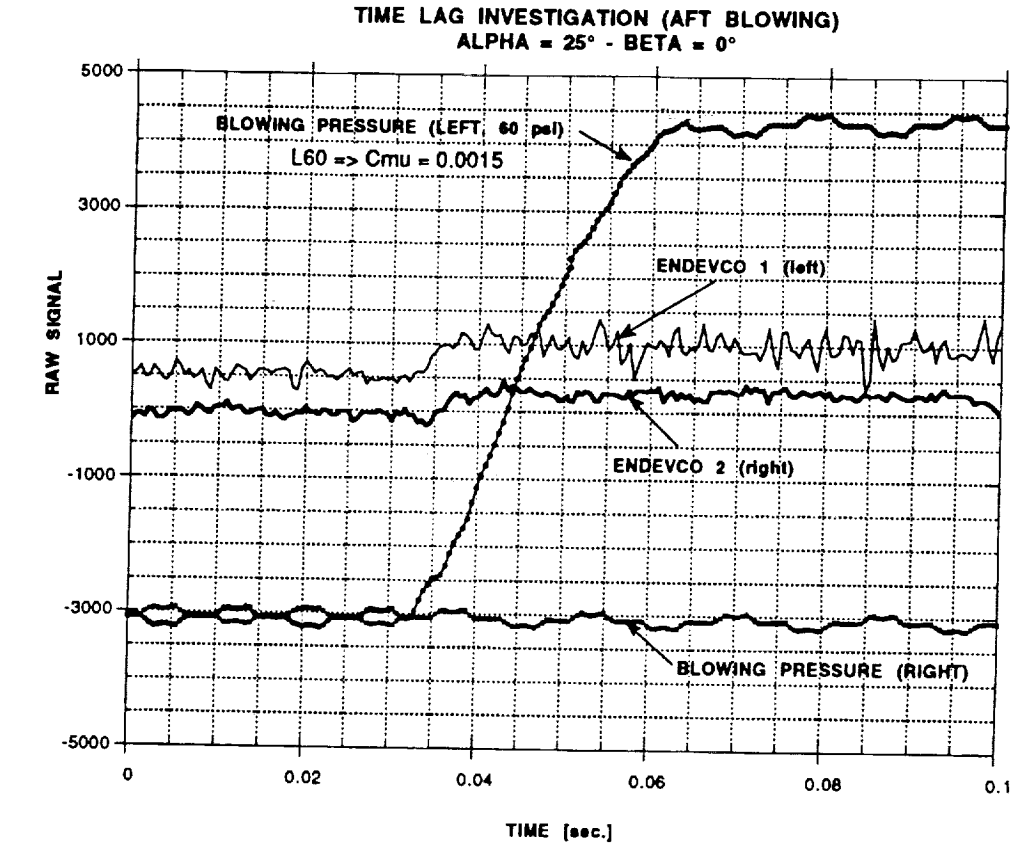

a)

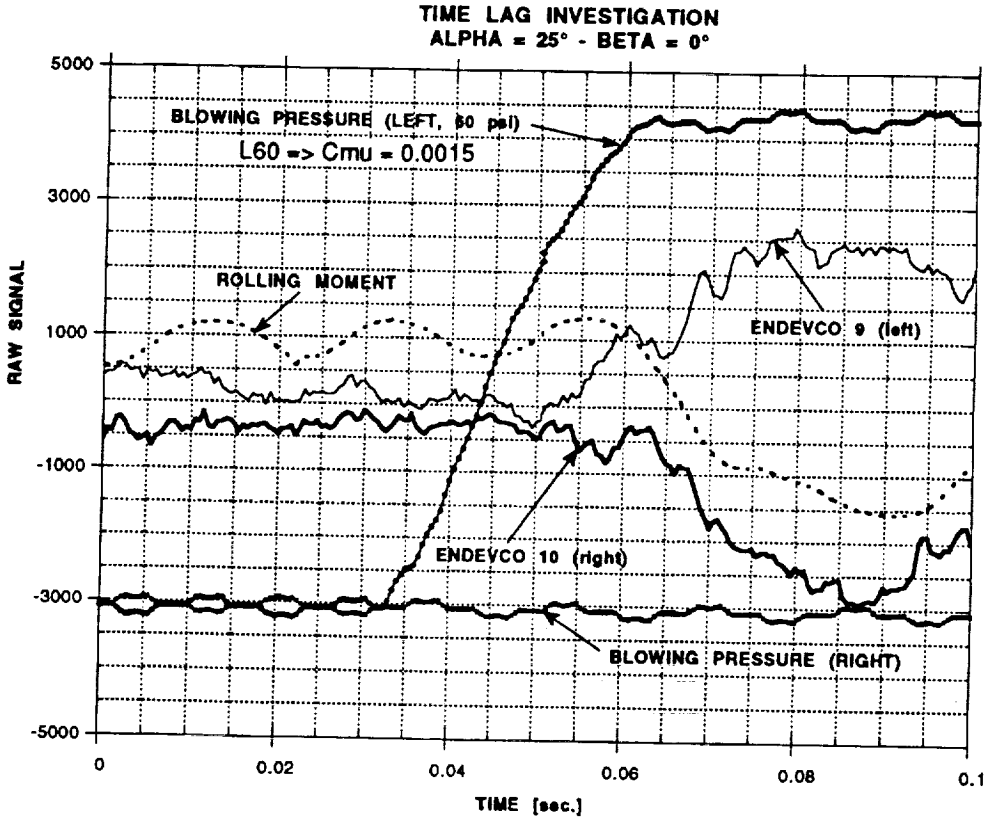

b)

Figure 51 - Time Response of Forces and Pressures to Blowing Inputs (Nozzle A, Left Blowing, $C\mu = 0.0015$, $\alpha = 25°$)

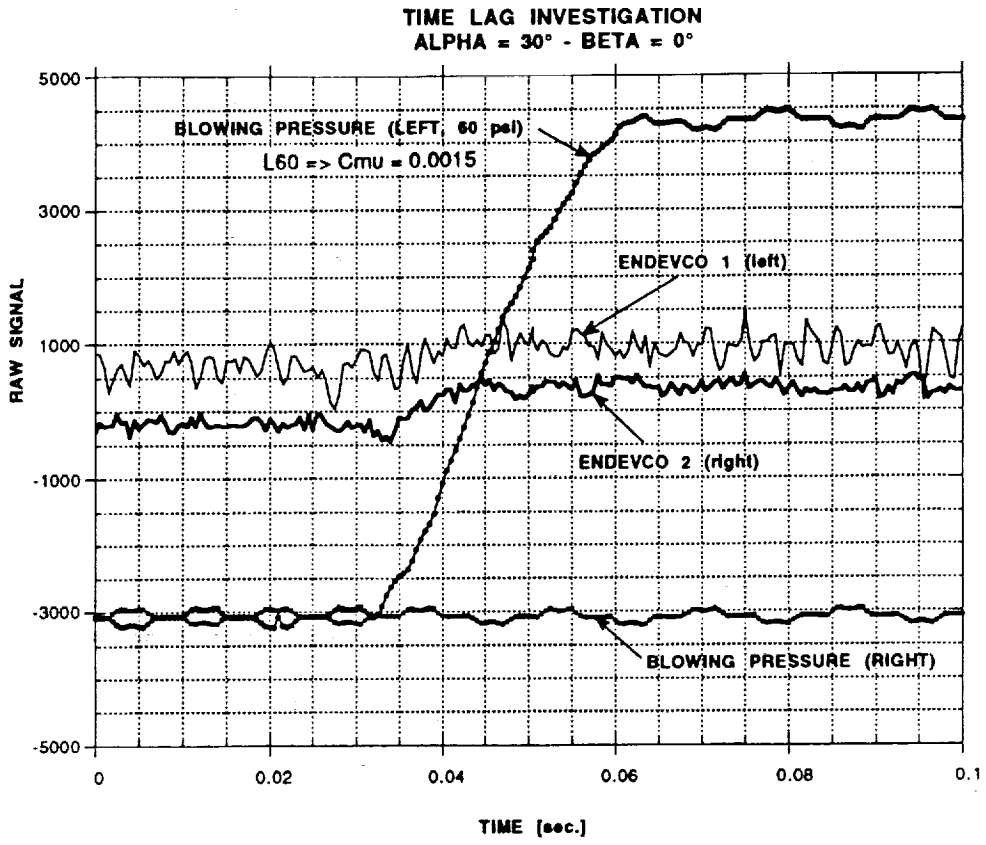

a)

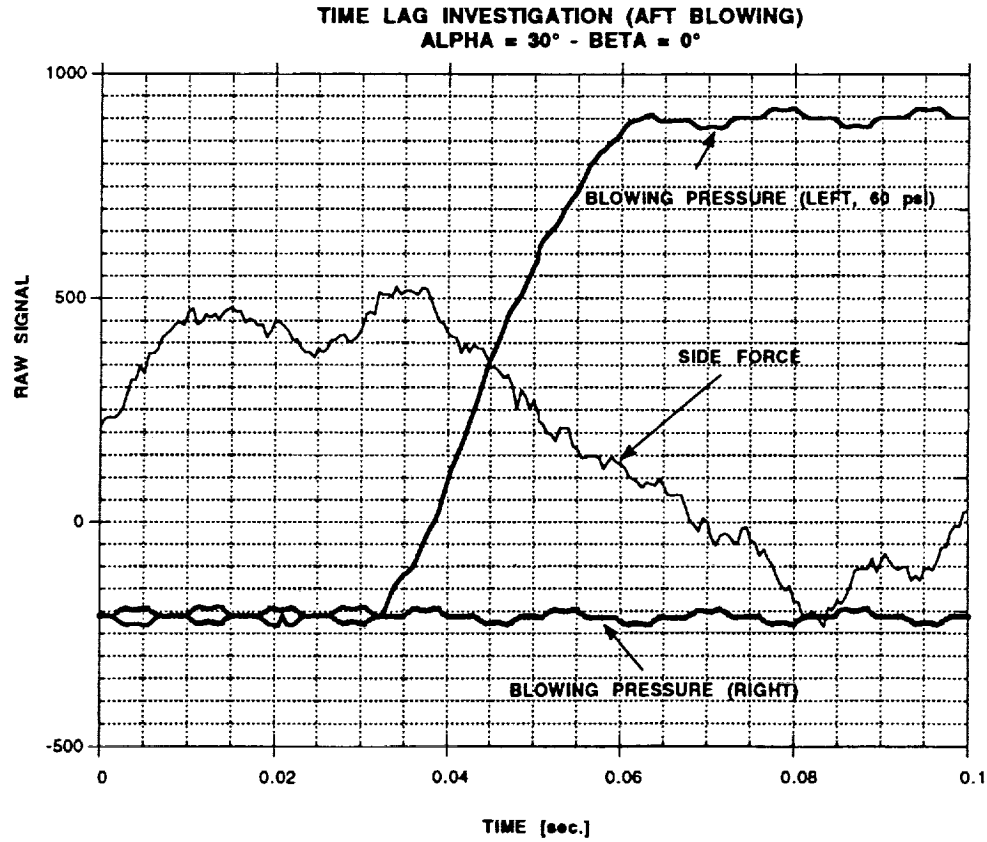

b)

Figure 52 - Time Response of Forces and Pressures to Blowing Inputs (Nozzle A, Left Blowing, $C\mu = 0.0015$, $\alpha = 30°$)

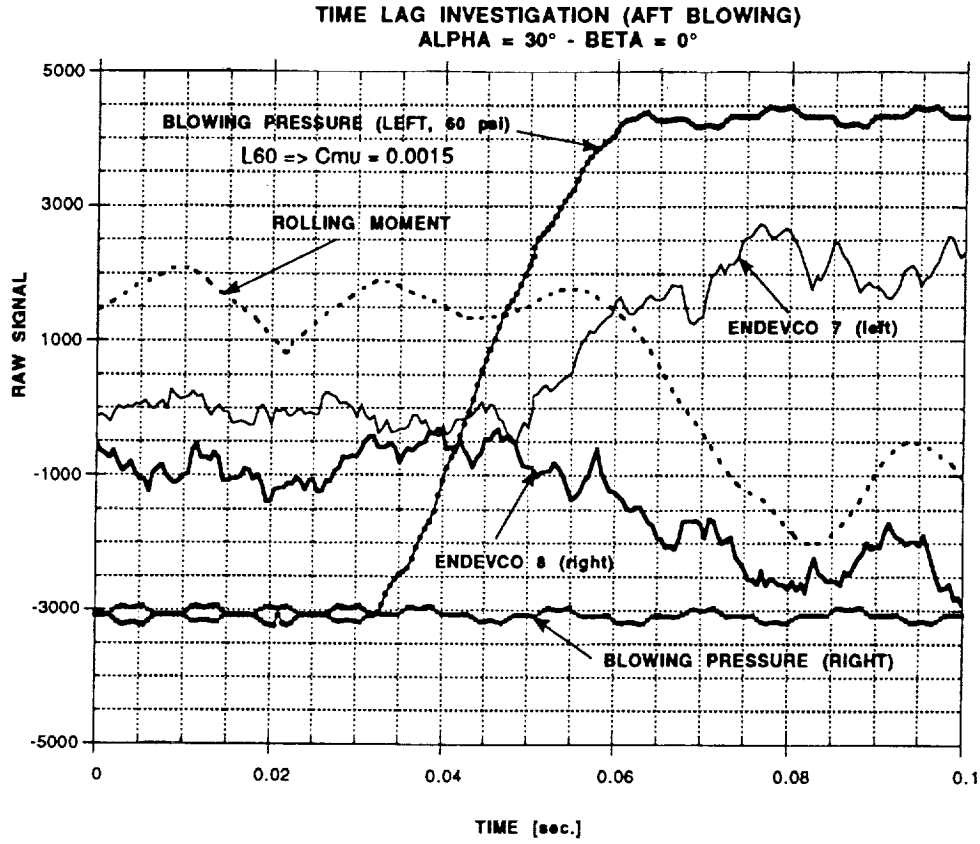

c)

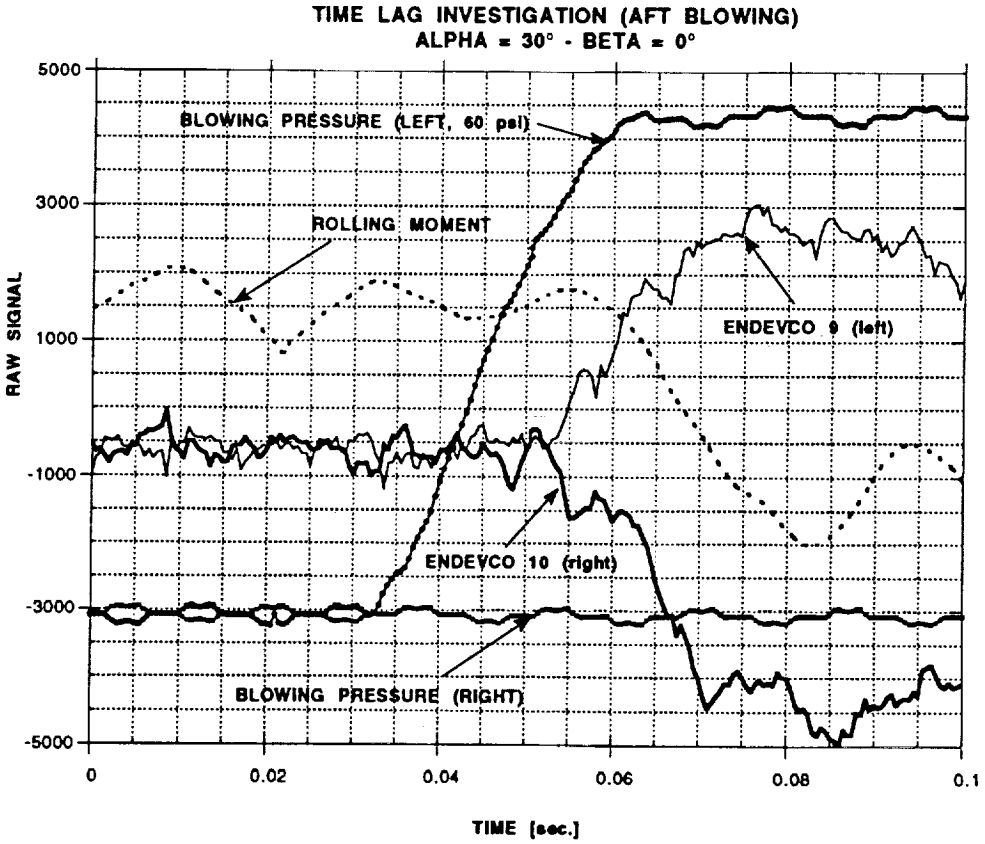

d)

Figure 52 - Concluded

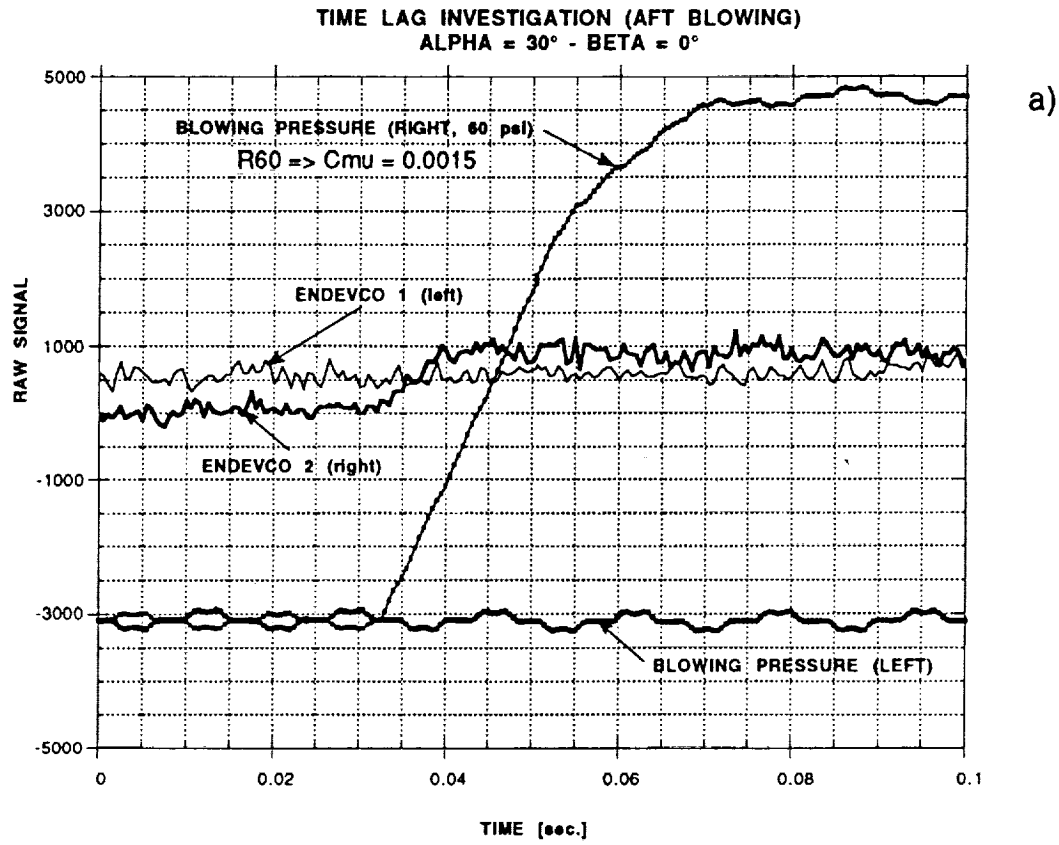

a)

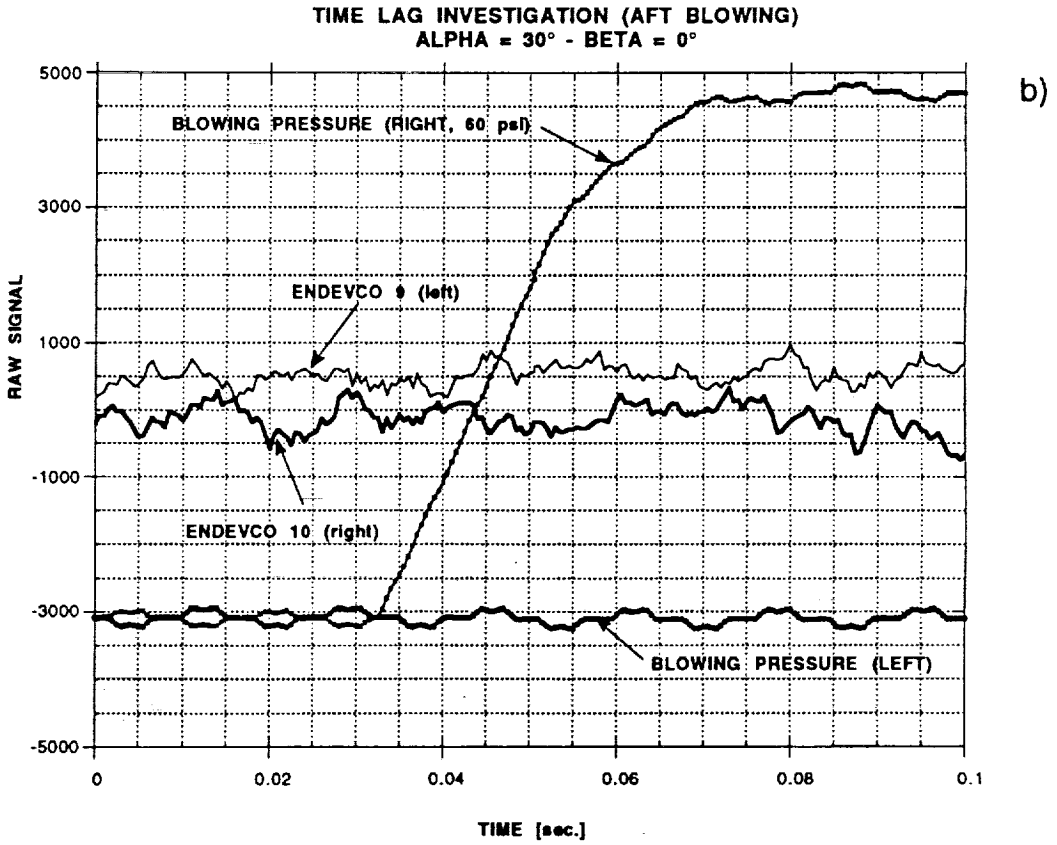

b)

Figure 53 - Time Response of Forces and Pressures to Blowing Inputs (Nozzle A, Right Blowing, Cμ = 0.0015, α = 30°)

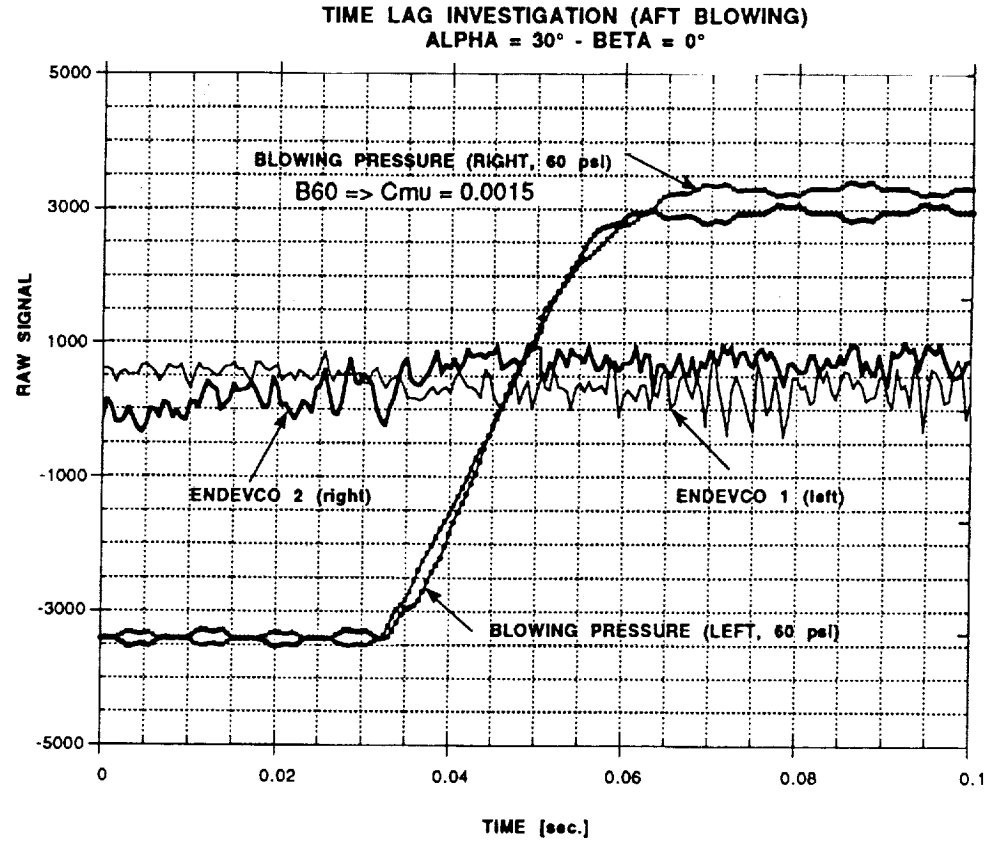

a)

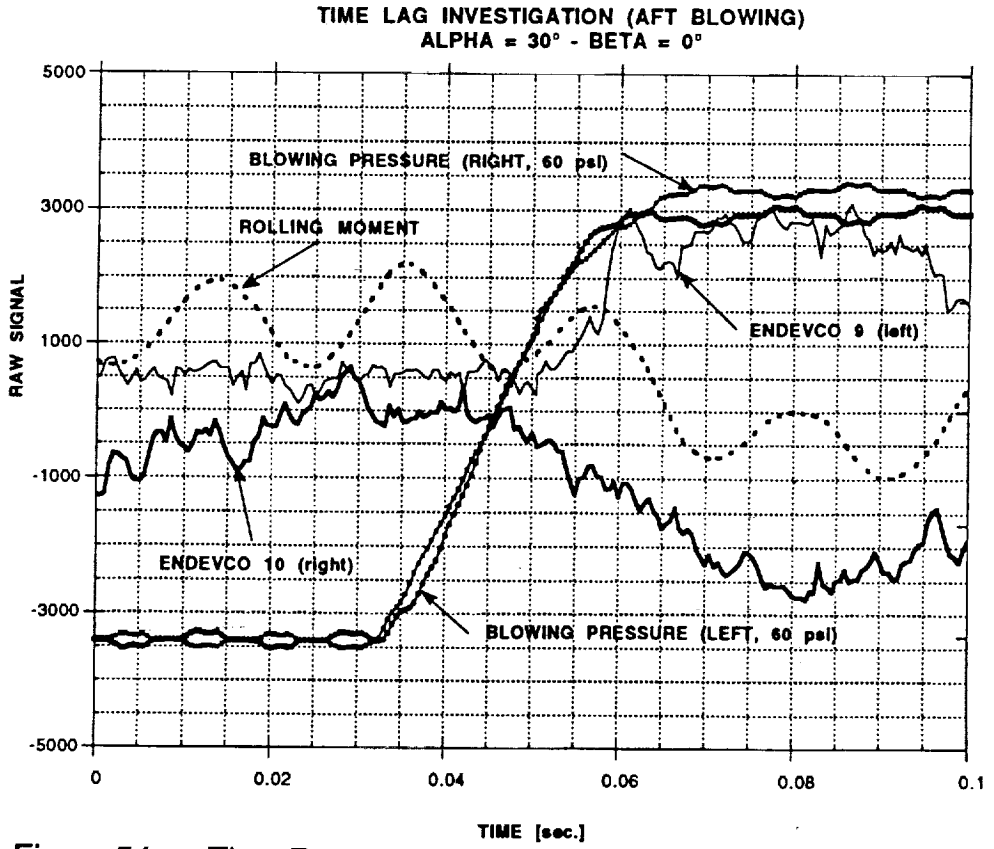

b)

Figure 54 - Time Response of Forces and Pressures to Blowing Inputs (Nozzle A, Simultaneous Blowing, $C\mu = 0.0015$, $\alpha = 30°$)

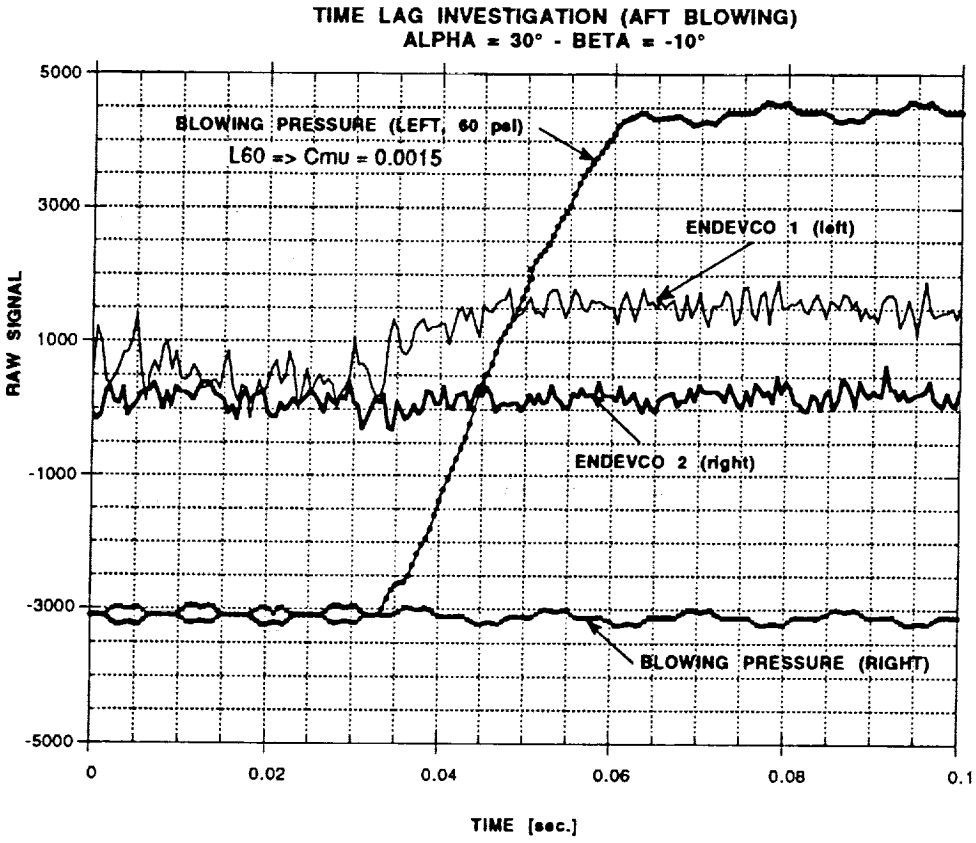

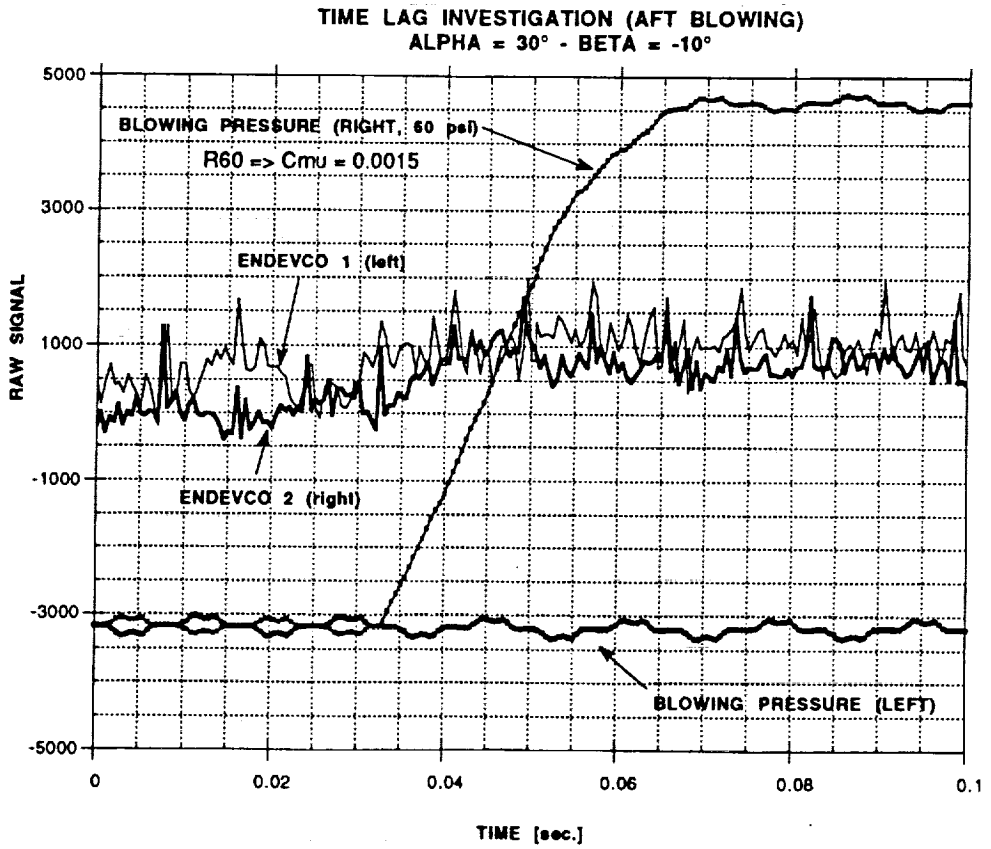

Figure 55 - Time Response of Forces and Pressures to Blowing Inputs (Nozzle A, Left and Right Blowing, $C\mu = 0.0015$, $\alpha = 30°$, $\beta = -10°$)

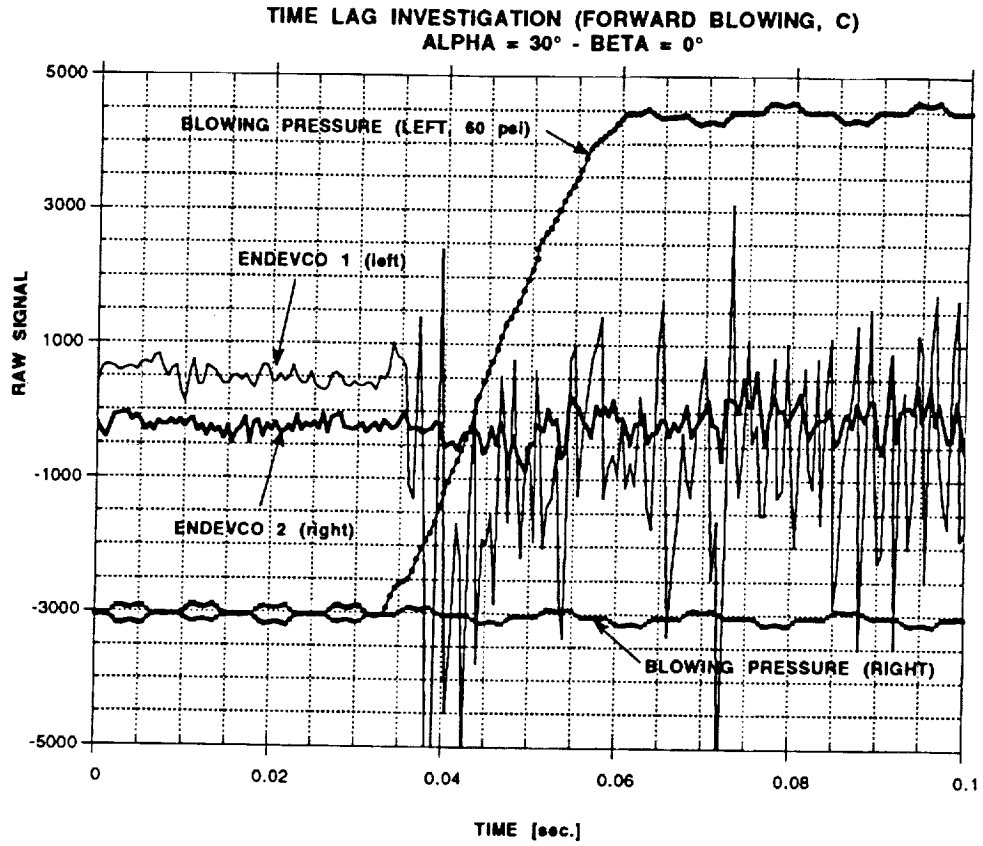

a)

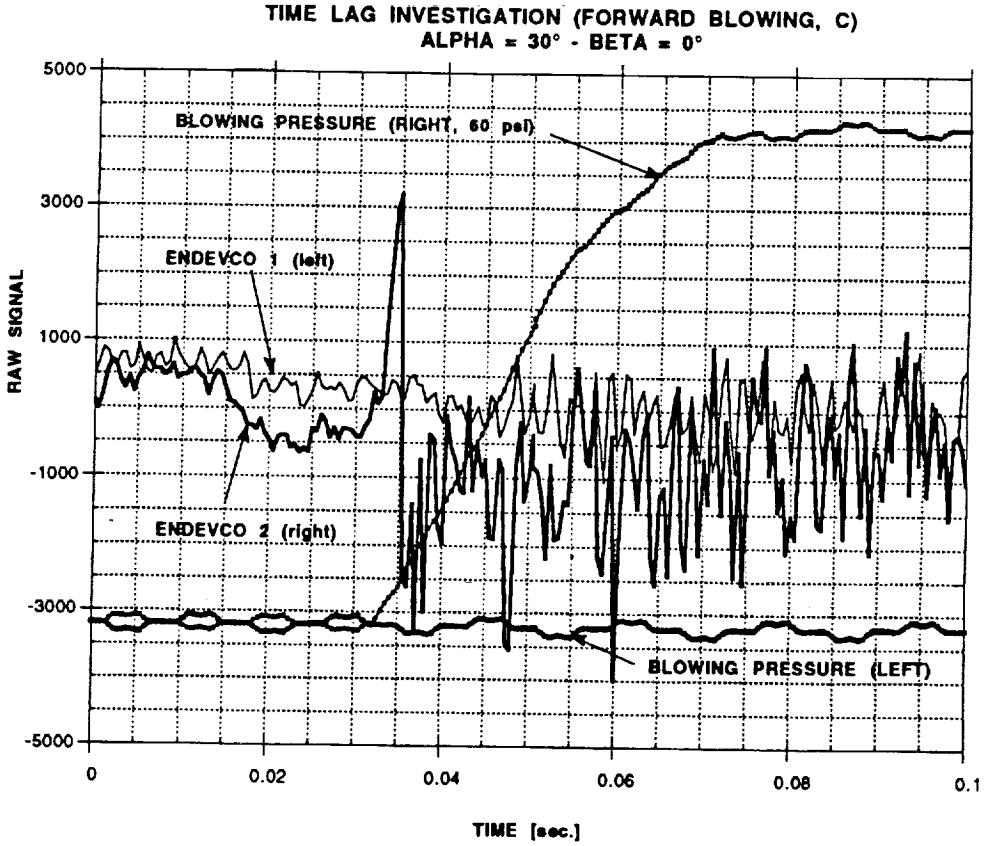

b)

Figure 56 - Time Response of Forces and Pressures to Blowing Inputs (Nozzle C, Left and Right Blowing, $C\mu = 0.0015$, $\alpha = 30°$)

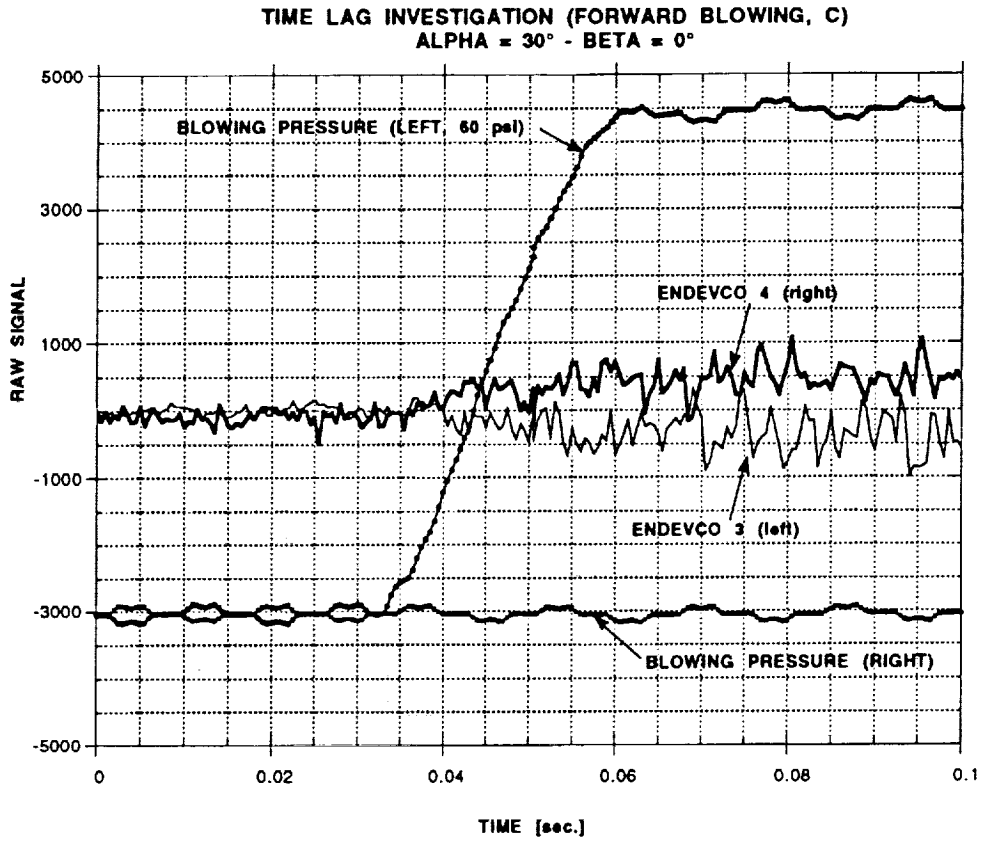

c)

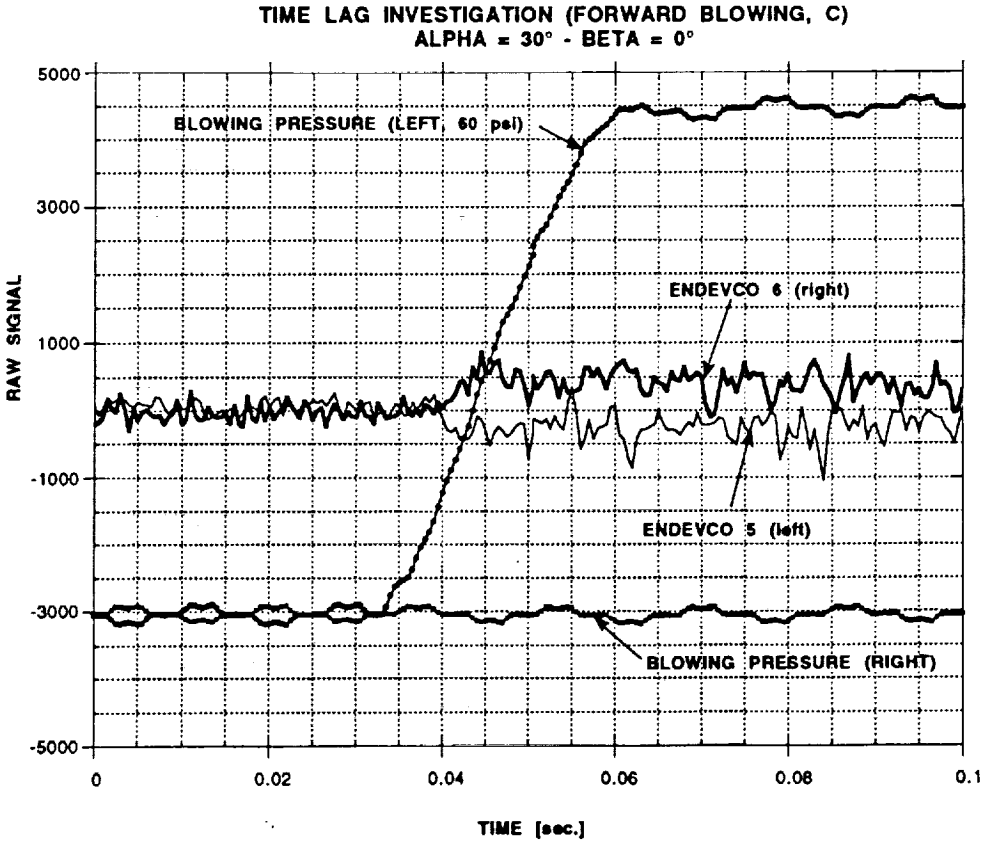

d)

Figure 56 - Continued

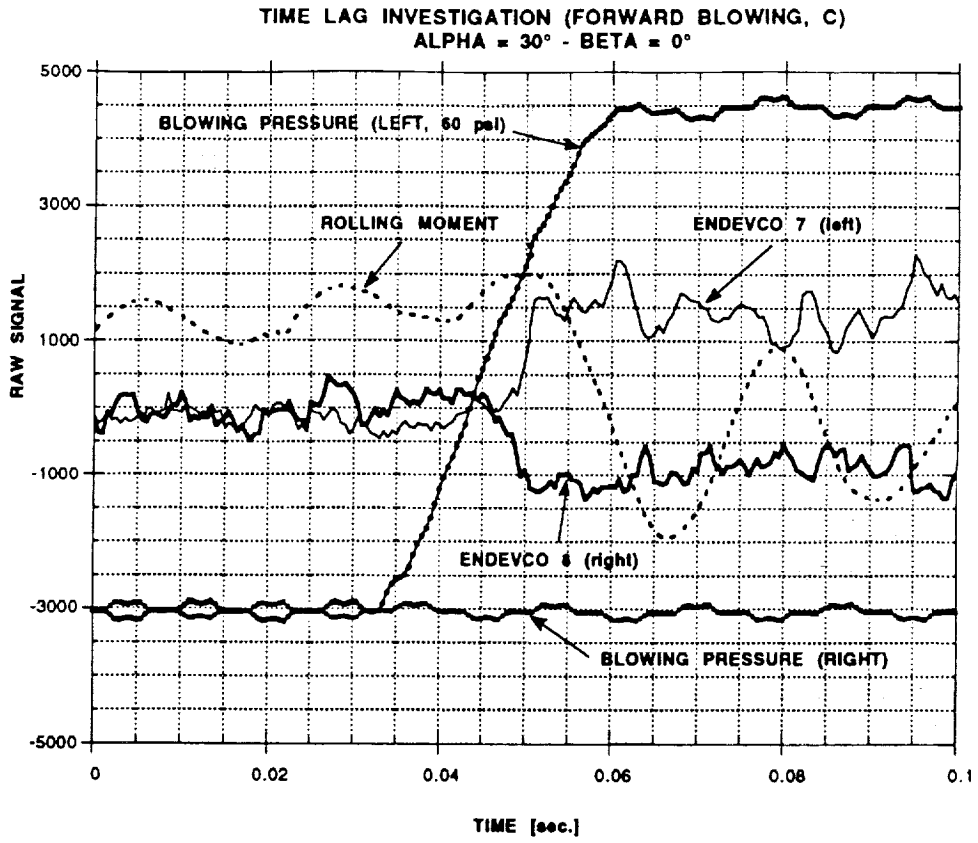

e)

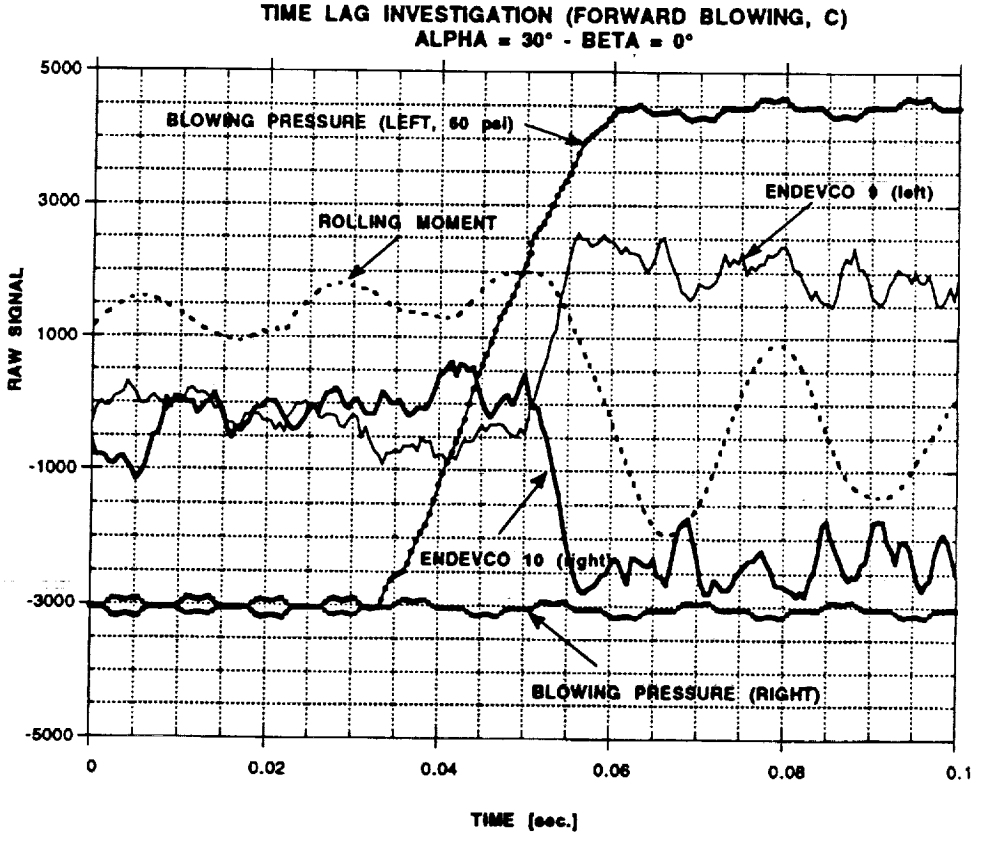

f)

Figure 56 - Concluded

REPORT DOCUMENTATION PAGE

Form Approved
OMB No. 0704-0188

1. AGENCY USE ONLY *(Leave blank)*	2. REPORT DATE	3. REPORT TYPE AND DATES COVERED
	September 1993	Contractor Report

4. TITLE AND SUBTITLE

Aerodynamic Control of NASP-Type Vehicles Through Vortex Manipulation, Volume II: Static Wind Tunnel Tests

5. FUNDING NUMBERS

NAS2-13196

6. AUTHOR(S)

Carlos Suárez, Brian R. Kramer, Brooke C. Smith, and Gerald N. Malcolm

7. PERFORMING ORGANIZATION NAME(S) AND ADDRESS(ES)

Eidetics International, Inc.
3415 Lomita Blvd.
Torrance, CA 90505

8. PERFORMING ORGANIZATION REPORT NUMBER

A-93138

9. SPONSORING/MONITORING AGENCY NAME(S) AND ADDRESS(ES)

National Aeronautics and Space Administration
Washington, DC 20546-0001

10. SPONSORING/MONITORING AGENCY REPORT NUMBER

NASA CR-177626

11. SUPPLEMENTARY NOTES

Point of Contact: Larry Meyn, Ames Research Center, MS 247-2, Moffett Field, CA 94035-1000
(415) 604-5038

12a. DISTRIBUTION/AVAILABILITY STATEMENT

Unclassified-Unlimited
Subject Category – 02

12b. DISTRIBUTION CODE

13. ABSTRACT *(Maximum 200 words)*

Forebody Vortex Control (FVC) has been explored in this research program for potential application to a NASP-type configuration. Wind tunnel tests have been conducted to evaluate a number of jet blowing schemes. The configuration tested has a slender forebody and a 78° swept delta wing. Blowing jets were implemented on the leeward side of the forebody with small circular tubes tangential to the surface that could be directed aft, forward, or at angles in between. The effects of blowing are observed primarily in the yawing and rolling moments and are highly dependent on the jet configuration and the angle of attack. Results show that the baseline flow field, without blowing activated, is quite sensitive to the geometry differences of the various protruding jets, as well as being sensitive to the blowing, particularly in the angle of attack range where the forebody vortices are naturally asymmetric. The time lag of the flow field response to the initiation of blowing was also measured. The time response was very short, on the order of the time required for the flow disturbance to travel the distance from the nozzle to the specific airframe location of interest at the free stream velolcity. Overall, results indicate that sizable yawing and rolling moments can be induced with modest blowing levels. However, direct application of this technique on a very slender forebody would require thorough wind tunnel testing to optimize the jet location and configuration.

14. SUBJECT TERMS

Generic hypersonic configuration, Forebody vortex control, Wing rock suppression, Experimental/simulation, Aerodynamic control

15. NUMBER OF PAGES

144

16. PRICE CODE

A07

17. SECURITY CLASSIFICATION OF REPORT	18. SECURITY CLASSIFICATION OF THIS PAGE	19. SECURITY CLASSIFICATION OF ABSTRACT	20. LIMITATION OF ABSTRACT
Unclassified	Unclassified		